

# **DIFFUSION WEIGHTED IMAGING OF THE NEONATAL BRAIN**

*Jeroen Dudink*

ISBN: 9789090256023

Cover design: Ton Everaers & Jeroen Dudink

Thesis layout: Ton Everaers

Printed by Print Partners Ipskamp

Part of the research in this thesis was financially supported by the "Prinses Beatrix Fonds".

The print and reproduction of this thesis was kindly supported by:

Esaote – Pie Medical Benelux B.V., Dräger Medical Netherlands B.V., LMT Lammers Medical Technology, Nutricia Nederland B.V., UCB Pharma B.V., Waldmann B.V.

Copyright © 2010 Jeroen Dudink

All rights reserved. No part of this thesis may be reproduced, distributed, stored in a retrieval system or transmitted in any form or by any means, without permission of the author, or, when appropriate, of the publishers of the publications.



# **DIFFUSION WEIGHTED IMAGING OF THE NEONATAL BRAIN**

*Diffusie gewogen beeldvorming  
van het neonatale brein*

*Proefschrift*

ter verkrijging van de graad van doctor aan de  
Erasmus  
Universiteit Rotterdam  
op gezag van de  
rector magnificus

Prof. dr. H.G. Schmidt

en volgens besluit van het College voor Promoties.

De openbare verdediging zal plaatsvinden op

woensdag 1 september 2010 om 15:30 uur

door

Jeroen Dudink  
Geboren te Amsterdam



# **promotiecommissie**

## ***Promotor***

Prof.dr. J.B. van Goudoever

## ***Overige leden***

Prof.dr. W.F.M. Arts

Prof.dr. G.P. Krestin

Prof.dr. D. Tibboel

## ***Copromotoren***

dr. P.P. Govaert

dr. M.H. Lequin

*Deze thesis draag ik op aan Judith Bosman-Vermeeren*

# Table of contents

<b>Chapter 1</b>	Introduction and aims	9
<b>Chapter 2</b>	Connecting the developing preterm brain <i>Early Hum Dev. 2008;84:777-82</i>	31
<b>Chapter 3</b>	Fractional anisotropy in white matter tracts of very-low-birth-weight infants <i>Pediatr Radiol. 2007;37:1216-23</i>	51
<b>Chapter 4</b>	Diffusion tensor imaging of cortical plate and subplate in very-low-birth-weight infants <i>Pediatr Radiol. 2010;40:1379-404</i>	67
<b>Chapter 5</b>	High b-value diffusion tensor imaging of the neonatal brain at 3T <i>AJNR Am J Neuroradiol. 2008;29:1966-72</i>	85
<b>Chapter 6</b>	Magnetic resonance imaging in neonatal stroke <i>Semin Fetal Neonatal Med. 2009;14:299-310</i>	107
<b>Chapter 7</b>	Evolution of unilateral perinatal arterial ischemic stroke on conventional and diffusion weighted MR imaging <i>AJNR Am J Neuroradiol. 2009;30:998-1004</i>	139
<b>Chapter 8</b>	Network injury to pulvinar with neonatal arterial ischemic stroke <i>Neuroimage. 2008;39:1850-7</i>	161

<b>Chapter 9</b>	Diffusion tensor imaging reveals acute network injury in neonatal arterial ischemic stroke <i>Submitted</i>	181
<b>Chapter 10</b>	General discussion, Future directions Summary in Dutch (Samenvatting) Dankwoord List of publications Curriculum vitae	197
<b>Color section</b>		227





# Chapter 1

## INTRODUCTION AND AIMS

---

## INTRODUCTION

### Preterm and Term neonatal brain injury

Although in the last decades advances in fetal and neonatal medicine have reduced mortality in neonatal intensive care units in the Western world, the morbidity due to brain injury remains high<sup>1-3</sup>. Patterns of neonatal brain injury can be roughly divided in (1) term and (2) preterm patterns. Table 1 shows the number of infants admitted to the NICU in the Sophia Children's Hospital between March 2008 and March 2010 with a typical 'neurological' diagnosis. The table highlights differences in diagnoses between preterm and term infants in relation to gender. In preterm infants the most common diagnoses are: persistent flaring (hypersignal intensity seen in periventricular white matter using cranial ultrasound), intraventricular haemorrhage and venous infarction. In term infants perinatal asphyxia and perinatal stroke are most often reported.

Early prediction of neurodevelopmental outcome after neonatal brain injury would provide important information to parents, doctors and researchers. Important, because many studies show a high incidence of neurodevelopmental disability among survivors of preterm birth<sup>4-6</sup>. Early recognition of a high risk of abnormal development would offer parents and health care workers the possibility to take action in optimizing outcome. For example by starting early targeted physiotherapy, speech therapy, pedagogic advice etc. Several of these neurological deficits, which occur following neonatal brain injury, are linked to white matter injury and more recently also to subplate injury<sup>7</sup>.

In term infants there is a high reported incidence of stroke (Table 1). Incidence rates of neonatal arterial ischemic stroke are currently estimated at approximately 1 in 2300 live births<sup>8</sup>, higher than the annual rate of adult large vessel stroke. The morbidity of perinatal stroke lasts a lifetime, which lays a heavy burden on individuals, families, and society. Up to 75% of survivors of perinatal stroke show neurological deficits or epilepsy<sup>9</sup>.



---

Early recognition of neonatal brain injury and assessment of risks of later impairment is difficult. Clinical and biochemical tests are of limited use to predict several aspects of long-term outcome. This is why advanced neuroimaging techniques are needed. To improve our knowledge of diagnosis, timing and evolution of perinatal brain injury such as stroke and preterm white matter and subplate injury is pivotal to be able to provide early proxy outcome measurements.

Magnetic resonance imaging (MRI) is a non-ionizing and non-invasive neuroimaging tool, which provides unique anatomical detail of neonatal brain tissue. It offers good spatial resolution and high quality soft tissue contrast and allows visualizing and quantifying the micro-architecture of brain structures *in vivo*<sup>10</sup>.

Thus, MRI presents clinicians and researchers with objective, *in vivo* information regarding brain anatomy, pathology and -due to recent advances- functional and physiological characteristics<sup>10</sup>.

Described by Le Bihan et al. in 1986, diffusion-weighted (DW) imaging has rapidly evolved and is now routinely used<sup>11</sup>. The most common application of DWI is the early detection of ischemia. By incorporating directionality into diffusion weighted measurements, diffusion-tensor images (DTI) can be obtained. DTI provides means of investigating tissue microstructure *in vivo*.

DTI measurements offer great potential in the study of white matter- and subplate damage in preterm infants. So far, however, the clinical use of this technique is restricted by the lack of normal reference values for preterm infants. Part of this thesis is aimed at providing reference values of both white matter tracts and the subplate for the clinical interpretation of DTI images in preterm infants.

DWI plays an important role in diagnosing neonatal stroke. However, the evolution of DWI in neonatal stroke is less well described. New DTI postprocessing techniques allows to visualize secondary network injury. Thus DTI may lead to better understanding of the variability in neurological outcomes seen in perinatal stroke.

This thesis explores diffusion weighted imaging (including DTI) in the newborn brain, and attempts to focus on clinical and research questions likely to be encountered by neonatologists and paediatric radiologists regarding neonatal neuroimaging. The research described in this thesis focuses on 'normal' white matter development and subplate evolution of the very low birth weight infant and on term born neonatal stroke. First an introduction to diffusion tensor imaging is given.

**Table 1**

Showing the number of infants with a neurological diagnosis admitted on the NICU of the Sophia's Childrens Hospital in 2 years (March 2008-March 2010). A total of 1420 children were admitted in those two years of which 766 (54%) male. (Research database 'Dudink/Roon').

Diagnosis	Preterm (M/F)	Term (M/F)
IVH grade 2 and 3	40 (22/18)	2 (2/0)
Venous infarction	11 (7/4)	0
PHVD	8 (7/1)	1 (1/0)
Persistent flaring on CUS (>1w)	60 (32/28)	0
PVL-cystic	1 (0/1)	0
Intrapartum asphyxia	9 (5/4)	38 (21/17)
Meningitis	5 (4/1)	6 (4/2)
Stroke	5 (2/3)	22 (18/4)
Neonatal seizures eci	2 (1/1)	7 (2/5)
Congenital brain anomalies	9 (6/3)	7 (4/3)
Cerebellar haemorrhage	9 (6/3)	0
Cranial birth trauma	5 (3/2)	5 (3/2)
<b>Total No Infants (M/F)</b>	<b>164 (95/69)</b>	<b>88 (55/33)</b>

*M = male, F = female, IVH= intraventricular haemorrhage, PHVD = post haemorrhagic ventricular dilatation, CUS = cerebral ultrasound, PVL = periventricular leucomalacia, eci = e causa ignota.*

## Introduction to Diffusion Tensor Imaging (DTI)

Diffusion tensor imaging (DTI) provides an opportunity to quantify the micro-architecture of biological tissue *in vivo*. This is especially important in studies that involve biological samples in which the boundaries influencing diffusion are so small that they cannot be displayed by

conventional magnetic resonance imaging techniques. In recent years studies have shown that DTI is a promising method for characterizing micro-structural changes or differences associated with neurodevelopment, neuropathology and neuroprotection strategies<sup>12</sup>.

This chapter describes the physical basis of diffusion in tissue and how this can be used. It is a brief and basic description of DTI and for further reading I would like to refer to the recently published book of Dr. Johansen-Berg and Dr. Behrens 'Diffusion MRI; from quantitative measurement to in vivo neuroanatomy'<sup>13</sup>.

## Basics of diffusion

Robert Brown (1773-1858), a Scottish botanist, made an important discovery in 1827: he noted pollen grains, which were suspended in water, were constantly moving (now called 'Brownian motion'). Brown had unintentionally described the phenomenon of self-diffusion of water molecules; i.e. the constant random thermal motion of all molecules above zero degrees Kelvin.

In 1905 another historical figure played an important role in the 'theory of diffusion': Albert Einstein. He proved that the square displacement of molecules from their starting point over time (t), averaged over all the molecules in a sample  $[r^2]$ , is directionally proportional to the observation time (t).

$$[r^2] = 6Dt$$

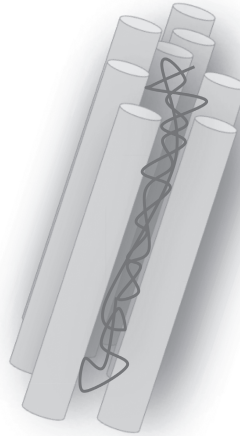
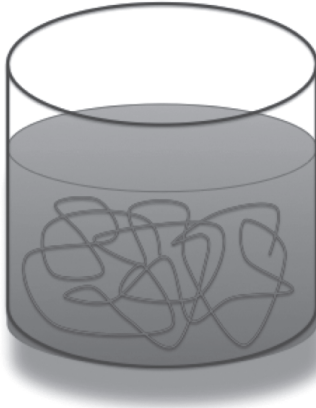
The constant (D) is the diffusion coefficient.

The distribution of squared displacements takes a Gaussian form, with the peak beginning at zero displacement. The diffusion coefficient of pure water at 20°C is roughly  $2.0 \times 10^{-3} \text{ mm}^2/\text{s}$  and increases at higher temperatures (e.g. the diffusion of water at body temperature (37°C) is  $3 \times 10^{-3} \text{ mm}^2/\text{s}$ ).

With diffusion MRI the diffusion coefficient is not measured directly, but it is deduced from the observations of the displacements over a given time period. When water molecules encounter any hindrance along their random walk such as cell membranes, the mean square displacement per time unit will be lower than when observed in 'free' water. When applying Einstein's equation to compute the diffusion coefficient it will "appear" that the diffusion coefficient is lower. So we refer to the 'apparent diffusion coefficient' (abbreviated to ADC)<sup>15</sup>.

## Biological diffusion

The diffusion of water in biological tissues occurs inside, outside, around, and through cellular structures. As mentioned above, the diffusion of water is primarily caused by random thermal fluctuations but is also modulated by the interactions with cellular membranes, and sub-cellular structures and organelles. Cellular membranes hinder the diffusion of water, causing water molecules to take more complex paths, thereby decreasing the mean squared displacement. The diffusion tortuosity increases and corresponding apparent diffusivity decreases either because of cellular swelling or because of increased cellular density<sup>16</sup>. Both hindered and restricted diffusion reduce the apparent diffusivity of water. Liquefaction due to necrosis, as a result of a breakdown of cellular membranes, decreases tortuosity and increases the ADC. In fibrous tissues including muscle tissue and cerebral white matter, water diffusion is relatively unrestricted in the direction parallel to the fiber orientation. On the other hand, water diffusion is highly restricted and hindered in the directions perpendicular to the fibers. Thus, the diffusion in fibrous tissues is anisotropic.



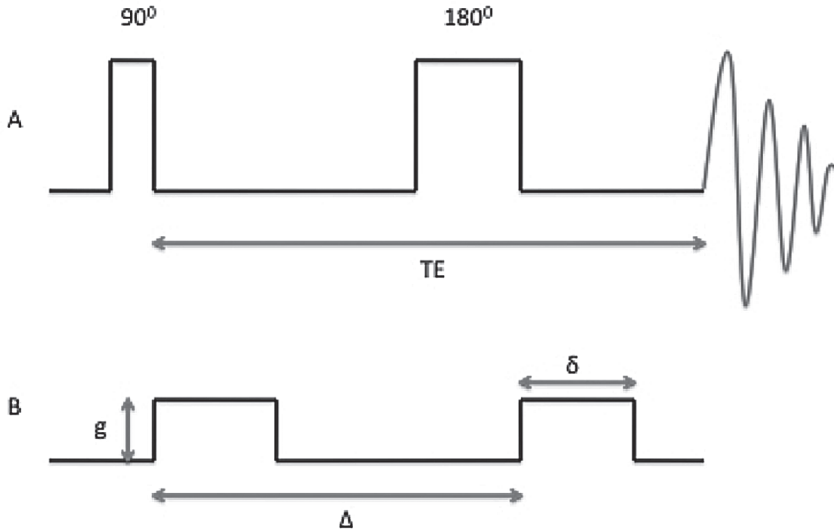
Figures representing free diffusion of water in an isotropic sample: e.g. the random walk water molecules in a glass of water (left) versus restricted diffusion in an anisotropic sample: e.g. a bundle of axons (right). In the isotropic case the diffusion is similar in all directions, in the anisotropic case the diffusion is larger in one direction (parallel to the direction of the axons) than in the other (perpendicular to the fiber bundle).

## How can we measure water diffusion using MRI?

DTI is based on traditional MRI. A book explaining MRI physics in an accessible, beginning-level way is 'From picture to proton' by McRobbie et al<sup>17</sup>.

MR sequences can be rendered sensitive to diffusion by adding magnetic field gradients (the magnetic field is varied in a linear manner over the volume of interest). The most basic MR equation is the Larmor equation, which states: the precessional frequency of spins in a magnetic field is directly proportional to the strength of the field. Thus a gradient imposes a position dependent precessional frequency of spins. When spins are precessing at different frequencies with respect to each other over a period of time they will acquire a certain phase difference with respect to each other. This phase effect is reversed by the application of a similar gradient of opposite polarity or of the same amplitude, duration and polarity but following the application of a 180 degrees refocusing pulse such as in a 'spin-echo experiment'.

The MR method mostly used for diffusion measurements is the ‘pulsed gradient spin echo’ method. It was introduced by Stejskal and Tanner: they incorporated two diffusion-sensitizing linear magnetic-field gradients into a ‘spin-echo sequence’ one placed on either side of the 180 degree radio-frequency pulse of the MR coil<sup>18</sup>.



Diffusion sensitized spin-echo sequence. (A) The 90-degree excitation and 180 degree refocusing pulses form a spin-echo at the echo-time TE. (B) The pulse sequence can be sensitized for diffusion by applying a pair of pulsed-field gradients, with amplitude  $g$ , surrounding the 180 degree pulse. The definition of the gradient pulse duration,  $\delta$ , and the time separation between the gradient pulses,  $\Delta$ , are indicated.

The phase shift ' $\phi$ ' of a gradient pulse of magnitude ' $g$ ' of duration ' $\delta$ ' on a spin at position ' $r$ ' is given by:

$$\phi(r) = \gamma \delta g r$$

for static spins and by:

$$\phi = \int \gamma \delta g r(t) dt$$

for moving spins

---

*'Y' is the gyromagnetic ratio, which is a nuclei specific constant. For hydrogen  $\gamma = 42,6 \text{ MHz/Tesla}$ .*

Only motion in the direction of the gradient causes a change in phase of the spin. When there is no diffusion, the phase difference is zero. The phase shift is cancelled out, because the 180-degree pulse in the spin-echo sequence reverses the sign of the phase angle. This causes the static spins to be all in phase with respect to other spins at the same spatial location, which gives a maximum echo signal. Diffusing spins will not be in phase with respect to the other spins at the same spatial location, which is leading to signal attenuation<sup>19</sup>. The amount of attenuation 'A' caused by diffusion is determined by the ADC and a so-called 'b-factor' (b), which describes the strength of the diffusion sensitivity.

$$A = \exp(-bADC)$$

and

$$b = \gamma^2 g^2 \delta^2 (\Delta - \delta/3)$$

In which ' $\gamma$ ' is the gyromagnetic ratio, ' $\delta$ ' the duration of the gradient pulse, and ' $\Delta$ ' the time between the onsets of the two gradient pulses.

The intensity of the signal is also affected by T2 relaxation. To know the amount of this effect, a measurement that is not diffusion weighted ( $S(0)$ ) is required. The measured signal  $S(b)$  is:

$$S(b) = AS(0)$$

Now ADC can be calculated:

$$ADC = -1/\ln(S(b))$$

**Table 2**

Shows mean ADC values (+/- SD) for different brain structures in healthy term born infants as found in literature.

	Mean ADC x 10–3 mm <sup>2</sup> /second (+/-SD)
<b>Grey Matter:</b>	
Thalamus	0,99 (0,08) <sup>20-25</sup>
Basal ganglia	1,17 (0,06) <sup>20-22,24</sup>
Cortex	1,21 (0,04) <sup>20,21,23,25</sup>
<b>White matter:</b>	
ALIC	1,14 (0,04) <sup>20,21,25,26</sup>
PLIC	1,05 (0,02) <sup>20-22,24,25</sup>
CSO	1,53 (0,07) <sup>20-27</sup>
<b>Cerebellum:</b>	1,13 (0,03) <sup>20-22,24</sup>

ALIC = anterior limb of internal capsule, PLIC = posterior limb of internal capsule, CSO= centrum semi ovale.

## The diffusion tensor

When the diffusion is anisotropic it cannot be described by a single scalar coefficient. Instead it is now dependent on a (three-dimensional) direction. The amount of signal attenuation  $A$  is now dependent on the relative position between the principal diffusion direction and the applied magnetic gradient vector  $B$ . Commonly, and similarly to the one-dimensional equation a multivariate Gaussian model is used for the attenuation. This Gaussian model is not valid in areas where fibers intersect. Instead, more complex models, such as mixtures of Gaussians, will be used.

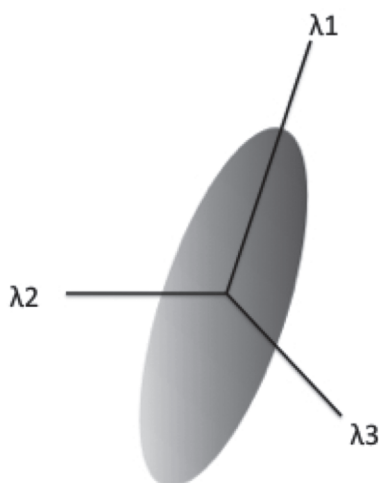
A tensor representation ( $\underline{D}$ ) is then required:

$$\underline{D} = \begin{pmatrix} D_{xx} & D_{xy} & D_{xz} \\ D_{yx} & D_{yy} & D_{yz} \\ D_{zx} & D_{zy} & D_{zz} \end{pmatrix}$$



The diagonal elements  $D_{xx}$ ,  $D_{yy}$  and  $D_{zz}$  represent the ADC along the axes  $x$ ,  $y$  and  $z$  in the frame in which the gradients are applied. The off diagonal elements allow for the principal diffusion direction to be different from one of the main axes  $x$ ,  $y$  and  $z$  in the frame. To determine the diffusion tensor, diffusion weighted images along at least 6 directions have to be collected and an image that is not diffusion weighted ( $b = 0$ ).

The diffusion tensor is often thought of in terms of an ellipsoid with an internal reference frame: the eigensystem. The principal axes of the ellipsoid are given by eigenvectors and the lengths are given by the diffusional distance variance in a given time (eigenvalues:  $\lambda_1, \lambda_2, \lambda_3$ ). The eigenvector-eigenvalue pairs together contain all information available in the original tensor.



Ellipsoids are used to represent diffusion displacements for the diffusion tensor. The diffusion is highly anisotropic in fibrous tissues such as white matter and the direction of greatest diffusivity is generally assumed to be parallel to the local direction of white matter bundles.

## Anisotropy Indices

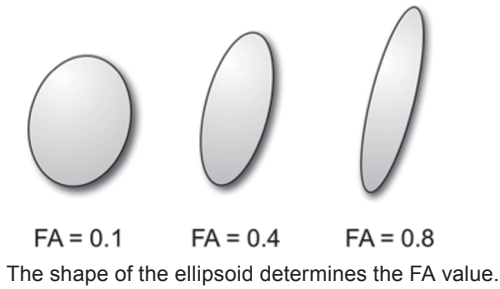
Several indices represent the amount of diffusion anisotropy of the diffusion tensor. The indices are based on the eigenvalues of the tensor. Some indices only distinguish between anisotropic and isotropic diffu-

sion, other indices also divide the anisotropy in two types: linear (cigar shape) and planar (pancake shape) anisotropy. Two anisotropy indices most used in literature are fractional anisotropy (FA) and relative anisotropy (RA)<sup>28</sup>.

$$FA = \frac{\sqrt{(\lambda_1 - \lambda_2)^2 + (\lambda_2 - \lambda_3)^2 + (\lambda_1 - \lambda_3)^2}}{\sqrt{2(\lambda_1^2 + \lambda_2^2 + \lambda_3^2)}}$$

$$RA = \frac{\sqrt{(\lambda_1 - \lambda_2)^2 + (\lambda_2 - \lambda_3)^2 + (\lambda_1 - \lambda_3)^2}}{\sqrt{2}(\lambda_1 + \lambda_2 + \lambda_3)}$$

The range of FA and RA is between one (anisotropic) and zero (isotropic).



Although FA appears to be sensitive to a large spectrum of pathological conditions in humans and animals, the full tensor shape cannot be simply described using a single scalar measure. Different eigenvalue combinations can give the same values of FA and thus shows that diffusion anisotropy does not describe the full tensor shape or distribution. Several studies have suggested that eigenvalue combinations will add information to the underlying pathology. For instance radial diffusivity  $((\lambda_2 + \lambda_3)/2)$  appears to be modulated by myelin in white matter, whereas the axial diffusivity  $(\lambda_1)$  is more specific to axonal degeneration<sup>29</sup>.

The tensor orientation (described by the major eigenvector) is another important measure. It is assumed that in diffusion tensors with high anisotropy, the major eigenvector direction is parallel to the direction of white matter tracts. This is often represented using an RGB (red-green-blue) color map to indicate eigenvector orientations<sup>30</sup>. These color maps

are very useful for surveying the organization of white matter in the brain and for identifying major white matter tracts in 2D.

DTI has a great ability to identify specific white matter tracts on the eigenvector color maps<sup>31</sup>. DTI has been proven useful for mapping white matter anatomy relative to lesions for preoperative planning and post-operative follow-up<sup>32</sup>.

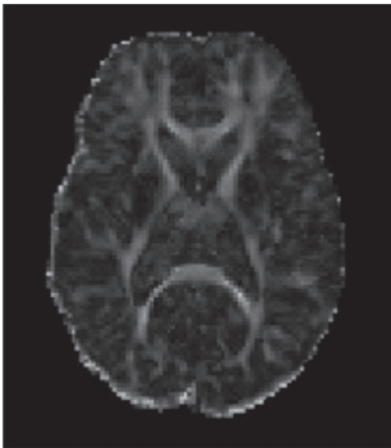


Figure showing a typical DTI color map: the major eigenvector direction indicated by color (red = R/L, green = A/P, blue = S/I) weighted by the FA (note that specific tract groups can be identified). (A full color version of this illustration can be found in the color section).

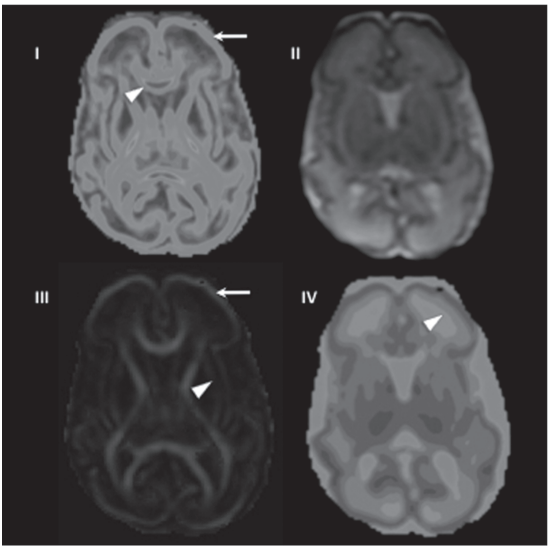
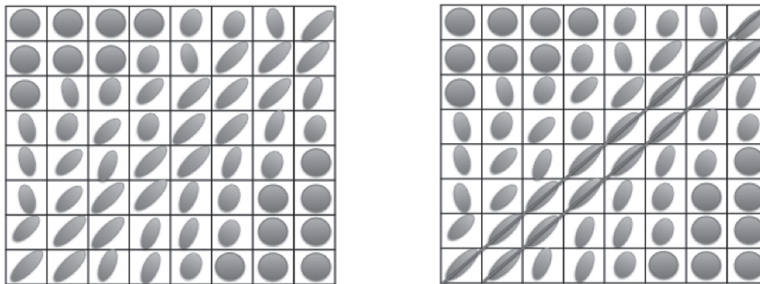


Figure showing different representations of a DTI scan of a patient of 30 weeks gestation. (I) FA-map showing a relatively high FA values (green) of the cortex (arrow) and the highest FA values (red) of the genu of the corpus callosum (arrowhead). (II) Showing a B0 map. (III) Color map in which the major eigenvector direction is indicated by color (red = R/L, green = A/P, blue = S/I) signal intensity weighted by FA values. Different white matter tracts can be delineated such as the external capsule (arrowhead). Note the radial organization of the cortex (arrow). (IV) ADC map showing a clear radial organization of the cortex (cortical plate and subplate). (A full color version of this illustration can be found in the color section).

## Tensor Visualization

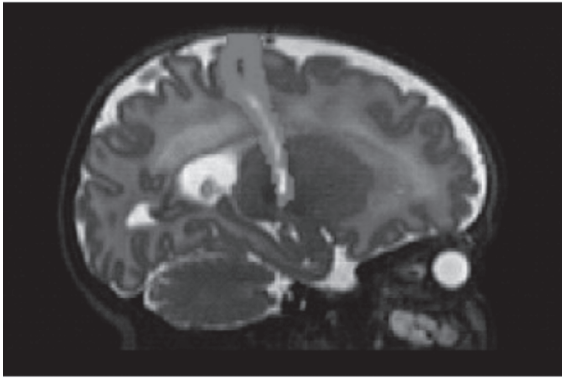
Another approach for visualizing white matter tracts is in 3D, by using white matter tractography<sup>33</sup>. ‘Fiber tracking’ algorithms can be broadly classified into two types: deterministic and probabilistic. Initial research focused mainly on deterministic tractography. The assumption is that the principal eigenvector is parallel to the underlying dominant fiber orientation in each voxel.

This algorithm proceeds from an initially determined point in the direction of the principal eigenvector from voxel to voxel. In deterministic tractography two thresholds are often applied. The first is a minimum value of anisotropy: the tracking is terminated if the tract enters a region below this value. A second threshold is an angular threshold: the maximum angle a path can turn between each step to prevent impossible turns in fiber orientation.



Figures showing an abstract representation of an 8 x 8 grid (left and right). Within the voxels the averaged ellipsoids are shown. Streamline tractography (right) propagates a fiber tract (red lines) in the direction of principal eigenvector, preserving voxel-to-voxel directional information. (A full color version of this illustration can be found in the color section).

There are limitations to the deterministic approach, including: (1) only one reconstructed trajectory per seed point is produced and it will not show branching of white matter tracts, (2) no indication towards the confidence of the reconstructed trajectory is given (3) voxels containing multiple fibers of different orientations have a reduced net anisotropy and the fiber tracking program can terminate the tractography.



Sagittal image of connectivity distributions in the corticospinal tracts in a preterm infant imaged at 42 weeks gestational age obtained using probabilistic tractography. (A full color version of this illustration can be found in the color section).

Probabilistic algorithms work in the same way to the deterministic approach but instead of

reconstructing a single trajectory from a seedpoint, a large number of pathways are propagated from the seedpoint. The direction for each next step is drawn from a distribution of possible orientations<sup>33</sup>. Probabilistic algorithms facilitate the reconstruction of trajectories into and from areas of low anisotropy such as deep matter<sup>34</sup>.

Using probabilistic tractography it is now possible to visualize connections between the thalamus and the cortex in adults and in children<sup>34,35</sup>.

Despite the promising results, there are several limitations of tractography. In the discussion (chapter 10) of this thesis I will elaborate on these limitations of DTI.

## How to interpret DTI measurements?

Interpretation of changes in the measured diffusion tensor should be performed with care. Many studies focus on the diffusion anisotropy (mostly FA), which may not be enough to characterize the tissue changes. For example, white matter neuropathology often causes anisotropy to decrease, which may result from either increased radial (perpendicular) diffusivity and/or reduced axial (parallel) diffusivity<sup>12</sup>. Interpretation is further complicated by other factors including image noise (both thermal and physiologic), artifacts (misregistration of DW images from eddy currents or head motion), partial volume averaging between tissues in large

voxels (signal mixing), and regions of crossing WM tracts. However, despite these limitations, DTI is a sensitive marker of neuropathology. The best example is how in the acute phase of brain ischemia, the mean diffusivity significantly decreases in the lesion. After several days (~5–7), it starts to pseudo-normalize, but chronic ischemic lesions (> 2 weeks) typically demonstrate significantly increased mean diffusivity. Another example is how demyelination seems to cause the radial diffusivity to increase, with minimal influence on the axial diffusivity. The effects of vasogenic edema on DTI measurements are similar to that of inflammation: diffusivity is increased and the anisotropy is decreased. In Chapter 2 of this thesis the use of DWI in the neonatal period is discussed.

With increasing number of reports focusing on the research and clinical application of DTI appearing every year and DTI postprocessing tools continuously being more advanced, exciting times seem to be ahead of us.

## **Aims of the study**

The general aim of this thesis was to use state-of-the-art DTI to help researchers and clinicians answer remaining questions concerning important common term- and preterm brain injuries: white matter- and subplate injury of the preterm and arterial ischemic stroke of the term infant.

This thesis describes the results of 6 original studies and 2 reviews. The studies in chapters 5 and 7 were performed at the Hammersmith Hospital, Imperial College London (United Kingdom). The other studies were performed at the Sophia Children's Hospital, ErasmusMC, Rotterdam (The Netherlands).

The specific aims of the studies presented in this thesis are:

- To review the present literature on the applications of DTI in the neonate,

- 
- To use DTI to evaluate 'normal' brain maturation of white matter tracts,
  - To use DTI to evaluate the 'normal' involution of the subplate,
  - To study the effects of high  $b$  values on DTI images of the neonatal brain,
  - To review the present literature on magnetic resonance imaging of neonatal stroke; focusing on diffusion weighted imaging,
  - To evaluate the evolution of neonatal stroke on diffusion weighted imaging,
  - To evaluate network injury in neonatal stroke, using diffusion weighted imaging.

The studies addressing these aims are described in this thesis. First Chapter 2 presents an overview of the literature on the applications of diffusion tensor imaging in the neonate. Chapter 3 describes the results of a DTI study evaluating the 'normal' maturation of white matter tracts of VLBW infants scanned in the first week of life at different gestational ages. Chapter 4 reports the results of a DTI study on the 'normal' involution' of the subplate of VLBW infants of different gestational ages. In chapter 5 the results are reported of the effect of high  $b$ -values on DTI indices and assessment of brain pathology in the neonatal brain. Chapter 6 reviews the state-of-the-art imaging techniques in neonatal stroke, focussing on diffusion weighted imaging and network lesions. Chapter 7 assesses the evolution of unilateral perinatal arterial ischemic stroke on diffusion weighted and conventional MR imaging. Chapter 8 systematically describes imaging findings of DWI scans of perinatal brain lesions looking for early secondary changes in pulvinar associated with primary cortical or white matter injury. Chapter 9 reports the findings of a study that reveals acute network injury in neonatal stroke using DTI. Chapter 10 gives an overview of the main findings and conclusions of the reviews and original studies of this thesis, and after a general discussion possible future directions are discussed. The thesis is then summarized in Dutch.

## References

1. C.V. Ananth, K.S. Joseph, Y. Oyelese et al. Trends in preterm birth and perinatal mortality among singletons: United States, 1989 through 2000. *Obstet Gynecol* 2005;105:1084-91
2. K. Costeloe, E. Hennessy, A.T. Gibson et al. The EPICure study: outcomes to discharge from hospital for infants born at the threshold of viability. *Pediatrics* 2000;106:659-71
3. R.E. Piecuch, C.H. Leonard, B.A. Cooper et al. Outcome of extremely low birth weight infants (500 to 999 grams) over a 12-year period. *Pediatrics* 1997;100:633-9
4. N.S. Wood, N. Marlow, K. Costeloe. Neurologic and developmental disability after extremely preterm birth. *N Engl J Med* 2000;343:378-84
5. M. Hack, H.G. Taylor, N. Klein et al. Functional limitations and special health care needs of 10- to 14-year-old children weighing less than 750 grams at birth. *Pediatrics* 2000;106:554-60
6. H.G. Taylor, N. Klein, M. Hack et al. School-age consequences of birth weight less than 750 g: a review and update. *Dev Neuropsychol* 2000;17:289-321
7. J.J. Volpe. Brain injury in premature infants: a complex amalgam of destructive and developmental disturbances. *Lancet Neurol* 2009;8:110-24
8. J.K. Lynch. Epidemiology and classification of perinatal stroke. *Semin Fetal Neonatal Med* 2009;14:245-9
9. S.K. Sran, R.J. Baumann. Outcome of neonatal strokes. *Am J Dis Child* 1988;142:1086-8
10. Counsell SJ, Tranter SL, Rutherford MA. Magnetic resonance imaging of brain injury in the high-risk term infant. *Semin Perinatol* 2010;34:67-78
11. D. Le Bihan, E. Breton, D. Lallemand et al. MR imaging of intravoxel incoherent motions: application to diffusion and perfusion in neurologic disorders. *Radiology* 1986;161:401-7
12. A.L. Alexander, J.E. Lee, M. Lazar, A.S. Field. Diffusion Tensor Imaging of the Brain. *Neurotherapeutics* 2007;4(3):316-29
13. H. Johansen-Berg, T.E.J. Behrens (Eds.), *Imaging brain pathways - Diffusion MRI: from quantitative measurement to in-vivo neuroanatomy*. Elsevier, 2009



14. A. Einstein. Investigations on the Theory of the Brownian Movement. Dover Publications, Inc; 1956. p17
15. D. Le Bihan. Molecular diffusion, tissue microdynamics and microstructure. *NMR Biomed* 1995;8:375–86
16. C. Beaulieu, P.S. Allen. Determinants of anisotropic water diffusion in nerves. *Magn Reson Med* 1994;31:394–400
17. McRobbie DW. From picture to proton. New York, NY: Cambridge University Press, 2003
18. E.O. Stejskal, J.E. Tanner. Spin diffusion measurements: spin echoes in the presence of a time-dependent field gradient. *J Chem Phys* 1965;42:288–91
19. P.J. Basser and C. Pierpaoli. Microstructural and physiological features of tissues elucidated by quantitative-diffusion-tensor MRI. *J Magn Reson B* 1996;111:209–19
20. J.J. Neil, S.I. Shiran, R.C. McKinsty, G.L. Schefft, A.Z. Snyder, C.R. Almli, E. Akbudak, J.A. Aronovitz, J.P. Miller, B.C. Lee, T.E. Conturo. Normal brain in human newborns: Apparent diffusion coefficient and diffusion anisotropy measured by using diffusion tensor MR imaging. *Radiology* 1998;209:57-66
21. R.L. Wolf, R.A. Zimmerman, R. Clancy et al. Quantitative apparent diffusion coefficient measurements in term neonates for early detection of hypoxic-ischemic brain injury: Initial experience. *Radiology* 2001;218:825-33
22. P. Ward, S. Counsell, J. Allsop et al. Reduced fractional anisotropy on diffusion tensor magnetic resonance imaging after hypoxic-ischemic encephalopathy. *Pediatrics* 2006;117:619-30
23. A.I Bartha, K.R. Ya, S.P. Miller et al. The normal neonatal brain: MR imaging, diffusion tensor imaging, and 3D MR spectroscopy in healthy term neonates. *AJNR* 2007;28:1015-21
24. M. Rutherford, S. Counsell, J. Allsop et al. Injury: A Comparison With Site of Lesion and Time From Birth Diffusion-Weighted Magnetic Resonance Imaging in Term Perinatal Brain. *Pediatrics* 2004;114;1004-14
25. J.S. Coats, A. Freeberg, E.G. Paiela et al. Meta-analysis of apparent diffusion coefficients in the newborn brain. *Pediatric Neurology* 2009;41(4):263-74
26. V. Engelbrecht, A. Scherer, M. Rassek et al. Diffusion-weighted MR imaging in the brain in children: Findings in the normal brain and in the brain with white matter diseases. *Radiology* 2002;222:410-8

27. C. Van Pul, J. Buijs, M.J. Janssen et al. Selecting the best index for following the temporal evolution of apparent diffusion coefficient and diffusion anisotropy after hypoxic-ischemic white matter injury in neonates. *AJNR* 2005;26:469-81
28. P.J. Basser, J. Mattiello, D. LeBihan. Estimation of the effective self-diffusion tensor from the NMR spin echo. *J Magn Reson B* 1994;103:247-54
29. S.K. Song, S.W. Sun, M.J. Ramsbottom et al. Dysmyelination revealed through MRI as increased radial (but unchanged axial) diffusion of water. *Neuroimage* 2002;17:1429-36
30. S. Pajevic, C. Pierpaoli. Color schemes to represent the orientation of anisotropic tissues from diffusion tensor data: Application to white matter fiber tract mapping in the human brain. *Magn Reson Med* 1999;42:526-40
31. S. Mori, B.J. Crain, V.P. Chacko et al. Three-dimensional tracking of axonal projections in the brain by magnetic resonance imaging. *Ann Neurol* 1999;45:265-9
32. A.S. Field, A.L. Alexander. Diffusion tensor imaging in cerebral tumor diagnosis and therapy. *Top Magn Reson Imaging* 2004;15:315-24
33. D.K. Jones, Studying connections in the living human brain with diffusion MRI, *Cortex* 2008;44:936-52
34. T.E. Behrens, H. Johansen-Berg, M.W. Woolrich et al. Noninvasive mapping of connections between human thalamus and cortex using diffusion imaging. *Nat Neurosci* 2003;6:750-7
35. S.J. Counsell, L.E. Dyet, D.J. Larkman et al. Thalamo-cortical connectivity in children born preterm mapped using probabilistic magnetic resonance tractography. *NeuroImage* 2007;34:896-904







# Chapter 2

## CONNECTING THE DEVELOPING PRETERM BRAIN

---

J. Dudink  
J.L. Kerr  
K. Paterson  
S.J. Counsell

*Early Hum Dev. 2008;84(12):777-82*

## **Abstract**

White matter injury and abnormal maturation are thought to be major contributors to the neurodevelopmental disabilities observed in children and adolescents who were born preterm. Early detection of abnormal white matter maturation is important in the design of preventive, protective, and rehabilitative strategies for the management of the preterm infant.

Diffusion Tensor Imaging (DTI) allows non-invasive, in vivo visualization and quantification of white matter tracts and has become a valuable tool in assessing white matter maturation in children born preterm. We will review the use of DTI to study white matter maturation and injury in the preterm brain.

---

## Introduction

Advances in neonatal intensive care have led to significant improvements in the survival of very premature infants, but have not yet reduced the high incidence of neurodevelopmental disability<sup>1,2</sup>. The most common cerebral neuropathology observed in premature infants is believed to be white matter injury and its effects on the overlying cerebral cortex from sensory deafferentation and/or axotomy<sup>3-5</sup>.

Although postmortem histo- and pathophysiology studies have given insights into cerebral injury in the premature infant, the development of specific preventive, protective, and rehabilitative strategies for preterm brain damage is still restricted by a lack of understanding of white matter injury<sup>5</sup>.

Diffusion tensor imaging (DTI) allows us to study white matter maturation in vivo. DTI is unique in its ability to non-invasively visualize and quantify white-matter tracts in the human brain<sup>6,7</sup>. It is superior to T1-weighted and T2-weighted imaging in detecting unmyelinated or premyelinated fibre tracts and in assessing the microstructural organization of the developing white matter<sup>8</sup>. Quantitative measures derived from DTI provide objective and reproducible assessment of white matter and offer great potential in the study of white matter damage in preterm infants<sup>9,10</sup>.

In this review, we introduce the technical aspects of neonatal DTI. We then discuss changes in DTI parameters associated with brain maturation and injury seen in infants born preterm.

## Technical aspects of neonatal DTI

If diffusion-sensitizing gradients are applied during an MR experiment, the resulting MR image become sensitive to the random (Brownian) motion of water along the direction of the gradient<sup>11</sup>. When motion of water along six or more non-collinear directions is analyzed, a mathematical tensor can be calculated that describes the motion of water in the stud-

ied tissue<sup>7</sup>. This tensor can be conceptualised as an ellipsoid of which the long axis represents the direction with the highest diffusivity; the magnitude of its diffusivity is given by the major eigenvalue ( $\lambda_1$ ) and its direction is called the major eigenvector. Perpendicular to the major eigenvector are the two short axes: the median and minimum eigenvectors, with their eigenvalues  $\lambda_2$  and  $\lambda_3$ <sup>12,13</sup>.

Structures within the brain tissue such as cell membranes, macromolecules, and WM fibres hinder water motion. In cerebral WM water diffuses preferentially along the direction of axons and is restricted perpendicular to axons. This directional dependence is termed anisotropy. The degree of anisotropy of white matter is thought to result from factors such as: number of axons and their parallel orientation, degree of myelination and presence of other cells such as glial cells<sup>14</sup>.

Using DTI, the separate values of  $\lambda_1$ ,  $\lambda_2$ ,  $\lambda_3$  in an imaging voxel can be quantified.

Averaged mean diffusivity ( $D_{av}$ ) then can be calculated as one third of the trace of the diffusion tensor,  $(\lambda_1, \lambda_2, \lambda_3)/3$ , and provides the overall magnitude of water diffusion.  $D_{av}$  is independent of anisotropy.  $D_{av}$  is a useful parameter which can serve as an indicator of brain maturation and/or injury<sup>15,16</sup>. Various anisotropy indexes exist to describe the ratio between the eigenvalues. Although many different kinds of anisotropy indexes exist (see table), there is still some debate which index is most sensitive to detect changes in anisotropy in the neonatal brain<sup>17</sup>. For neonatal brain studies the anisotropy indexes that are mostly used are fractional anisotropy (FA) and relative anisotropy (RA).

Index	Introducing Authors	Equation
FA	Basser and Pierpaoli <sup>6</sup>	$\frac{1}{2} \sqrt{2} \sqrt{\frac{(\lambda_1 - \lambda_2)^2 + (\lambda_2 - \lambda_3)^2 + (\lambda_3 - \lambda_1)^2}{(\lambda_1)^2 + (\lambda_2)^2 + (\lambda_3)^2}}$
RA	Basser and Pierpaoli <sup>6</sup>	$\frac{1}{2} \sqrt{2} \sqrt{\frac{(\lambda_1 - \lambda_2)^2 + (\lambda_2 - \lambda_3)^2 + (\lambda_3 - \lambda_1)^2}{(\lambda_1 + \lambda_2 + \lambda_3)^2}}$



The DTI information can be assessed using various visualization techniques, usually based on anisotropy indexes. Red-green-blue (RGB) colour-coded directionality maps (colour-maps) indicate the orientation of the major eigenvector of the diffusion tensor. In colour maps the major eigenvectors are colour-coded, showing position and direction of white matter tracts (by convention: red for left-right, blue for superior-inferior, and green for anterior-posterior). The brightness in colour maps is weighted by the fractional anisotropy in a given voxel (Figure 1).

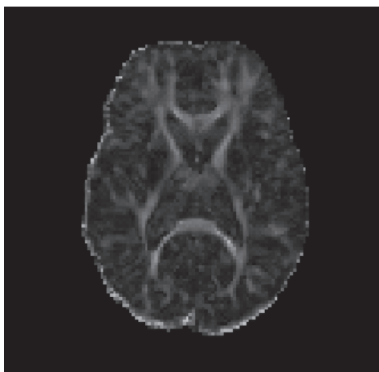


**Figure 1.**

Red-green-blue FA color map. Red represents fibres in the left-right direction, blue represents fibres in the superior-inferior direction and green represents fibres in the anterior-posterior direction. (A full color version of this illustration can be found in the color section).

Fibre tracking algorithms can be broadly classified into two types: deterministic and probabilistic. Initial research focused mainly on deterministic tractography. The assumption is

that the principal eigenvector is parallel to the underlying dominant fibre orientation in each voxel. This algorithm proceeds from an initially determined point in the direction of the principal eigenvector from voxel to voxel. In deterministic tractography two thresholds are often applied. The first is a minimum value of anisotropy: the tracking is terminated if the tract enters a region below this value. Using a minimum FA value, tract reconstruction can avoid entering gray matter and regions of poorly defined principal fibre orientation. A second threshold is an angular threshold: the maximum angle a path can turn between each step to prevent impossible turns in fibre orientation. In the literature there seems to be no consensus on the maximum curvature threshold<sup>18</sup>. When applying these thresholds a lot of factors have to be taken into account including: age at scanning, anatomy, step size and voxel dimensions<sup>18</sup>.

Postmortem histology studies have shown that cerebral white matter is largely composed of different white matter tracts running closely together, making it difficult to define a single ROI on a DTI image that includes

only the fibres of the white matter tract of interest. A solution can be to define an additional ROI, which the reconstructed pathway either has to include or exclude<sup>19</sup>.

There are limitations to the deterministic approach, including: (i) only one reconstructed trajectory per seed point is produced and it will not show branching of white matter tracts, (ii) voxels containing multiple fibres of different orientations have a reduced net anisotropy and fibre tracking can terminate the tractography (iii) no indication towards the confidence that one can assign to a reconstructed trajectory is given.

Probabilistic algorithms work in the same way but instead of reconstructing a single trajectory from a seedpoint, a large number of pathways are propagated from the seedpoint. The direction for each next step is drawn from a distribution of possible orientations<sup>18</sup> (Figure 2).

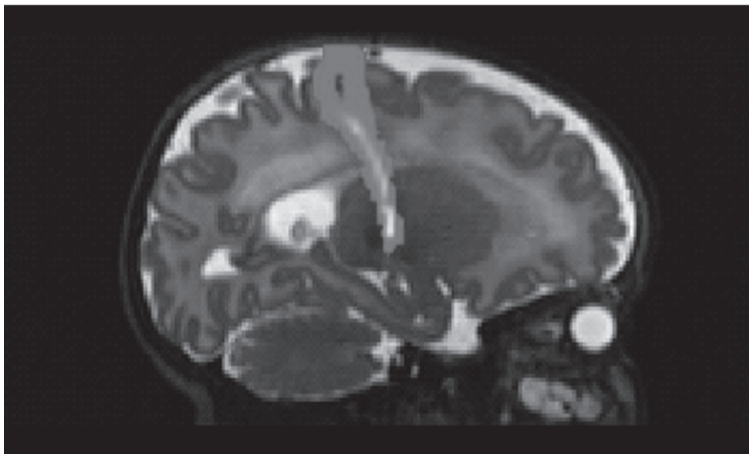


**Figure 2.**

Sagittal image of connectivity distributions in the corticospinal tracts in a pre-term infant imaged at 42 weeks gestational age obtained using probabilistic tractography. (A full color version of this illustration can be found in the color section).

Probabilistic algorithms are less dependent upon well defined principal eigenvectors, and typically do not have an anisotropy threshold as a termination criteria, but the only stopping criterion is the angular deviation between successive steps. This facilitates the reconstruction of trajec-

tories into and from areas of low anisotropy such as the gray matter<sup>20,21</sup>. There are various probabilistic algorithms available; the main difference between them is the mechanism by which a sample is drawn from the inherent distribution of fibre orientations. The result is a map quantifies the confidence that a pathway can be found, between each voxel and the seedpoint<sup>18</sup>.

Using probabilistic tractography it is now possible visualize and quantify connections between the thalamus and the cortex in adults and in children<sup>20,22</sup>. Volumes of thalamo-cortical projections in a two year old ex preterm were reduced on the side ipsilateral brain injury<sup>22</sup> (Figure 3).

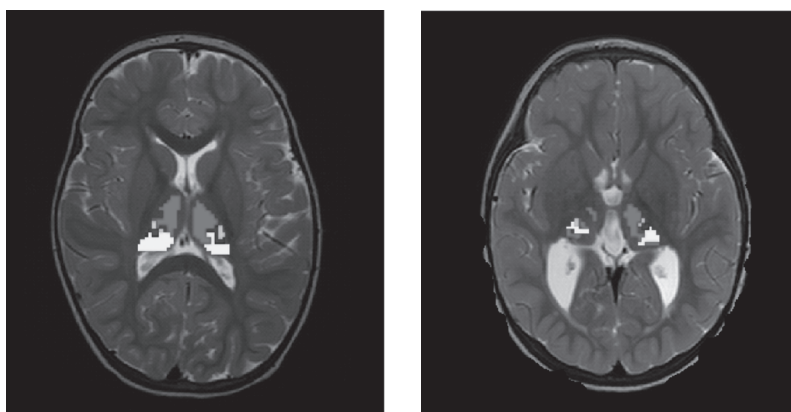


**Figure 3.**

Thalamo-cortical projections displayed on the infants native T2 weighted image in (a) infant with normal imaging and (b) infant with porencephalic cyst (key: red = connections from frontal/temporal cortex, y = connections from parietal/occipital cortex, green = connections from motor cortex and blue = connections from somato-sensory cortex). Reprinted from SJ Counsell, LE Dyet, DJ Larkman, RG Nunes, JP Boardman, JM Allsop, JA Fitzpatrick, L Srinivasan, FM Cowan, JV Hajnal, MA Rutherford, AD Edwards. Thalamo-cortical connectivity in children born preterm mapped using probabilistic magnetic resonance tractography. *NeuroImage* 2007; 34: 896-904 with permission from Elsevier. (A full color version of this illustration can be found in the color section).

The ability to visualize and quantify connections between thalamus and cortex offers the possibility of studying normal development and aberrant neural connectivity in infants and may improve our understanding of the aetiology of the cognitive deficits associated with preterm birth.

To measure diffusion values in different areas in the brain ‘regions of interest’ (ROIs) can be placed directly onto diffusion tensor images, however the global changes occurring in the developing neonatal brain cannot be fully captured by ROI analysis. Also, studies using ROI are subjective, and require a priori definitions of the spatial locations of different brain structures, which is difficult when comparing many brain regions or large subject groups. Automated whole-brain measurement techniques for analyzing MRI data can overcome these problems and are being increasingly used. A common technique is voxel-based morphometry. VBM uses image registration to bring brain images from different subjects into a common coordinate system for analysis<sup>23</sup>.

A limitation of VBM however, is to determine whether apparent differences highlighted using VBM are due to differences in brain regions or to local misalignment. Tract-based spatial statistics overcomes some of the limitations of both ROI and VBM approaches to analyze neonatal data. TBSS aligns diffusion tensor FA data from different subjects via a nonlinear registration algorithm. The mean FA image is then created and thinned to create a mean FA skeleton, which represents the centres of all tracts common to the group. Each subject's aligned FA data is then projected onto this skeleton prior to applying voxelwise statistics<sup>24</sup>. The method therefore represents an observer-independent method of analyzing neonatal DTI data without requiring spatial smoothing and can offer new insights into the development of the preterm brain.

In a recent study using TBSS Anjari et al demonstrated significantly lower FA in the centrum semiovale, frontal white matter and genu of the corpus callosum in a group of preterm infants at term equivalent age compared to age and sex-matched term-born controls, with the most immature infants displaying additional and more extensive reductions in FA<sup>25</sup> (Figure 4). In addition, using a combination of TBSS and probabilistic diffusion tractography to assess the association between structure and function in the visual system in preterm infants at term equivalent age, FA in the optic radiations was found to be correlated with contemporaneous visual assessment score<sup>26</sup> (Figure 5).

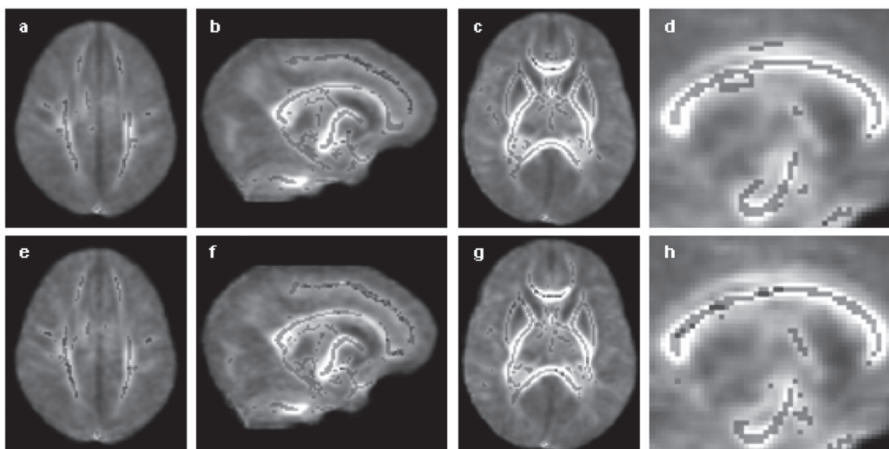


**Figure 4.**

The effect of preterm birth on FA at term equivalent age. Mean FA skeleton overlaid on the mean FA map. Regions of the mean FA skeleton in green represent areas where there were no significant differences in FA values in the preterm infants imaged at term compared to the term-born controls. Areas in blue are regions where the FA was significantly lower in the preterm group (a–d), and can be observed in the centrum semiovale (a), frontal white matter (b) and genu of the corpus callosum (c). Those infants born  $\leq 28$  weeks gestational age (e–h) had greater regions of reduced anisotropy within the centrum semiovale (e), frontal white matter (f) and genu of the corpus callosum (g), and displayed additional reductions in FA in the posterior aspect of the posterior limb of the internal capsule (g) and the external capsule (g). Reprinted from: M Anjari, L Srinivasan, JM Allsop, JV Hajnal, MA Rutherford, AD Edwards, SJ Counsell. Diffusion tensor imaging with tract-based spatial statistics reveals local white matter abnormalities in preterm infants. *NeuroImage* 2007;35: 1021-7 with permission from Elsevier. (A full color version of this illustration can be found in the color section).

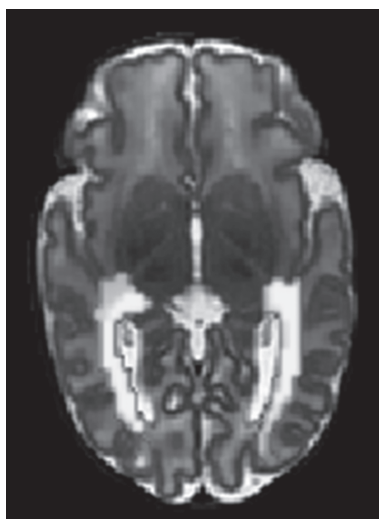


**Figure 5.**

Probabilistic tractography of the optic radiations in an infant who was born at 26 weeks gestational age and imaged at 40 weeks post-menstrual age shown on the infant's native T2 weighted image. Reprinted from: L Bassi, D Ricci, A Volzone, JM Allsop, L Srinivasan, A Pai, C Ribes, LA Ramenghi, E Mercuri, F Mosca, AD Edwards, FM Cowan, MA Rutherford, SJ Counsell. Probabilistic Diffusion Tractography of the Optic Radiations and Visual Function in Preterm Infants at Term Equivalent Age. *Brain* 2008; 131: 573-582. by permission of Oxford University Press. (A full color version of this illustration can be found in the color section).

There are many technical factors that affect image quality in diffusion imaging which include: the acquisition sequence, magnet field strength, and gradient amplitude and b-value used. We have not discussed these considerations here but recommend a recent article by Mukherjee et al in which the major technical factors that affect image quality in diffusion MR imaging are evaluated in detail<sup>27</sup>.

## **WM maturation in the preterm brain**

Changes in DTI parameters during early development provide unique in vivo insight into the structural basis of WM maturation. WM average apparent diffusion coefficient (Dav) values differ between the premature and term brain. Dav values decrease with increasing age during development until they reach adult values. This is reflected by a 30–50% higher ADC in neonates than in adults<sup>9,15,28,29</sup>. In early development, changes in Dav take place more rapidly and are not simultaneous in all brain regions. Also Dav maps of the preterm brain show contrast between white and gray matter (Dav values for white matter are higher than those for gray)<sup>28</sup>. These findings of contrast between white and gray matter Dav maps of the preterm brain despite their similar water content is consistent with the idea that white matter is less restrictive to overall water motion than gray matter.

Brain water content decreases dramatically with increasing gestational age and it can explain the rapid decrease of Dav values observed between early gestation and term age. Also increasing complexity of white matter structures with increasing myelination constrict water motion and contribute to the decrease in Dav values. This is reflected by a 40–60% lower anisotropy in neonates than in adults<sup>9,15,28,29</sup>. Measurements of the three separate eigenvalues ( $\lambda_1$ ,  $\lambda_2$ ,  $\lambda_3$ ) confirm this notion. During white matter development decreases in diffusion are observed principally in  $\lambda_2$ ,  $\lambda_3$  (and not in  $\lambda_1$ ), which reflect changes in water diffusion perpendicular to white matter fibres<sup>30</sup>. This decrease in radial (lambda horizontal) diffusivity indicates changes due to premyelination and myelination.

WM anisotropy indices values also differ between preterm and term brain. For children beyond term and for adults, FA and RA values for cortical gray matter are consistent with zero, meaning that water diffusion in gray matter is essentially isotropic at the resolution achievable in vivo. FA and RA values for white matter areas, on the other hand, are relatively low in infants and increase steadily with increasing age<sup>15,30-32</sup>.

The increase in anisotropy values of white matter during development appears to take place in two phases: (i) showing an increase before the histological appearance of myelin, attributed to changes in white matter structure which accompany the 'premyelinating state'<sup>8</sup>. The 'premyelinating state' is characterized by a number of histological changes: axon calibre changes, increasing numbers of axonal microtubule-associated proteins and number of oligodendrocytes, together with an increase in axonal conduction velocity and changes in Na/K-ATPase activity<sup>8</sup>. The increase in anisotropy associated with premyelination takes place before the histological appearance of myelin and in the absence T1- or T2-weighted imaging changes (ii) a second increase in anisotropy values is associated with the histological appearance of myelin and its maturation<sup>14</sup>. However, it is important to note that myelin accounts for only about 20% of anisotropy in white matter. Other factors playing a role in anisotropy are: axon packing, internal axonal structure, membrane permeability to water and tissue water content<sup>14</sup>. As an example the commissural fibres in the splenium and the genu of corpus callosum show the highest anisotropy values in the preterm human brain even although these fibres are largely unmyelinated in the newborn period<sup>32</sup>. Their high anisotropy is in part due to a high degree of parallel organization.

When studying early human WM maturation using DTI one has to take into account that WM of the preterm infant has a high vulnerability to inflammatory mechanisms and oxidative processes and a high injury risk during the postnatal preterm period<sup>5</sup>. Also developing preterm brains are exposed to different stimuli in the NICU compared to the environment of the uterus. Growing evidence shows that this will effect the WM maturation<sup>25,33</sup>. Solution to this would be to study normal WM maturation in the foetal brain<sup>34,35</sup>. Foetal motion is a major problem for in utero diffusion

tensor imaging. However, new methodologies to achieve 3D high resolution in utero foetal brain DTI show promising results<sup>36</sup>.

## **Preterm WM injury assessed with DTI**

In addition to providing information on WM maturation, DTI can be used to assess brain injury. Changes in diffusion characteristics can provide early evidence of both focal and diffuse brain injuries associated with preterm birth.

Over the past decades advances in neonatal intensive care have resulted in improved survival rates of preterm infants<sup>37,38</sup>. However, long-term neurological deficits amongst the survivors are increasingly recognized. Literature reports an incidence of spastic motor deficits in 10% of preterm survivors and up to 50% ex-preterms show learning difficulties or have behavioural problems in adolescence<sup>1,2,39</sup>.

Several forms of brain injury are observed in premature infants including: intraventricular hemorrhage (IVH), periventricular haemorrhagic infarction (PVHI), and periventricular white matter injury (PWMI). PWMI includes a spectrum of cerebral injury ranging from focal to general WM lesions (e.g. punctate WM lesions, diffuse excessive high signal intensity (DHESI) and cystic periventricular leucomalacia (PVL))<sup>40</sup>. Whereas the incidence of IVH and cystic PVL has decreased with advanced medical treatment strategies, the incidence of PWMI seems to be stable<sup>41</sup>. PWMI is now considered the most common cause of brain injury in preterm infants and the leading cause of chronic neurologic morbidity<sup>42</sup>. Factors implicated in the pathogenesis of PWMI during prematurity include hypoxia, ischemia, and chronic exposure to infection and inflammation<sup>42</sup>. DTI allows recognizing injury in specific WM tracts in children and has become a useful tool to assess WM damage.

DWI/DTI can be extremely useful for highlighting regions of acute white matter injury (Figure 6). However, the quantitative measures obtained from DWI/DTI can provide further insight into the nature of white mat-



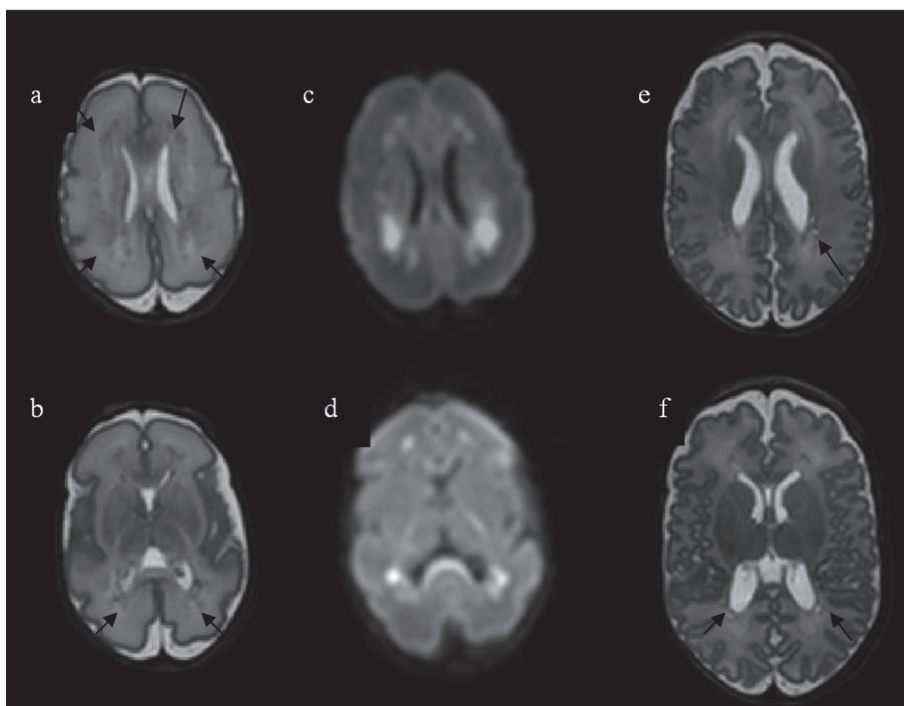


**Figure 6.**

Preterm infant born at 29 weeks GA and imaged at 30 weeks (a-d) and 40 weeks (e and f) post-menstrual age. T2 weighted image at the mid-ventricular level (a) and basal ganglia level (b) demonstrating multiple abnormalities in the white matter (arrows). DT image at the mid-ventricular level (c) and basal ganglia level (d) showing these regions as high signal intensity. Cystic lesions have developed at term equivalent age (e and f).

ter injury/ mal-development. Miller et al. reported a significant increase in ADC values with increasing GA in the frontal white matter and visual association areas in infants with moderate white matter injury<sup>43</sup>. In addition, the normal maturational increase in RA was absent in a number of white matter regions in infants with moderate white matter injury and in the frontal region in infants with only minimal white matter injury<sup>43</sup>.

Diffuse excessive high signal intensity (DEHSI) on T2 weighted imaging is a common finding in preterm infants at term-equivalent age but the neuropathologic correlates of DEHSI are unknown<sup>44</sup>. DWI has showed that infants with DEHSI have WM ADC values similar to preterm infants

with major focal lesions, suggesting DEHSI to be a diffuse WM abnormality, consistent with widespread axonal and oligodendrocyte abnormalities<sup>45,46</sup>.

Huppi et al compared quantitative measures of diffusion at term among premature infants with perinatal WM injury (including PVL) with infants without WM injury. They found a lower RA in the central WM area, but also in the underlying posterior limb of the internal capsule<sup>47</sup>. The lower RA in the cerebral WM site of injury (central WM) suggested a destruction of central fibre tracts or an impaired subsequent development or both.

A number of DTI studies have investigated the effect of PVL on brain development in later childhood to adulthood using anisotropy indices and scoring systems based on a visual assessment colour-coded maps<sup>48-51</sup>. These studies have shown that although injury to the corticospinal tracts is thought to be the major determinant of motor impairment in children with PVL, sensory pathways (including the posterior thalamic radiation) may be playing an even more important role<sup>48</sup>. These studies are indicative of the complexity of white matter involvement in PVL<sup>46,50,51</sup>.

Tractography studies have shown involvement of the sensory and motor pathways, corpus callosum, posterior limb of the internal capsule and superior longitudinal fasciculus and disrupted connections between the thalamus and the cortex (Figure 3) in children and adolescents with PVL and HPI<sup>22,48-50,51</sup>. Nagae et al showed that in patients with PVL (scanned at a mean age of 6 years) both the retrolenticular part of the internal capsule and the posterior thalamic radiation (which include thalamocortical and corticothalamic white matter tracts) were affected the most<sup>51</sup>.

## Summary

Improved understanding of early white matter damage in preterm infants is essential if more effective preventive, protective, and rehabilitative strategies are to be developed. DTI has been shown to provide non-

invasive and quantitative means for evaluating preterm brain maturation and injury in vivo. DTI allows us to study brain connectivity and plasticity and has contributed to our understanding of preterm WM maturation, WM injury and plasticity. Recent advances in the DTI postprocessing such as probabilistic tractography and TBSS have given new insights in subtle abnormalities of cerebral white matter associated with preterm birth which are thought to be responsible for neurobehavioral sequelae. DTI research offers great potential to gain new insights and bring us a step further in reducing WM damage of the preterm infant.

## References

1. A.T. Bhutta, M.A. Cleves, P.H. Casey et al. Cognitive and behavioral outcomes of school-aged children who were born preterm: a meta-analysis. *JAMA* 2002;288:728-37
2. N. Marlow, E.M. Hennessy, M.A. Bracewell et al; EPICure Study Group. Motor and executive function at 6 years of age after extremely preterm birth. *Pediatrics* 2007;120:793-804
3. M. Marin-Padilla. Developmental neuropathology and impact of perinatal brain damage: III. Grey matter lesions of the neocortex. *J Neuropathol Exp Neurol* 1999;58:407-29
4. S.A. Back, S.A. Rivkees. Emerging Concepts in Periventricular White Matter Injury. *Semin Perinatol* 2004;28:405-14
5. S. Rees, T. Inder. Fetal and neonatal origins of altered brain development. *Early Hum Develop* 2005;81:753-61
6. P.J. Basser, C. Pierpaoli. Microstructural and physiological features of tissues elucidated by quantitative-diffusion-tensor MRI. *J Magn Reson B* 1996;111:209-19
7. P.J. Basser, J. Mattiello, D. Le Bihan. Estimation of the effective self-diffusion tensor from the NMR spin echo. *J Magn Reson B* 1994;103:247-54
8. D.M. Wimberger, Roberts TP, Barkovich AJ, Prayer LM, Moseley ME, Kucharczyk J. Identification of "premyelination" by diffusion-weighted MRI. *J Comput Assist Tomogr* 1995;19:28-33

9. J. Neil, J. Miller, P. Mukherjee et al. Diffusion tensor imaging of normal and injured developing human brain – a technical review. *NMR Biomed* 2002;15:543–52
10. P.S. Huppi, J. Dubois. Diffusion tensor imaging of brain development. *Semin Fetal Neonatal Med* 2006;11:489-97
11. E.O. Stejskal, J.E. Tanner. Spin diffusion measurements: spin-echoes in the presence of a time-dependent field gradient. *J Chem Phys* 1965;42:288-92
12. D. LeBihan, J.F. Mangin, C. Poupon et al. Diffusion Tensor Imaging: Concepts and Applications. *J Magn Reson Imag* 2001;13:534-46
13. S. Mori, J. Zhang. Principles of diffusion tensor imaging and its applications to basic neuroscience research. *Neuron* 2006;51:527-39
14. C. Beaulieu. The basis of anisotropic water diffusion in the nervous system: a technical review. *NMR Biomed* 2002;15:435–55
15. P.S. Huppi, S.E. Maier, S. Peled et al. Microstructural development of human newborn cerebral white matter assessed in vivo by diffusion tensor magnetic resonance imaging. *Pediatr Res* 1998;44:584-90
16. R.C. McKinstry, J.H. Miller, A.Z. Snyder et al. A Prospective, longitudinal diffusion tensor imaging study of brain injury in newborns. *Neurology* 2002;59:824–33
17. C. Van Pul, J. Buijs, M.J.A. Janssen et al. Selecting the best index for following the temporal evolution of apparent diffusion coefficient and diffusion anisotropy after hypoxic-ischemic white matter injury in neonates. *AJNR Am J Neuroradiol* 2005;26:469–81
18. D.K. Jones. Studying connections in the living human brain with diffusion MRI. *Cortex* 2008;44:936-52
19. T.E. Conturo, N.F. Lori, T.S. Cull et al. Tracking neuronal fibre pathways in the living human brain. *Proceedings of the National Academy of Sciences United States of America* 1999;96:10422–7
20. T.E. Behrens, H. Johansen-Berg, M.W. Woolrich et al. Noninvasive mapping of connections between human thalamus and cortex using diffusion imaging. *Nat Neurosci* 2003;6:750–7
21. T.E. Behrens, H. Johansen-Berg, S. Jbabdi et al. Probabilistic diffusion tractography with multiple fibre orientations: what can we gain? *NeuroImage* 2007; 34:144–55

- 
22. S.J. Counsell, L.E. Dyet, D.J. Larkman et al. Thalamo-cortical connectivity in children born preterm mapped using probabilistic magnetic resonance tractography. *NeuroImage* 2007;34:896–904
  23. J. Ashburner, K.J. Friston. Why voxel-based morphometry should be used. *NeuroImage* 2001;14:1238-43
  24. S.M. Smith, M. Jenkinson, H. Johansen-Berg et al. Tract-based spatial statistics: voxelwise analysis of multi-subject diffusion data. *NeuroImage* 2006;31:1487–505
  25. M. Anjari, L. Srinivasan, J.M. et al. Diffusion tensor imaging with tract-based spatial statistics reveals local white matter abnormalities in preterm infants. *NeuroImage* 2007;35:1021-7
  26. L. Bassi, D. Ricci, A. Volzone, J.M. Allsop et al. Probabilistic diffusion tensor tractography of the optic radiations and visual function in preterm infants at term equivalent age. *Brain* 2008;131:573-82
  27. P. Mukherjee, S.W. Chung, J.I. Berman et al. Diffusion tensor MR imaging and fibre tractography: technical considerations. *AJNR Am J Neuroradiol* 2008;29:843-52
  28. J.J. Neil, S.I. Shiran, R.C. McKinstry et al. Normal brain in human newborns: apparent diffusion coefficient and diffusion anisotropy measured by using diffusion tensor MR imaging. *Radiology* 1998;209:57–66
  29. C. Lebel, L. Walker, A. Leemans et al. Microstructural maturation of the human brain from childhood to adulthood. *NeuroImage* 2008;40:1044-55
  30. S.C. Partridge, P. Mukherjee, J.I. Berman et al. Tractography based quantitation of diffusion tensor imaging parameters in white matter tracts of preterm newborns. *J Magn Reson Imaging* 2005;22:467–74
  31. J.I. Berman, P. Mukherjee, S.C. Partridge et al. Quantitative diffusion tensor MRI fibre tractography of sensorimotor white matter development in premature infants. *Neuroimage* 2005;27:862-71
  32. J. Dudink, M. Lequin, C. VanPul et al. Fractional anisotropy in white matter tracts of very-low-birth-weight infants. *Pediatr Radiol* 2007;37:1216-23
  33. M. Gimenez, M.J. Miranda, A.P. Born et al. Accelerated cerebral white matter development in preterm infants: a voxel based morphometry study with diffusion tensor MR imaging. *NeuroImage* 2008;41:728-34
  34. T. Bui, J.L. Daire, F. Chalard et al. Microstructural development of human brain assessed in utero by diffusion tensor imaging. *Pediatr Radiol* 2006;36:1133-40

35. G. Kasprian, P.C. Brugger PC, M. Weber et al. In utero tractography of fetal white matter development. *NeuroImage* 2008;43:213-24
36. S. Jiang, H. Xue, S.J. Counsell et al. In-utero three dimension high resolution fetal brain diffusion tensor imaging. *Med Image Comput Comput Assist Interv Int Conf Med Image Comput Comput Assist Interv* 2007;10:18-26
37. K. Costeloe, E. Hennessy, A.T. Gibson et al. The EPICure study: outcomes to discharge from hospital for infants born at the threshold of viability. *Pediatrics* 2000;106:659–71
38. D.J. Field, J.S. Dorling, B.N. Manktelow, E.S. Draper. Survival of extremely born premature babies in an geographically defined population: prospective cohort study of 1994-9 compared with 2000-5. *BMJ* 2008;336:1199-200
39. M. Hack, A.A. Fanaroff. Outcomes of children of extremely lowbirthweight and gestational age in the 1990s. *Semin Neonatol* 2000;5:89–106
40. S.A. Back, A. Riddle, M.M. McClure. Maturation-dependent vulnerability of perinatal white matter in premature birth. *Stroke* 2007;38:724-30
41. S. Hamrick, S.P. Miller, C. Leonard et al. Trends in severe brain injury and neurodevelopmental outcome in premature newborn infants: the role of cystic periventricular leukomalacia. *J Pediatr* 2004;145:593-9
42. O. Khwaja, J.J. Pathogenesis of cerebral white matter injury of prematurity. *Arch Dis Fetal Neonatal Ed* 1008;93:153-61
43. S.P. Miller, D.B. Vigneron, R.G. Henry et al. Serial quantitative diffusion tensor MRI of the premature brain: development in newborns with and without injury. *J Magn Reson Imaging* 2002;16:621-32
44. E.F. Maalouf, P.J. Duggan, M.A. Rutherford et al. Magnetic resonance imaging of the brain in a cohort of extremely preterm infants. *J Pediatr* 1999;135:351-7
45. S.J. Counsell, J.M. Allsop, M.C. Harrison et al. Diffusion-weighted imaging of the brain in preterm infants with focal and diffuse white matter abnormality. *Pediatrics* 2003;112:1-7
46. S.J. Counsell, Y. Shen, J.P. Broadman et al. Axial and radial diffusivity in preterm infants who have diffuse white matter changes on magnetic resonance imaging at term-equivalent age. *Pediatrics* 2006;117:376-86

- 
47. P.S. Huppi, B. Murphy, S.E. Maier et al. Microstructural brain development after perinatal cerebral white matter injury assessed by diffusion tensor magnetic resonance imaging. *Pediatrics* 2001;107:455-60
  48. A.H. Hoon, W.T. Lawrie, E.R. Melhem et al. Diffusion tensor imaging of periventricular leukomalacia shows affected sensory cortex white matter pathways. *Neurology* 2002;59:752-6
  49. B. Thomas, M. Eyssen, R. Peeters R et al. Quantitative diffusion tensor imaging in cerebral palsy due to periventricular white matter injury. *Brain* 2005;28:2562-77
  50. G.G. Fan, B. Yu, S.M. Quan et al. Potential of diffusion tensor MRI in the assesment of periventricular leukomalacia. *Clinical Radiology* 2006;61:358-4
  51. L.M. Nagae, A.H. Hoon, E. Stashinko et al. Diffusion tensor imaging in children with periventricular leukomalacia: variability of injuries to white matter tracts. *AJNR Am J Neuroradiol* 2007;28:1213-22
  52. M. Staudt, C. Braun, C. Gerloff, M. Erb, W. Grodd, I. Krageloh-Mann. Developing somatosensory projections bypass periventricular brain lesions. *Neurology* 2006;67:522-5







## Chapter 3

### FRACTIONAL ANISOTROPY OF WHITE MATTER TRACTS IN VERY-LOW-BIRTH-WEIGHT INFANTS

---

J. Dudink  
M.H. Lequin  
C. van Pul  
J. Buijs  
N. Conneman  
J.B. van Goudoever  
P.P. Govaert

*Pediatr Radiol.* 2007;37(12):1216-23

## **Abstract**

### ***Background and purpose***

Advances in neonatal intensive care have not yet reduced the high incidence of neurodevelopmental disability among very low birth weight (VLBW) infants. As neurological deficits are related to white matter injury, early detection is important. Diffusion tensor imaging (DTI) could be an excellent tool for assessment of white matter injury. Our purpose was to provide DTI fractional anisotropy (FA) reference values for white matter tracts of VLBW infants for clinical use.

### ***Materials and methods***

We retrospectively analyzed DTI images of 28 VLBW infants (26-32 weeks gestational age) without evidence of white matter abnormalities on conventional MRI sequences, and normal developmental outcome (assessed at age 1-3 years). For DTI an echoplanar sequence with diffusion gradient ( $b=1000$  s/mm<sup>2</sup>) applied in 25 non-collinear directions was used. We measured FA and apparent diffusion coefficient (ADC) of different white matter tracts within 4 days of life.

### ***Results***

Our quantitative investigation characterized the age related trends in fractional anisotropy in pyramidal tracts (right PLIC:  $r=0.530$ ,  $p<0.01$ , left PLIC:  $r=0.405$ ,  $p<0.05$ ).

### ***Conclusion***

Normative data are provided for white matter tracts in preterm infants. Fractional anisotropy of the pyramidal tracts, measured in the first few days after birth, is related to gestational age.

---

## Introduction

The last decade has seen improved survival for very low birth weight (VLBW) preterm infants<sup>1,2</sup>. The survivors, however, still show high incidence of neurodevelopmental disability, despite advances in foetal and neonatal intensive care<sup>3-5</sup>. These neurological deficits are usually related to white matter injury<sup>6,7</sup>. So early detection of abnormal white matter maturation will be important in the design of preventive, protective, and rehabilitative strategies for the management of the critically ill newborn<sup>8,9</sup>.

The clinical evaluation of these infants may not provide either adequate diagnostic or prognostic information on white matter injury. Various neuroimaging techniques have become available, however, that may be of help. Cranial ultrasound is such a technique used in premature infants but is not as sensitive as MR imaging, which shows better soft tissue contrast<sup>10</sup>. Yet, conventional T1- and T2-weighted MR imaging sequences also have limited value in the evaluation of the preterm brain, as they do not allow visualization of specific white matter tracts before the onset of myelination. Most white matter tracts of the premature cerebrum are unmyelinated, except for a few pathways – e.g. the pyramidal tract – that mature early, as the infant approaches term-equivalent age<sup>11,12</sup>.

Diffusion tensor imaging (DTI) is unique in its ability to visualize and quantify white matter tracts in the human brain. It is superior to T1 and T2-weighted imaging in detecting unmyelinated or pre-myelinated fiber tracts and therefore likewise in assessing the microstructural organization of the developing white matter<sup>13</sup>. DTI anisotropy measurements offer great potential in the study of white matter damage in VLBW infants. So far, however, the clinical use of this technique is restrained by the lack of normal reference values for VLBW infants.

Four groups have described reference values for white matter DTI parameters at different gestational ages (Table 1). Nevertheless, the populations studied each included no more than four infants without white matter damage on conventional imaging, scanned within days after birth and gestational age less than 32 weeks<sup>14-17</sup>. And then, as sizes and shapes of the regions of interests (ROIs) in these studies differ, compari-

son between the studies is difficult. We therefore set up a retrospective study aimed at providing reference values for the clinical interpretation of DTI images in VLBW infants.

**Table 1**  
Overview of relevant literature

Reference	Gestational age (weeks)	Scan week	No. of patients	No. with gestational age <32 weeks	MR field strenght (T)	ROI
[14]	<37w	28-43	27	<5	1.5	FT <sup>a</sup>
[15]	24-36	28-39	17	<5	1.5	Manual
[16]	24-36	28-39	14	<5	1.5	Manual
[17]	26-30	28-40	6	<5	1.5	Manual

<sup>a</sup>ROI placement with fiber tracking

## Material and Methods

### Subjects

The Erasmus MC Ethical Review Board approved the study, and written informed parental consent was obtained for each subject. The images used in this study had been obtained within the framework of a study in which premature infants of different gestational age underwent serial conventional and DTI acquisitions to evaluate white matter development. The inclusion criteria for our study were birth at gestational age of 25 to 32 weeks, no evidence of white matter injury on conventional MR and scanned within four days of life. Besides, developmental outcome assessed at age 1-3 years needed to be normal. Gestational age was calculated from the mother's last menstrual period or estimated from early ultrasound (<18 weeks of pregnancy). Exclusion criteria were intraventricular hemorrhage, ventriculomegaly, congenital infection, brain malformation or a multiple congenital anomaly syndrome. Furthermore, preterm infants whose images were severely motion degraded were excluded since evaluation of these scans was not possible. During the 25 months of the study period (between March 2004 and April 2006), 41 infants were scanned and 32 met our study criteria. Four MR exams were excluded due to severe motion artefacts, so 28 patients were included.

---

### ***Neurodevelopment monitoring***

The infants' hospital charts were reviewed for neurodevelopmental outcome. They had all been neurologically assessed at 3, 6, 12 and 24 months, and Denver scores were used to monitor neurodevelopment<sup>18</sup>. At 24 months the Bayley Scales of Infant Development second edition (BSID-II) had been administered as well<sup>19</sup>. All patients had shown normal neurodevelopment according to the most recent examination.

### ***Conventional MR imaging***

Images had been acquired using standard scanning protocols. All imaging was performed on a 1,5 Tesla GE EchoSpeed scanner (GE Medical Systems, Milwaukee, WI). The imaging protocol included a T1-weighted (spin echo, TR/TE = 500/11ms) and a T2-weighted sequence (spin echo with TR/TE = 3000/120ms) with a slice thickness of 4 mm and a 0.4 mm gap. For DTI an echoplanar sequence with diffusion gradients ( $b=1000$  s/mm<sup>2</sup>) applied in 25 non-collinear directions was used with a slice thickness of 3 mm with no gap. An average of 20 slices was recorded within 4 minutes using TR/TE = 9150/98-91 ms. The FOV was 20 cm, the scan matrix 128 x 128 and the reconstruction matrix 256x256.

All patients were scanned using a MR-compatible incubator with a specialized high-sensitivity neonatal head coil (LMT), which allowed DTI imaging at high spatial resolution and high SNR. The incubator provided for controlled temperature and humidity, as well as MR compatible pulse oximetry and ventilator. This set-up allowed for imaging in this most vulnerable patient population in a stable and safe microenvironment<sup>20-22</sup>. We used mouldable earplugs and neonatal earmuffs to reduce the noise. No sedation was given. Pads around the infant's head kept movement to a minimum.

### ***Diffusion tensor post-processing***

Diffusion tensor images were transferred to a GE Advantage Windows workstation (General Electric Medical Systems, Milwaukee, WI) for post processing using Functool 2000 software (General Electrics). DTI measures the diffusion of water in each voxel and the extent to which water

diffuses in particular directions as a result of the micro structural characteristics of the tissue imaged. High anisotropy indicates that the magnitude of diffusion is very unequal in different directions. The complex nature of anisotropic diffusion in the brain has been described by a diffusion tensor, which contains information about the magnitude of diffusion in different directions. Each tensor contains a set of three eigenvalues, which are related to the major, intermediate, and minor axes of a diffusion ellipsoid. The principal eigenvector (1) specifies the direction in which water diffusion is greatest. Fractional anisotropy (FA) measures the fraction of the magnitude of the diffusion tensor that can be ascribed

to anisotropic diffusion<sup>23-25</sup>. For isotropic diffusion ( $\lambda_1 = \lambda_2 = \lambda_3$ ), FA is zero, and in the case where there is a strongly preferred direction of diffusion ( $\lambda_1 \gg \lambda_2 = \lambda_3$ ), FA approaches one.

The tracts selected for quantization in the study included commissural tracts (corpus callosum: splenium and genu), projection tracts ((posterior limb of the internal capsule (PLIC), anterior limb of the internal capsule (ALIC)) and optic radiation (OR)) and association tracts (external capsule (EC)).

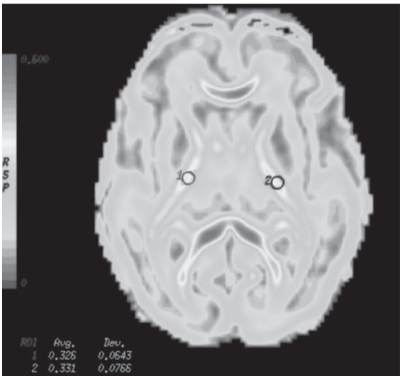
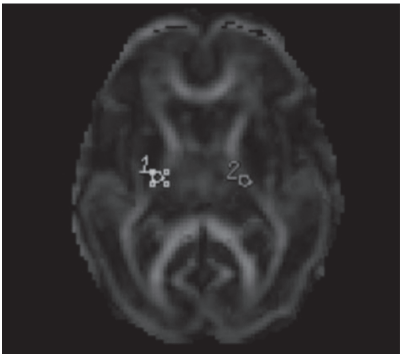


**Figure 1**  
Example of a fractional anisotropy map (gestational age 30 weeks) on which the ROIs were placed. (A full color version of this illustration can be found in the color section).



**Regions of interest**

DTI measurements were taken from multiple ROIs positioned bilaterally within individual white matter tracts.

**Figure 2**  
We performed fiber tracking in each of the ROIs to confirm the right location (example showing the corticospinal tracts (gestational age 28 weeks). (A full color version of this illustration can be found in the color section).



**Figure 3**  
We confirmed ROI placement on the color-maps (example showing the colormaps of a patient with gestational age of 30 weeks). (A full color version of this illustration can be found in the color section).

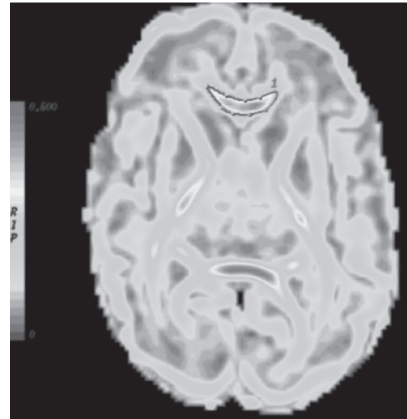


**Figure 4**  
Delineating the Corpus Callosum with a free hand ROI placement on a FA map. (A full color version of this illustration can be found in the color section).

For the placement we used standard size, round shaped 16 pixels ROIs. ROI placement was done on the FA maps and was validated against corresponding average diffusion ( $D_{av}$ ) maps and color maps [Figure 1, Figure 2, Figure 3]. We also performed fiber tracking in each of the ROIs to confirm the right location. We then looked for the maximum pixel value within the ROI [Figure 4, Figure 5].

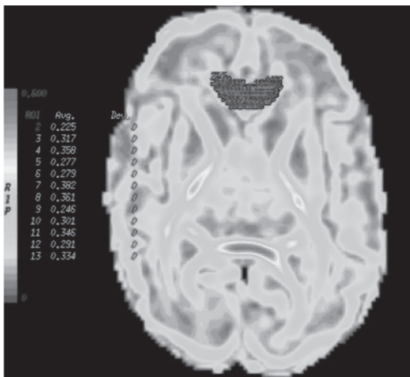


**Figure 5**  
Automating calculation of the maximum FA pixel value within the ROI on a FA map. (A full color version of this illustration can be found in the color section).

Two researchers experienced in neonatal DTI did all measurements. Statistical analysis of the relationship between FA of the white matter tracts and gestational age was analyzed by correlation analysis (Pearson product moment correlation, SPSS 13.0.1).

**Table 2**  
Tract statistics (FA and ADC mean values and standard deviations) and significant differences in FA and ADC between tracts

Structure	FA	ADC
	Mean (SD)	Mean (SD)
Posterior limb of the internal capsule	0.349 (0.028)	1.09 (0.05)
Anterior limb of the internal capsule	0.242 (0.033)	1.27 (0.091)
External capsule	0.175 (0.188)	1.29 (0.097)
Optic radiation	0.270 (0.042)	1.30 (0.126)
Corpus callosum (genu)	0.42 (0.048)	1.24 (0.111)
Corpus callosum (splenium)	0.442 (0.056)	1.27 (0.131)

## Results

### *Patient characteristics*

Gestational ages at birth ranged from 26 to 32 weeks (mean 28 weeks and 5 days) (Table 2). Mean weight at birth was 1148 grams and mean head circumference was 26.4 cm. All patients had shown normal neurodevelopment as defined by the Denver- or Bayley scoring system according to the most recent examination.

### *FA and ADC of standard pixel size ROIs*

We plotted average FA and ADC values of 16 pixel ROIs of the different white matter tracts against gestational age. We found a significant correlation between gestational age and FA of the right PLIC ( $r=0.530$ ,  $p<0.01$ ) as well as the left PLIC ( $r=0.405$ ,  $p<0.05$ ) [Figure 6, Figure 7]. No significant correlations were found for the other tracts. We found no correlation between average ADC values and gestational age in the



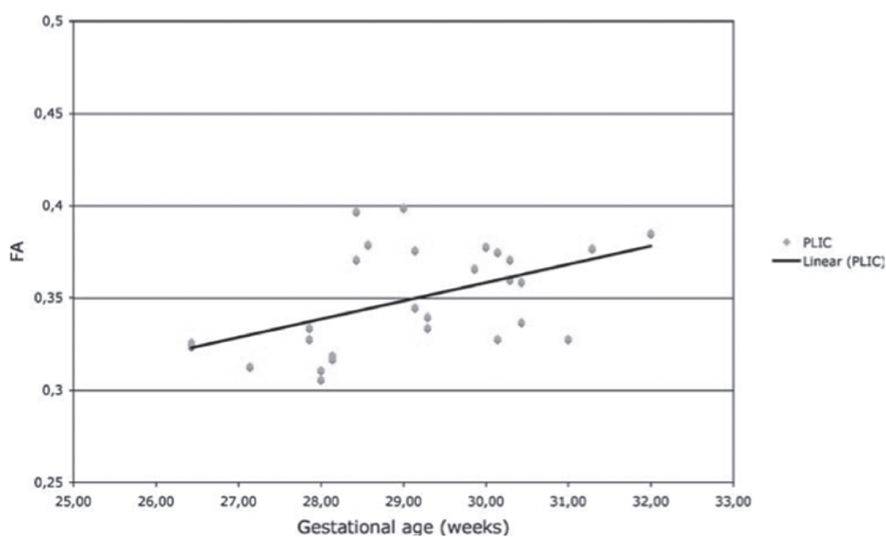


**Figure 6**  
Average FA values of 16 pixel ROIs of the PLIC.

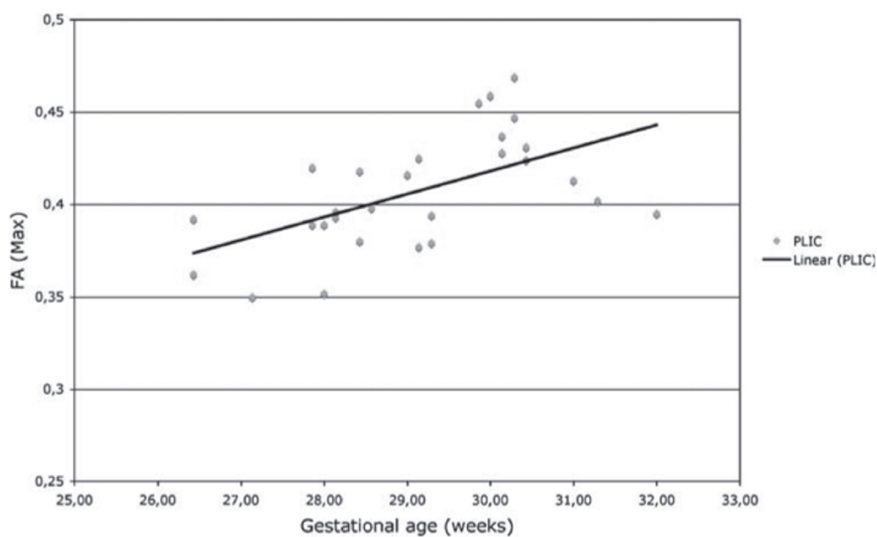


**Figure 7**  
Maximum FA ROI values of the PLIC.

studied tracts. Maximum FA values of the PLIC The maximum FA values of the ROI were plotted against gestational age and also showed a significant correlation between gestational age and FA of the right PLIC ( $r=0.517$ ,  $p<0.01$ ) and the left PLIC ( $r=0.530$ ,  $p<0.01$ ). Except for the right external capsule we saw no other significant correlations between FA and gestational age. Compared with standard size ROI mean FA values of the PLIC, the maximum values were a mean 0.05 higher.

### ***Comparison between tracts***

DTI values varied between white matter structures. FA was highest in the commissural tracts of the corpus callosum (splenium>genu), deep projection tracts (internal capsule). FA was lowest in association tracts (external capsule).

## **Discussion**

Our aim was to provide clinicians with reference values for the evaluation of diffusion tensor images of white matter tracts in VLBW infants. A literature search identified four similar studies. Comparison with these studies seems irrelevant as each included no more than four infants evaluated below a gestational age of 32 weeks within the first days of life. We were able to study scans of 28 infants VLBW without white matter damage within the first four days of life. We found a statistically significant correlation between gestational age and FA of the PLIC. Differences were observed between white matter tracts: FA was highest in commissural, followed by deep projection and association tracts. Others found the same hierarchy in the perinatal brain and in fully myelinated adult tracts<sup>16,26</sup>.

Different anisotropy indexes can be used to study the anisotropy of white matter tracts: fractional anisotropy (FA), relative anisotropy (RA), axial anisotropy (Am) etc. We focused on FA, the most frequently used anisotropy index. FA has a high sensitivity for studying anisotropy in white matter tracts<sup>16</sup>; it has a higher signal to noise ratio than RA for anisotro-

---

pic regions<sup>27,28</sup>. Previous studies showed that FA was the most sensitive significantly discriminating DTI parameter in pair wise comparisons between different tracts in premature infants<sup>16</sup>. In most tracts FA increases significantly by the week, whereas weekly decreases in apparent diffusion coefficients (ADC) values are smaller and less discriminative in most regions<sup>16</sup>. A growing number of studies have reported FA values of injured tracts<sup>29,30</sup>. Nevertheless, we should realize that FA is only one of the functions that describe the diffusion tensor. Although aberrant FA values seem to be a sensitive detector of abnormal tissue one could also use the relative magnitudes of the 3 principal eigenvectors to describe diffusion.

What determines anisotropy in white matter tracts? The value of the anisotropic index is determined by size, shape and composition of physical obstructions, as well as the space between them. Myelin, fast axonal transport, the axonal cytoskeleton (neurofilaments and microtubules), and local susceptibility gradients do not seem to have any major impact on anisotropic water diffusion<sup>32,33</sup>. Indeed, intact membranes are thought to be the main contributing factor to anisotropy. The corpus callosum, with a coherent parallel organization, has the highest FA values. Callosal fibre tracts, however, do not show a significant increase of FA with increasing gestational age, as the PLIC does. This might be due to the fact that myelination progress in the callosal fibers is slower than in the projection fibres at this age.

Studying DTI parameters of VLBW white matter tracts is challenging for many reasons. One of these challenges was to determine a standard for the size and shape of the ROIs. A ROI is a controlled identification of a given area of an image for numerical analysis and the area of anatomy being scanned that is of particular importance in the image. Different authors have used different ways to set their ROIs. The reason we compared two techniques was to achieve better reproducibility. Maximum values might be an alternative in which the value is given by the software. Fiber tracking, colormaps and ADC maps are established but time consuming techniques for the verification of tracts. We trust that automatic verification will become common practice in the future. A possible solution for ROI comparisons between researchers is the use of

a neonatal brain atlas coordinate system. Individual brain images could then be transformed into a common coordinate space and the ROIs can be placed at specific topographic coordinates. Our research group is currently looking into this option.

Another serious challenge was the signal-to-noise ratio (SNR) and spatial resolution constraints due to the very low anisotropy of premyelinating white matter and the tiny size of white matter tracts in premature newborns. Using a custom-made MR-compatible incubator with a high sensitivity neonatal head coil that improved image quality, spatial resolution and patient comfort we were able to overcome this challenge.

Better understanding of normal preterm white matter development is essential to encourage the use of DTI for evaluation and treatment of white matter injury. Early diagnosis of white matter abnormalities means that early intervention might be possible. We are exploring the feasibility of perinatal brain repair, and new MR imaging techniques like DTI will enable us to improve our understanding of how the developing brain responds to our interventions.

## Conclusion

In conclusion, our study gives anisotropy values for VLBW children with normal outcome that can be used as reference values. This work adds to our understanding of normal preterm white matter development.

## References

1. K. Costeloe, E. Hennessy, A.T. Gibson et al. The EPICure study: outcomes to discharge from hospital for infants born at the threshold of viability. *Pediatrics* 2000;106:659-71
2. R.E. Piecuch, C.H. Leonard, B.A. Cooper, et al. Outcome of extremely low birth weight infants (500 to 999 grams) over a 12-year period.

---

Pediatrics 1997;100:633–9

3. N.S. Wood, N. Marlow, K. Costeloe et al. Neurologic and developmental disability after extremely preterm birth. *N Engl J Med* 2000;343:378–4
4. M. Hack, H.G. Taylor, N. Klein et al. Functional limitations and special health care needs of 10- to 14-year-old children weighing less than 750 grams at birth. *Pediatrics* 2000;106:554–60
5. H.G. Taylor, N. Klein, M. Hack. School-age consequences of birth weight less than 750 g: a review and update. *Dev Neuropsychol* 2000;17:289–321
6. P.D. Barnes. Neuroimaging and the timing of fetal and neonatal brain injury. *J Perinatol* 2001;21:44–60
7. J.J. Volpe. Brain injury in the premature infant. *Clin Perinatol* 1997;24:567–87
8. P.S. Huppi, T.E. Inder. Magnetic resonance techniques in the evaluation of the perinatal brain: recent advances and future directions. *Semin Neonatol* 2001;6:195–210
9. N.J. Robertson, J.S. Wyatt. The magnetic resonance revolution in brain imaging: impact on neonatal intensive care. *Arch Dis Child Fetal Neonatal Ed* 2004;89:193–7
10. K.J. Rademaker, C.S. Uiterwaal, F.J. Beek et al. Neonatal cranial ultrasound versus MRI and neurodevelopmental outcome at school age in children born preterm. *Arch Dis Child Fetal Neonatal Ed* 2005;90:489–93
11. P.I. Yakovlev, A.R. Lecours (1967). The myelogenetic cycles of regional maturation of the brain. In: Mankowski A, ed. *Regional development of the brain in early life*. Oxford: Blackwell Scientific Publications: 3–69
12. L.T. Sie, M.S. van der Knaap, G. van Wezel-Meijler et al. MRI assessment of myelination of motor and sensory pathways in the brain of preterm and term born infants. *Neuropediatrics* 1997;28:97–105
13. D.M. Wimberger, T.P. Roberts, A.J. Barkovich et al. Identification of “premyelination” by diffusion-weighted MRI. *J Comput Assist Tomogr* 1995;19:28–33
14. J.I. Berman, P. Mukherjee, S.C. Partridge et al. Quantitative diffusion tensor MRI fiber tractography of sensorimotor white matter development in premature infants. *Neuroimage* 2005;27:862–71

15. P.S. Huppi, S.E. Maier, S. Peled et al. Microstructural development of human newborn cerebral white matter assessed in vivo by diffusion tensor magnetic resonance imaging. *Pediatr Res* 1998;44:584-90
16. S.C. Partridge, P. Mukherjee, J.I. Berman et al. Tractography-based quantitation of diffusion tensor imaging parameters in white matter tracts of preterm newborns. *J Magn Reson Imaging* 2005;22:467-74
17. S.S. Yoo, H.J. Park, J.S. Soul et al. In vivo visualization of white matter fiber tracts of preterm- and term-infant brains with diffusion tensor magnetic resonance imaging. *Invest Radiol* 2005;40:110-5
18. W.K. Frankenburg, B.W. Camp, P.A. van Natta. Validity of the Denver developmental screening test. *Child Dev* 1971;42:475-85
19. N. Bayley (1993). *Scales of Infant Development*. 2nd ed. San Antonio, TX: Psychological Corp
20. F.G. Shellock, J.V. Crues. MR procedures: biologic effects, safety, and patient care. *Radiology* 2004;232:635-52
21. F. Groenendaal, C. Leusink, M. Nijenhuis et al. Neonatal life support during magnetic resonance imaging. *J Med Eng Technol* 2002;26:71-4
22. M. Battin, E.F. Maalouf, S.J. Counsell et al. Physiological stability of preterm infants during magnetic resonance imaging. *Early Hum Develop* 1998;52:101-10
23. P.J. Basser, C. Pierpaoli. Microstructural and physiological features of tissues elucidated by quantitative-diffusion-tensor MRI. *J Magn Reson B* 1996;111:209-19
24. C. Pierpaoli, P.J. Basser. Toward a quantitative assessment of diffusion anisotropy. *Magn Reson Med* 1996;36:893-906
25. D. Le Bihan, J.F. Mangin, C. Poupon et al. Diffusion tensor imaging: concepts and applications. *J Magn Reson Imaging* 2001;13:534-46
26. J.S. Shimony, R.C. McKinstry, E. Akbudak et al. Quantitative diffusion-tensor anisotropy brain MR imaging: normative human data and anatomic analysis. *Radiology* 1999;212:770-84
27. K.M. Hasan, A.L. Alexander, P.A. Narayana. Does fractional anisotropy have better noise immunity characteristics than relative anisotropy in diffusion tensor MRI? An analytical approach. *Magn Reson Med* 2004;51:413-7

- 
28. C. Van Pul, J. Buijs, M.J. Janssen et al. Selecting the best index for following the temporal evolution of apparent diffusion coefficient and diffusion anisotropy after hypoxic-ischemic white matter injury in neonates. *ANJR Am J Neuroradiol* 2005;26:469-81
  29. S.J. Counsell, J.M. Allsop, M.C. Harrison et al. Diffusion-weighted imaging of the brain in preterm infants with focal and diffuse white matter abnormality. *Pediatrics* 2003;112:1-7
  30. P.S. Huppi, B. Murphy, S.E. Maier et al. Microstructural brain development after perinatal cerebral white matter injury assessed by diffusion tensor magnetic resonance imaging. *Pediatrics* 2001;107:455-60
  31. Z. Nagy, H. Westerberg, S. Skare et al. Preterm children have disturbances of white matter at 11 years of age as shown by diffusion tensor imaging. *Pediatr Res* 2003;54:672-9
  32. C. Beaulieu. The basis of anisotropic water diffusion in the nervous system: a technical review. *NMR Biomed* 2002;15:435-55
  33. S. Wakana, H. Jiang, L.M. Nagae-Poetscher et al. Fiber tract-based atlas of human white matter anatomy. *Radiology* 2004;230:77-87







# Chapter 4

## DIFFUSION TENSOR IMAGING OF CORTICAL PLATE AND SUBPLATE IN VERY-LOW-BIRTH-WEIGHT INFANTS

---

J. Dudink  
J. Buijs  
P.P. Govaert  
A.L. van Zwol  
N. Conneman  
J.B. van Goudoever  
M.H. Lequin

*Pediatr Radiol. 2010;40:1379-404*

## **Abstract**

### ***Background and purpose***

Many intervention studies in preterms aim to improve neurodevelopmental outcome, but short term proxy outcome measurements are lacking. Cortical plate and subplate development could be such a marker. Our aim was to provide normal DTI reference values for the cortical plate and subplate of preterm infants.

### ***Materials and Methods***

As part of an ongoing study we analyzed DTI images of 19 preterm infants without evidence of injury on conventional MRI, with normal outcome (Bayley-II assessed at age 2), and scanned in the first four days of life. Fractional anisotropy (FA) and apparent-diffusion-coefficient (ADC) values in frontal and temporal subplate and cortical plate were measured in single and multiple voxel regions-of-interest placed on predefined regions.

### ***Results***

Using single voxel ROIs, statistically significant inverse correlation was found between gestational age and FA of the frontal ( $r=-0.5938, p=0.0058$ ) and temporal ( $r=-0.4912, p=0.0327$ ) cortical plate. ADC values had a significant positive correlation with gestational age in the frontal ( $r=0.5427, p=0.0164$ ) and temporal ( $r=0.5540, p=0.0138$ ) subplate.

### ***Conclusion***

Diffusion tensor imaging allows in vivo exploration of evolving cortical plate and subplate. We show FA and ADC values of subplate and cortical plate in VLBW infants with normal developmental outcome, which can be used as reference values.

---

## Introduction

Advances in neonatal intensive care have led to significant improvement in survival of very low birthweight (VLBW) infants<sup>1,2</sup>. However survivors of preterm birth still show a high incidence of neurodevelopmental disability. Up to 25-50 % of VLBW infants have cognitive and attention deficits, often without marked motor deficits<sup>3-5</sup>. Early detection of abnormal brain maturation is important in the design of preventive, protective and rehabilitative strategies for the management of VLBW infants. White matter injury is believed to be the most common type of injury seen in preterm infants and is associated with neurological deficits seen in VLBW infants later in life<sup>6,7</sup>. However, it is difficult to relate cognitive and attention deficits entirely to white matter disease. Instead it seems more likely that these deficits are secondary to sensory deafferentation and/or axotomy<sup>8</sup>.

The human cerebral cortex develops through a series of stages during which complex histogenetic events occur in several transient anatomic layers. Many of these layers disappear as the fetus approaches term. The laminar structure of the developing cortex comprises the marginal zone, cortical plate (CP) and the subplate (a band of cells lying below the developing cortical plate).

The subplate is a transient laminar compartment of the human fetal cerebral wall, which plays an important role in the developing cortical architecture. The subplate develops around week 13 of gestation and gradually disappears at 32-34 weeks. The structure is thought to be the main synaptic zone of the human fetal cortex based on the rich input of 'waiting' afferents from cortical plate and thalamus. It plays a major role during the phase of cortical target area selection<sup>9</sup>. The subplate is a site of early neural activity, it is seen as substrate for functional plasticity and is considered to be selectively vulnerable for hypoxic/ischemic injury. All this renders the subplate a structure of great interest in the study of preterm brain injury<sup>9-12</sup>.

The subplate can be visualized with conventional and diffusion tensor magnetic resonance imaging (DTI)<sup>13-16</sup>. In contrast to conventional ana-

tomical imaging, DTI can provide information about the microstructural organization within the neural tissue *in vivo*<sup>17</sup>. Studies have shown that diffusion anisotropy can be used to study brain development<sup>15,18</sup>. DTI can thus be used to quantify microstructural organization of the subplate *in vivo*. Maas et al. used DTI to delineate early laminar organization of the cerebrum in two extremely premature infants<sup>14</sup>. Gupta et al performed DTI on 15 aborted fetuses and 5 term infants to look at regional FA values including the subplate<sup>15</sup>. There is a lack of DTI reference values for the subplate in healthy VLBW infants in the first week of life. Reference values of the subplate could be used as a tool to quantify the efficacy of interventions in clinical trials. In addition, these reference values might enable the pediatrician to identify infants at risk for suboptimal development already in the first phase of life.

We set up a prospective study aimed at providing DTI reference values for the CP and subplate zone VLBW infants.

## **Materials and Methods**

### ***Subjects***

The Erasmus MC Ethical Review Board approved the study and written informed parental consent was obtained for each subject. The MR scans used in this study had been obtained within the framework of a study in which premature infants of different gestational ages underwent serial conventional and DTI acquisitions to evaluate white matter development. All MR scans were obtained without sedation. The inclusion criteria for our study were birth at gestational age 25–32 weeks, no evidence of cerebral injury on conventional MRI (T1- and T2-weighted images) and scanned within 4 days of birth. Developmental outcome assessed at age of 2 years needed to be normal. Gestational age was calculated from the mother's last menstrual period or estimated from early US (<18 weeks of pregnancy). Exclusion criteria were ventriculomegaly, congenital infection, brain malformation or a multiple congenital anomaly syndrome. During the 25 months of the study period (March 2004 to April 2006), 41 infants were scanned and 32 met our study criteria. Four MR exami-

---

nations were excluded due to severe motion degradation and 9 due to other artifacts, so 19 patients were included.

### ***Neurodevelopment monitoring***

All children were neurologically assessed at 2 years of age and Bayley scales of infant development second edition (BSIDII) were used to monitor neurodevelopment<sup>19</sup>. All patients had shown normal neurodevelopment according to their neurological examination and Bayley scores (Bayley scores within one standard deviation of the mean were considered within normal limits; i.e. > 85).

### ***Conventional MR imaging***

Images were acquired using standard scanning protocols. All imaging was performed on a 1.5-T GE EchoSpeed scanner (GE Medical Systems, Milwaukee, Wis.). The imaging protocol included T1-W (spin echo, TR/TE 500/ 11 ms) and T2-W sequences (spin echo, TR/TE 3,000/ 120 ms) with a slice thickness of 4 mm and 0.4 mm gap. For DTI an echoplanar sequence with diffusion gradients applied in 25 non-collinear directions was used with a slice thickness of 3 mm and no gap ( $b=1,000$  s/mm<sup>2</sup>). An average of 20 slices was recorded within 4 min using TR/ TE 9,150/98–91 ms. The FOV was 20 cm, the scan matrix 128×128 and the reconstruction matrix 256×256. All patients were scanned using an MR-compatible incubator with a specialized high-sensitivity neonatal head coil (Lammers Medical Technology, Lubeck, Germany). Pads around the infant's head kept movement to a minimum. Moldable earplugs and neonatal earmuffs were used to reduce noise. The incubator provided controlled temperature and humidity as well as MR compatible pulse oximetry and ventilation.

### ***Diffusion tensor postprocessing***

Diffusion tensor images were transferred to a GE Advantage Windows workstation (General Electric Medical Systems, Milwaukee, Wis.) for postprocessing using 'Functool' software (General Electrics).

DTI measures the diffusion of water in each voxel and the extent to which water diffuses in particular directions as a result of the micro-structural characteristics of the tissue imaged. FA measures the fraction of the magnitude of the diffusion tensor that can be ascribed to anisotropic diffusion<sup>20-22</sup>. For isotropic diffusion ( $\lambda_1=\lambda_2=\lambda_3$ ), FA is zero, and in the case where there is a strongly preferred direction of diffusion ( $\lambda_1>>\lambda_2=\lambda_3$ ), FA approaches a value of one. The apparent diffusion tensor (ADC) was calculated from the eigenvalues for each voxel as follows:  $(\lambda_1 + \lambda_2 + \lambda_3)/3$ , and provides the overall magnitude of water diffusion. ADC is independent of anisotropy and also a useful parameter for brain maturation<sup>23</sup>.

Two strategies for regions of interest (ROI) placement were used. First we placed two rows (right and left hemisphere) of single voxel ROIs along a straight line on an axial slice through the foramen of Moro (Figure 1); this line prolonged the long axis of the lateral ventricle through the subplate and CP. Next we placed two rows on an axial slice through the pedunculi of the brainstem from the top of the temporal horn to the CP right and left (Figure 1). We identified the voxel most representing the

cortical plate and subplate visually on the b0-reference image. We cross-correlated this with the T1- and T2 weighted scans and the ADC and FA maps.

In the second method we placed standard-size, round-shaped 16-voxel ROIs in the region of the subplate

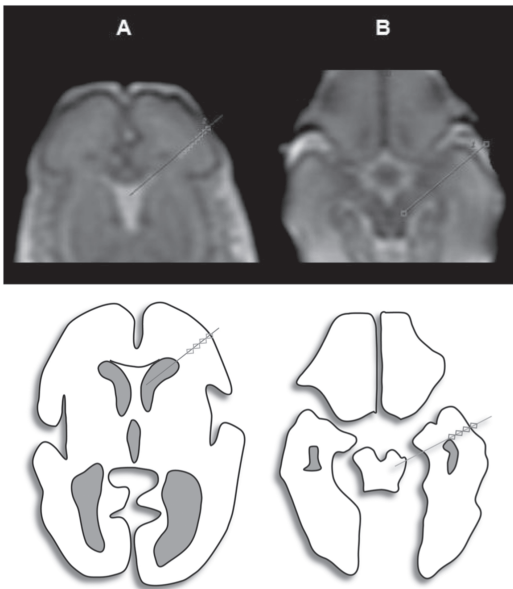


**Figure 1.** Top image shows ROI placement (row of single voxels) both frontal (A) and temporal (B) regions. The image below shows the same ROI placement on a cartoon. (A full color version of this illustration can be found in the color section).

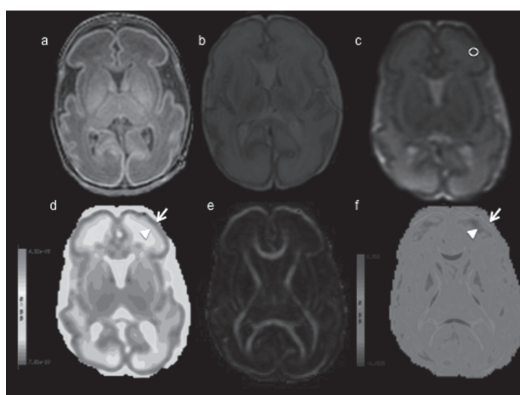


**Figure 2.**

Showing different scan sequences of the same patient (GA 30w). (a) T1-weighted image, (b) T2-weighted image, (c) B0-image showing low signal intensity (SI) of CP and a ROI placed in area of the subplate, (d) ADC map showing low (dark blue) ADC value of the cortex (arrow) and intermediate ADC values of the subplate (arrowhead), (e) colour map (red representing right-left, green representing antero-posterior, and blue representing supero-inferior anatomical directions), (f) FA map, showing high FA values of the cortex (arrow) and low FA values (blue) of the subplate zone (arrowhead). (A full color version of this illustration can be found in the color section).

on the same axial slices as mentioned in the first method. In temporal regions it was more difficult to place the 16 voxel ROI in the centre of the cortical plate and we decided to use this method for the subplate only because else we suspected too much interference from partial-volume effects. We identified the subplate visually on the b0-reference image. We cross-correlated this with the T1- and T2 weighted scans and the ADC and FA maps (Figure 2). Two researchers experienced in neonatal DTI achieved consensus on ROI place-

ment and measurements readings. For every ROI,  $\lambda_{1,2,3}$  was measured and FA and ADC were calculated.

## **Statistical analysis**

The relationship between FA and ADC of the CP and gestational age and between the subplate and gestational age was analyzed by correlation analysis (Pearson product moment correlation, SPSS 13.0.1).

## **Results**

### **Patient characteristics**

Gestational ages at birth ranged from 26 to 31 weeks (mean 29 weeks 1 day). All infants were appropriate for gestational age. Mean weight at

birth was 1,135 g and mean head circumference was 26 cm, 9 of the infants were girls. In 91% antenatal steroids were given. The median APGAR score at 5 minutes was 9 (range 5-10). No infections were reported in the first week of life. Except for one patient, all infants received respiratory support in the first week of life.

### ***FA and ADC calculations***

For both ROI methods, we plotted the calculated FA and ADC values of the CP and the subplate against GA. No statistically significant differences based on a two tailed paired Student's t-test (at a significance level of  $P < 0.05$ ) were found comparing FA and ADC values between the left and right hemispheres in each subject. Therefore, the values obtained from the left and right were averaged to obtain the mean FA and ADC of the different ROIs (Table1).

### ***FA and ADC of single voxel ROIs***

A statistically significant inverse correlation was found between GA and FA of the frontal ( $r = -0.5938$ ,  $p = 0.0058$ ) and temporal ( $r = -0.4912$ ,  $p = 0.0327$ ) CP (figure 3,4). No significant correlations between ADC and the CP were detected. ADC had a significant correlation with GA in the frontal ( $r = 0.5427$ ,  $p = 0.0164$ ) and temporal ( $r = 0.5540$ ,  $p = 0.0138$ ) subplate (Figure 3). No correlation was found between FA values in the frontal and temporal subplate and GA.

### ***FA and ADC of ROIs of standard 16 pixel size***

A statistically significant correlation was found between GA and ADC of the frontal ( $r = 0.505$ ,  $p = 0.027$ ) and temporal ( $r = 0.301$ ,  $p = 0.015$ ) subplate (Figure 4).



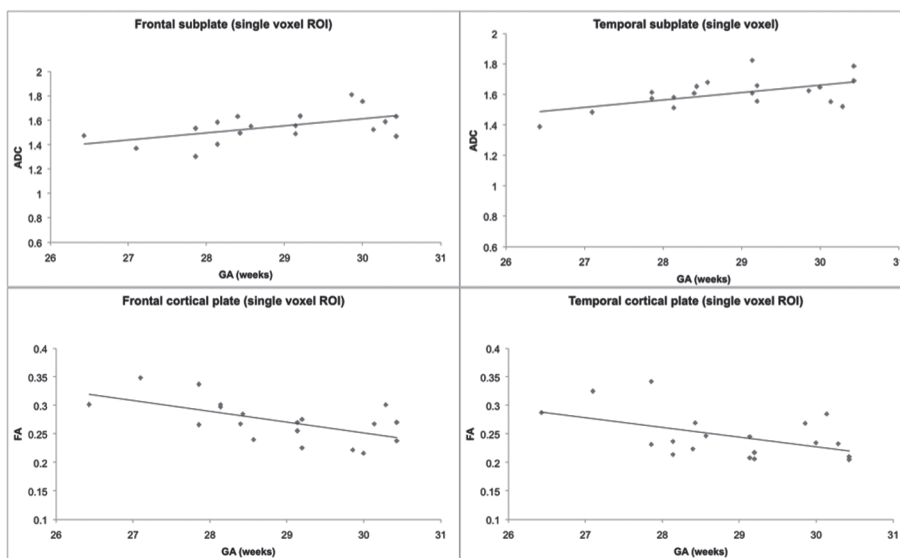


**Figure 3. FA and ADC of single voxel ROIs**

A statistically significant inverse correlation was found between gestational age (GA) and fractional anisotropy (FA) of the frontal ( $r=-0.5938$ ,  $p=0.0058$ ) and temporal ( $r=-0.4912$ ,  $p=0.0327$ ) cortical plate (CP). No significant correlations between apparent diffusion coefficient (ADC) and the CP were detected. ADC had a significant correlation with GA in the frontal ( $r=0.5427$ ,  $p=0.0164$ ) and temporal ( $r=0.5540$ ,  $p=0.0138$ ) subplate.

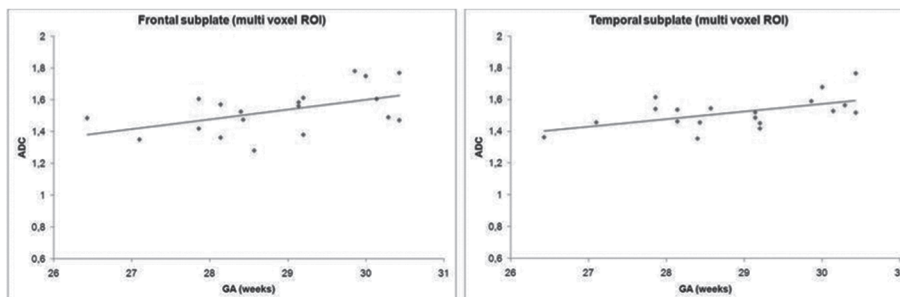


**Figure 4. ADC of ROIs of standard 16 pixel size**

A statistically significant correlation was found between gestational age (GA) and apparent diffusion coefficient (ADC) of the frontal ( $r=0.505$ ,  $p=0.027$ ) and temporal ( $r=0.301$ ,  $p=0.015$ ) subplate.

Table 1

Single voxel ROI	Frontal subplate		Temporal subplate	
	mean (SD)		mean (SD)	
	Right	Left	Right	Left
FA	0,069 (0,02)	0,061 (0,02)	0,08 (0,02)	0,075 (0,02)
ADC x 10–3 mm <sup>2</sup> /second	1,539 (0,14)	1,519 (0,13)	1,593 (0,14)	1,609 (0,16)

16 voxel ROI	Frontal subplate		Temporal subplate	
	mean (SD)		mean (SD)	
	Right	Left	Right	Left
FA	0,09 (0,03)	0,08 (0,03)	0,103 (0,02)	0,09 (0,02)
ADC x 10–3 mm <sup>2</sup> /second	1,509 (0,16)	1,52 (0,17)	1,509 (0,09)	1,527 (0,12)

Mean FA and ADC values in the frontal and temporal subplate

Discussion

We provide clinicians with reference values for the evaluation of diffusion tensor images of the CP and subplate in VLBW infants with normal outcome at two years of age. A statistically significant inverse correlation was measured between GA and FA values of the frontal and temporal cortical CP. ADC values were found to have a significant positive correlation with GA in the frontal and temporal subplate.

ADC and FA values of cortical plate

Our observation of decreased cortical FA values with increasing gestational age after 26 weeks seems consistent with published data<sup>15,18,24</sup>. Before 26 weeks a gradual increase in the cortical FA values has been reported. Neurons that form the cerebral CP migrate to their destinations along radial glial fibers<sup>25</sup>. It is thought that the observed increase in the cortical FA values during early GA (<27 weeks) could be associated with this radial organization and with the radial orientation of the apical dendrites of pyramidal cells<sup>26</sup>. The decline in the cortical FA after 27 weeks probably reflects a degradation in the radial organization. In time radial glial cells differentiate into astrocytes and gradually retract their ventricular and pial attachments, also neocortical maturation will take place which results from neuronal growth, afferents ingrowth, dendrites

elaboration and synapse formation<sup>26,27</sup>. These processes are an important basis of later functional connectivity. In agreement with others we have demonstrated a low cortical ADC. We did not find a significant correlation between GA and ADC values of CP, which is probably due to the close age range of our patients. McKinstry et al did find an increase in ADC values of the CP until 32 weeks and a decrease hereafter<sup>18</sup>. These divergent findings might reflect a difference of ROI location between the two studies. It is known that the rate of CP development varies, depending on its location which could also explain the differences found.

### ***ADC and FA values of subplate***

The subplate is a transient fetal cerebral zone, which serves as the 'waiting compartment' for growing cortical afferents<sup>9</sup>. The SP is a laminar structure, which consists of tissue with large extracellular spaces and an abundance of glycosaminoglycans<sup>28</sup>. It is most prominent around 22 weeks and disappears at around 32-34 weeks. In the ROIs corresponding with the subplate region we measured medium diffusivity and low anisotropy values. These findings seem to be consistent with earlier findings and might reflect the relatively lower cellularity of this region<sup>14</sup>. The finding of low FA values in the subplate region are consistent with observation of more randomly scattered cells seen on histology, perhaps also due to the mixture of interdigitating radial and tangential fibers within this lamina<sup>14,29</sup>. We found an increase of ADC values in the region of the subplate between 26 and 31 weeks of gestation. These findings might be explained by the assumption that either a decrease in cellularity (associated with programmed cell death) in certain areas or the loss of interconnections of the brain could outweigh the decrease in overall water content during brain maturation<sup>30-32</sup>.

Studying DTI parameters of the subplate of VLBW infants is challenging for many reasons. One of the challenges is to determine a practical ROI size, shape and location. We choose to examine subplate in the temporal and frontal lobe because the subplate is clearly visible during the gestational ages studied and these regions are related to associative or 'executive' functions, which are increasingly recognized as being impaired in children born preterm.

A limitation of this study is that at 2 years of age it remains difficult to exclude global injury or interference with normal development with certainty. Although the developmental testing of premature infants at two years of age with the use of the Bayley Scales of Infant Development provides an early opportunity to estimate future developmental capabilities, the correlation of developmental assessments with ultimate developmental achievement would be greater for assessments at five years of age or even later. So in future studies longer follow up is necessary.

We compared two techniques to achieve better reproducibility. However both methods have limitations. In the single-voxel method, we use the best corresponding voxel out of a row of voxels on a line crossing the subplate and CP. This technique will be more prone to artefacts than a standard multi-voxel ROI. The multi-voxel ROI placed in the middle of a structure such as the subplate will be more prone to partial-volume effects. Because single voxel ROI placement allows us to follow the changes of  $\lambda_1$ ,  $\lambda_2$ ,  $\lambda_3$  values seen in cross sections of the brain we found the single voxel method a useful way to study DTI parameters of the SP and CP. We found that the voxels with the lowest FA values correlated well with the voxels representing the middle of the SP region. However because of the limitations mentioned we do recommend using the multi voxel ROI method.

Using interobserver independent (semi-) automatic subplate segmentation might be the best way to cope with these limitations and will allow measurements of the complete subplate instead of a limited number of locations. However, the use of (semi-) automatic postprocessing algorithms does require specialized computing knowledge and will be less accessible for clinical purposes.

In this study we used a  $b$  value of 1,000 s/mm<sup>2</sup> to allow exact comparisons between early and later scans of the study subjects made at different ages (including scans made at 6 weeks and 1 year). We realize a lower  $b$  value for scanning the preterm brain would be optimal. The optimal  $b$  value can be calculated as indicated by Jones et al<sup>33</sup>. The choice of dti scan parameters (including b-values) have shown to effect both ADC and FA values. In a recent study we examined the effect of high  $b$

---

values on FA and ADC in different neonatal brain regions. ADC values decreased with increasing b-value in all regions studied. In white matter, there was an approximately linear trend in the reduction of ADC with increasing b-value, whereas in the thalamus ADC declined more slowly at higher b-values. There was no consistent change in FA with increasing b-value in the neonatal brain<sup>34</sup>.

Another serious challenge is the signal to noise ratio (SNR) and spatial resolution constraints due to the very low anisotropy of premyelinating white matter and the tiny size of white-matter tracts in premature newborns. Using a custom-made MR-compatible incubator with a high-sensitivity neonatal head coil that improved image quality and spatial resolution we were able to overcome these problems.

## **Conclusion**

Secondary disturbances of cortical connectivity seem a logical anatomical substrate for some of the neurodevelopmental deficits seen in a large number of VLBW infants. Early diagnosis of subplate abnormalities is important for developing intervention strategies and for exploring different ways of perinatal brain repair.

Given the important role of the subplate in normal development of the CP and its selective vulnerability to hypoxic–ischemic brain injury, a better understanding of normal subplate development is essential. Our study provides normal DTI reference values for evaluation of cortical brain maturation.

## References

1. K. Costeloe, E. Hennessy, A.T. Gibson et al. The EPICure study: outcomes to discharge from hospital for infants born at the threshold of viability. *Pediatrics* 2000;106:659–71
2. R.E. Piecuch, C.H. Leonard, B.A. Cooper et al. Outcome of extremely low birth weight infants (500 to 999 grams) over a 12-year period. *Pediatrics* 1997;100:633–9
3. N.S. Wood, N. Marlow, K. Costeloe et al. Neurologic and developmental disability after extremely preterm birth. *N Engl J Med* 2000;343:378–84
4. M. Hack, H.G. Taylor, N. Klein et al. Functional limitations and special health care needs of 10- to 14-year-old children weighing less than 750 grams at birth. *Pediatrics* 2000;106:554–60
5. H.G. Taylor, N. Klein, M. Hack et al. School-age consequences of birth weight less than 750 g: a review and update. *Dev Neuropsychol* 2000;17:289–321
6. P.D. Barnes. Neuroimaging and the timing of fetal and neonatal brain injury. *J Perinatol* 2001;21:44–60
7. J.J. Volpe. Brain injury in the premature infant. *Clin Perinatol* 1997;24:567–87
8. J.J. Volpe JJ. Brain injury in premature infants: a complex amalgam of destructive and developmental disturbances. *Lancet Neurol* 2009;8:110-24
9. I. Kostovi, N. Jovanov-Milošević. Subplate zone of the human brain historical perspective and new concepts. *Coll. Antropol* 2008;32:3-8
10. J.J. Volpe. Subplate neurons-missing link in brain injury of the premature infant? *Pediatrics* 1996;97:112-3
11. P.S. McQuillen, R.A. Sheldon, C.J. Shatz et al. Selective vulnerability of subplate neurons after early neonatal hypoxia-ischemia. *Neurosci* 2003;23:3308-15
12. A. Ghosh, C.J. Shatz CJ. A role for subplate neurons in the patterning of connections from thalamus to neocortex. *Development* 1993;117:1031-47
13. M. Rados, M. Judas, I. Kostovic. In vitro MRI of brain development. *Eur J Radiol* 2006;57:187–98

14. L.C. Maas, P. Mukherjee, J. Carballido-Gamio et al. Early laminar organization of the human cerebrum demonstrated with diffusion tensor imaging in extremely premature infants. *Neuroimage* 2004;22:1134-40
15. R.K. Gupta, K.M. Hasan, R. Trivedi R et al. Diffusion tensor imaging of the developing human cerebrum. *J Neurosci* 2005;15:172-8
16. L. Perkins, E. Hughes, L. Srinivasan et al. Exploring cortical subplate evolution using magnetic resonance imaging of the fetal brain. *Dev Neurosci* 2008;30:211-20
17. D. Le Bihan. Looking into the functional architecture of the brain with diffusion MRI. *Nat Rev Neurosci* 2003;4:469–80
18. R. McKinstry, A. Mathur, J.H. Miller et al. Radial organization of developing preterm human cerebral cortex revealed by non-invasive water diffusion anisotropy MRI. *Cereb Cortex* 2002;12:1237-43
19. N. Bayley (1993) Bayley scores of infant development, 2nd edn. Psychological Corporation, San Antoni, TX
20. P.J. Basser, C. Pierpaoli. Microstructural and physiological features of tissues elucidated by quantitative-diffusion-tensor MRI. *J Magn Reson B* 1996;111:209–19
21. C. Pierpaoli, P.J. Basser. Toward a quantitative assessment of diffusion anisotropy. *Magn Reson Med* 1996;36:893–906
22. D. Le Bihan, J.F. Mangin, C. Poupon et al. Diffusion tensor imaging: concepts and applications. *J Magn Reson Imaging* 2001;13:534–46
23. J. Dudink, J.L. Kerr, K. Paterson et al. Connecting the developing preterm brain. *Early Hum Dev* 2008;84:777-82
24. R. Trivedi, R.K. Gupta, N. Husain et al. Region specific maturation of cerebral cortex in human fetal brain: diffusion tensor imaging and histology. *Neuroradiol* 2009;51:567-76
25. P. Rakic. Developmental and evolutionary adaptation of cortical radial glia. *Cereb Cortex* 2003;13:541-9
26. R.L. Sidman, P. Rakic. Neural migration with special reference to developing human brain: a review. *Brain Res* 1973;62:1-35
27. J.J. Volpe (2008) *Neurology of the Newborn*. 5th ed. Philadelphia: Elsevier.
28. I. Kostovic, M.E. Molliver. A new interpretation of the laminar development of the cerebral cortex: synaptogenesis in different layers of neopallium in the human fetus. American association of anatomists. Eighty seventh annual session. *Anat Rec* 1974;178:395

29. S. Mori, R. Xue, J. Zhang et al. High resolution anatomical study of human fetal brain development based on diffusion tensor imaging [abstract]. *Proc Int Soc Magn Reson Med* 2002;10:1305
30. W.Y. Chan, D.T. Yew. Apoptosis and Bcl-2 oncoprotein expression in the human fetal central nervous system. *Anat Rec* 1998;252:165–75
31. J. Dobbing, J. Sands. Quantitative growth and development of human brain. *Arch Dis Child* 1973;48:757–67
32. M. Cannie, F. De Keyzer, J. Meersschaert et al. A diffusion-weighted template for gestational age-related apparent diffusion coefficient values in the developing fetal brain. *Ultrasound Obstet Gynecol* 2007;30:318–24
33. D.K. Jones, M.A. Horsfield, A. Simmons. Optimal strategies for measuring diffusion in anisotropic systems by magnetic resonance imaging. *Magn Reson Med* 1999;42:117–21
34. J. Dudink, D.J. Larkman, M. Kappellou et al. High b-value diffusion tensor imaging of the neonatal brain at 3T. *AJNR Am J Neuroradiol* 2008;29:196-72









# Chapter 5

## HIGH B VALUE DIFFUSION TENSOR IMAGING OF THE NEONATAL BRAIN AT 3 TESLA

---

J. Dudink  
D.J. Larkman  
O. Kapellou  
J.P. Broadman  
J.M. Allsop  
F.M. Cowan  
J.V. Hajnal  
A.D. Edwards  
M.A. Rutherford  
S.J. Counsell

*AJNR Am J Neuroradiol. 2008;29(10):1966-72*

## **Abstract**

### ***Background and Purpose***

Diffusion weighted magnetic resonance (MR) imaging studies of the adult brain have shown that contrast between lesions and normal tissue is increased at high  $b$  values. We considered whether diffusion tensor imaging (DTI) obtained at high  $b$  values would be useful in assessing pathology in the neonatal brain.

### ***Materials and Methods***

We studied 17 neonates, median (range) age of 10 (2-96) days, who were undergoing MR imaging for clinical indications. DTI was performed on a Philips 3 Tesla Intera system with  $b$  values of 350, 700, 1500 and 3000 s/mm<sup>2</sup>. Regions of interest were positioned in the central white matter at the level of the centrum semiovale, frontal and occipital white matter, splenium of the corpus callosum, posterior limb of the internal capsule and the thalamus.

### ***Results***

Isotropic diffusion image contrast and lesion to normal tissue contrast increased with increasing  $b$  value. ADC values decreased with increasing  $b$  value in all regions studied. However, there was no change in FA with increasing  $b$  value.

### ***Conclusion***

The increase in diffusion image contrast observed at high  $b$  values may be useful in identifying lesions in the neonatal brain.

---

## Introduction

Diffusion weighted magnetic resonance (MR) imaging is increasingly being used to investigate neonatal cerebral pathology. Previous studies have shown that diffusion weighted imaging (DWI) is able to demonstrate lesions that are not always discernable on conventional MR imaging and the utility of this imaging technique for assessing infarction and metabolic disorders in the neonatal brain is established<sup>1-5</sup>. In addition to the qualitative assessment of injury, diffusion tensor imaging (DTI) provides directionally invariant measurements of mean diffusivity and diffusion anisotropy. These objective measurements provide information regarding water molecular mobility, which reflect tissue microstructure and thereby provide insight into mechanisms of brain development and disease processes.

Diffusion weighted MR imaging with  $b$  values over 2000 s/mm<sup>2</sup> has been performed in animal studies, in the adult brain and in infants<sup>6-15</sup>. These studies suggest that diffusion contrast characteristics are altered at higher  $b$  values. In addition, adult studies of cerebral infarction and white matter disease have shown increased lesion conspicuity at higher  $b$  values and so it is possible that high  $b$  value DTI in neonates may also improve lesion conspicuity<sup>13,14</sup>.

To our knowledge, the only studies investigating the effects of high  $b$  value diffusion imaging in the neonatal brain were done on infants whose conventional MR imaging was considered normal and did not examine the full diffusion tensor<sup>8,15</sup>. In this study we considered whether diffusion imaging at high  $b$  values enhances contrast between lesions and normal tissue in neonates, and thereby increases lesion conspicuity. Furthermore, we acquired diffusion data in 6 non-collinear directions of sensitisation, enabling us to examine the effects of high  $b$  values on diffusion anisotropy.

The aims of this study were i) to assess isotropic diffusion weighted image contrast and lesion conspicuity at  $b$  values between 350 and 3000s/mm<sup>2</sup> and ii) to assess whether apparent diffusion coefficient (ADC) or fractional anisotropy (FA) in the neonatal brain change with increasing  $b$  value.

## Methods

Ethical permission for this study was granted by the Hammersmith Hospitals Research Ethics Committee. Written, informed parental consent was obtained for each infant prior to scanning.

## Subjects

The study group consisted of 17 neonates, 8 male and 9 female, of gestational ages ranging from 26 to 42 weeks, who underwent MR imaging for clinical indications. The median (range) age of the infants at scanning was 10 (2-96) days [median post menstrual age at scanning = 41 (39 - 45) weeks]. One infant was imaged twice. The characteristics of the infants and clinical indications for imaging are described in Table 1. Neonates were sedated for imaging with oral chloral hydrate (20-50 mg/kg). Pulse oximetry and electrocardiograph were monitored throughout the procedure. Ear protection was used for each infant (Natus MiniMuffs, Natus Medical Inc., San Carlos CA, USA). An experienced neonatologist, trained in MR imaging procedures, was in attendance throughout the MR examination.

## MR Imaging

MR imaging was performed on a Philips 3 Tesla Intera system (Philips Medical Systems, Best, The Netherlands) using a 6 channel phased array head coil. Transverse T2 weighted fast spin echo (FSE) and 3D MPRAGE images were acquired prior to obtaining DTI. The conventional MR images were assessed by an experienced neonatal neuro-radiologist (MAR).

Single shot echo planar imaging DTI was acquired in 6 non-collinear directions with  $b$  values of 0, 350, 700, 1500 and 3000 s/mm<sup>2</sup>. The pulse sequence parameters used were as follows; TR 5000ms, TE 100ms,

**Table 1.** Characteristics of the infants

Infant	Age (days)	Gestational age	Male/female	Indication for imaging	Imaging findings – conventional MR imaging
1	7	41w	female	Perinatal asphyxia.	Posterior fossa and hemispheric subdural haemorrhage. Small foci of abnormal signal intensity in posterior lateral lentiform nucleus.
2	3	38w	male	Ventricular dilatation noted on antenatal ultrasound.	Extensive subependymal heterotopias and abnormal cortical folding. No myelin within PLIC and abnormal signal intensity in thalamus and lentiform. Hypoplastic cerebellar vermis.
3	96	26w3d	female	Bilateral IVH on early ultrasound. Term imaging assessment.	Mild bilateral lateral ventricular dilatation. Residual hemorrhage evident on ventricular wall. Myelin appropriate for gestational age.
4	5	40w	male	Right sided focal seizures.	Left sided anterior branch middle cerebral artery infarct. Abnormal signal intensity in left PLIC and thalamus.
5	18	40w	female	Repetitive jerking episodes. Diagnosis: Benign sleep myoclonus.	Focal regions of short T2 in temporal white matter.
6	25	39w4d	female	Hypotonic at birth and poor feeding.	Foci of abnormal signal intensity in the globus pallidum and thalamus. Myelin not present in the PLIC. Abnormal long T1 and T2 throughout the white matter. Injury probably established antenatally.
7	9	42w	female	Hypotonia. Hip contractures. Poor feeding. Diagnosis: Prader-Willi syndrome.	Narrow bifrontal diameter of the skull with an enlarged anterior extracerebral space. Subdural hemorrhage over the right hemisphere and in the posterior fossa. Abnormal folding of the frontal cortex.
8	12	40w6d	male	Perinatal asphyxia.	No abnormality.
9	17	41w	male	Seizures. Hypoglycemia. Hypotonia. Early hyperhomocysteinaemia. Later diagnosis: Sotos syndrome.	Increased T1 and T2 in white matter. Foci of increased T2 in basal ganglia and thalamus

10	2	37w	male	Investigation of early neonatal encephalopathy.	Haemorrhage within right cerebellar hemisphere. Basal ganglia and thalamus appear normal.
11	4	41w	female	Neonatal seizures.	Left middle cerebral artery infarct with abnormal signal intensity within the left PLIC and thalamus.
12	3	38w4d	female	Cerebellar hypoplasia suspected on antenatal ultrasound.	Normal imaging appearances.
13	16	37w6d	female	Neonatal and ongoing seizures. Intrauterine growth restriction. No definite diagnosis.	No abnormality.
14	5	41w6d	male	Perinatal asphyxia.	No abnormality.
15	75	29w6d	female	Prolonged rupture of membranes (6 weeks). Term imaging assessment as part of research cohort.	Very high signal intensity within the white matter on T2 weighted imaging. Subependymal cyst. No focal lesions.
16	3	38w4d	male	Periventricular cystic lesions observed on cranial ultrasound. Later Diagnosis: methylmalonic acidemias.	Generalised long T1 and long T2 in the white matter. Foci of abnormal signal intensity within the cerebellum. Bilateral periventricular cysts anteriorly. Suggestive of metabolic disorder or congenital infection.
17	6	38w	male	Perinatal asphyxia. Severe anaemia from fetal maternal loss.	Bilateral abnormal signal intensity within the basal ganglia and thalami extending into the brainstem. Multiple small "hemorrhagic" foci within the white matter.



slice thickness 4mm, FOV 220mm, matrix 96 x 96. NSA was increased with increasing  $b$  value; 2 NSA ( $b = 350 \text{ s/mm}^2$ ), 4 NSA ( $b = 750 \text{ s/mm}^2$ ), 6 NSA ( $b = 1500$  and  $3000 \text{ s/mm}^2$ ). The duration of the diffusion gradient pulses was 36 ms and the time interval between their leading edges was 49 ms for all  $b$  values. The  $b$  value was increased by increasing the amplitude of the diffusion gradients (maximum 21 mT/m). In addition, DTI was obtained using the same parameters described above on a spherical phantom containing dimethyl sulfoxide (DMSO).

## Data Analysis

### *Phantom data*

Measurements were taken from a circular region of interest (ROI) measuring  $740\text{mm}^2$ . In order to assess hardware or pulse sequence errors, ADC and FA values were plotted against  $b$  value.

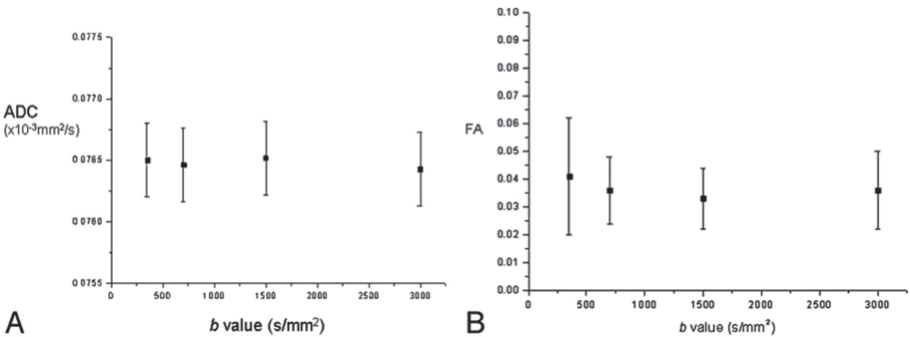
### *Infant data*

Image contrast and lesion conspicuity at each  $b$  value were assessed visually by 2 investigators (SJC and MAR) and by calculating the contrast ratio as described by Meyer<sup>16</sup>. The contrast ratio between unmyelinated white matter (WM) (frontal WM) and central gray matter (GM) (thalamus), between unmyelinated WM and partially myelinated WM (central WM at the level of the centrum semiovale), and between partially myelinated, highly anisotropic WM (PLIC) and central GM was determined using equation [1]<sup>13</sup>. The contrast ratio between lesions and adjacent tissue in infant 4 and infant 17 was also assessed.

$$\text{CR} = \frac{S_1 - S_2}{S_1 + S_2} \quad [1]$$

CR = contrast ratio,  $S_1$  and  $S_2$  are the signal intensities of regions on the isotropic diffusion images.

In addition, ROIs were positioned in the central WM at the level of the centrum semiovale, frontal WM at the level of the basal ganglia, occipital WM, the splenium of the corpus callosum, the posterior limb of the internal capsule (PLIC) and the thalamus on the ADC and FA maps. ADC and FA values were plotted against *b* value for each region.



**Figure 1**  
a. Graph demonstrating ADC value versus *b* value in a spherical DMSO phantom.  
b. Graph demonstrating FA value versus *b* value in a spherical DMSO phantom.

## Results

### *Phantom data*

Phantom data showed little change in ADC (Figure 1a) or FA (Figure 1b) over the range of *b* values.

### *Infant data*

Visual assessment of isotropic diffusion weighted images

At  $b = 350 \text{ s/mm}^2$  unmyelinated WM was high signal intensity relative to central GM and the cortex. Highly anisotropic WM regions such as the PLIC were demonstrated as very slightly hyperintense relative to the thalamus.

At  $b = 700 \text{ s/mm}^2$  there was little contrast between unmyelinated WM and central GM. The PLIC was seen as very slightly hyperintense relative to the thalamus.

At  $b = 1500 \text{ s/mm}^2$  unmyelinated WM was low signal intensity relative to central and cortical GM. Highly anisotropic WM regions were hyperintense relative to both GM and unmyelinated WM.

At  $b = 3000 \text{ s/mm}^2$  unmyelinated WM was extremely low signal relative to central and cortical GM. Highly anisotropic WM fibre bundles were markedly hyperintense relative to other brain tissues. The cerebellum was demonstrated as very high signal intensity.

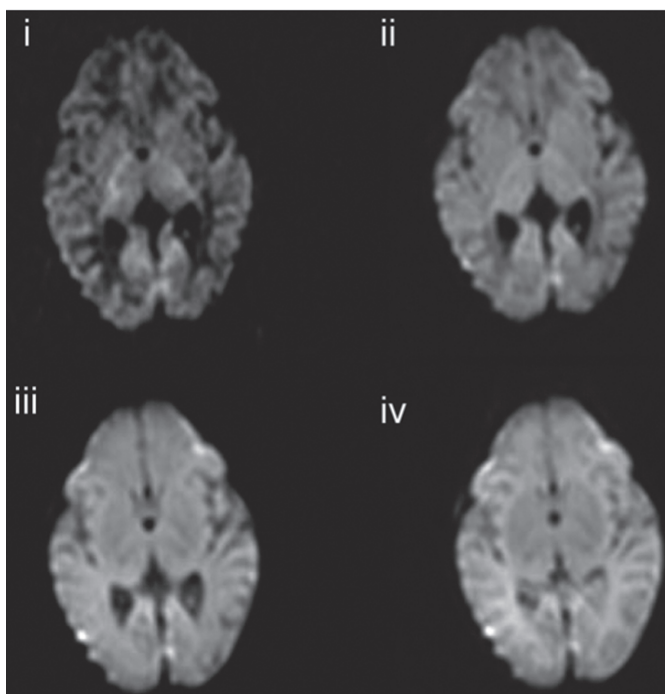


**Figure 2**

Isotropic diffusion weighted image at the level of the basal ganglia in an infant (infant 3) who had no evidence of abnormality on conventional or diffusion weighted imaging.

I.  $b = 3000 \text{ s/mm}^2$

II.  $b = 1500 \text{ s/mm}^2$

III.  $b = 700 \text{ s/mm}^2$

IV.  $b = 350 \text{ s/mm}^2$

Figure 2 shows isotropic diffusion weighted images at the level of the centrum semiovale and the basal ganglia level for the 4 different  $b$  values in an infant who had no evidence of abnormality on conventional MR or diffusion imaging (infant 3).

### ***Visual assessment of lesion conspicuity on isotropic diffusion weighted images and ADC maps***

In the cases of acute infarction, no new lesions were identified on isotropic diffusion weighted images obtained at higher  $b$  values compared

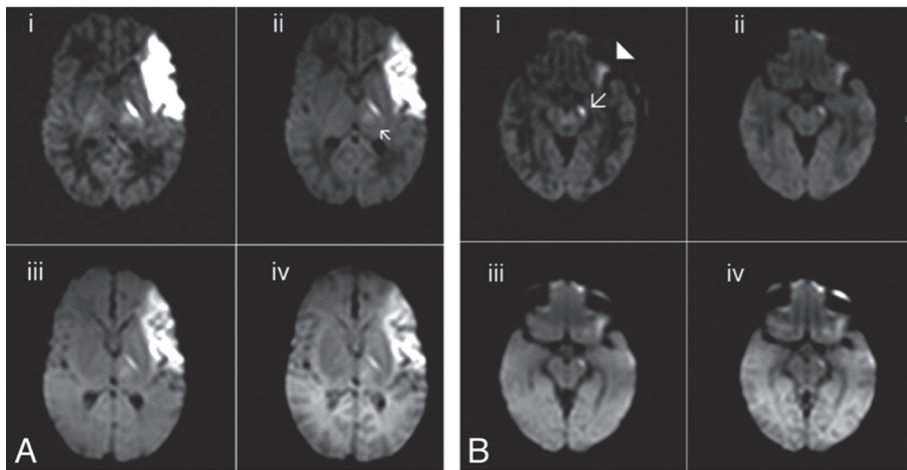


**Figure 3**

A. Isotropic diffusion weighted images and b. ADC maps demonstrating a left middle cerebral infarct in a term born infant (infant 4) and abnormal signal intensity in the left posterior limb of the internal capsule and left thalamus (arrow).

I.  $b = 3000 \text{ s/mm}^2$

II.  $b = 1500 \text{ s/mm}^2$

III.  $b = 700 \text{ s/mm}^2$

IV.  $b = 350 \text{ s/mm}^2$

B. Isotropic diffusion weighted images demonstrating Wallerian degeneration in the cortico-spinal tracts of the left mesencephalon (arrow). Susceptibility artefact appears reduced on the higher  $b$  value isotropic diffusion weighted images, thereby allowing the infarct in the left temporal lobe to be more clearly visualised (arrowhead).

I.  $b = 3000 \text{ s/mm}^2$

II.  $b = 1500 \text{ s/mm}^2$

III.  $b = 700 \text{ s/mm}^2$

IV.  $b = 350 \text{ s/mm}^2$

to those observed at lower  $b$  values. However, the contrast between regions of abnormality and adjacent tissue increased with increasing  $b$  value. Signal intensity change in the corticospinal tracts distal to the region of infarction consistent with Wallerian degeneration was much more clearly seen on the ADC map obtained from the  $b = 3000 \text{ s/mm}^2$  diffusion data than on those obtained at the lower  $b$  values. High  $b$  value DTI also clearly showed abnormal signal intensity of thalamic nuclei related to the injured cortex. Figure 3 shows isotropic diffusion weighted images of a left anterior branch middle cerebral artery infarction with abnormal signal intensity in the PLIC (Figure 3a), and Wallerian degen-

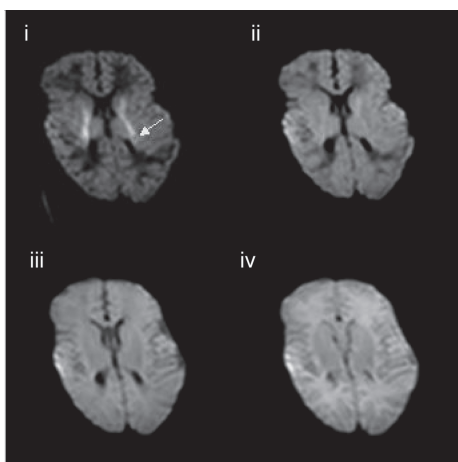


**Figure 4**

Isotropic diffusion weighted images of a term-born infant with transient hyperhomocysteinemia and Sotos syndrome (infant 9) demonstrating low signal intensity lesions in PLIC

I.  $b = 3000 \text{ s/mm}^2$

II.  $b = 1500 \text{ s/mm}^2$

III.  $b = 700 \text{ s/mm}^2$

IV.  $b = 350 \text{ s/mm}^2$

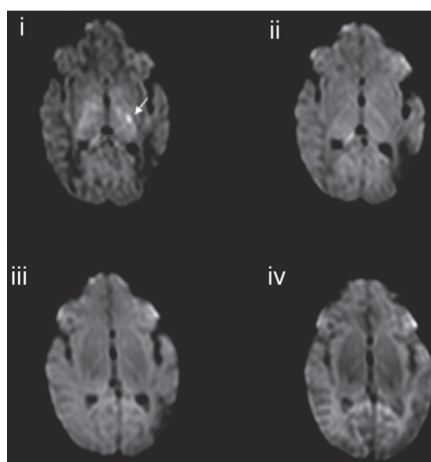


**Figure 5**

Isotropic diffusion weighted images in a term-born infant with a left sided middle cerebral artery infarction (infant 11) at 4 weeks of age demonstrating residual abnormal high signal intensity in the posterior limb of the internal capsule on the left on the  $b = 3000 \text{ s/mm}^2$  isotropic diffusion weighted image (arrow). Not demonstrated on the images obtained at lower  $b$  values. T2 shine through in the region of the infarct is reduced at high  $b$  values.

I.  $b = 3000 \text{ s/mm}^2$

II.  $b = 1500 \text{ s/mm}^2$

III.  $b = 700 \text{ s/mm}^2$

IV.  $b = 350 \text{ s/mm}^2$

eration in the mesencephalon (Figure 3b). Susceptibility artefact in the frontal and temporal regions appeared diminished on the high  $b$  value diffusion weighted images and a region of infarction in the left temporal region was more clearly seen on the  $b = 3000$  and  $b = 1500$  s/mm<sup>2</sup> isotropic diffusion weighted images compared to those obtained at lower  $b$  values (Figure 3b).

In an infant with transient hyperhomocysteinaemia and a later diagnosis of Sotos syndrome (infant 9), regions of low signal intensity representing cystic lesions were observed within the PLIC and the corona radiata on the  $b = 3000$  s/mm<sup>2</sup> isotropic diffusion image. These lesions were not identified on the isotropic diffusion images obtained at lower  $b$  values (Figure 4). Additionally, follow up images at one month of age in infant 11 with a left posterior branch middle cerebral artery infarct demonstrated abnormal high signal intensity within the left PLIC on the  $b = 3000$  s/mm<sup>2</sup> isotropic diffusion image. This lesion was not observed at lower  $b$  values. T2 shine-through in the region of infarction was observed on the isotropic diffusion weighted images obtained at  $b = 350$  s/mm<sup>2</sup>. This was reduced at  $b = 700$  s/mm<sup>2</sup>, and was not observed on the  $b = 1500$  and  $b = 3000$  s/mm<sup>2</sup> isotropic diffusion weighted images (Figure 5).

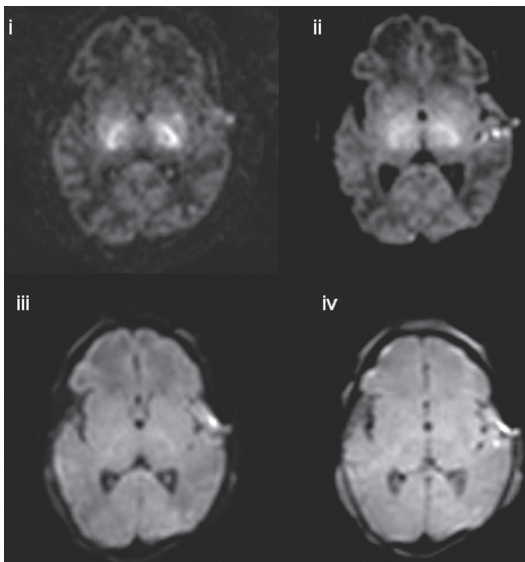


**Figure 6**

Isotropic diffusion weighted image at the level of the basal ganglia in a term born infant who had a history of perinatal asphyxia (infant 17). Lesions in the basal ganglia and in the mesencephalon were visualised on the isotropic diffusion weighted images obtained at  $b = 3000$  and  $b = 1500$ , which were not seen at lower  $b$  values.

I.  $b = 3000$  s/mm<sup>2</sup>

II.  $b = 1500$  s/mm<sup>2</sup>

III.  $b = 700$  s/mm<sup>2</sup>

IV.  $b = 350$  s/mm<sup>2</sup>

In 3 out of the 4 infants presenting with hypoxic-ischemic encephalopathy (HIE) (infants 8,10,14) no new lesions were identified on high  $b$  value DTI. However, in infant 17, lesions in the basal ganglia and in the mesencephalon were visualised on the isotropic diffusion weighted images obtained at  $b = 3000$  and  $b = 1500$ , which were not seen on those obtained at lower  $b$  values (Figure 6).

***Contrast ratio on normal appearing isotropic diffusion weighted images***

The contrast ratio between unmyelinated WM (frontal WM) and central GM (thalamus) and partially myelinated WM (central WM at the level of the centrum semiovale) increased with increasing  $b$  value for those infants who had no focal lesions on conventional MR or diffusion imaging. The contrast ratio between the thalamus and the PLIC also increased with increasing  $b$  value. Figure 7 shows contrast ratios for PLIC versus thalamus, thalamus versus frontal WM and the central WM of the centrum semiovale versus the frontal WM for infant 3.

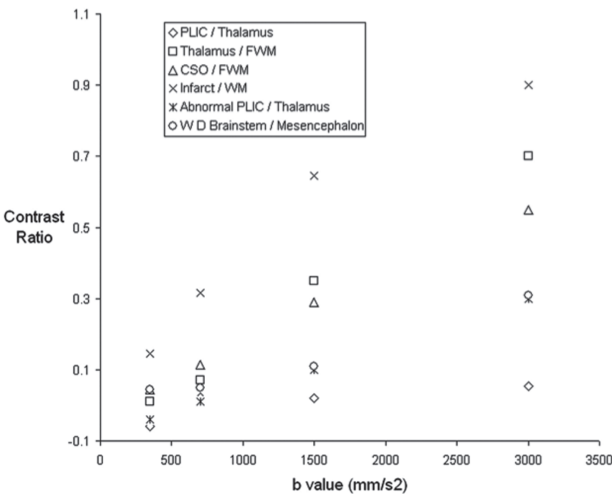


**Figure 7**  
Graph demonstrating contrast ratios between adjacent tissues on isotropic diffusion weighted images of an infant whose conventional and diffusion weighted imaging appeared normal (infant 3) and between areas of abnormal signal intensity and adjacent tissues on isotropic diffusion weighted images (infant 4).

**Contrast ratio of lesions to adjacent tissue on Isotropic diffusion weighted images**

Figure 7 shows the contrast ratios obtained for the signal intensity of the isotropic diffusion weighted images of a left sided middle cerebral artery territory infarct (infant 4) versus adjacent WM, the abnormal PLIC versus the adjacent thalamus and the region of Wallerian degeneration in the corticospinal tracts versus the adjacent mesencephalon tissue. The contrast ratio between lesion and adjacent tissue increased with increasing *b* value for all regions of abnormality examined.

**ADC values**

ADC values decreased with increasing *b* value in all regions studied. In WM there was an approximately linear trend in the reduction of ADC with increasing *b* value, whereas in the thalamus ADC declined more slowly at higher *b* value. Figure 8a shows change in ADC with *b* value for infant 3 who had no evidence of pathology on conventional MR or diffusion weighted imaging.

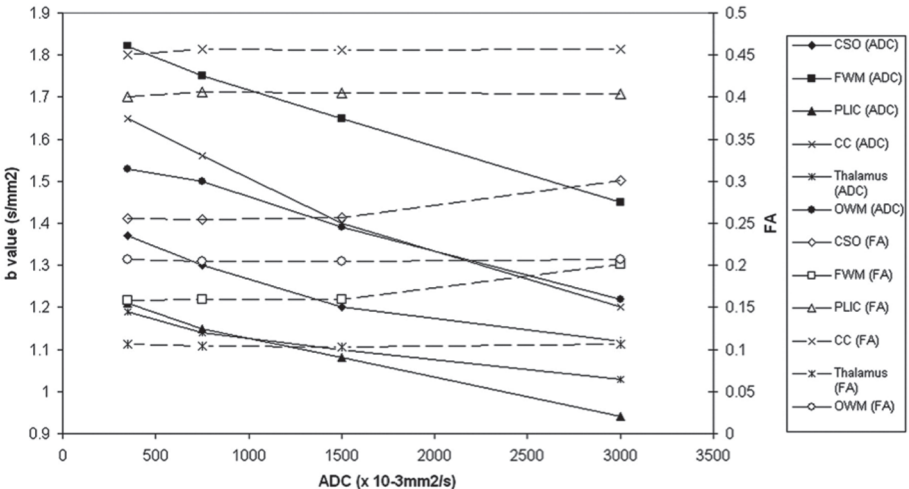


**Figure 8**  
a. Graph demonstrating ADC values versus *b* value for an infant whose conventional and diffusion weighted imaging appeared normal (infant 3).  
b. Graph demonstrating FA values versus *b* value for an infant whose conventional and diffusion weighted imaging appeared normal.



---

### **FA values**

There was no consistent change in FA with increasing  $b$  value in the neonatal brain. Figure 8b shows change in FA with  $b$  value for infant 3.

## **Discussion**

This study shows that image contrast and lesion conspicuity on isotropic diffusion weighted images increases with increasing  $b$  value. Our results show that, for  $b$  values between 350 and 3000 s/mm<sup>2</sup>, FA values are not altered by increasing  $b$  value, but ADC values in the white matter and central gray matter decrease with increasing  $b$  value.

We observed that contrast on isotropic diffusion weighted images increases at  $b$  values over 700 s/mm<sup>2</sup>. Similar to adult studies of infarction, our instances of acute infarction demonstrated that lesion conspicuity was increased at higher  $b$  values<sup>13</sup>. This was particularly striking in showing abnormal signal intensity changes distal to the infarction consistent with early Wallerian degeneration in the brain stem and in the PLIC. In addition, high  $b$ -value DTI made abnormal signal intensity in the ipsilateral thalamus more conspicuous. It has been shown that newborn stroke involving extensive parts of cerebral cortex immediately leads to secondary network injury in the thalamus presenting as hypersignal on DWI<sup>19</sup>. Amongst our cohort in a neonate with an anterior branch middle cerebral artery infarction, higher  $b$ -values revealed more clearly abnormal signal intensity of the thalamic nuclei related to the injured cortex. The relevance of network injury for prognosis is as yet unknown. The use of higher  $b$ -values to reveal acute network injury might give more insights.

New lesions were identified in one infant with Wallerian degeneration in the posterior limb of the internal capsule on follow-up imaging and in one infant with early but transient hyperhomocysteinaemia and Sotos syndrome on the isotropic diffusion weighted images obtained at a  $b$  value of 3000 s/mm<sup>2</sup>, that were not observed on the images obtained at lower  $b$  values. This suggests that the increase in isotropic diffusion image contrast with increasing  $b$  value may have an important clinical utility in

identifying lesions in some pathologies in the neonatal brain. In acute asphyxia, for example, the diagnostic role of DWI/DTI in the evaluation of deep gray matter injury is still not clear. In some cases DWI underestimated the extent of lesions or provided no further information compared to conventional MR imaging, whilst in other cases lesion detection was increased on DWI<sup>20</sup>. Future studies using high  $b$  value DTI in acute asphyxia are required to ascertain whether there is a role for this technique in assessing brain lesions in acute perinatal asphyxia.

Reductions in ADC values with increasing  $b$  values have previously been demonstrated in animal adult and paediatric studies<sup>6,7,8,9,11-13</sup>. In the adult brain, the ADC value of myelinated white matter becomes lower than that of gray matter with increasing  $b$  value<sup>9,10</sup>. In this study, ADC values in the partially myelinated PLIC became lower than ADC values in the thalamus at higher  $b$  values. However, ADC values in the other white matter regions studied here remained higher than those obtained in the central gray matter at all  $b$  values, reflecting the higher ADC of unmyelinated white matter compared to myelinated white matter<sup>23,24</sup>. In addition, whilst the reduction in ADC with increasing  $b$  value was approximately linear in the white matter, the rate of reduction in ADC values in the thalamus decreased at higher  $b$  values, suggesting that the difference between ADC values in the fast and slow compartments is less in central gray matter than in unmyelinated white matter. The change in measured ADC with different  $b$  values must be taken into account when attempting to compare diffusion data obtained at different imaging centres.

To our knowledge, the change in diffusion anisotropy with increasing  $b$  value has not been previously investigated in neonates, and the results of previous studies in adults are conflicting. One study observed no change in FA with increasing  $b$  value, consistent with the findings of our study, and suggests that the reduction in ADC is proportional for all eigenvectors of the diffusion tensor<sup>9</sup>. However, a more recent DTI study observed that FA of the slow component was significantly higher than that of the faster component<sup>11</sup>. This concurs with previous estimates of anisotropy (the anisotropy index) in the different compartments<sup>9-12</sup>. The reasons for the differing results between these adult brain studies are not clear, as both examined central gray matter and the PLIC and used  $b$

---

values up to 5000 s/mm<sup>2</sup>. However, it is possible that the differing results are due to the different approaches to calculating FA. Yoshiura et al used the same method as that used in our study to calculate FA at each *b* value, whilst Maier et al obtained fits for the fast and slow components of diffusion on a pixel by pixel basis using all measured *b* values, and then calculated FA separately for the 2 components<sup>9,11</sup>. Further DTI studies, over an extended range of *b* values and using the method described by Maier are required to confirm that FA does not change with increasing *b* value in the neonatal brain<sup>11</sup>.

Our results show a wide range of ADC and FA values in different regions in infants with no abnormalities identified on conventional or diffusion weighted imaging. These findings are in agreement with previous DTI studies in neonates at low *b* values, which have demonstrated greatest anisotropy in the highly organised white matter bundles of the corpus callosum and PLIC<sup>23</sup>. The lower ADC values and larger FA values in the central white matter of the centrum semiovale compared to the frontal and occipital white matter probably reflect the more advanced maturation of this white matter region, as the corticospinal tracts of the pre and post central sulcus show evidence of myelination in term neonates, but the occipital white matter does not show evidence of myelination until 3 months and the frontal white matter until around 6 months after birth<sup>25</sup>. Diffusion anisotropy in the thalamus is lower than in the white matter in adults and neonates which is consistent with the cytoarchitecture of this structure<sup>24-27</sup>.

One of the disadvantages of high *b* value DTI is that SNR is reduced. Whilst the higher SNR afforded by imaging at 3Tesla means that high *b* value DTI of the neonatal brain is feasible, even at this field strength, multiple signal averages were required to achieve adequate SNR. This increases image acquisition time and hence susceptibility to image degradation due to patient motion, which is of particular importance when imaging neonates. In order to avoid prohibitively long examination times, we investigated only 4 different *b* values in this study. This prevented us from exploring the possible non-monoexponential nature of diffusion signal decay at high *b* values.

## Conclusions

Our results show that up to  $b$  values of 3000 s/mm<sup>2</sup>, FA is not altered by increasing  $b$  value, but ADC values in the white matter and central gray matter decrease with increasing  $b$  value. In all of the white matter regions we studied this decrease was approximately linear, however in the thalamus the decrease in ADC with increasing  $b$  value appeared to be non-linear. Isotropic diffusion image contrast and lesion conspicuity increased with increasing  $b$  value. In acute infarction DTI obtained at high  $b$  values more clearly revealed secondary network injury in the ipsilateral thalamus and some lesions were identified in other pathologies on high  $b$ -values that were not visible at lower  $b$  values. Therefore, high  $b$  value DTI may have an important clinical utility in identifying lesions in the neonatal brain and understanding the timing and site of injury secondary to primary insults.

## References

1. F.M. Cowan, J.M. Pennock, J.D. Hanrahan, K.P. Manji, A.D. Edwards AD. Early detection of cerebral infarction and hypoxic ischemic encephalopathy in neonates using diffusion weighted magnetic resonance imaging. *Neuropediatrics* 1994;25:172-5
2. K.S. Krishnamoorthy, T.B. Soman, M. Takeoka, P.W. Schaefer. Diffusion-weighted imaging in neonatal cerebral infarction: clinical utility and follow-up. *J Child Neurol* 2000;15:592-602
3. F. Groenendaal, M.J. Benders, L.S. de Vries. Pre-wallerian degeneration in the neonatal brain following perinatal cerebral hypoxia-ischemia demonstrated with MRI. *Semin Perinatol* 2006;30:146-50
4. J. Mourmans, C.B. Majoie, P.G. Barth, M. Duran, E.M. Akkerman, B.T. Poll-The. Sequential MT imaging changes in nonketotic hyperglycinemia. *AJNR Am J Neuroradiol* 2006;27:209-11
5. H. Parmar, Y.Y. Sitoh, L. Ho. Maple syrup urine disease: diffusion-weighted and diffusion-tensor magnetic resonance imaging findings. *J Comput Assist Tomogr* 2004;28:93-7

6. T. Niendorf, R.M. Dijkhuizen, D.G. Norris, C.M. van Lookeren, K. Nicolay. Biexponential diffusion attenuation in various states of brain tissue: implications for diffusion-weighted imaging. *Magn Reson Med* 1996;36:847-57
7. J. Pfeuffer, S.W. Provencher, R. Gruetter. Water diffusion in rat brain in vivo as detected at very large b values is multicompartmental. *MAGMA* 1999;8:98-108
8. R.V. Mulkern, S. Vajapeyam, R.L. Robertson, P.A. Caruso, M.J. Rivkin, S.E. Maier. Biexponential apparent diffusion coefficient parametrization in adult vs newborn brain. *Magn Reson Imaging* 2001;19:659-68
9. T. Yoshiura, O. Wu, A. Zaheer, T.G. Reese, A.G. Sorensen. Highly diffusion-sensitized MRI of brain: dissociation of gray and white matter. *Magn Reson Med* 2001;45:734-40
10. M.C. DeLano, T.G. Cooper, J.E. Siebert, M.J. Potchen, K. Kuppusamy. High-b-value diffusion-weighted MR imaging of adult brain: image contrast and apparent diffusion coefficient map features. *AJNR Am J Neuroradiol* 2000;21:1830-6
11. S.E. Maier, S. Vajapeyam, H. Mamata, C.F. Westin, F.A. Jolesz, R.V. Mulkern. Biexponential diffusion tensor analysis of human brain diffusion data. *Magn Reson Med* 2004;51:321-30
12. C.A. Clark, D. Le Bihan. Water diffusion compartmentation and anisotropy at high b values in the human brain. *Magn Reson Med* 2000;44:852-9
13. J.R. Meyer, A. Gutierrez, B. Mock, D. Hebron, J.M. Prager, M.T. Gorey et al. High-b-value diffusion-weighted MR imaging of suspected brain infarction. *AJNR Am J Neuroradiol* 2000;21:1821-9
14. Y. Assaf, D. Ben Bashat, J. Chapman, S. Peled, I.E. Biton, M. Kafri et al. High b-value q-space analyzed diffusion-weighted MRI: application to multiple sclerosis. *Magn Reson Med* 2002;47:115-26
15. R.A. Jones, S. Palasis, J.D. Grattan-Smith. The evolution of the apparent diffusion coefficient in the pediatric brain at low and high diffusion weightings. *J Magn Reson Imaging* 2003;18:665-74
16. O. Dietrich, S. Heiland, K. Sartor. Noise correction for the exact determination of apparent diffusion coefficients at low SNR. *Magn Reson Med* 2001;45:448-53

17. D. Le Bihan, E. Breton, D.ALLEMAND, P. Grenier, E. Cabanis, M. Laval-Jeantet. MR imaging of intravoxel incoherent motions: application to diffusion and perfusion in neurologic disorders. *Radiology* 1986;161:401-7
18. P.J. Basser, C. Pierpaoli. Microstructural and physiological features of tissues elucidated by quantitative-diffusion-tensor MRI. *J Magn Reson B* 1996;111:209-19
19. P.P. Govaert, A. Zingman, Y.H. Jung, J. Dudink, R. Swarte, A. Zecic, V. Meersschaut, S. van Engelen, M. Lequin. Network injury to pulvinar with neonatal arterial ischemic stroke. *Neuroimage* 2008;39:1850-7
20. A.M. Roelants-van Rijn, P.G. Nikkels, F. Groenendaal, G.J. van der, P.G. Barth, I. Snoeck. Neonatal Diffusion-Weighted MR Imaging: Relation with Histopathology or Follow-Up MR Examination. *Neuropediatrics* 2001;32:286-94
21. J.S. Soul, R.L. Robertson, A.A. Tzika, A.J. du Plessis, J.J. Volpe. Time course of changes in diffusion-weighted magnetic resonance imaging in a case of neonatal encephalopathy with defined onset and duration of hypoxic-ischemic insult. *Pediatrics* 2001;108:1211-4
22. R.L. Robertson, L. Ben Sira, P.D. Barnes, R.V. Mulkern, C.D. Robson, S.E. Maier et al. MR line-scan diffusion-weighted imaging of term neonates with perinatal brain ischemia. *AJNR Am J Neuroradiol* 1999;20:1658-70
23. P.S. Huppi, S.E. Maier, S. Peled, G.P. Zientara, P.D. Barnes, F.A. Jolesz et al. Microstructural development of human newborn cerebral white matter assessed in vivo by diffusion tensor magnetic resonance imaging. *Pediatr Res* 1998;44:584-90
24. J.J. Neil, S.I. Shiran, R.C. McKinstry, G.L. Schefft, A.Z. Snyder, C.R. Almli et al. Normal brain in human newborns: apparent diffusion coefficient and diffusion anisotropy measured by using diffusion tensor MR imaging. *Radiology* 1998;209:57-66
25. A.J. Barkovich, B.O. Kjos, D.E. Jackson, D. Jr., Norman. Normal maturation of the neonatal and infant brain: MR imaging at 1.5 T. *Radiology* 1988;166:173-80
26. J.S. Shimony, R.C. McKinstry, E. Akbudak, J.A. Aronovitz, A.Z. Snyder, N.F. Lori et al. Quantitative diffusion-tensor anisotropy brain MR imaging: normative human data and anatomic analysis. *Radiology* 1999;212:770-84

- 
27. P. Mukherjee, J.H. Miller, J.S. Shimony, T.E. Conturo, B.C. Lee, C.R. Almli et al. Normal brain maturation during childhood: developmental trends characterized with diffusion-tensor MR imaging. *Radiology* 2001;221:349-58







# Chapter 6

## MAGNETIC RESONANCE IMAGING IN NEONATAL STROKE

---

M.H. Lequin  
J. Dudink  
K.A. Tong  
A. Obenaus

*Semin Fetal Neonatal Med.* 2009;14(5):299-310

## **Abstract**

Neonatal stroke occurs in 1 in 2300–5000 live births, the incidence of which is lower than that in adults, but still higher than that in childhood. The higher incidence of perinatal stroke in preterm and term infants compared to stroke in childhood may be partly explained by higher detection rates using routine fetal ultrasound and postnatal cranial sonography. In addition, there is greater availability of magnetic resonance imaging (MRI) for neuroimaging in preterm and full-term infants, which is due in part to the availability of MR-compatible incubators and MR systems at or near the neonatal intensive care unit. In addition, the wide range of MR techniques, such as T2-, diffusion- and susceptibility-weighted imaging allows improved visualization and quantification of neonatal stroke or hypoxic–ischemic injury. This chapter reviews the MR neuroimaging modalities that actually assist the clinician in the detection of neonatal stroke.

---

## **Rationale for magnetic resonance imaging (MRI)**

In contrast to adult stroke, the clinical presentation of neonatal stroke is often non-specific, including seizures, apnea, lethargy, poor feeding, hypotonia and asymmetrical weakness.<sup>1</sup> Ambiguous neonatal symptoms often delay the diagnosis, which can affect neurological outcome. The delay in diagnosis eliminates a reasonable therapeutic window for possible neuroprotection. In an attempt to minimize this delay as much as possible, physicians (neonatologists, pediatricians, and pediatric neurologists) have several non-invasive imaging options.

The first and often easiest option is cranial sonography, but this technique suffers from operator dependence and has not been found to be an objective tool for the detection and monitoring of neonatal stroke. An exception may be perforator stroke, which can be easily detected with cranial sonography.<sup>2</sup> A second option is computed tomography (CT) of the brain. Its advantage of rapid image acquisition and minimal use of sedation is tempered by its clear disadvantages that include radiation exposure and its low sensitivity for detection of early, small or infratentorial infarcts.

The third non-invasive imaging choice is MRI, which is the most sensitive technique to detect early stroke, particularly in the posterior circulation. MRI also carries no radiation risk and has multiple image contrasts that allow visualization of blood vessels of the neck and head and can be performed without having to administer intravenous contrast agents. Despite logistical issues, such as the need for sedation (which can be minimized or eliminated in the very early neonate) and competition for scanner time, MRI is the imaging modality of choice, especially for pial stroke. It not only allows early detection of stroke, but also eliminates various differential diagnoses by its unique ability to acquire multiple contrasts between different tissues by adjusting imaging parameters, without loss of significant signal, resolution, or anatomical detail.

We will focus on commonly used sequences for the detection of neonatal stroke: T1-weighted (T1WI), T2-weighted (T2WI) and diffusion-weighted

imaging (DWI) and their changes over time. Furthermore, we will discuss additional techniques, such as diffusion tensor imaging (DTI), MR angiography (MRA), perfusion-weighted MRI (PWI), MR proton spectroscopy (MRS), susceptibility weighted imaging (SWI), and functional MRI (fMRI). These additional techniques may provide a more accurate diagnosis and allow determination of time of onset and the underlying cause of neonatal stroke. More importantly, these neuroimaging approaches could provide and define a window for neuroprotective therapy. Finally, we will describe some new features for post-processing of neuroimaging data that could enable more accurate assessment of the extent of brain damage from neonatal stroke and the expected neurological outcome.

## **Current MRI modalities for neonatal stroke**

### ***T1- and T2-weighted MRI***

Within the first week after neonatal stroke, T2WI shows increased signal intensity (SI) in the affected cortex and white matter. Vasogenic edema in combination with cytotoxic edema increases the overall water content in the infarcted tissue, resulting in prolonged T2 relaxation times. This can make the infarct visible on T2WI between 24 and 48 h after its onset,<sup>3</sup> although it is sometimes poorly delineated due to the normal T2 hyperintensity of immature white matter. The visual disappearance of the affected cortical ribbon during this stage represents the so-called 'missing cortex sign'.<sup>4</sup> On T1WI the affected cortex exhibits low SI in the first week, from about day 2 after the onset of stroke. It is important to remember that the immature brain, particularly in the neonate, has a high water content that can confound MRI results (Fig. 1).<sup>5, 6</sup>

Next, from 1 week to 1 month, high SI is seen in the cortex on T1WI (cortical highlighting) and low cortical SI is seen on T2WI. Tanaka et al. showed an increase in lipid-laden microglia by day 7 in a rat model of focal brain ischemia.<sup>7</sup> Lectin staining revealed a correlation between T1 values and number of microglia observed.<sup>8</sup> The high protein content and accumulation of manganese in reactive astrocytes has also been

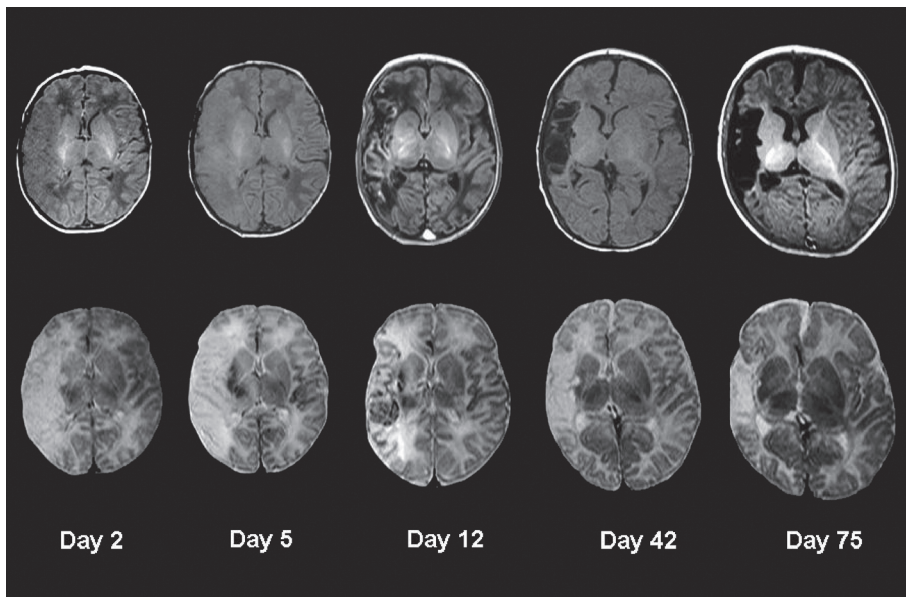


**Figure 1**

T1- and T2-weighted imaging of neonatal stroke. Serial T1 (upper row) and T2 (lower row)-weighted sequences within the first 3 months following perinatal stroke at term, involving the right middle cerebral artery (MCA) in its cortical area, sparing deep grey matter (complete pial MCA stroke). Stages of organization visualized here are discussed in the text. Tissue loss starts at the end of the second week. Reprinted from: Dudink J, Mercuri E, Al-Nakib L, Govaert P, Counsell SJ, Rutherford MA, Cowan FM. Evolution of unilateral perinatal arterial ischemic stroke on conventional and diffusion weighted MR imaging. *AJNR Am J Neuroradiol*, first published on Feb 26, 2009 as ©by American Society of Neuroradiology.

suggested to be integral to the SI changes on T1WI.<sup>9</sup> The low cortical SI seen on T2WI is thought to be related to petechial hemorrhages, release of myelin lipids, and/or calcifications.<sup>4</sup>

An intermediate variegated or ‘checkerboard’ pattern of mixed high and low SI in the areas of infarction can appear after 2–3 weeks in the neonate and subsequently progresses into areas of cystic tissue loss after 1–2 months.

### ***Diffusion-weighted imaging***

Numerous animal experiments have shown restricted diffusion within the infarcted parenchyma minutes after ischemia – possibly due to a net shift

of water from the extracellular space to the ‘slow’ diffusion compartment of the intracellular space.<sup>10</sup> The resultant cytotoxic edema is due to a net slowing of the water diffusion, with resultant high DWI SI.<sup>11, 12</sup>

DWI findings in the first week after ischemic injury are characterized by a hyperintense SI, with little change in the first few days after symptom onset, but a slowly decreasing SI thereafter.<sup>13</sup> DWI SI is not only influenced by water diffusibility but also by intrinsic T2 properties. This effect is called ‘T2 shine-through’ and can contribute to differences seen in DWI SI evolution between adults and newborns.<sup>14, 15</sup>

The quantitative measure of DWI, the apparent diffusion coefficient (ADC), is a reflection of water mobility within the tissues and is without T2 influence. Quantifiable ADC maps can help determine the age of ischemic lesions as shown in several adult stroke studies.<sup>15, 16, 17</sup> Early after injury the SI is opposite to DW images, such that shortly after stroke the infarcted area is hypointense due to cellular swelling that restricts water movement.<sup>18</sup> The lowest ADC values seem to occur around day 3 after lesion onset and may take 4–21 days for pseudonormalization.<sup>16, 17, 19</sup> A recent review of ADC values within normal neonates and those with strokes demonstrates significant regional differences between white and grey matter regions in the neonatal brain.<sup>6</sup> The value of DWI and ADC in neonatal stroke imaging is that it is the most sensitive marker for delineation of infarction and hypoxic–ischemic injury compared to more conventional imaging modalities such as T2WI. Thus, the first line of imaging of a putative neonatal stroke patient should be DWI.

### ***Diffusion tensor imaging***

A recent variant of DWI is application of diffusion gradients in multiple directions, to obtain water motion along different directions within the cerebral tissue. Thus, DTI allows the quantification and visualization of white matter pathways in vivo.<sup>20, 21</sup> DTI can also provide information about the organization of brain tissue and is sensitive to microstructural changes, even in the absence of abnormalities on conventional MR images. DTI characterizes the 3D spatial distribution of water diffusion in each MRI voxel. In cerebral white matter (WM), water diffuses preferentially along

the direction of axons and is restricted perpendicular to axons by myelin (Fig. 2).<sup>22</sup> This directional dependence is termed anisotropy.

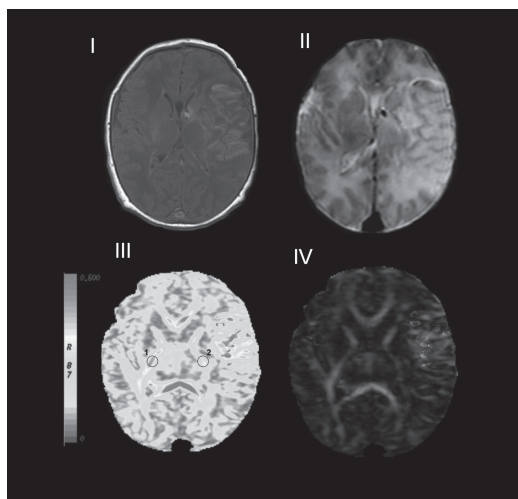


**Figure 2**

Diffusion tensor imaging. A magnetic resonance image of a term infant with left complete middle cerebral artery infarction: (I) T1-weighted image, (II) T2-weighted image, (III) fractional anisotropy (FA) map showing distorted FA values in the region of the infarction and (IV) RGB (red–green–blue) directionality color map. Two regions of interest (ROIs) are placed on the FA map (III) on the posterior limbs of the internal capsules showing clear differences in FA values between the contralateral (1 = 0.447) and the ipsilateral (2 = 0.295) sides. (A full color version of this illustration can be found in the color section).

Averaged mean diffusivity ( $D_{av}$ , or Trace) can be calculated as one-third of the trace of the diffusion tensor, and provides the overall magnitude of water diffusion.  $D_{av}$  is a useful parameter (similar to ADC) that can serve as an indicator of brain maturation and/or injury. Various anisotropy indices have been developed to describe the ratio between the eigenvalues (directional vectors from DTI) but there is still some debate as to which index is most sensitive for detecting anisotropy changes within the neonatal brain.<sup>23</sup> The anisotropy indices used primarily for neonatal brain studies are relative anisotropy (RA) and fractional anisotropy (FA). Quantification of these indices provides a comparative measure to standardized controls and may be useful in subtle instances of neonatal stroke or hypoxic–ischemic injury.

DTI information can be assessed using various visualization techniques, the most popular being red–green–blue (RGB)-coded directionality maps indicating the orientation of the major eigenvector of the diffusion tensor (Fig. 2). The directionality information allows for another DTI visualization technique, ‘fiber tracking’, which allows reconstruction of 3D white matter tracts by assuming that the orientation of the largest

component of the diagonalized diffusion tensor represents the orientation of dominant axonal tracts.<sup>24</sup> However, tractography requires longer imaging time and significant computational post-processing to visualize these data sets.

DTI, like DWI, can serve as an early indicator of stroke as it often demonstrates abnormalities on water diffusion maps well before conventional MRI.<sup>25</sup> A wealth of DTI data is available on animals and adults, but DTI data in human neonatal stroke are limited.<sup>26</sup> In contrast to ADC alone, the improved ability of DTI to distinguish between white and grey matter can allow separate quantitative assessment of these tissues in response to stroke. A future role for DTI could allow evaluation of neuroprotective strategies and assessment of their efficacy in different cerebral tissues. Maturation of white matter after stroke and its consequences for white matter connectivity can be followed throughout an infant's development, by correlating abnormalities on DTI and neurologic cognitive outcome.<sup>27</sup>

### ***Magnetic resonance angiography/venography***

In neonates with suspected stroke, the initial MR brain imaging protocol should include magnetic resonance angiography (MRA) and/or magnetic resonance venography (MRV) of the great arteries and veins at the neck and head. In children and adults MRA is as sensitive as conventional angiography for the detection of vasculopathy of the internal carotid and major cerebral arteries, but less sensitive for detection of smaller vessels.<sup>28, 29, 30</sup> Compared to adults, neonates have smaller vessels with lower blood flow velocities, making MRA and MRV of the neonatal brain a challenging procedure, not only to visualize the vascular anatomy, but also for assessing diameter and flow. MRA can be used to obtain anatomical and hemodynamic information at the level of the internal carotid arteries, vertebrobasilar arteries and circle of Willis. MRV can give anatomical and hemodynamic information of the superficial and deep venous system.

Three MRA/MRV methods are currently available: time of flight (TOF), phase contrast (PC) and contrast-enhanced (CE) MRA. TOF MRA (2D or 3D) visualizes the arterial lumen by inflow of unsaturated blood through



an image slice with pre-saturated static tissue.<sup>31</sup> The 2D TOF technique is more sensitive to slow arterial or venous flow whereas the 3D TOF MRA has the ability to cover a larger volume, which allows visualization of a larger trajectory of arteries with a high spatial resolution and a high signal-to-noise ratio (SNR). Especially in cases of suspected dissection of one of the cervical arteries, 3D TOF MRA is a better option than 2D TOF MRA. An important drawback of TOF MRA is its susceptibility to flow void artifacts, especially distal to a severe stenosis due to turbulence of blood flow,<sup>32</sup> which can result in exaggeration of stenosis. In addition, thrombus with T1 bright signal can also mimic flow signal, resulting in misinterpretation of patent vasculature.

PC MRA uses the phase shift in the signal induced by flowing blood where the signal intensity is directly correlated to the blood velocity and enables visualization of small vessels with slow-flowing blood. An advantage of PC MRA is the ability to create phase velocity maps that can be used for quantitative measurements of blood volume flowing through

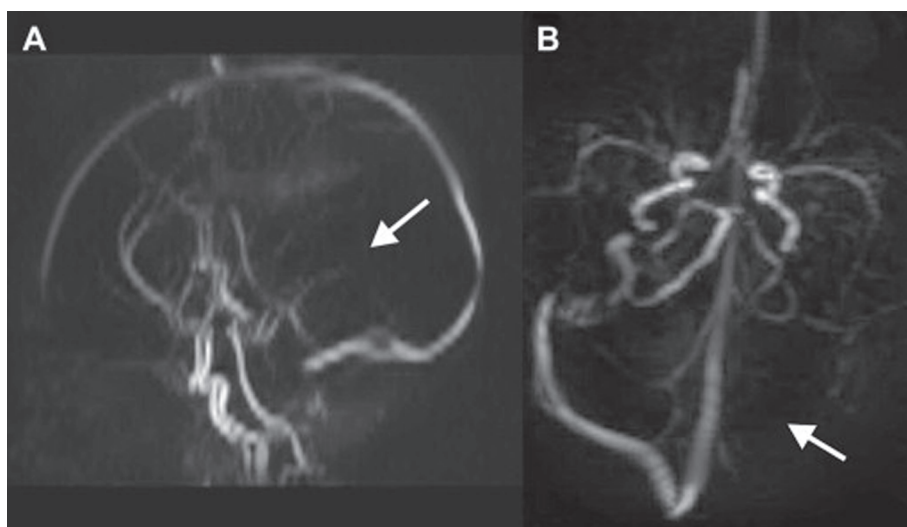


**Figure 3**

Phase contrast (PC) magnetic resonance angiography (MRA). A 5-day-old term boy who presented with inconsolable crying and apnea. The 3D PC MRA shows no filling of straight sinus or deep veins (A) and transverse sinus on the left side (B) suggestive of deep venous thrombosis. Operator-selected velocity thresholding may on the other hand also be the cause of non-visualization of veins, therefore sonographic confirmation of absence of flow in the left transverse sinus will establish the diagnosis.

a vessel. It also provides for better suppression of background brain tissue than the TOF MRA method (Fig. 3). Moreover, PC MRA gives information on flow direction and presence of collateral flow. This information can be crucial, given the large interindividual variability in the anatomy of the circle of Willis.<sup>33</sup> PC MRA can also be performed in a 2D and 3D mode but the 3D mode has a disadvantage of relatively long scanning time, introducing potential venous contamination.

CE MRA is another MRA method to visualize the head and neck arteries.<sup>34, 35</sup> It uses an intravenous bolus of gadolinium, a contrast agent, to shorten T1 relaxation of the blood. This allows utilization of larger flip angle to generate a stronger signal with improved background suppression in combination with less signal saturation (Fig. 4 and Fig. 5). To avoid venous contamination, the CE MRA sequences need to be fast and bolus-triggered. The advantages of CE over PC and TOF MRA include better visualization of small vessels and collaterals, as well as fewer flow-related artifacts (compare 3D PC MRV of Fig. 3A to CE MRV of Fig. 4A, performed in the same patient).

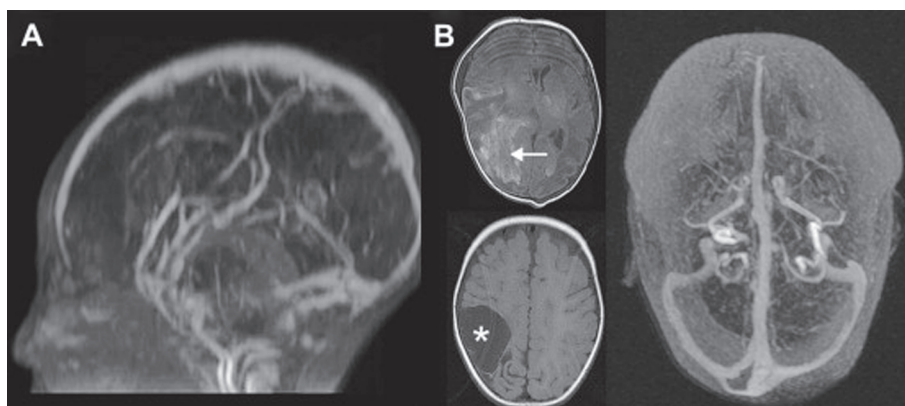


**Figure 4**

Two different patients illustrating Magnetic Resonance Angiography (MRA). (A) A late arterial phase 3D contrast-enhanced (CE) MRA in a 5-day-old term boy reveals no enhancement of the internal cerebral veins. The straight sinus and the vein of Galen enhance but there is no enhancement of the internal cerebral veins, suggesting deep venous thrombosis. (B) A 3D CE MRA follow-up of a 1-year-old girl who had bleeding in the right parieto-occipital region at birth (white arrow). The follow-up was performed to rule out an underlying vascular malformation and the MRA demonstrated no malformation. It was concluded that there was a posterior trunca infarction in the MCA territory (\*), likely due to thromboembolism.

---

In all MRA/MRV methods, maximum intensity projections (MIPs) can be reconstructed, providing multiple views of the vascular anatomy. These can be helpful in demonstrating anatomic variation and extracranial sources of collateral circulation. Due to very low flow in the deep and superficial intracranial venous system, MRV can give the false interpretation of an occlusion, especially when using the TOF or PC technique. Correlation with the sonographic findings is highly recommended.

In summary, all MRA/MRV methods can demonstrate absence of flow, suggesting total occlusion, anatomical variants, or reduced flow within the affected artery or vein, indicative of partial vessel occlusion. PC MRA provides additional information about the direction of flow in the affected and surrounding vessels. An unanswered question remains whether anatomical variations in vasculature predispose to injury, but future studies may resolve these issues (Table 1).

### ***Perfusion-weighted MRI***

Perfusion-weighted MRI (PWI) allows the assessment of cerebral hemodynamics from semi-quantitative maps of cerebral blood flow (CBF), cerebral blood volume (CBV), mean transit time (MTT), and time to peak (TTP). CT PWI is routinely performed in adults suspected of having a stroke, but MRI-derived PWI may be preferable for children, and especially neonates, as there is no radiation exposure, acquisition times are short, and better spatial coverage is achieved. Theoretically, PWI is even better suited to neonates as they have faster heart rate and smaller perfusion cross-sectional brain area than adults. But in spite of all this, PWI is not routinely used in neonates suspected of having had a stroke. One important reason is that the interpretation of the semiquantitative maps is complex due to age-related changes in brain perfusion and lack of normative data (similar issues are present for much of neonatal imaging). For the detection and understanding of pathology it would seem essential to have the requisite knowledge of changes in brain hemodynamics, both for normal neonates and for those with stroke. Another difficulty with PWI studies of the neonatal brain is the occurrence of motion artifacts, which prevent reliable quantification.

Today, two different MR PWI methods are available. The method most commonly applied is the so-called dynamic susceptibility contrast technique. It is based on a decrease of T2 or T2\* effect related to the passage of paramagnetic contrast material through the capillary bed.<sup>36</sup> Using the

**Table 1.** Magnetic resonance angiography (MRA) techniques.

MRA technique	Advantage	Disadvantage	Indications
TOF MRA 2D	No intravenous contrast necessary	Worse background suppression than PC MRA Flow void artifacts	Vascular anatomy
TOF MRA 3D	No intravenous contrast necessary Larger scan volume Better SNR than 2D	Worse background suppression than PC MRA Flow void artifacts	Vascular anatomy
PC MRA 2D	No intravenous contrast necessary Flow direction information	Small area of coverage	Vascular anatomy and hemodynamics (flow volume and direction)
PC MRA 3D	No intravenous contrast necessary Flow direction information Larger scan volume Better SNR than 2D	Relatively long scanning time	Vascular anatomy
CE MRA	High SNR Faster scanning time than TOF and PC	Need for bolus tracking in the case of MRA in arterial phase	Vascular anatomy
Perfusion: dynamic susceptibility contrast	Assessment of brain perfusion	Need for contrast agent	Hemodynamics
Arterial spin labelling	No intravenous contrast assessment of brain perfusion within selected intracranial arteries	Difficult to perform in neonates due to high heart rate	Hemodynamics

CE, contrast-enhanced; PC, phase contrast; SNR, signal-to-noise ratio; TOF, time of flight; 2/3D, two/three-dimensional.

---

drop in MR signal intensity we can assess multiple cerebral hemodynamics. For example, the time evolution of the contrast agent concentration can be monitored by acquiring dynamic images of the brain. Using this technique, Takahashi et al. found a lower CBF in neonates compared to older children and adults.<sup>37</sup> They also described age-dependent regional differences in cerebral perfusion, related to physiological development within the brain. In the neonate, the cerebral perfusion of the occipital lobe is prominent compared to the other brain regions. The frontal association cortex is the last region to show an increase in cerebral perfusion, far beyond the neonatal period, predominately during adolescence. A large study by Ball and Holland showed age-dependent differences in normal CBV between grey-to-white-matter.<sup>38</sup> The normal CBV ratio in neonates was not established because only a few neonates were included in this study. The most important finding from this study was that CBV, CBF and MTT maps should be symmetrical for both hemispheres in healthy children. Susceptibility-weighted PWI in neonates is further complicated by the difficulty of administering an adequate bolus of contrast agent and the need for a central line.

The second PWI method is arterial spin labeling (ASL), where inflowing protons (in red blood cells) are given a different magnetic state than the surrounding static tissues. The change in tissue magnetization is directly related to local cerebral perfusion. Unlike the dynamic susceptibility contrast technique, ASL does not require administration of a contrast agent and has the possibility of selective assessment of the contributions of all the great arteries feeding the brain. Thus, each vessel's perfusion territory can be mapped separately. There are two major categories: pulsed ASL and continuous ASL.<sup>39</sup> Each can be used for selective perfusion territory mapping of the internal carotid artery (ICA), vertebro-basilar artery (VBA), anterior cerebral artery (ACA) and middle cerebral artery (MCA) territories.<sup>40</sup> Quantification of CBF in children with severe steno-occlusive disease, such as sickle cell disease, can be problematic with ASL, owing to the relatively large contribution of collateral flow to the cerebral perfusion. In addition, labeled blood, flowing via collateral pathways, will arrive to the brain parenchyma with some delay, which results in overestimation of MTT delay and underestimation of the CBF. Several compensatory methods have been developed to correct for dif-

ferent arterial transit times.<sup>41, 42</sup> Fortunately, severe steno-occlusive disease is rare in neonates. Only a few research groups worldwide have some experience with ASL as a tool for assessment of brain perfusion in the pediatric population.<sup>43</sup> In neonates ASL is not routinely feasible due to a rapid heart rate.

Both PWI methods can assess focal or global cerebral hypoperfusion, such as in neonates who suffer a traumatic or spontaneous vascular dissection<sup>44</sup> or thromboembolic vessel occlusion. In adults suspected of having had a stroke, PWI is mostly performed primarily to compare with DWI or DTI results, to identify brain tissue at risk for progressing damage or future infarction. Regional differences between PWI and DWI yield information about the core and penumbra of ischemic tissues and can be important in clinical management decisions in the neonate. At the present time it is not clear, regrettably, whether a penumbra exists in some neonates suspected of stroke. One reason is the variability in tissue response. After the onset of ischemia PWI can show hypo- or hyperperfusion. For example, it is not clear whether hyperperfusion in an area of focal infarction with reduced ADC values is a normal reperfusion response of the neonatal brain. However, instead of preventing further infarction, it is more likely that reperfusion triggers neovascularisation and increased delivery of metabolites, which can result in increased tissue injury. Further research using serial PWI in neonates is needed to understand these processes as the response of the immature neonatal brain to ischemia may differ from that in adults.

### ***Proton MR spectroscopy***

It is beyond the scope of this review to provide the physical basis of proton MR spectroscopy (MRS) but a review by Roberts and Mikulis is comprehensive.<sup>45</sup> Proton MRS provides information about common metabolites such as: N-acetyl-aspartate (NAA) as a neuronal marker, choline-containing compounds (Cho) which reflect membrane turnover, creatine (Cr) as a bioenergetic marker, glutamate/glutamine (Glx) which are involved in many metabolic pathways, myoinositol (mIns) that is involved in the activation of protein C kinase, and finally, lactate/lipids that may reflect ischemic or necrotic processes.<sup>46</sup> Lactate can often be

---

observed in MRS spectra from ischemic brain tissue, due to anaerobic glycolysis. To date, only a few studies have used MRS for stroke detection<sup>47, 48, 49</sup> but MRS has been used with great success in neonatal and pediatric trauma.<sup>50</sup> As in severe asphyxia, brain tissue damaged by a neonatal stroke is characterized by reduced NAA and increased lactate, although to some extent this is dependent on the time interval between insult and scanning.

## **Emerging MR modalities for neonatal stroke**

### ***Functional magnetic resonance***

Functional magnetic resonance imaging (fMRI) is an effective method to study brain function, using changes in blood-oxygen-level-dependent (BOLD) signals related to increased neuronal activity.<sup>51</sup> Many researchers have applied this method to examine brain activity in patients suffering or having suffered from a variety of different diseases.<sup>51, 52, 53, 54</sup> Although sensitivity and speed of fMRI has improved due to faster acquisition techniques, stronger computational power and new processing algorithms, only a few studies have used fMRI to study neonatal stroke. These few studies focused primarily on the plasticity of the brain after stroke, whereas fMRI has not been used for evaluation of the neonatal brain in the setting of acute stroke. In summary, fMRI may be useful for short- and long-term follow-up to monitor for relocation of cortical function. The usefulness of fMRI in evaluation of neonatal stroke remains uncertain.

### ***Volumetric determination of stroke volumes***

Volumetric analysis is an established method for studying a variety of neurological disorders in the adult and pediatric populations.<sup>55, 56, 57</sup> Recently Ashwal et al., in an animal study using 3D volume measurement, demonstrated that lesion volume and location correlated with the degree of functional deficit.<sup>58</sup> Volumetric analysis may improve the assessment of the total and regional extent of injury needed for clinical decision-



making of therapeutic options and monitoring the effectiveness of neuroprotective strategies. Although current volumetric analysis of adult or neonatal stroke is still uncommon,<sup>59</sup> work is in progress to minimize the drawbacks. The primary reasons for limited clinical use of volumetric data are: (i) post-processing time for volumetric reconstruction of the 3D data set, (ii) the need for sophisticated software, (iii) current requirements for manual operator-dependent analysis, and (iv) overlay of volumetric data with localization to anatomical regions. Currently, only manual segmentation methods can reliably delineate the ischemic margins and tissues and this approach is very operator dependent.

Obenaus and Ashwal have developed an automated computational analysis for 3D data sets (Fig. 6).<sup>18</sup> Manual segmentation can take 2–3 h but the automated computer analysis can be less than 1 min and has

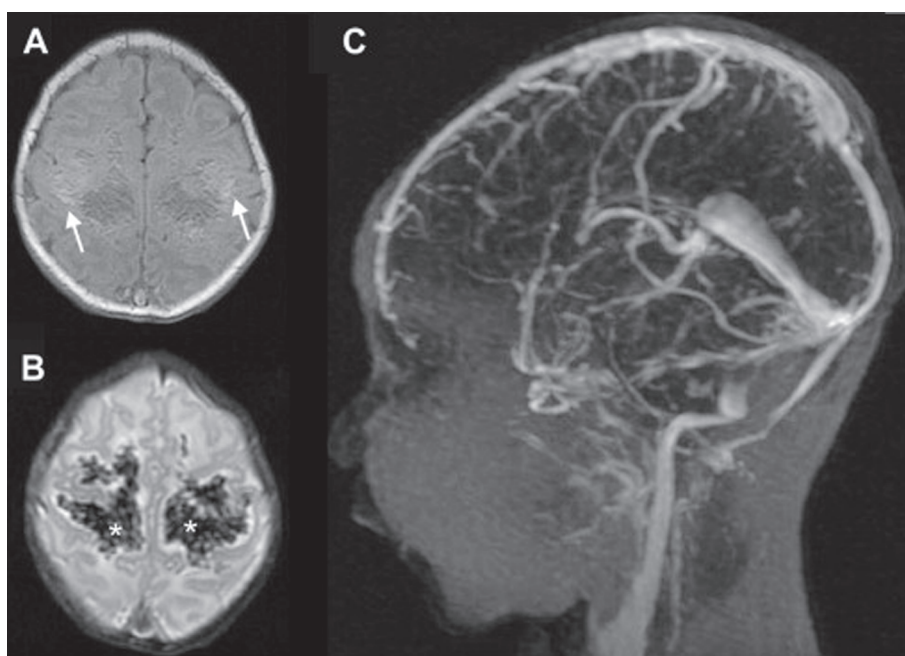


**Figure 5**

Venous phase contrast-enhanced magnetic resonance venography (CE MRV). A term girl presented with perinatal asphyxia; the T1-weighted image (A) demonstrated bleeding with a feathery shape (arrows) in the deep white matter. This was confirmed by the large deposits of blood (\*) on T2-weighted images (B). The 3D CE MRV (C) shows normal enhancement of the venous structures and ultrasound confirmed patency of both internal cerebral veins, the superior sagittal and both transverse sinus.



excellent concordance with ‘ground-truth’ manual segmentation (<5% variance). Aiming at better discriminatory power to distinguish between normal and ischemic brain tissue, which then would allow better assessment of severity and regional distribution, they used a whole-brain histogram analysis method.<sup>18</sup> Others have applied this method as well, primarily in tumors,<sup>60</sup> but Holtmannspotter et al.<sup>61</sup> also used it for evaluation of adult stroke patients, by analysing ADC histograms for assessment of severity and therapeutic evaluations. These ADC histograms can be used for automated threshold discrimination between normal and injured

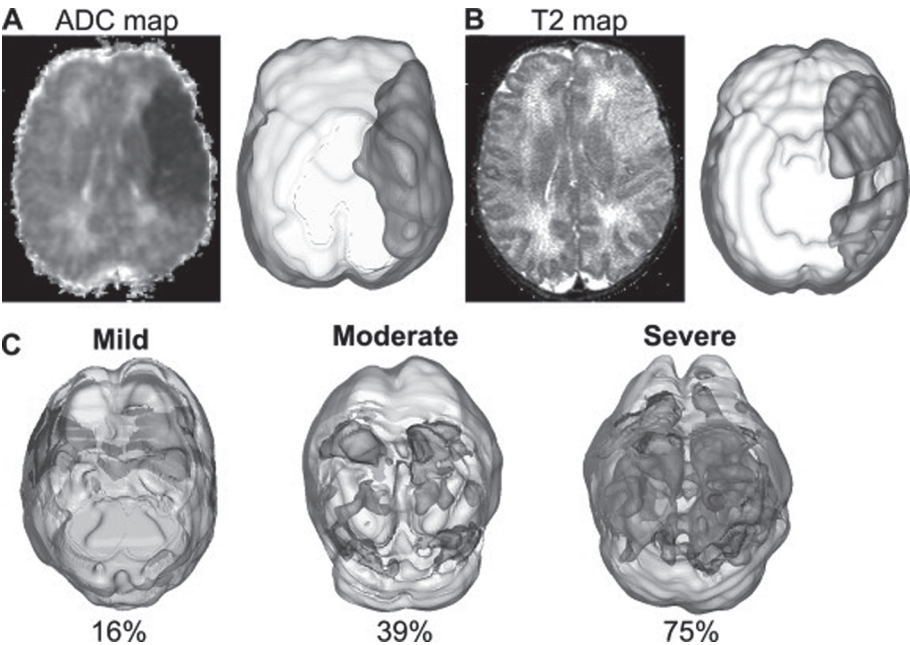


**Figure 6**

Volumetric reconstructions assist in localizing neonatal hypoxic ischemic injury. Volumetric reconstructions of magnetic resonance datasets can assist in localizing regions of injury in the arterial ischemic stroke and hypoxic ischemic injury neonate. (A) Using apparent diffusion coefficient (ADC) maps we can threshold for all ADC values below a value ( $<50 \times 10^{-6} \text{ mm}^2/\text{s}$ ), allowing rapid 3D localization of the lesion (patient was scanned at 4 days after birth). (B) In the same patient the T2 maps can also be used to localize the lesion. Note that the injury location and volume are different within this patient between the two imaging modalities and these differences may represent salvageable tissues. The 12-month outcome of this left middle cerebral artery occlusion patient was right hemiplegic cerebral palsy. (C) 3D volumetric hypoxic ischemic injury volumes from axial MRI scans of three newborns. The severity scaling (mild, moderate, severe) was determined from 12-month outcomes using their neurological outcome score. Individuals with poorer outcomes had higher percentage of injury (Courtesy of S. Ashwal). (A full color version of this illustration can be found in the color section).

regions. These early studies could have a great impact on the clinical decision-making process regarding neuroprotective treatment choices.

### ***Higher field strength***

The current clinical standard of 1.5T for MRI is rapidly being replaced by 3T MRI. The major advantage of 3T imaging is increased SNR, which allows for better DTI and MRA (as well as improved future use of MRS and fMRI). The increased susceptibility effects at 3T also make susceptibility-weighted PWI more robust (although still not quantitative). The higher field strengths can be used either to acquire MRI of similar quality (similar SNR to 1.5T) in a significantly shorter time period, or to acquire imaging of a higher quality (improved SNR compared to 1.5T) in the same amount of time. Standard neuroanatomic imaging can be performed in less time, allowing additional acquisition of other useful MR modalities, for example DTI and PWI. DTI, in turn, will be of better quality, allowing for higher resolution Dav and FA maps, and for better quality assessment of white matter imaging and fiber tracking, respectively. These parameters, in turn, can be used to quantify the amount of damage to regions of white matter and specific white matter tracts.<sup>62, 63</sup> Unfortunately, the noise from gradient switching on 3T scanners is significantly louder than that on 1.5T imagers, so it is essential to provide protection for children's ears. These and other considerations may make it more difficult to perform scans without sedation in the neonate.

### ***Susceptibility-weighted imaging***

This is a relatively new technique and is composed of a velocity-compensated 3D gradient-echo sequence, with unique post-processing. While 3D gradient echo imaging has been used previously to detect blood products, the novelty and power of SWI is that it uses both the magnitude and phase MR information.<sup>64, 65</sup> These two pieces of MR data are then combined after post-processing to provide high resolution SW images that have higher contrast-to-noise ratios, due to local susceptibility differences between tissues. SWI has been shown to be useful in measuring iron content, blood products and calcium deposits. Several investigators have showed applicability in a variety of different diseases,

such as multiple sclerosis, trauma, tumors, vascular malformations, as well as stroke.<sup>64, 65, 66, 67, 68, 69</sup> SWI can explain the occurrence of stroke due to sinovenous thrombosis much better than conventional imaging, as this condition is characterized by a higher concentration of intravascular deoxyhemoglobin due to venous stasis and greater prominence of collateral veins due to a nearby obstruction. SWI can also show thrombus in acute arterial stroke where the clot appears hypointense on SWI due to high concentrations of deoxyhemoglobin (Fig. 7).<sup>65</sup>

SWI is optimized to delineate the extent of parenchymal brain hemorrhage often seen in sinovenous infarction (Fig. 7). In addition Tong et al., in a recent review of pediatric and neonatal applications of SWI, described improved visibility of deep medullary veins in the penumbra region around an infarct, suggesting impaired CBF in the penumbra.<sup>70</sup> In particular, they reported an asymmetry in prominence of the medullary

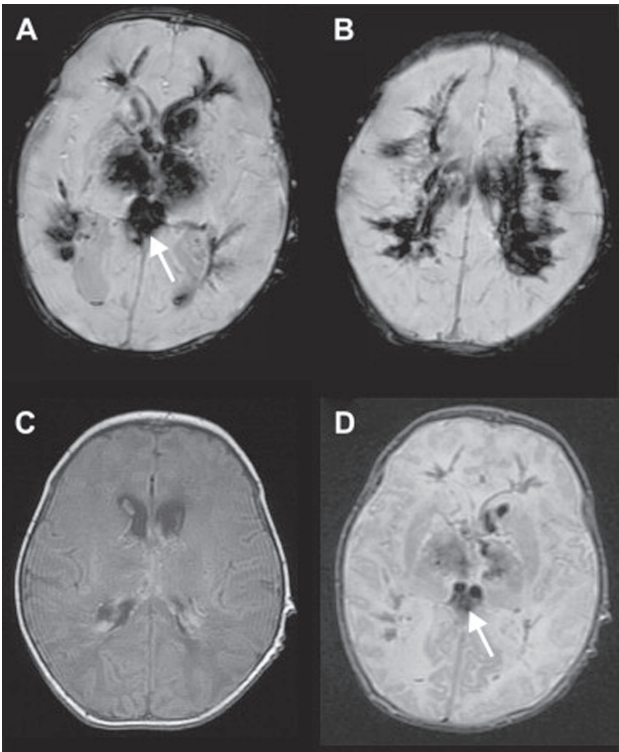


**Figure 7**  
Susceptibility-weighted imaging for hemorrhage in a term neonate illustrating extensive hemorrhage (A, B) due to a deep venous thrombosis that can be visualized with this new imaging method. The hemorrhage is also visible to a lesser extent on T1- (C) and T2-weighted images (D). The SWI and T2-weighted images shows the enlarged internal cerebral veins due to thrombosis (arrow). The primary occlusion was at the great cerebral vein of Galen.

veins just above the area of infarction, and speculated that this may be due to increased oxygen extraction in the penumbra region – possibly correlating with salvageable tissue at risk. Similar evidence from term neonates with global hypoxia or asphyxia would appear to lend support to this hypothesis but more research is required for validation of this interesting finding (Fig. 8)

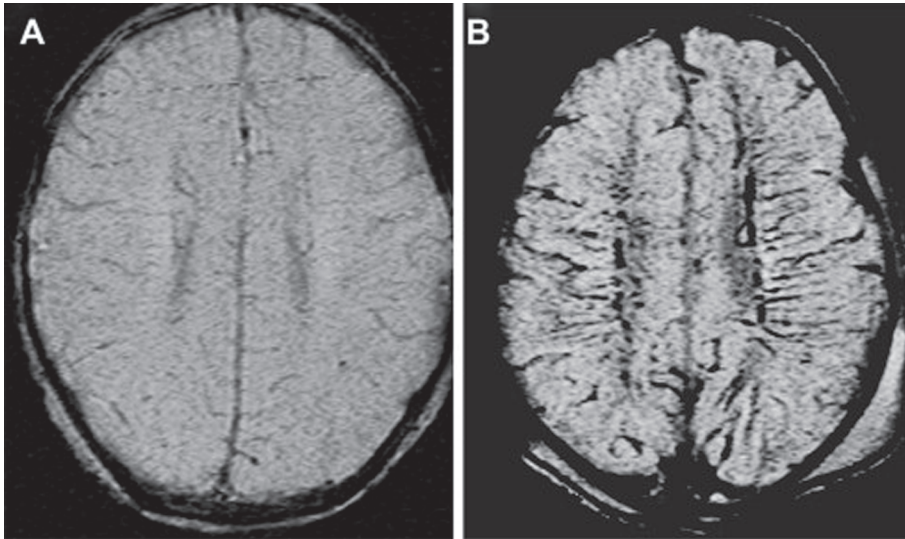


**Figure 8**

Susceptibility weighted imaging of prominent veins in neonatal hypoxia. (A) Control neonate showing a normal distribution of prominent veins. (B) In a profoundly hypoxic neonate the number of observable veins increases dramatically. It has been hypothesized that the appearance of these veins is due to increased extraction of oxygen and metabolic substrates after severe injury (Courtesy of D. Kido).

Thus, SWI can provide useful additional information in stroke and other neonatal conditions. However, clinical implementation is hampered by limited commercial availability. In addition, acquisition and post-processing techniques often vary between manufacturers. Also, the relative lack of availability of higher field strength (3T) MRI scanners is slowing the introduction of SWI for assessment of neonatal and pediatric populations. However, given the additional information it provides to the clinician, it is likely that SWI will become part of routine pediatric MRI protocols.

## Network injury

Awareness of network injury has increased due to the possibility of combining visible abnormalities from different MR modalities with expert knowledge about complex functional brain anatomy. This intriguing concept may lead to better understanding of the variability in neurological outcomes in perinatal stroke.

Recently, Govaert et al. presented the concept of secondary axonal effects of cell injury in nuclei connected to the primary lesion sites in neonates with arterial ischemic stroke.<sup>71</sup> Such effects are expected as axonal changes may first transmit excitotoxic injury and later result in cell death due to lack of trophic support. This study evaluated seven term infants with cortical stroke, showing hyperintensities in the pulvinar on DWI (Fig. 9).

Injury types included complete MCA, posterior cerebral artery, internal carotid artery, and multiple arterial territory strokes. ADC values in the secondarily injured pulvinar were significantly higher than in the region of the primary cortical injury. Because the pulvinar was outside of the

primary territory of infarction, and because these infants showed no evidence of hypoxia, the authors concluded that imaging suggested acute secondary injury to the pulvinar, i.e. following primary damage of their cortical targets and/or connecting axons.



**Figure 9**

Network injury, showing secondary injury to the pulvinar region of the thalamus (arrow) in a term neonate with left complete middle cerebral artery infarction as the primary injury.

Also the early stage of Wallerian degeneration in the corticospinal tract affected by stroke may be a manifestation of this network injury concept.<sup>72, 73, 74, 75, 76, 77</sup> Corticospinal tract hypersignals on DWI (with decreased ADC values) follows hyperintensities within the stroke area by hours (although it may be absent within the first day after the insult) and then subsides in the second to third week after the event. Often at later time points there is a return to normal diffusion in the stroke area (pseudonormalization). These hypersignals likely correspond to axonal swelling and restriction of axoplasmic transport.<sup>73</sup> The timing fits the early stage of Wallerian degeneration where axonal breakdown precedes myelin breakdown, the latter starting after about 4 weeks with first protein and later lipid dissolution in the myelin sheath, often resulting in permanent T2 hypersignal. A readily accessible method to quantify, in the acute stage, the extent of hypersignal in descending tracts can be obtained by thresholding grey values in the affected versus unaffected side. This approach refines the hypersignal, demonstrating that the middle part of the cerebral peduncle is an important prognostic site for cerebral palsy.<sup>78</sup> The interplay between axonal and myelin degeneration and injury can also be exquisitely assessed using radial and axial diffusion tensor metrics (see DTI above).

Many other studies have shown these secondary axonal effects by visualizing or measuring ADC differences in many brain regions in neonates – not only for stroke but also for global forebrain ischemia and leukomalacia.<sup>79, 80</sup> Tractography studies demonstrate reduced FA and axonal fiber count in corticospinal and corticobulbar tracts in adolescents with perinatal white matter lesions and cerebral palsy.<sup>81, 82</sup> These and future studies will uncover new patterns of network injury in the near future (Fig. 10).

The concept of secondary lesions is complex where acute injury may lead to cell necrosis followed by the maturation phenomenon where the time course of necrosis is dependent on the severity of injury. Apoptosis can follow a similarly fast time course, but in some instances it may take up to a week for a neuron to slowly die. The different time span between insult and admission to the hospital as well as the diversity in vulnerability of different brain regions currently make treatment difficult.



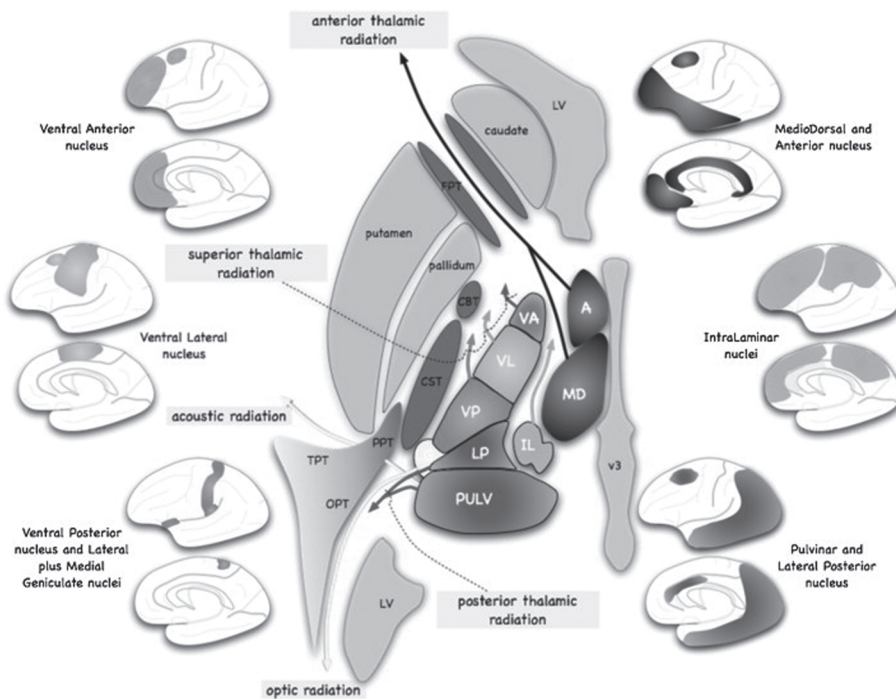


**Figure 10**

Corticothalamic network injury. Examples of possible network injuries from primary injury to various cortical areas resulting in secondary injury to different nuclei (in matching colors). (A full color version of this illustration can be found in the color section).

Therefore, keeping neuronal networks partially functioning by application of neuroprotective treatments, such as pharmacological therapy and cooling, may be an approach for improved neurological outcomes. Future research efforts should be directed at determining the relevance of delineating network injury, its influence on prognosis, and the impact of early treatment of a newborn with stroke.

## Conclusion

There are numerous MRI modalities available to the clinician to diagnose and monitor prognosis in the neonatal brain after stroke. While much still needs to be learned about the current MR armamentarium, new methods and approaches to MR imaging will expand the toolkit available to

help neonates. While development of new sequences is critical to the advancement of neonatal imaging, computational and post-processing methods are equally important. Thus, neonatal stroke imaging is still in its infancy and much research and clinical application of novel approaches are needed to assist the clinical evaluation of neonatal stroke.

## References

1. K.B. Nelson, Perinatal ischemic stroke. *Stroke* 2007;38:742–5
2. L. Abels, M. Lequin and P. Govaert, Sonographic templates of newborn perforator stroke. *Pediatr Radiol* 2006;36:663–9
3. A.J. Barkovich, The encephalopathic neonate: choosing the proper imaging technique. *AJNR Am J Neuroradiol* 1997;18:1816–20
4. A.J. Barkovich, K. Westmark, C. Partridge, A. Sola and D.M. Ferriero, Perinatal asphyxia: MR findings in the first 10 days. *AJNR Am J Neuroradiol* 1995;16: 427–38
5. V. Engelbrecht, A. Scherer, M. Rassek, H.J. Witsack and U. Modder, Diffusion-weighted MR imaging in the brain in children: findings in the normal brain and in the brain with white matter diseases. *Radiology* 2002;222:410–18
6. Coats JS, Freeberg AM, Pajela EG, Obenaus A, Ashwal S. A meta-analysis of apparent diffusion coefficients in the newborn brain. *Pediatr Neurol*, 2009;41:263-74
7. R. Tanaka, M. Komine-Kobayashi and H. Mochizuki et al., Migration of enhanced green fluorescent protein expressing bone marrow-derived microglia/macrophage into the mouse brain following permanent focal ischemia. *Neuroscience* 2003;117:531–9
8. D.E. Shan, H.C. Pan, D.M. Ho, M.M. Teng and C. Chang, Presence of activated microglia in a high-signal lesion on T1-weighted MR images: a biopsy sample re-examined. *AJNR Am J Neuroradiol* 2007;28:602
9. W.D. Heiss, J. Sobesky and V. Hesselmann, Identifying thresholds for penumbra and irreversible tissue damage. *Stroke* 2004;35:2671–4



10. T. Neumann-Haefelin, A. Kastrup and A. de Crespigny et al., Serial MRI after transient focal cerebral ischemia in rats: dynamics of tissue injury, blood–brain barrier damage, and edema formation. *Stroke* 2000;31:1965–72
11. P.A. Barber, L. Hoyte, D. Kirk, T. Foniok, A. Buchan and U. Tuor, Early T1- and T2-weighted MRI signatures of transient and permanent middle cerebral artery occlusion in a murine stroke model studied at 9.4T. *Neurosci Lett* 2005;388:54–9
12. M. Qiao, K.L. Malisza, M.R. Del Bigio and U.I. Tuor, Transient hypoxia–ischemia in rats: changes in diffusion-sensitive MR imaging findings, extracellular space, and Na<sup>+</sup>-K<sup>+</sup>-adenosine triphosphatase and cytochrome oxidase activity. *Radiology* 2002;223:65–75
13. J. Dudink, D.J. Larkman and O. Kapellou et al., High b-value diffusion tensor imaging of the neonatal brain at 3T. *AJNR Am J Neuroradiol* 2008;29:1966–72
14. A.J. Barkovich, MR imaging of the neonatal brain, *Neuroimaging Clin N Am* 16 (2006), pp. 117–135 viii–ix.
15. J.B. Fiebach, O. Jansen, P.D. Schellinger, S. Heiland, W. Hacke and K. Sartor, Serial analysis of the apparent diffusion coefficient time course in human stroke. *Neuroradiology* 2002;44:294–8
16. H.L. Lutsep, G.W. Albers, A. DeCrespigny, G.N. Kamat, M.P. Marks and M.E. Moseley, Clinical utility of diffusion-weighted magnetic resonance imaging in the assessment of ischemic stroke. *Ann Neurol* 1997;41:574–80
17. G. Stoll, S. Jander and M. Schroeter, Inflammation and glial responses in ischemic brain lesions. *Prog Neurobiol* 1998;56:149–71
18. A. Obenaus and S. Ashwal, Magnetic resonance imaging in cerebral ischemia: focus on neonates, *Neuropharmacology* 2008;55:271–80
19. G. Schlaug, B. Siewert, A. Benfield, R.R. Edelman and S. Warach, Time course of the apparent diffusion coefficient (ADC) abnormality in human stroke. *Neurology* 1997;49:113–9
20. P.J. Basser, J. Mattiello and D. LeBihan, Estimation of the effective self-diffusion tensor from the NMR spin echo. *J Magn Reson B* 1994;103:247–54
21. P.J. Basser and C. Pierpaoli, Microstructural and physiological features of tissues elucidated by quantitative-diffusion-tensor MRI. *J Magn Reson B* 1996;111:209–19
22. C. Beaulieu, The basis of anisotropic water diffusion in the nervous system – a technical review. *NMR Biomed* 2002;15:435–55

23. C. van Pul, J. Buijs, M.J. Janssen, G.F. Roos, M.T. Vlaardingerbroek and P.F. Wijn, Selecting the best index for following the temporal evolution of apparent diffusion coefficient and diffusion anisotropy after hypoxic–ischemic white matter injury in neonates. *AJNR Am J Neuroradiol* 2005;26:469–81
24. D.K. Jones, Studying connections in the living human brain with diffusion MRI, *Cortex* 2008;44:936–52
25. C.H. Sotak, The role of diffusion tensor imaging in the evaluation of ischemic brain injury – a review. *NMR Biomed* 2002;15:561–9
26. M.L. Seghier, F. Lazeyras and S. Zimine et al., Combination of event-related fMRI and diffusion tensor imaging in an infant with perinatal stroke. *Neuroimage* 2004;21:463–72
27. P.S. Huppi and J. Dubois, Diffusion tensor imaging of brain development. *Semin Fetal Neonatal Med* 2006;11:489–97
28. B. Husson and P. Lasjaunias, Radiological approach to disorders of arterial brain vessels associated with childhood arterial stroke – a comparison between MRA and contrast angiography. *Pediatr Radiol* 2004;34:10–5
29. N. Rollins, M. Dowling, T. Booth and P. Purdy, Idiopathic ischemic cerebral infarction in childhood: depiction of arterial abnormalities by MR angiography and catheter angiography. *AJNR Am J Neuroradiol* 2000;21:549–56
30. B. Husson, G. Rodesch, P. Lasjaunias, M. Tardieu and G. Sebire, Magnetic resonance angiography in childhood arterial brain infarcts: a comparative study with contrast angiography. *Stroke* 2002;33:1280–5
31. D.L. Parker, D.J. Parker, D.D. Blatter, Y.P. Du and K.C. Goodrich, The effect of image resolution on vessel signal in high-resolution magnetic resonance angiography. *J Magn Reson Imaging* 1996;6:632–41
32. R.M. Hoogeveen, C.J. Bakker and M.A. Viergever, Phase-derivative analysis in MR angiography: reduced Venc dependency and improved vessel wall detection in laminar and disturbed flow. *J Magn Reson Imaging* 1997;7:321–330
33. A.W. Hoksbergen, C.B. Majoie, F.J. Hulsmans and D.A. Legemate, Assessment of the collateral function of the circle of Willis: three-dimensional time-of-flight MR angiography compared with transcranial color-coded duplex sonography. *AJNR Am J Neuroradiol* 2003;24:456–62

- 
34. P.J. Nederkoorn, Y. van der Graaf and M.G. Hunink, Duplex ultrasound and magnetic resonance angiography compared with digital subtraction angiography in carotid artery stenosis: a systematic review. *Stroke* 2003;34:1324–32
  35. W.A. Willinek, J. Gieseke and R. Conrad et al., Randomly segmented central k-space ordering in high-spatial-resolution contrast-enhanced MR angiography of the supraaortic arteries: initial experience. *Radiology* 2002;25:583–8
  36. T.A. Huisman and A.G. Sorensen, Perfusion-weighted magnetic resonance imaging of the brain: techniques and application in children. *Eur Radiol* 2004;14:59–72
  37. T. Takahashi, R. Shirane, S. Sato and T. Yoshimoto, Developmental changes of cerebral blood flow and oxygen metabolism in children. *AJNR Am J Neuroradiol* 1999;20:917–22
  38. W.S. Ball Jr. and S.K. Holland, Perfusion imaging in the pediatric patient. *Magn Reson Imaging Clin N Am* 2001;9:207–30
  39. M. Wintermark, M. Sesay and E. Barbier et al., Comparative overview of brain perfusion imaging techniques. *Stroke* 2005;36:83–99
  40. R. Werner, D.G. Norris, K. Alfke, H.M. Mehdorn and O. Jansen, Continuous artery-selective spin labeling (CASSL). *Magn Reson Med* 2005;53:1006–12
  41. J.B. Gonzalez-At, D.C. Alsop and J.A. Detre, Cerebral perfusion and arterial transit time changes during task activation determined with continuous arterial spin labeling. *Magn Reson Med* 2000;43:739–46
  42. J. Hendrikse, M.J. van Osch and D.R. Rutgers et al., Internal carotid artery occlusion assessed at pulsed arterial spin-labeling perfusion MR imaging at multiple delay times. *Radiology* 2004;233:899–904
  43. J. Wang, D.J. Licht and G.H. Jahng et al., Pediatric perfusion imaging using pulsed arterial spin labeling. *J Magn Reson Imaging* 2003;18:404–13
  44. M.H. Lequin, E.A. Peeters, H.C. Holscher, R. de Krijger and P. Govaert, Arterial infarction caused by carotid artery dissection in the neonate. *Europ J Paediatr Neurol* 2004;8:155–60
  45. T.P. Roberts and D. Mikulis, Neuro MR: principles. *J Magn Reson Imaging* 2007;26:823–37
  46. T. Michaelis, K.D. Merboldt, H. Bruhn, W. Hanicke and J. Frahm, Absolute concentrations of metabolites in the adult human brain in vivo: quantification of localized proton MR spectra. *Radiology* 1993;187:219–27

47. P. Gideon, O. Henriksen and B. Sperling et al., Early time course of N-acetylaspartate, creatine and phosphocreatine, and compounds containing choline in the brain after acute stroke. A proton magnetic resonance spectroscopy study. *Stroke* 1992;23:1566–72
48. S.K. Shu, S. Ashwal, B.A. Holshouser, G. Nystrom and D.B. Hinshaw Jr., Prognostic value of <sup>1</sup>H-MRS in perinatal CNS insults. *Pediatr Neurol* 1997;17:309–18
49. A. Venkataraman, P.B. Kingsley and P. Kalina et al., Newborn brain infarction: clinical aspects and magnetic resonance imaging. *CNS Spectr* 2004;9:436–44
50. S. Ashwal, B.A. Holshouser and K.A. Tong, Use of advanced neuroimaging techniques in the evaluation of pediatric traumatic brain injury. *Dev Neurosci* 2006;28:309–26
51. S. Ogawa, T.M. Lee, A.S. Nayak and P. Glynn, Oxygenation-sensitive contrast in magnetic resonance image of rodent brain at high magnetic fields. *Magn Reson Med* 1990;14:68–78
52. S.S. Kannurpatti, B.B. Biswal and A.G. Hudetz, Regional dynamics of the fMRI-BOLD signal response to hypoxia–hypercapnia in the rat brain. *J Magn Reson Imaging* 2003;17:641–7
53. S.G. Kim and S. Ogawa, Insights into new techniques for high resolution functional MRI. *Curr Opin Neurobiol* 2002;12:607–15
54. R.S. Menon, Imaging function in the working brain with fMRI. *Curr Opin Neurobiol* 2001;11:630–6
55. S.K. Schiemanck, M.W. Post, G. Kwakkel, T.D. Witkamp, L.J. Kappelle and A.J. Prevo, Ischemic lesion volume correlates with long-term functional outcome and quality of life of middle cerebral artery stroke survivors. *Restor Neurol Neurosci* 2005;23:257–63
56. J.N. Fink, M.H. Selim and S. Kumar et al., Is the association of National Institutes of Health Stroke Scale scores and acute magnetic resonance imaging stroke volume equal for patients with right- and left-hemisphere ischemic stroke? *Stroke* 2002;33:954–8
57. P.S. Huppi and T.E. Inder, Magnetic resonance techniques in the evaluation of the perinatal brain: recent advances and future directions. *Semin Neonatol* 2001;6:195–210
58. S. Ashwal, B. Tone, H.R. Tian, S. Chong and A. Obenaus, Comparison of two neonatal ischemic injury models using magnetic resonance imaging. *Pediatr Res* 2007;61:9–14

- 
59. D. Mungas, B.R. Reed and W.J. Jagust et al., Volumetric MRI predicts rate of cognitive decline related to AD and cerebrovascular disease. *Neurology* 2002;59:867-73
  60. S.C. Steens, F. Admiraal-Behloul and J.A. Schaap et al., Reproducibility of brain ADC histograms. *Eur Radiol* 2004;14:425-30
  61. M. Holtmannspotter, N. Peters and C. Opherck et al., Diffusion magnetic resonance histograms as a surrogate marker and predictor of disease progression in CADASIL: a two-year follow-up study. *Stroke* 2005;36:2559-65
  62. S.P. Miller, D.B. Vigneron and R.G. Henry et al., Serial quantitative diffusion tensor MRI of the premature brain: development in newborns with and without injury, *J Magn Reson Imaging* 2002;16:621-32
  63. S.C. Partridge, P. Mukherjee and J.I. Berman et al., Tractography-based quantitation of diffusion tensor imaging parameters in white matter tracts of preterm newborns, *J Magn Reson Imaging* 2005;22:467-74
  64. E.M. Haacke, S. Mittal, Z. Wu, J. Neelavalli and Y.C. Cheng, Susceptibility-weighted imaging: technical aspects and clinical applications, part 1. *AJNR Am J Neuroradiol* 2009;30:19-30
  65. S. Mittal, Z. Wu, J. Neelavalli and E.M. Haacke, Susceptibility-weighted imaging: technical aspects and clinical applications, part 2. *AJNR Am J Neuroradiol* 2009;30:232-52
  66. T. Babikian, M.C. Freier and K.A. Tong et al., Susceptibility weighted imaging: neuropsychologic outcome and pediatric head injury. *Pediatr Neurol* 2005;33:184-94
  67. B. Thomas, S. Somasundaram and K. Thamburaj et al., Clinical applications of susceptibility weighted MR imaging of the brain – a pictorial review. *Neuroradiology* 2008;50:105-16
  68. J. Hu, Y. Yu and C. Juhasz et al., MR susceptibility weighted imaging (SWI) complements conventional contrast enhanced T1 weighted MRI in characterizing brain abnormalities of Sturge-Weber syndrome. *J Magn Reson Imaging* 2008;28: 300-7
  69. L.J. Bagley, R.I. Grossman and K.D. Judy et al., Gliomas: correlation of magnetic susceptibility artifact with histologic grade. *Radiology* 1997;202:511-6
  70. K.A. Tong, S. Ashwal, A. Obenaus, J.P. Nickerson, D. Kido and E.M. Haacke, Susceptibility-weighted MR imaging: a review of clinical applications in children. *AJNR Am J Neuroradiol* 2008;29:9-17

71. P. Govaert, A. Zingman and Y.H. Jung et al., Network injury to pulvinar with neonatal arterial ischemic stroke. *Neuroimage* 2008;39:1850–7
72. R.C. McKinstry, J.H. Miller and A.Z. Snyder et al., A prospective, longitudinal diffusion tensor imaging study of brain injury in newborns. *Neurology* 2002;59:824–33
73. A. Mazumdar, P. Mukherjee, J.H. Miller, H. Malde and R.C. McKinstry, Diffusion-weighted imaging of acute corticospinal tract injury preceding Wallerian degeneration in the maturing human brain. *AJNR Am J Neuroradiol* 2003;24:1057–66
74. A. Uchino, A. Sawada, Y. Takase, R. Egashira and S. Kudo, Transient detection of early wallerian degeneration on diffusion-weighted MRI after an acute cerebrovascular accident. *Neuroradiology* 2004;46:183–8
75. R.W. Hunt, J.J. Neil, L.T. Coleman, M.J. Kean and T.E. Inder, Apparent diffusion coefficient in the posterior limb of the internal capsule predicts outcome after perinatal asphyxia, *Pediatrics* 2004;114:999–1003
76. L.S. De Vries, J. Van der Grond, I.C. Van Haastert and F. Groenendaal, Prediction of outcome in new-born infants with arterial ischaemic stroke using diffusion-weighted magnetic resonance imaging, *Neuropediatrics* 2005;36:12–20
77. F.M. Cowan and L.S. de Vries, The internal capsule in neonatal imaging. *Semin Fetal Neonatal Med* 2005;10:461–74
78. A. Kirton, M. Shroff, T. Visvanathan and G. deVeber, Quantified corticospinal tract diffusion restriction predicts neonatal stroke outcome. *Stroke* 2007;38:974–80
79. D. Ricci, S. Anker and F. Cowan et al., Thalamic atrophy in infants with PVL and cerebral visual impairment. *Early Hum Dev* 2006;82:591–5
80. M. Rutherford, S. Counsell and J. Allsop et al., Diffusion-weighted magnetic resonance imaging in term perinatal brain injury: a comparison with site of lesion and time from birth. *Pediatrics* 2004;114:1004–14
81. S.J. Counsell, L.E. Dyet and D.J. Larkman et al., Thalamo-cortical connectivity in children born preterm mapped using probabilistic magnetic resonance tractography. *Neuroimage* 200;734:896–904
82. B. Thomas, M. Eyssen and R. Peeters et al., Quantitative diffusion tensor imaging in cerebral palsy due to periventricular white matter injury. *Brain* 2005;128:2562–77









# Chapter 7

## EVOLUTION OF UNILATERAL PERINATAL ARTERIAL ISCHEMIC STROKE ON CONVENTIONAL AND DIFFUSION WEIGHTED MAGNETIC RESONANCE IMAGING

---

J. Dudink  
E. Mercuri  
L. Al-Nakib  
P.P. Govaert  
S.J. Counsell  
M.A. Rutherford  
F.M. Cowan

*AJNR Am J Neuroradiol. 2009;30(5):998-1004*

## **Abstract**

### ***Background and purpose***

Knowledge of the sequence of signal intensity (SI) change on conventional and diffusion weighted (DW) imaging following perinatal arterial ischemic stroke (PAIS) is limited, adding to the difficulty in timing the onset of PAIS. We report PAIS evolution on serial conventional and DW MR scans from symptomatic term infants.

### ***Materials and Methods***

We documented serial changes on T1 and T2-weighted and DW images over 3 post-natal months after unilateral PAIS. A visual SI scoring system was used (-1=lower, 0=equal, 1=higher) compared to the contralateral hemisphere.

### ***Results***

We analyzed 43 scans (mean age first scan day 4) from 21 term infants. Changes in SI on conventional T1 and T2 images were remarkably consistent between infants. The cortex was of low SI on T1 and high SI on T2 until day 6 when SIs reversed and cortical highlighting was seen for 1-2 months. The white matter was high SI on T1 in the first 8-9 days and on T2 for >2 weeks before becoming low SI. Secondary SI changes remote from the infarction were seen in the thalamus and brainstem in the first week and atrophy was seen from 4 weeks. All DW images showed high SI of the affected region until at least day 4, which fell to =/below that of the contralesional hemisphere by day 12.

### ***Conclusion***

The pattern of SI change on conventional and DW images following PAIS was remarkably consistent between patients suggesting that PAIS in symptomatic term-born infants occurs within a very limited time frame around birth.

---

## Introduction

Perinatal arterial ischemic stroke (PAIS) is an important cause of long-term neurologic morbidity including cerebral palsy, epilepsy and cognitive impairment<sup>1-6</sup>. The incidence of neonatally symptomatic PAIS is at least 1/4000 term liveborn infants<sup>7</sup>. Newborn term infants with PAIS most often present with seizures having been thought well after birth with Apgar scores and cord pH values that were considered normal<sup>1</sup>. These seizures may be, but are not always, contralateral to the site of infarction, are mostly clonic in nature, and can be subtle<sup>8</sup>; sometimes the presenting symptoms are apnea, duskiness, poor feeding, hypotonia and irritability<sup>9,10</sup>. PAIS is occasionally associated with hypoxic-ischemic encephalopathy (HIE)<sup>11,12</sup>. The timing of presentation is often more than 12 hours after birth and may be up to 3-4 days.

MRI is the neuroradiologic investigation of choice for PAIS<sup>13,14</sup>. Diffusion-weighted (DW) imaging can detect neonatal ischemic brain injury within 24 hours of its onset with the acute changes being seen for several days<sup>15,16</sup>. As the initial clinical symptoms can be subtle and knowledge of the exact time of onset of the stroke in neonates is usually uncertain care must be exercised in the interpretation of DWI for timing the onset of the lesion<sup>17</sup>. Literature on radiologic criteria for timing of PAIS onset combining conventional and DW imaging is limited and includes mostly case descriptions<sup>15,16-23</sup>. The aim of the study was to evaluate the time course of SI changes assessed visually from conventional and DW MRI in term-born infants with unilateral PAIS.

## Subjects and Methods

### *Patients*

The study is part of a longitudinal project documenting the evolution of neonatal brain lesions of both inborn and referred infants at the Hammersmith and Queen Charlotte's Hospitals, London, UK. Data were collected between 1994 and 2004. As part of this study all infants who presented with neonatal seizures or other symptoms known to occur with

stroke for which no other explanation was found underwent neonatal brain MRI. Study approval was granted by the Research Ethics Committee of the Hammersmith Hospitals Trust, and parental consent was obtained for all scans.

Only infants  $\geq 36$  weeks gestation with unilateral PAIS in the territory of a main cerebral artery with a first MRI scan within the first postnatal month were included in this study. We also evaluated all subsequent scans up to 3 months post-natal age. Exclusion criteria were bilateral infarction seen on MRI, congenital infection, major brain or other malformation, multiple dysmorphic features, chromosomal abnormality or evidence of HIE. The infarcts were classified according to the vessel territory involved.

### ***Conventional MR Imaging and DWI***

From 1994-1999 the infants were scanned on a 1.0-T Picker system (Cleveland, OH) using conventional T1-weighted spin echo (CSE; TR 860/TE 20 ms) and T2-weighted spin echo (SE; TR 3000/TE<sub>eff</sub> 120 ms) sequences. After 1999, images were acquired on a 1.5-T Eclipse system (Philips Medical Systems, Cleveland, OH) using conventional T1-weighted spin echo (CSE; TR 500/TE 15 ms) and T2-weighted fast spin echo (FSE; TR 4500/TE<sub>eff</sub> 210 ms) at 5-mm slice thickness. Single-shot echo planar DW images were also acquired. A reference image was obtained with a b value of 0 and DW images were obtained with a b value of 1000 s/mm<sup>2</sup>. For some of the early scans only single slice DW images including the stroke areas were made; in these cases the DW sequence used a cardiac gated pulsed gradient spin echo sequence with a b value of 600 s/mm<sup>2</sup>. The infants were usually sedated for imaging with oral chloral hydrate (30-50mg/kg). Pulse oximetry and electrocardiograph were monitored throughout the procedure. Ear protection was used (Natus MiniMuffs, Natus Medical Inc, San Carlos, CA). An experienced pediatrician, trained in MRI procedures, was in attendance throughout the examination.

## Scoring system

The infarcts were classified according to the arterial territory involved. We used a scoring system comparing the SI of infarcted tissue to that of the equivalent tissue in the contralesional hemisphere as an internal control documenting the SI as higher (1), equal (0) or lower (-1). We evaluated the SI of the white matter, cortical gray matter and also white matter-cortical gray matter contrast, the delineation of the stroke borders and evidence of swelling, atrophy or tissue loss (Table 1). We also evaluated the SI of the basal ganglia (caudate nucleus, putamen and globus pallidus), the posterior limb of the internal capsule (PLIC) and brainstem. To evaluate the DW images we classified the SI of the infarcted tissue into 4 groups: (i) severe hyperintensity (HI), (ii) moderate HI, (iii) mild HI and (iv) no HI.

**Table 1**

The scoring system: comparing infarcted tissue using the contralesional hemisphere as an internal control.

Score	1	0	-1
SI White matter	higher	equal	lower
SI Cortex	higher	equal	lower
White matter - cortex contrast	increased	equal	decreased
Stroke borders	clearer	equal	lost
Swelling or atrophy	swelling	equal	atrophy

## Results

### *Patient Characteristics*

During the study period 28 term-born infants were diagnosed with unilateral PAIS; 7 were not included in this study because their first scan was >1 month after birth. We analyzed 43 conventional MRI scans all taken within in the <3 post-natal months (mean age first scan 4 days) from 21 infants (Table 2). All were born after a period in labor and none by elective caesarean section (CS); 6 were born by spontaneous vaginal delivery, 7 by forceps or ventouse and 8 by emergency CS for fetal distress, prolonged 2<sup>nd</sup> stage or failed instrumental delivery. In 10 patients a prolonged 2<sup>nd</sup> stage of labour (≥2hours) was recorded. The infants had a median gestational age of 40 weeks [range: 38–42 weeks] and median

weight 3554 grams [range: 2845-4450grams]. Twelve infants were male. All had Apgar scores  $\geq 5$  at 5 minutes (median 10, range 5-10). Median cord pH was 7.26 [range:7.00-7.38]. All infants went to the postnatal wards initially and were later admitted to the neonatal unit. All but one (infant 8) had overt clinical seizures (median day 1, range 1-3). Infant 8 was scanned as a “normal control” to a primigravid mother but had been born by CS after failed forceps and ventouse attempts and was jittery when examined on day 5.

Five infants had a main branch middle cerebral artery (c-MCA) territory infarction involving hemispheric tissue and the basal ganglia. Four infants had infarction within anterior MCA branch territory and 9 infants within posterior MCA branch territory; 2 infants had a posterior cerebral artery (PCA) territory infarction and 1 infant had an anterior cerebral artery (ACA) territory + an anterior branch MCA infarction. The lesions were left sided in 16 infants. 15 infants had DW imaging (median age first scan 4 days of age, range 2-14 days).

### ***Conventional Imaging Findings***

SI levels in white matter and cortex in the regions of infarction as compared to the contralateral hemisphere on T1- and T2 weighted imaging are summarized in Figures 1 and 2. On both T1-weighted and T2-weighted images tissue swelling of the region of infarction was seen on the first scans and this lasted until about day 8.

### ***T1-weighted imaging***

On T1-weighted images the affected cortex was always initially of low SI changing to high SI, so-called cortical highlighting, after day 6. Loss of cortical tissue in the areas of infarction started to be seen from 14 days but was most marked after 1 month. The cortical highlighting remained visible until 2 months in remaining cortex (Figure 1).

The white matter on T1-weighted images was of moderately higher SI than the white matter in the contralateral hemisphere in the first 9 post-natal days, although in the first 5 days when the cortex was of low SI

**Table 2**

Patient characteristics: Including: Sex (M=male, F=female), gestational age at birth (GA), Apgar scores, mode of delivery (Em-CS= emergency cesarean section, SVD= spontaneous vaginal delivery, VE=ventouse delivery), cord pH (n.a.=not-available), artery involved, side of infarction, postnatal day of seizure onset, postnatal day of T1- and T2-weighted MRI and postnatal day of DW MRI (nd=not done).

Patient	Sex	GA (weeks)	APGAR scores at 1 and 5 min	Mode of delivery	Artery involved	Cord pH	Side	Postnatal day of onset seizures	Postnatal day of T1 and T2 weighted MRI scans	Postnatal day of DWI MRI scans
1	M	40	8,9	Em-CS	c-MCA	738	R	1	2,5,12,42,75	2,5,12,42
2	F	40	9,10	Forceps	PCA	727	R	1	2,5,40	2,5,40
3	F	41	9,10	Em-CS	post-MCA	730	L	1	3	3
4	F	42	6,9	NSVD	PCA	n.a.	L	2	3	3,10
5	M	40	8,9	Em-CS	c-MCA	n.a.	L	1	4,6,40	4,6
6	M	40	9,10	NSVD	post-MCA	n.a.	L	1	4,6,28	4,28
7	M	40	6,9	VE	ant-MCA	732	L	3	4,45	4
8	M	38	9,10	Em-CS VE	post-MCA	n.a.	L	-	4,7	4
9	F	39	5,8	Em-CS	ant-MCA	717	L	2	6,14,28	5,12,14,28
10	M	41	6,10	Em-CS	post-MCA	702	R	1	6	6
11	M	39	9,10	NSVD	post-MCA	n.a.	L	1	8	8
12	M	41	9,9	Em-CS	post-MCA	700	L	1	9	9
13	F	40	8,10	Forceps	ant-MCA	726	R	2	10,33	10,33
14	M	41	9,10	Em-CS	c-MCA	734	L	1	11,16	11,16
15	M	41	9,10	Forceps	ant-MCA	730	L	1	5,56	5,56
16	M	40	5,7	Forceps VE	c-MCA	n.a.	L	1	6	nd
17	F	41	8,10	NSVD	post-MCA	729	L	1	4	nd
18	M	39	7,10	NSVD	post-MCA	707	L	2	4,8,48	nd
19	F	42	8,9	VE	c-MCA	n.a.	L	2	14,43	nd
20	F	41	9,9	Em-CS	post-MCA	723	L	1	11	nd
21	M	38	3,5	NSVD	ant-MCA + ACA	706	L	1	7,22,70	nd

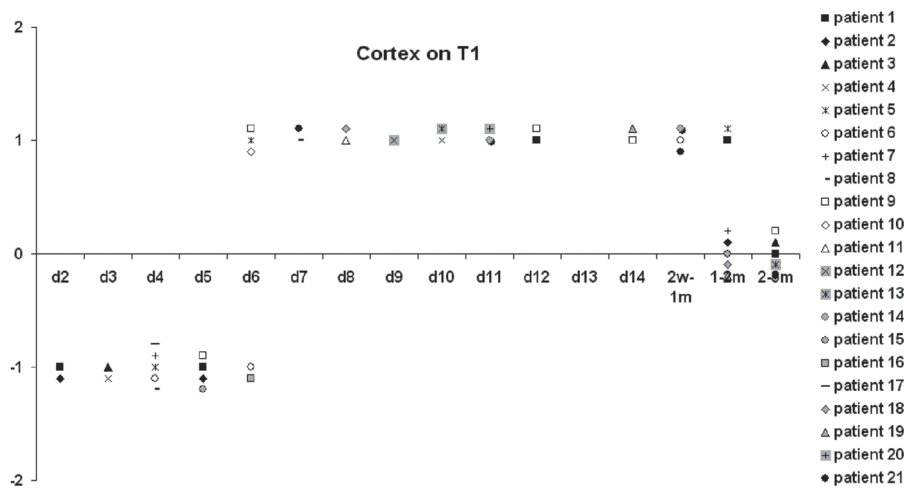


**Figure 1**  
This shows the SI score (y-axis) of the infarcted cortex on T1-weighted MR images from each postnatal day (x-axis).

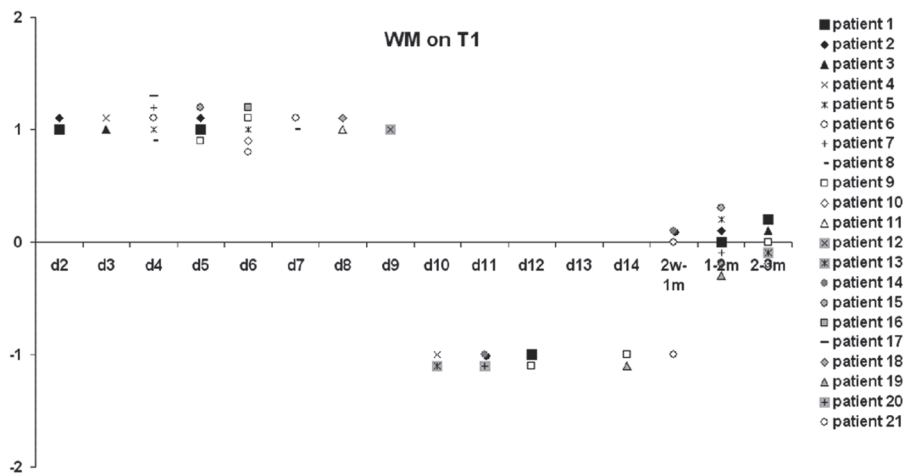


**Figure 2**  
This shows the SI score (y-axis) of the infarcted WM on T1-weighted MR images from each postnatal day (x-axis).

this was more difficult to discern as the initial visual impression was that the SI in the white matter was lower than the contralateral hemisphere. After day 9 the SI became lower than the other hemisphere until about



1 month after birth when it became of equal SI (Figure 2). The first appearance of tissue loss often with cyst formation in the areas of infarction was seen between 14 days and 1 month, but was most marked after 1 month.

The basal ganglia were clearly involved in the five patients with cMCA infarction and in the first 4 days were of low SI intensity on T1-weighted images; this changed to high SI from days 5 -7. From day 7 until day 14 we saw a variegated (checkerboard) pattern. After 1 month, tissue atrophy or cysts were seen (Figure 3).

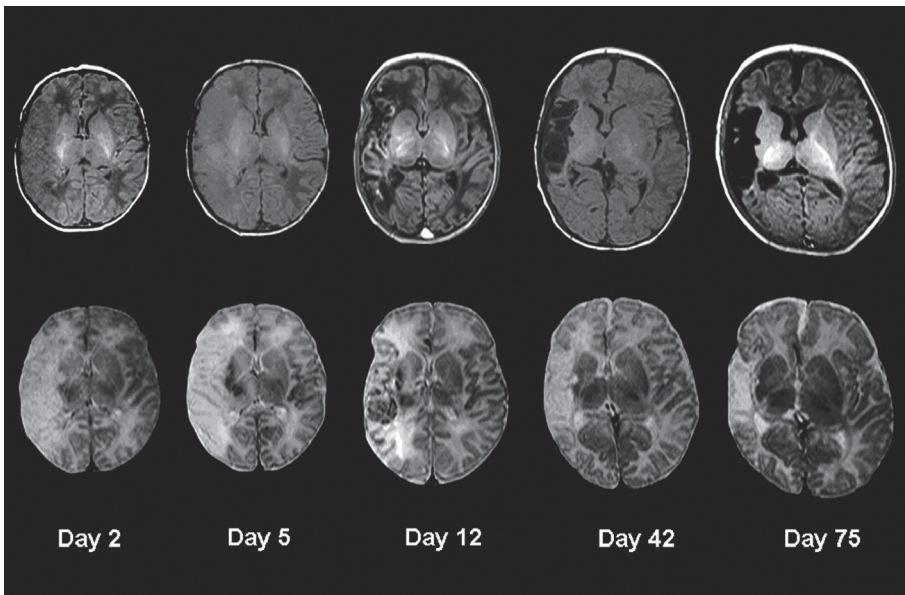


**Figure 3**

This shows the temporal evolution of a right-sided main branch MCA territory infarction (patient 1) on T1-weighted images (top row), and T2-weighted images (bottom row) scanned on days 2,5,12,42 and 75 post-delivery.

Asymmetry of the ipsilateral PLIC compared to the contralesional side was seen in 9 patients (infants 1,5,7,10,14,15,18-20). During the study period a lower SI was seen in the ipsilateral PLIC.

No clear visual SI changes were seen in the ipsilateral brainstem on the T1-weighted images in the time period studied. Ipsilateral peduncles became smaller in size in those with T2-weighted changes after 1 month.

Although the thalamus was not initially involved in the stroke in any infant, a reduction in ipsilateral thalamic size was seen in 10 (infants 1,2,5,9,10,13,14,17,18,20) on later scans within the first 3 postnatal months. The degree of thalamic reduction appeared to relate positively with the size of the original area of infarction.

**T2-weighted imaging**

On T2-weighted images the cortex in the region of infarction was initially of high SI but became of low SI after day six. Loss of cortical tissue in the areas of infarction was seen from day 14 and was most marked after 1 month. During the period of 1-2 months of age there was no difference in SI compared to the contralateral side in the remaining tissue (Figure 4).

The white matter was of high SI on T2-weighted images until 2-3 weeks of age (Figure 5) when the SI of the remaining tissue became isointense

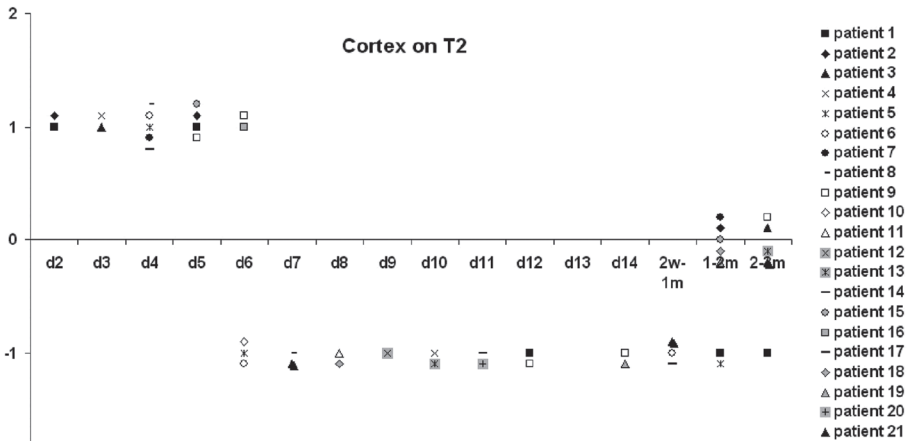


**Figure 4**  
This shows the SI score (y-axis) of the infarcted cortex on T2-weighted MR images from each postnatal day (x-axis).

with the contralesional side. Tissue atrophy often with cyst formation was evident after 1 month but started between 14 days and 1 month.

The basal ganglia were of high SI in the first 4 days and became of low SI from day 4 until day 7. From day 7 until day 14 we saw a checker-board pattern and after 1 month atrophy or cysts were seen (Figure 3).

During the study period a higher SI was seen in the ipsilateral PLIC in 9 patients compared in the contralesional PLIC, suggesting abnormal myelination.

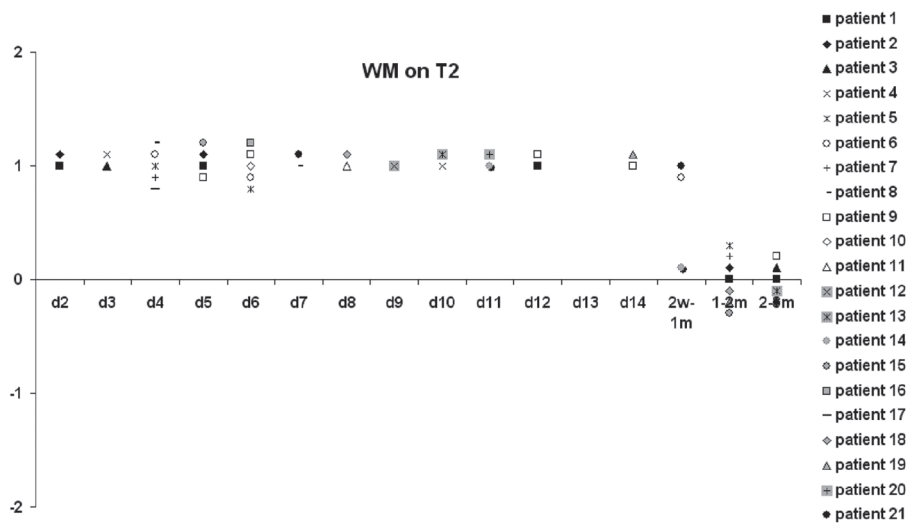


**Figure 5**

This shows the SI score (y-axis) of the infarcted WM on T2-weighted MR images from each postnatal day (x-axis).

In 5 patients we saw high SI in the ipsilateral brainstem on the T2-weighted images in the first postnatal week. No SI differences were seen after 1 month. In 4 of these patients (infants 1,5,14,18) who had late scanning ipsilateral brainstem atrophy presumed to be due to Wallerian degeneration (shrunk pyramidal tract at mesencephalic level) was seen by 1 month of age.

On both the T2-weighted images and DW images we saw high SI in the ipsilateral thalamus in the first postnatal week. These findings might reveal acute corticothalamic network injury, showing the secondary changes in distant nuclei and tracts associated with primary cortical or white matter injury [Figure 6].

### ***Cortical – white matter contrast and stroke borders***

The evolution of changes in stroke border recognition and contrast between white matter and cortex are described in Figure 7 where a composite of the scoring sys-

tem for all the infants is given. During the first 5 postnatal days the infarcted cortex became increasingly isointense with white matter, increasing the definition of the margins of the infarct with the affected cortex appearing absent: the “missing cortex sign” [8]. Around day 6 SI in cortex and white matter were more varied making recognition of the stroke borders more difficult. After day 6 white matter and cortex contrast became sharper, rendering the borders visible. After 1-month the combination of tissue loss (often with cysts) and slowly fading contrast between white matter and cortex contrast made the borders again inconspicuous.

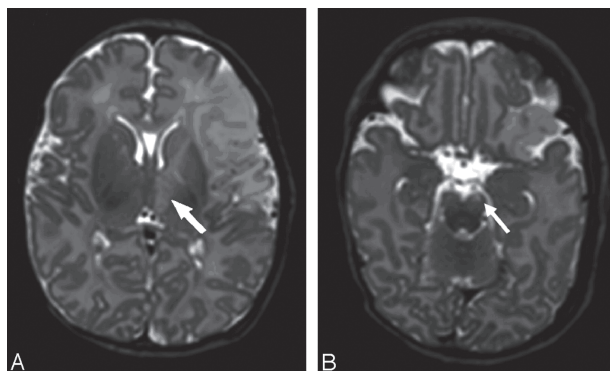


**Figure 6** This shows T2-weighted images of a patient with an infarction within anterior MCA branch territory on day 5 (patient 15), showing high SI changes within (A) the ipsilateral thalamus (arrow) and (B) the ipsilateral brain stem (arrow).

### ***Diffusion Weighted Imaging Findings***

The results from DW imaging are summarized in Figure 8. All DW images showed high SI in the white matter until day 4 after birth, which fell to equal to or below the contralateral hemisphere by day 12. The extent of tissue involvement was usually the same on DW and conventional im-

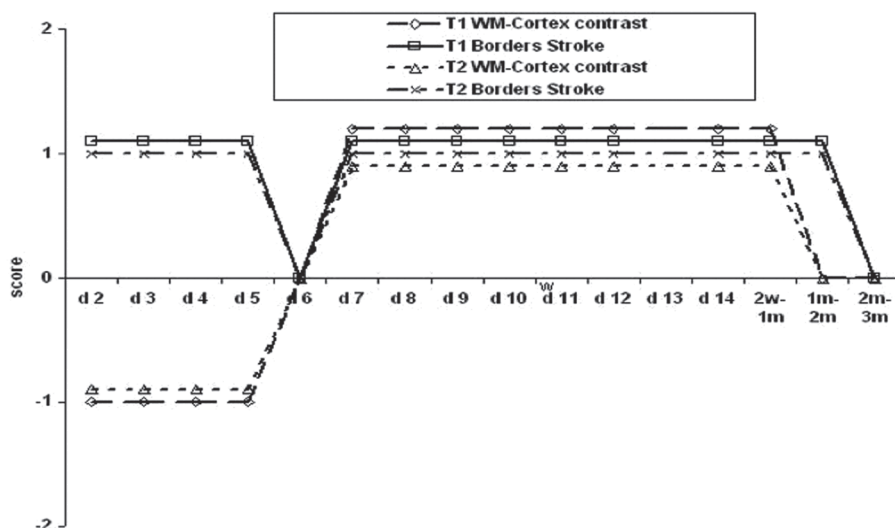


**Figure 7**

This figure shows the evolution of changes in stroke border recognition and contrast between white matter using a composite of the scoring system.

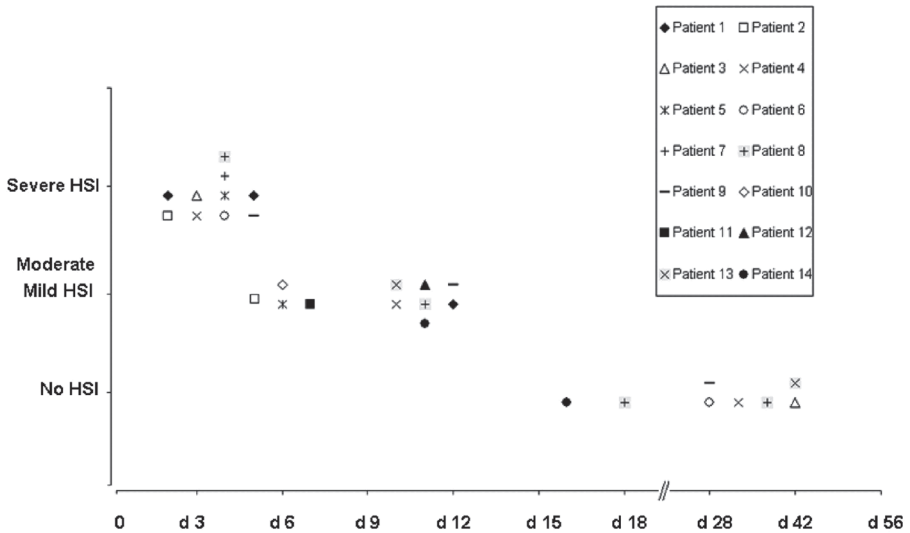
ages in the first week and seemed to be equal or less on the repeated DW scans. DW changes tended marginally to overestimate the size of the infarct at 4-8 weeks. In the first week the lesion SI on the DW images were all higher than the SIs seen on T1- and T2 weighted images, making lesion contrast most apparent on the DW images. Increased SI was clearly seen in parts of the ipsilateral thalamus in 5 infants on DW images.

## Discussion

Our results demonstrate that the patterns of SI change on conventional and DW images following PAIS were consistent between infants suggesting that PAIS in our infants who were symptomatic soon after birth occurred within a limited time frame around birth. Insights into the natural evolution of MR characteristics of neonatal stroke are important for estimating the age of a lesion, especially when the time of symptom onset can be unclear. Knowledge of neonatal stroke evolution on MR can

**Figure 8**

This shows the SI score (y-axis) of the infarcted tissue on DW MR images from each postnatal day (x-axis).



also be used to interpret the results of medical intervention strategies and for determining optimal timing for imaging. Because the literature on radiologic timing of neonatal stroke onset in humans is limited, our data adds to the understanding of the evolution of neonatal stroke. Since changes in MR parameters reflect histopathological changes in brain tissue we will discuss how our findings relate to the literature on the histo- and pathophysiologic evolution of arterial ischemic stroke, most of which is based on adult and animal studies.

In our patients SI increase on DW imaging consistent with restricted diffusion was seen within the infarcted area for up to 14 days but was most marked in the first 4 days. For all of the studied infants the first DW image showed the highest signal intensity consistent with a recent insult (Figure 8). After ischemic arterial injury, energy depletion and impaired ion homeostasis cause cytotoxic edema with restricted diffusion of water and shrinkage of the extracellular compartment translating into a high DWI signal<sup>24-25</sup>. Post-mortem studies have shown astrocytic swelling microscopically within 30 minutes after the onset of severe ischemia and by 4-6 hours swelling of oligodendroglial nuclei and cytoplasm is seen<sup>26</sup>.

DW imaging studies have shown changes in water diffusion within minutes after stroke in animals<sup>27</sup>. Our DW imaging findings in the first week are consistent with adult stroke literature on DW SI evolution, in which acute ischemic lesions are characterized by very hyperintense signal and show little change in the first 7 days after symptoms onset but decrease in SI thereafter<sup>28,29</sup>. However in adult stroke patients the high SI is reported to last for several weeks. DW SI is not only influenced by water diffusibility but also by intrinsic T2 properties (“T2 shinerthrough”) and field strength; this may contribute to the differences seen in DW imaging SI evolution between adults and newborns. The quantitative measure of DW MR is the computed apparent diffusion coefficient (ADC), which is without the influence of T2 signal. Because the visual classification of the degree of hypersignal intensity can be difficult, quantifiable ADC maps have been useful in determining the age of ischemic lesions in several adult studies<sup>28,30,31</sup>. The lowest ADC values in adult ischemic brain tissue seem to occur around day 3 after lesion onset and take 4–21 days for pseudonormalization<sup>29–31</sup>. Because of our rather heterogeneous imaging datasets we were not able to measure ADC values across the group.

In the first postnatal week (from day 2) T2-weighted images in our patients show clear increased SIs in the cortex and white matter. Once the blood-brain barrier is disrupted, vasogenic edema in combination with cytotoxic edema increase the overall water content in the infarcted tissue, which accounts for the prolonged T2 relaxation times making the infarct readily visible on T2-weighted images between 24–48 hours after its onset<sup>29</sup>. The visual disappearance of the cortical ribbon in the affected area during this stage represents the so-called “missing cortex sign”<sup>19</sup>. Animal histology studies have shown that from 4–6 hours after the onset of stroke to about 6 days damage to the endothelium and breakdown of the blood-brain barrier takes place associated with vasogenic edema and coagulation necrosis<sup>26,27</sup>.

On T1-weighted images the affected cortex showed low SI in the first week from day 2. This SI is generally attributed to vasogenic edema. However the white matter on T1-weighted images was of moderately higher SI than the white matter in the contralateral hemisphere in the

first 9 postnatal days, although in the first five days when the cortex was of low SI the overall impression was that the SI in the white matter was lower than the contralateral hemisphere. Whether cortical swelling is responsible for this appearance or whether there is actual shortening of the T1 relaxation time in white matter causing high SI on T1-weighted images during this period is unclear.

After approximately 1 week up to 1 month we documented high SI in the cortex on T1-weighted images (cortical highlighting) and low cortical SI on T2-weighted images. From post-mortem studies this time period seems to coincide with organization within the infarction, a process that involves gliosis, release of myelin lipids, microcyst formation, calcification and ingrowth of new vessels<sup>26,32</sup>. It is an ongoing process, which in adults takes place from 3 days to 6 weeks. In post-mortem studies neuronal breakdown products can be seen microscopically in macrophages after day 5 in adults<sup>26</sup>. Takana et al showed an increase in microglial cells, which changed to a form of lipid, laden phagocytes in rats subjected to focal brain ischemia on day 7<sup>33</sup>. Aoe et al. showed a clear correlation between T1 values and the number of microglia observed using lectin staining<sup>34</sup>. But also the high protein content and accumulation of manganese in reactive astrocytes have been suggested as being important in generating the SI changes on T1-weighted images<sup>35</sup>.

The low cortical SI on T2-weighted images is generally thought to be related to petechial hemorrhage, release of myelin lipids or calcification<sup>19</sup>. Around day 7 there is also evidence of newly formed capillaries. This neovascularisation is most marked in gray matter. At the same time the walls of the remaining blood vessels thicken<sup>26</sup>. These vascular changes will also contribute to the cortical changes seen on the conventional images after the first postnatal week.

The areas of infarction evolved into areas of tissue loss and cysts after 1-2 months following an intermediate variegated or “checkerboard” pattern of mixed high and low SI seen around 2-3 weeks.

Wallerian degeneration of the ipsilateral corticospinal tract and secondary degeneration of ipsilateral thalamus was seen in some of our pa-



---

tients after 1 month. These findings seem to be in accordance with the adult and neonatal literature on secondary degeneration<sup>36-38</sup>.

One of the limitations of our study is the use of the “healthy” hemisphere as an internal control. None of the infants was considered to have contralateral lesions or pathology on visual analysis of the scans. Trans-synaptic degeneration could cause network injury affecting the contralateral hemisphere making a case for using healthy term controls in future studies. The visual scoring system we used is practical in a clinical setting; however for research purposes relatively new but more time consuming post-processing techniques such as automatic segmentation will give more objective measurements of SI and volume change<sup>39</sup>.

Based on the mechanisms that can lead to arterial occlusion and known perinatal risk factors the arterial occlusion in our patients could have taken place during three periods: (i) in later labor (ii) the intrapartum period (iii) shortly after delivery, each period reflecting different risks factors<sup>12,14,40,41</sup>. In this study we could not differentiate between these different periods. All infants underwent labor, none being born by pre-labor caesarean section. In most infants labor was complicated in that delivery was only spontaneous in 6 infants and the second stage of labor was prolonged (lasted  $\geq 2$  hours) in 9 cases. No fetus had had problems recorded prior to the onset of labor and as is most usual for term-born infants with PAIS none had low Apgar scores or presented with symptoms of global hypoxia-ischemia immediately after birth. Abnormal DW imaging SI in our patients was always most marked on the first scan and the SI started to diminish after 4-6 postnatal days; extrapolating from the adult and animal literature this would support the onset of the stroke closely to the time of birth. We had consistent change in SI on DW and conventional images in the first week with the infarct always being seen even on T1-weighted images on first scan suggesting the infarcts had occurred at least 1-2 days before first imaging. This further supports the interpretation of our data to indicate that the stroke occurred within a limited time frame around or during delivery.

To our knowledge this is the first study in which the radiologic evolution of PAIS has been described in such a large number of infants. Future

intervention studies and medico-legal issues will require an even more detailed study of the temporal evolution of PAIS. Prospective studies with serial scanning (including quantitative diffusion tensor imaging) in combination with continuous EEG monitoring and detailed clinical histories might provide this.

## **Conclusion**

The pattern of SI change on conventional and DW images following PAIS was remarkably consistent between patients suggesting that PAIS in symptomatic term-born infants occurs closely around the time of birth.

## **References**

1. C. Sreenan, R. Bhargava, C.M. Robertson. Cerebral infarction in the term newborn: clinical presentation and long-term outcome. *J Pediatr* 2000;137:351-55
2. E. Mercuri, A. Barnett, M.A. Rutherford et al. Neonatal cerebral infarction and neuromotor outcome at school age. *Pediatrics* 2004;113:95-100
3. Y.W. Wu, J.K. Lynch, K.B. Neslon. Perinatal arterial stroke: understanding mechanisms and outcomes. *Semin Neurol* 2005;424-34
4. A. Kirton, G. deVeber. Cerebral palsy secondary to perinatal ischemic stroke. *Clin Perinatol* 2006;33:367-86
5. B.B. Wulfeck, D.A. Trauner, P.A. Tallal. Neurologic, cognitive, and linguistic features of infants after early stroke. *Pediatr Neurol* 1991;7:266-9
6. D.A. Trauner, C. Chase, P. Walker et al. Neurologic profiles of infants and children after perinatal stroke. *Pediatr Neurol* 1993;9:383-6
7. J.K. Lynch, K.B. Nelson. Epidemiology of perinatal stroke. *Curr Opin Pediatr* 2001;13:499-505

8. P.A. Filipek, K.S. Krishnamoorthy, K.R. Davis et al. Focal cerebral infarction in the newborn: a distinct entity. *Pediatr Neurol* 1987;3:141-7
9. S.R. Levy, I.F. Abrams, P.C. Marshall et al. Seizures and cerebral infarction in the full-term newborn. *Ann Neurol* 1985;17:366-70
10. S. Fujimoto, K. Yokochi, H. Togari et al. Neonatal cerebral infarction: symptoms, CT findings and prognosis. *Brain Dev* 1992;14: 48-52
11. F.M. Cowan, M.A. Rutherford, F. Groenendaal et al. Origin and timing of brain lesions in term infants with neonatal encephalopathy. *Lancet* 2003;361:736-42
12. V. Ramaswamy, S.P. Miller, A.J. Barkovich et al. Perinatal stroke in term infants with neonatal encephalopathy. *Neurology* 2004;62:2088-91
13. F.M. Cowan, E. Mercuri, F. Groenendaal et al. Does cranial ultrasound imaging identify arterial cerebral infarction in term neonates. *Arch Dis Child Fetal Neonatal Ed* 2005;90:252-6
14. A. Obernaus, S. Ashwal. Magnetic resonance imaging in cerebral ischemia: Focus on neonates. *Neuropharmacology* 2008;55:270-80
15. E. Mercuri, F.M. Cowan, M.A. Rutherford et al. Ischaemic and haemorrhagic brain lesions in newborns with seizures and normal Apgar scores. *Arch Dis Child Fetal Neonatal Ed* 1995;73:67-74
16. W. Küker, S. Möhrle, I. Mader et al. MRI for the management of neonatal cerebral infarctions: importance of timing. *Childs Nerv Syst* 2004;20:742-48
17. I. Mader, M. Schoning, U. Klose et al. Neonatal cerebral infarction diagnosed by diffusion-weighted MRI: pseudonormalization occurs early. *Stroke* 2002;33:1142-45
18. M.A. Rutherford. *MRI of the Neonatal Brain*, W.B. Saunders, Edinburgh (2002)
19. A. Barkovich. *Pediatric neuroimaging*. Lippincott, Williams & Wilkins, Philadelphia
20. F.M. Cowan, J.M. Pennock, J.D. Hanrahan et al. Early detection of cerebral infarction and hypoxic ischemic encephalopathy in neonates using diffusion-weighted magnetic resonance imaging. *Neuropediatrics* 1994;25:172-5
21. R.L. Robertson, L. Ben-Sira, P.D. Barnes et al. MR line-scan diffusion-weighted imaging of term neonates with perinatal brain ischemia. *AJNR Am J Neuroradiol* 1999;20:1658-70

22. R.L. Robertson, C.M. Glasier. Diffusion-weighted imaging of the brain in infants and children. *Pediatr Radiol* 2007;37:749-68
23. K.S. Krishnamoorthy, T.B. Soman, M. Takeoka et al. Diffusion-weighted imaging in neonatal cerebral infarction: clinical utility and follow-up. *J Child Neurol* 2000;15:592-602
24. P.A. Barber, L. Hoyte, D. Kirk et al. Early T1- and T2 weighted MRI signatures of transient and permanent middle cerebral artery occlusion in an murine stroke model studied at 9.4T. *Neurosci Lett* 2005;388:54-9
25. M. Qiao, K.L. Malisza, M.R. Del Bigio et al. Transient hypoxia-ischemia in rats: changes in diffusion-sensitive MR imaging findings, extracellular space, and Na<sup>+</sup>-K<sup>+</sup> -adenosine triphosphatase and cytochrome oxidase activity. *Radiology* 2002;233:65-75
26. D.I. Graham, P.L. Lantos. eds. *Greenfield's neuropathology*. 7th ed. London, Arnold;2002
27. T. Neumann-Haefelin, A. Kastrup, A. de Crespigny et al. Serial MRI after transient focal cerebral ischemia in rats: dynamics of tissue injury, blood-brain barrier damage, and edema formation. *Stroke* 2000;31:1965-72
28. J.B. Fiebach, O. Jansen, P.D. Schellinger et al. Serial analysis of the apparent diffusion coefficient time course in human stroke. *Neuroradiology* 2002;44:294-98
29. M.G. Lansberg, M.W. O'Brien, D.C. Tong et al. Evolution of cerebral infarct volume assessed by diffusion-weighted magnetic resonance imaging. *Arch Neurol* 2001; 58: 613–17
30. G. Schlaug, B. Siewert, A. Benfield et al. Time course of the apparent diffusion (ADC) abnormality in human stroke. *Neurology* 1997;49:113-19
31. H.L. Lutsep, G.W. Albers, A. DeCrespigny et al. Clinical utility of diffusion-weighted magnetic resonance imaging in the assessment of ischemic stroke. *Ann Neurol* 1997;41:574-80
32. G. Stoll, S. Jander, M. Schroeter. Inflammation and glial responses in ischemic brain lesions. *Prog Neurobiol* 1998;56:149-71
33. H. Aoe, Y. Takeda, H. Kawahara et al. Clinical significance of T1-weighted MR images following transient cerebral ischemia. *J Neurol Sci* 2006;241:19-24

- 
34. R. Takana, M. Komine-Kobayashi, H. Mochizuki et al. Migration of enhanced green fluorescent expressing bone marrow-derived microglia/macrophage into the mouse brain following permanent focal ischemia. *Neuroscience* 2003;117:531-39
  35. D.E. Shan, H.C. Pan, D.M. Ho et al. Presence of activated microglia in a high signal lesion on T1-weighted MR images: a biopsy sample re-examined. *AJNR Am J Neuroradiol* 2007;28:602
  36. W.D. Heiss, J. Sobesky, V. Hesselmann. Identifying thresholds for penumbra and irreversible tissue damage. *Stroke* 2004;35:2671-4
  37. P.P. Govaert, A. Zingman, Y.H. Jung et al. Network injury to pulvinar with neonatal arterial ischemic stroke. *Neuroimage* 2008;39:1850-7
  38. F. Groenendaal, M.J. Benders, L.S. de Vries. Pre-wallerian degeneration in the neonatal brain following perinatal cerebral hypoxia-ischemia demonstrated with MRI. *Semin Perinatol* 2006;30:146-50
  39. M.A. Jacobs, R.A. Knight, H. Soltanian-Zadeh et al. Unsupervised segmentation of multiparameter MRI in experimental cerebral ischemia with comparison to T2, diffusion, and ADC parameters and histopathological validation. *J Magn Reson Imaging* 2000;11:425-37
  40. L.R. Ment, C.C. Duncan, R.A. Ehrenkranz. Perinatal cerebral infarction. *Ann Neurol* 1984;16:559-68
  41. M.H. Lequin, E.A. Peeters, H.C. Holscher et al. Arterial infarction caused by carotid artery dissection in the neonate. *Eur J Paediatr Neurol* 2004;8:155-60





# Chapter 8

## NETWORK INJURY TO PULVINAR WITH NEONATAL ARTERIAL ISCHEMIC STROKE

---

P.P. Govaert  
A. Zingman  
Y. Hoa Jung  
J. Dudink  
R. Swarte  
A. Zecic  
V. Meersschaut  
S. van Engelen  
M.H. Lequin

*Neuroimage. 2008;39(4):1850-7*

## **Abstract**

### ***Background and purpose***

The purpose of this study is to establish that newborn stroke involving extensive parts of cerebral cortex immediately leads to secondary network injury in pulvinar.

### ***Materials and Methods***

Seven term infants with cortical stroke presented with hypersignal in pulvinar on DWI. Stroke types included: complete MCA stroke (n=4); PCA stroke, ICA stroke and multiple artery stroke (1 each). Age range at scanning was between day 2 and 6 after birth (except for 1 infant scanned within 7 days of acute presentation during ECMO).

### ***Results***

ADC values in secondarily injured pulvinar were significantly higher than in the area with primary (sub)cortical injury (all patients scanned with identical MR image acquisition).

### ***Conclusion***

In the absence of asphyxia and because pulvinar is outside of the primary area of infarction, we conclude there are suggestions from imaging for acute secondary injury to pulvinar following primary damage of their cortical targets and/or connecting axons. Acute secondary injury is probably due to excitotoxicity and deafferentiation. The relevance of network injury for prognosis and the impact of early treatment on it have yet to be studied, in stroke but also in other acute perinatal brain disorders.



---

## Introduction

Until recently classification of perinatal brain disease focused on primary lesions only: global forebrain ischemia with selective cell death and watershed injury, arterial and venous stroke, periventricular leukomalacia, meningitis and encephalitis, primary haemorrhage. Secondary effects of cell injury on connected projection tracts have now been recognized with diffusion-weighted MR imaging (DWI), and as such the significance of early stages of Wallerian degeneration has been recognized at the level of the posterior limb of the internal capsule and the cerebral peduncles in some of the above mentioned primary disease entities, mainly focal infarction<sup>1-8</sup>. There are no human imaging studies of the effect of tract changes on nuclei connected to the primary perinatal lesion sites.

The concept that primary cortical injury can lead to cell loss in thalamus was known to mid-20th century pathologists. Gliotic change in one thalamic nucleus, pulvinar, has been associated with a more severe type of periventricular leukomalacia in a pediatric MR study of ex preterms with spastic cerebral palsy and subsequent global thalamic shrinkage has been linked to perinatal preterm white matter injury<sup>9-11</sup>. The influence of perinatal venous white matter infarction on thalamus has been recently depicted at 2 years of age with probabilistic magnetic resonance imaging of white matter tracts and thalamocortical connections<sup>12</sup>. We are unaware of reports that focused on acute corticothalamic network injury in the human newborn brain. We reviewed our experience with acute DWI of perinatal brain lesions focusing on secondary changes in distant nuclei and tracts associated with primary cortical or white matter injury. The aim of this report is to describe one pattern of thalamocortical interaction where extensive cerebral injury from stroke led to changes in pulvinar (Fig. 1) and to speculate on the significance of these findings for acute management and prognosis.

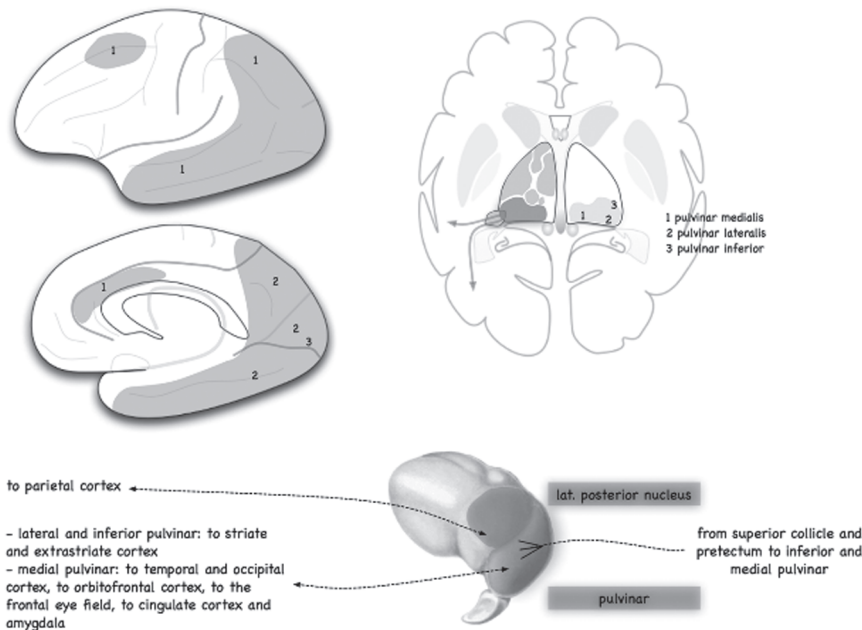


**Figure 1**  
Afferents and efferents of pulvinar and lateral posterior nucleus (adapted from Nieuwenhuys et al. 1988). Cortical connections are mainly with parietal, occipital and temporal lobes. (A full color version of this illustration can be found in the color section).

## Material and methods Study population

This analysis was retrospective, focusing on signal changes in pulvinar in DWI sequences. We analyzed in detail the images of patients with hypersignal in pulvinar on DWI that seemed to be outside of the area of primary injury in 7 term infants with acute and extensive cortical arterial ischemic stroke. Longstanding antepartum injury was excluded by routine first day ultrasound scanning in these infants. The cohort consisted of seven extensive cortical arterial ischemic stroke cases observed between January 2004 and 2006, scanned in the latter part of the first week and with artefact-less DWI sequence of similar acquisition mode. One infant was scanned 40 days after birth but 3 days following clinical seizures.

---

## **MR imaging technique**

### ***Image acquisition***

Images were acquired with a GE 1.5 Tesla scanning system (Milwaukee, WI, USA). All studies were performed according to a protocol that included axial dual T2 spin echo, axial T1 spin echo or axial T13D SPGR, sagittal T1 spin echo, axial PD (proton density) and coronal FLAIR. Diffusion tensor images (DTI) were acquired using multi repetition, single shot echo-planar sequence with a slice thickness of 3 mm with no gap. The images were gathered in 25 gradient directions with sensitivity of  $b = 1000 \text{ s/mm}^2$ , TR/TE = 8700-11725/83-98 ms, field of view 18-24 cm<sup>2</sup>. DW images were gathered in 6 gradient directions with sensitivity of  $b=1000\text{s/mm}^2$ , TR/TE = 8000/111.8-83.4 ms, one average, field of view 18-24 cm<sup>2</sup>, slice thickness 4 mm and a spacing of 0.4 mm.

### ***Quantitative image analysis***

For quantitative data analysis diffusion and apparent diffusion coefficient (ADC) maps of GE scans were reconstructed using Functool 3.1.23 (GE, Milwaukee, WI). Regions of interest (ROI) of varying size were manually placed in affected (sub)cortical areas, and in pulvinar in places that carried increased signal intensity on the diffusion images. All ROI placement was done on the  $b = 0 \text{ s/mm}^2$  images because of higher anatomic detail. ROI's were automatically superimposed on the functional maps by Functool. ADC-maps were used to exclude cerebrospinal fluid from measurements. Fractional anisotropy (FA) maps were used to avoid involvement of the corticospinal tract (posterior limb of the internal capsule) or the optic radiation when placing ROI's in pulvinar.

## **Visual image analysis**

To confirm hypersignal in pulvinar in relation to extra-thalamic injury we designed an extensive scoring system involving inexperienced medical students. Each patient was scored by two students and later by two physicians. Subjective visual scoring began with overall assessment of

damage based on a scale of hypo/hyperintensity on DWI. Both hemispheres were scored independently. These intensities were considered relative to 6 term DWI controls. These control scans were from term infants with suspected birth asphyxia, scanned between day 3 and 7, but without clinical seizures and with a subjectively reported normal scan. Hypointensity was scored as 0, expected intensity was scored as 1, hyperintensity that was either moderate or encompassed only part of the structure was scored as 2 and extreme hyperintensity of an entire structure was scored as 3. Scored structures included deep nuclei, white matter tracts, and lobar regions. The students scored individual nuclei of thalamus (ventral, anterior, medial, intralaminar, posterolateral including pulvinar) as well as each of the nuclei of the basal ganglia (caudate, putamen and pallidum). Among white matter tracts, we scored the optic chiasm, tracts, and radiations; the rostrum, genu, and splenium of the corpus callosum; the columns and fimbriae of the fornix; the corona radiata, anterior limb of the internal capsule (ALIC), posterior limb of the internal capsule (PLIC), medial and lateral crus cerebri. Cortical regions were subdivided in: the mesial, basal and lateral surfaces of the frontal lobe; the basal and lateral portions of the temporal lobe as well as the temporal poles; the cingulum, hippocampus, and amygdala; the striate and extrastriate areas of the occipital lobe; and the parietal lobe. When a lobar region was scored, it was recorded whether injury was cortical, subcortical, or in white matter. Scores were qualified in words. The medical students concluded their scoring assessment by consensus. The physicians but not the students had prior knowledge of the case histories. Discrepancies were debated by all four parties after initial blinded scoring by the students was complete. Primary source data, the images, were used again for all final analyses. Although in many patterns the primary lesion was of highest signal intensity, pulvinar hypersignal needed to be unequivocal (intensity score 2 or 3) in the final lesion cohort.

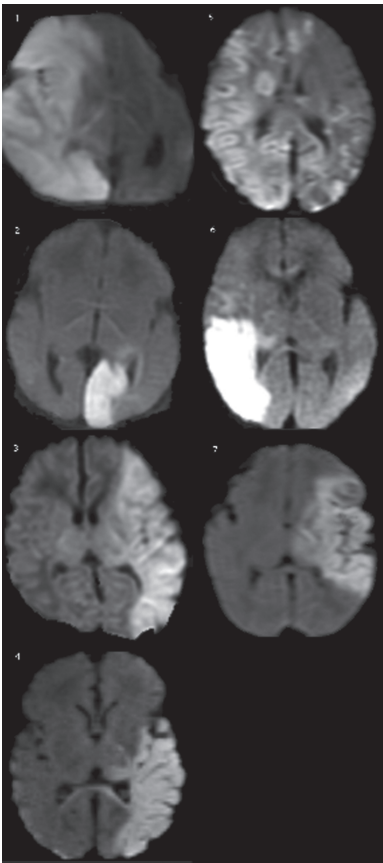
# Statistical method

Secondary pulvinar lesions were compared for ADC values with primary (sub)cortical lesions and healthy contralateral pulvinar, using the paired T-test with two tails (Graphpad Instat for Macintosh).

# Results

All stroke cases fulfilling the criteria mentioned under Study Population had definite hypersignal in pulvinar ipsilateral to the cortical area of infarction. Instances with pulvinar hypersignal in relation to large artery

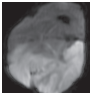
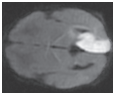
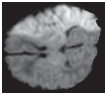
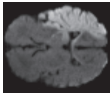
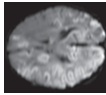
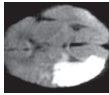
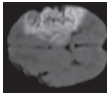
cortical stroke are listed in Table 1 (Figures 2-4). In axial sections through caudal thalamus, pulvinar hypersignal took the form of either complete hypersignal from midline to lateral geniculate or partial lateral hypersignal sparing medial pulvinar.



ADC values in pulvinar versus primary (sub)cortical lesions (Table 2, Fig. 5) Pulvinar changes were compared in a subset of scans for ADC values with the primary (sub)cortical injury areas and with contralateral supposedly healthy pulvinar. Average ADC in 7 patients was 0.51  $\mu\text{m}^2/\text{ms}$  in the primary lesion, 0.72  $\mu\text{m}^2/\text{ms}$  in ipsilateral and 0.98 0.72  $\mu\text{m}^2/\text{ms}$  in contralateral pulvinar. ADC values in pulvinar were

**Figure 2**  
Stroke lesions related to network injury in pulvinar. The DWI sections serve to illustrate the lesion extent, in all also demonstrating hypersignal in pulvinar (except patient 5 where the section is above thalamus).

Table 1 Pulvinar hypersignal in the absence of global forebrain ischaemia

	focal infarction	GA w	scan day	cortical injury	comments (including lesion to optic radiation)	
1	stroke ICA R and PCA R	40	4	FPOT	hypersignal in ALIC and PLIC	
2	stroke top of basilar, PCA L	40	2	O	optic radiation affected in the occipital subcortex only	
3	stroke MCAcomp L	40	6	FPT	primary visual cortex not affected; optic radiation affected along and behind atrium	
4	stroke MCAcomp L	39	5	FPT	primary visual cortex not affected; optic radiation affected along and behind atrium	
5	stroke MCAcomp R, PCA R, MCApost L, PCAL	39	4	FPOT	optic radiation and visual cortex bilaterally injured	
6	stroke MCAcomp R	40	3	FPT	primary visual cortex not affected, frontal lobe affected partially; optic radiation affected along and behind atrium	
7	stroke MCAcomp L, listeria meningitis	37	6	FPT	primary visual cortex not affected; optic radiation affected along and behind atrium	

MCA, ICA, PCA: middle cerebral, internal carotid, posterior cerebral artery  
F frontal, P parietal, T temporal, O occipital lobe  
ALIC, PLIC: anterior and posterior limb of the internal capsule

**Table 2** ADC values in (sub)cortex (I) versus pulvinar (II)

patient	I [ $\mu\text{m}^2/\text{ms}$ ]	II pulvinar [ $\mu\text{m}^2/\text{ms}$ ]	contralateral pulvinar	ratio I/II
1	POT = 0.42	0.67	1.08	0.62
2	O = 0.42	0.85	1.14	0.50
3	F = 0.56	0.78	1.08	0.72
4	FT=0.52	0.80	1.07	0.65
5	POT = 0.50	0.54	0.58	0.94
6	PT = 0.50	0.65	0.92	0.77
7	white matter = 0.63	0.77	0.98	0.82
statistics	$0.51 \pm 0.075$	$0.72 \pm 0.107$	$0.98 \pm 0.19$	0.72

*lesion vs pulvinar*                      *mean difference is -0.2157*      *P<0.05*  
*lesion vs healthy*                    *mean difference is -0.4714*      *P<0.001*  
*pulvinar vs healthy*                  *mean difference is -0.2557*      *P<0.01*

*F,P,O,T: frontal, parietal, occipital, temporal (sub)cortex*  
*frontal, parietal, occipital, temporal (sub)cortex*

therefore significantly higher than in the primary injury area but lower than in healthy pulvinar. Mean difference between healthy and affected pulvinar = + 0.26 (the 95% confidence interval of the difference: + 0.09 to 0.42).

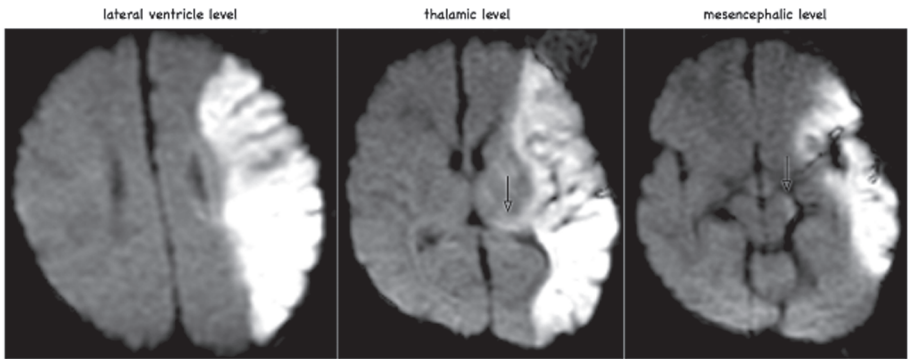


**Figure 3** (nr 4 in Table 1)

Complete left MCA stroke at term. DWI on day 6, following seizures on day 2. Hypersignal affects the stroke area, including the complete pial MCA area and lateral parts of striatum. Observe the presence of hypersignal in pulvinar on the affected side, outside of the MCA perfusion area (arrow). Some hypersignal is also present in PLIC and in the corticospinal (-bulbar) tract at mesencephalic level on the infarct side (arrow).

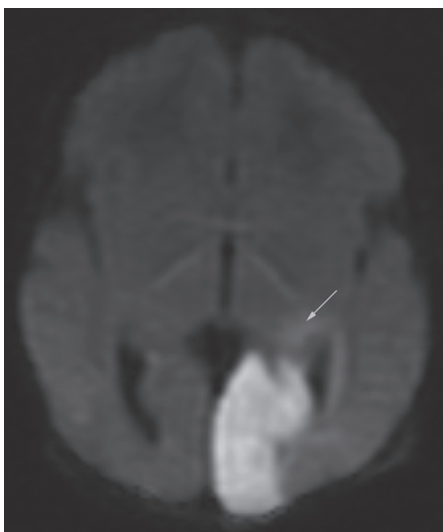


**Figure 4 (nr 3 in Table 1)**

PCA stroke in a term infant, due to embolism from the inferior vena cava. The arrow points to faint hypersignal in pulvinar. Notice high signal in the ipsilateral optic radiation.

## Discussion

We describe a pattern of injury to pulvinar associated with posterior (parietal, occipital and/or temporal) cortical damage caused by arterial ischemic infarction. Because tract changes are clearly present in these infants, one has to consider the possibility that signal intensity change in pulvinar is not due to neuronal but to axonal changes. As there are no large fiber tracts in pulvinar, this seems unlikely. In the only patient with PCA stroke (case 2) and hypersignal in pulvinar, one could theoretically suspect perforator stroke in pulvinar due to

occlusion of a thalamogeniculate branch, but patients with MCA or ICA stroke exhibit no primary lesion in pulvinar because that nucleus is perfused from the PCA. It is therefore highly probable that hypersignal in pulvinar is an immediate network reaction. The differences in ADC between ipsi- and contralateral pulvinar corroborate the finding of altered tissue characteristics in pulvinar connected to an area of extensive cortical necrosis, but more numerous prospective measurements are needed to confirm ADC characteristics in nuclei with secondary injury. To defend the hypothesis of acute network injury to pulvinar we need to discuss development and function of thalamus, and we need to document the existence of thalamic cell death in experimental work secondary to (sub) cortical primary injury.

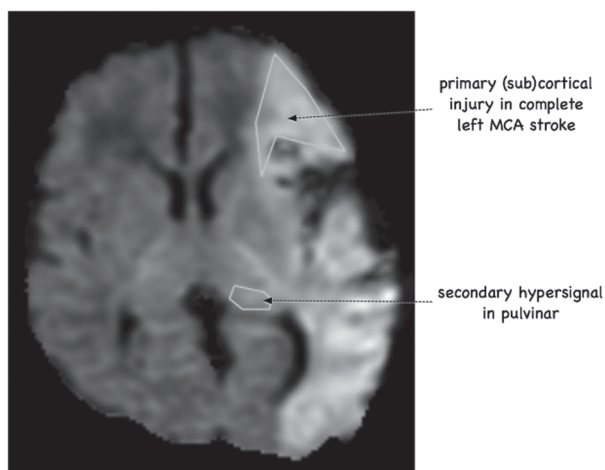
Development and function of thalamus (and especially pulvinar) is complex. After the fourteenth gestational week all major thalamic nuclei can be recognized following proliferative activity in matrix lining the third ventricle and subsequent migration around the transition from embryonic to fetal period<sup>13-15</sup>. Almost all of thalamus is diencephalic in origin,



stemming from third ventricle neuroepithelium. By 18 weeks pulvinar is only partly developed: it grows further from a proliferative structure called the corpus gangliothalamicum up to 34 weeks of gestation<sup>15,16</sup>. This conduit between lateral ganglionic eminence and diencephalic nuclei guides interneurons (GABAergic) into pulvinar, mediodorsal and anterior thalamic nuclei. Pulvinar is finally divided into at least 4 subdivisions<sup>17</sup>: lateral and medial, inferior and oral. Lateral and inferior pulvinar are connected to striate and extrastriate visual cortex; part of lateral and medial pulvinar is connected to parietal, frontal (a.o. the frontal eye field) and cingular cortex plus amygdala; cells projecting to temporal lobe are less well organized and lie ventrally; oral pulvinar is connected to parietal somatosensory cortex and area 5. Each connected cortical field has a separate set of projection neurons in pulvinar, even when these fields are adjacent and interconnected by themselves. The difference in maturational stage at term between ventral thalamic complex and regions like the pulvinar and mediodorsal nucleus was recently demonstrated in vivo with measurement of FA and ADC in preterms scanned at term equivalent<sup>18</sup>: pulvinar has higher ADC and lower FA than ventral nuclei. Pulvinar's role in vision is to entertain visual salience and to register position and movement of eyes and head at a higher order than purely retinotopic. Afferents to thalamus can be subdivided into drivers and modulators. Drivers are of first or higher order (Fig. 6). Topographical representation of the perceived quality is present in most thalamocortical projections, except for those from ventral anterior, midline, intralaminar

**Table 3** Expected network injury types in thalamus

thalamic subnucleus	type of function	expected (sub)cortical injury pattern leading to thalamic injury
ventral anterior, lateral, posterior	specific first order driver	premotor, MI, SI
pulvinar and lateral posterior intralaminar mediodorsal	higher order driver	parietal and occipital frontal and temporal orbitofrontal and prefrontal
ventral lateral	non-specific first order driver	premotor and MI in association with pallidal or cerebellar injury

**Figure 5**

Choice of regions of interest compared in patient nr 4.

nar and centromedian thalamic nuclei that project to large cortical areas with synapses mainly on layer 1 cells. Expected network injury patterns derived from such insight are in Table 3. Least vulnerable should be non-specific driver nuclei with a broad subcortical input and diffuse output. When cortical and striatal necrosis are associated, as in global forebrain ischaemia, thalamic nuclei that project to both cortex and striatum may be even more vulnerable, i.e. intralaminar and midline nuclei. Fibers in the external and extreme capsule along claustrum connect frontal and temporal, insular and parietal or insular and amygdalar areas; they can therefore acquire hypersignal in many variants of cortical injury<sup>19</sup>. In this report we have reported one of these expected patterns and predict more will be reported in the future.

The tools for studying the later effects of the acute changes we describe here, are available. Using a probabilistic tractography algorithm in diffusion tensor MR sequences, Behrens and coworkers noninvasively mapped connections between thalamus and cortex<sup>20,21</sup>. Their method was recently applied to scans of 2 year old ex-preterms without obvious neurological injury and changes in thalamocortical tracts and thalamic subnuclei were documented in an infant with focal white matter loss<sup>12</sup>.

The nature of secondary lesions is probably complex. Excitotoxic injury could play a role: cortical neurons suffering from electrographic seizures

transmit glutamatergic signals to connected thalamic nuclei<sup>21-23</sup>. Detailed measurement of lobar injury coupled to lobar electrographic seizure load may unravel the contribution of excitotoxicity in secondary injury to pulvinar. Following primary injury connected thalamic and brainstem nuclei may also undergo delayed neurodegeneration due to loss of trophic support from their cortical targets. This type of transsynaptic thalamic cell death is mainly apoptotic and develops over a period of a few days, peaking in intensity slightly later than necrosis in cortex or striatum<sup>24,25</sup>. Immature brains are more susceptible to this type of injury than mature ones, a.o. because the somatodendritic architecture is less arborized and thalamic axonal collaterals are scarcer. In this respect late cell migration into pulvinar may render it more injury-prone than other thalamic subnuclei. Natale et al. in 2002 reviewed lateral geniculate apoptosis, peaking already at 36 hours after cortical ablation without seizures in a mouse model<sup>26</sup>. Acute trophic thalamic cell death is therefore possible without seizures in this animal model. Necrosis follows the maturation phenomenon, i.e. the more severe an insult the shorter the time course of cells in their necrotic process, but in cortex and striatum the necrotic cycle is complete in around three days. Apoptosis can follow a similar fast course, but in some instances it may also take up to one week for a neuron to slowly die. For many reasons newborn infants with an insult - be it asphyxia, stroke or leukomalacia - are often scanned between 2 and 7 days after the event or the clinical presentation. In term birth asphyxia we strive for a scan on day 4. It is probably important that the infants with large artery stroke reported here were scanned during this time after the event. That ADC values in this report are lower in primary lesions in the (sub)cortex than in secondary lesion in pulvinar might be due to different mixtures of necrosis and apoptosis. Pre- and postcentral gyri in preterm infants between 25 and 38 weeks have significantly lower anisotropy than the superior occipital and superior frontal gyri, indicating that DTI is sensitive to regional heterogeneity in cortical development<sup>18</sup>. There is also a significant age-related decline in radial but not tangential diffusivities in all cortical areas. Such heterogeneity also exists in development of thalamic nuclei<sup>18</sup>. These findings prove that DWI-DTI differences between primary lesion and network injury also depend on location in the brain and on maturational stage.

Limitations of this study are: (1) the absence of a large cohort of normal ADC data in different thalamic subnuclei across different gestational ages; (2) the absence of a quantitative estimate of the burden of lobar injury (be it cortical or in white matter), that would permit finding thresholds above which distant tracts and nuclei become affected; (3) due to the retrospective nature it was not possible to calculate the load of lobar electrographic seizures in relation to injury to pulvinar; (4) the absence of histopathological studies of secondary pulvinar lesions; (5) because patients were scanned only once in the acute stage, this study is not in a position to answer questions about the optimal timing of DWI to pick up network injury. Because of these limitations these findings suggestive of acute network injury must be confirmed by other studies.

In conclusion, acute brain imaging in the latter part of the first week may depict transaxonal network injury. Within days changes in pulvinar follow focal infarction involving cortex and white matter. It would seem desirable in future intervention studies to document the effect of treatment not only on primary but also on network injury, using serial acute brain imaging<sup>27</sup>. Before that, the prognostic significance of network injury must be established in large prospective cohorts, not only for stroke but also for global forebrain ischemia and leukomalacia.

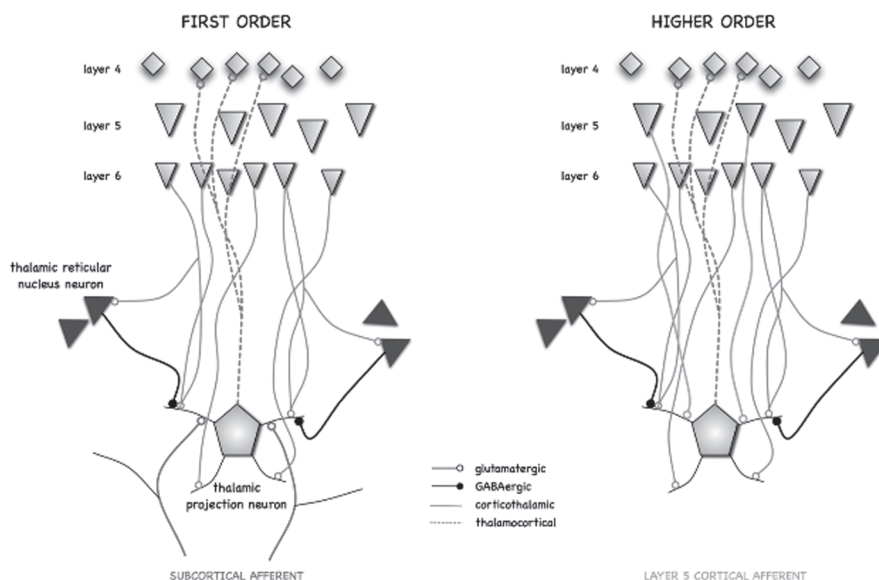


**Figure 6**

FIRST ORDER driving thalamic afferents transfer peripheral (subcortical) information to cortex for further processing. Specific first order afferents (mainly to layer 4, also to 3 and 6) come from thalamic relay nuclei in one of the sensory brain modes: VPL for somatosensory perception, lateral geniculate for visual and medial geniculate for auditory perception. The columnar cortical module is largely built on thalamocortical input. Reciprocal projections from these cortical areas to their thalamic nuclei and corresponding parts of the thalamic reticular nucleus come from layer 6. One thalamic cell forms synapses with many cells within a cortical column. The reciprocal corticothalamic axon number is an order of magnitude (at least 10 x) greater than the number of thalamocortical axons. Each cortical axon (most coming from layer 6) innervates many thalamic neurons, therefore there is considerable convergence and divergence in specific first order corticothalamic pathways. Non-specific first order afferents come from association thalamic nuclei that function in different systems: e.g. VL between cerebellum/pallidum and (pre)motor cortex in the motor system. There is more overlap in cortical areas innervated from these non-specific thalamic nuclei. Driving projections of HIGHER ORDER type come from neocortex onto nuclei like mediodorsal nucleus, pulvinar and intralaminar nuclei. Reciprocal connections emanate not only from layer 6 but also from layer 5 pyramidal cells to these thalamic nuclei, which depend heavily on the intact function of these neocortical areas because subcortical input to them is limited. Corticothalamic connections are glutamatergic. MODULATORS to thalamus come from thalamic reticular nucleus (inhibitory), hypothalamus, raphe nuclei, reticular formation, locus coeruleus. They filter information by switching the transmission mode of thalamic cells between tonic firing, rhythmic (quiet sleep or non-REM sleep) or arrhythmic bursting. When awake the burst mode acts like a "wake-up" system whereas the tonic mode works on a linear relay basis and permits faithful, detailed signal analysis. Thalamus as a whole filters and transforms information to the cortex and thereby becomes a tool for attention to events (adapted from Sherman and Koch 1998). (A full color version of this illustration can be found in the color section).

## References

1. M.K. Zarifi, L.G. Astrakas, T.Y. Poussaint, Ad.A. Plessis, D. Zurakowski, A.A. Tzika. Prediction of adverse outcome with cerebral lactate level and apparent diffusion coefficient in infants with perinatal asphyxia. *Radiology* 2002;225:859-70
2. R.C. McKinstry, J.H. Miller, A.Z. Snyder, A. Mathur, G.L. Schefft, C.R. Almlí, J.S. Shimony, S.I. Shiran, J.J. Neil. A prospective, longitudinal diffusion tensor imaging study of brain injury in newborns. *Neurology* 2002;24:824-33
3. A. Mazumdar, P. Mukherjee, J.H. Miller, H. Malde, R.C. McKinstry. Diffusion-weighted imaging of acute corticospinal tract injury preceding Wallerian degeneration in the maturing human brain. *AJNR Am J Neuroradiol* 2003;24:1057-66
4. A. Uchino, A. Sawada, Y. Takase, R. Egashira, S. Kudo. Transient detection of early wallerian degeneration on diffusion-weighted MRI after an acute cerebrovascular accident. *Neuroradiology* 2004;46:183-8
5. R.W. Hunt, J.J. Neil, L.T. Coleman, M.J. Kean, T.E. Inder. Apparent diffusion coefficient in the posterior limb of the internal capsule predicts outcome after perinatal asphyxia. *Pediatrics* 2004;114:999-1003
6. F.M. Cowan, L.S. de Vries. The internal capsule in neonatal imaging. *Seminars in Fetal and Neonatal Medicine* 2005;10:461-74
7. C. Boichot, P.M. Walker, C. Durand, M. Grimaldi, S. Chapui, J.B. Gouyon, F. Brunotte. Term neonate prognoses after perinatal asphyxia: contributions of MR imaging, MR spectroscopy, relaxation times, and apparent diffusion coefficients. *Radiology* 2006;239:839-48
8. F. Groenendaal, M.J. Benders, L.S. de Vries. Pre-wallerian degeneration in the neonatal brain following perinatal cerebral hypoxia-ischemia demonstrated with MRI. *Semin Perinatol* 2006;30:146-50
9. K. Yokochi. Thalamic lesions revealed by MR associated with periventricular leukomalacia and clinical profiles of subjects. *Acta Paediatr* 1997;86:493-6

10. Y. Lin, A. Okumura, F. Hayakawa, K. Kato, T. Kuno, K. Watanabe. Quantitative evaluation of thalami and basal ganglia in infants with periventricular leukomalacia. *Dev Med Child Neurol* 2001;43:481-5
11. D. Ricci, S. Anker, F.M. Cowan, M. Pane, F. Gallini, R. Luciano, V. Donvito, G. Baranello, L. Cesarini, F. Bianco, M.A. Rutherford, C. Romagnoli, J. Atkinson, O. Braddick, F. Guzzetta, E. Mercuri. Thalamic atrophy in infants with PVL and cerebral visual impairment. *Early Hum Dev* 2006;82:591-5
12. S.J. Counsell, L.E. Dyet, D.J. Larkman, R.G. Nunes, J.P. Boardman, J.M. Allsop, J. Fitzpatrick, L. Srinivasan, F.M. Cowan, J.V. Hajnal, M.A. Rutherford, A.D. Edwards. Thalamo-cortical connectivity in children born preterm mapped using probabilistic magnetic resonance tractography. *Neuroimage* 2007;34:896-904
13. Altman, J., Bayer, S.A., 1989. Development of the rat thalamus.
14. J. Mojsilovic, N. Zecevic. Early development of the human thalamus: Golgi and Nissl study. *Early Hum Dev* 1991;27:119-44
15. P. Rakic, R.L. Sidman. Telencephalic origin of pulvinar neurons in the fetal human brain. *Z Anat Entwicklungsgesch* 1969;129:53-82
16. K. Letinic, I. Kostovic. Transient fetal structure, the gangliothalamic body, connects telencephalic germinal zone with all thalamic regions in the developing human brain. *J Comp Neurol* 1997;384:373-95
17. K.L. Grieve, C. Acuna, J. Cudeiro. The primate pulvinar nuclei: vision and action. *Trends Neurosci* 2000;23:35-9
18. A.R. delpolyi, P. Mukherjee, K. Gill, R.G. Henry, S.C. Partridge, S. Veeraraghavan, H. Jin, Y. Lu, S.P. Miller, D.M. Ferriero, D.B. Vigneron, A.J. Barkovich. Comparing microstructural and macrostructural development of the cerebral cortex in premature newborns: diffusion tensor imaging versus cortical gyration. *Neuroimage* 2005;27:579-86
19. P. Gloor (1997). The temporal lobe and limbic system, subchapter capsula externa and interna, p 242
20. T.E. Behrens, H. Johansen-Berg, M.W. Woolrich, S.M. Smith, C.A. Wheeler-Kingshott, P.A. Boulby, G.J. Barker, E.L. Sillery, K. Sheehan, O. Ciccarelli, A.J. Thompson, J.M. Brady, P.M. Matthews. Non-invasive mapping of connections between human thalamus and cortex using diffusion imaging. *Nat Neurosci* 2003;6:750-7
21. B.S. Meldrum, R.A. Vigouroux, J.B. Brierley. Systemic factors and epileptic brain damage: prolonged seizures in paralyzed, artificially ventilated baboons. *Arch Neurol* 1973;29:82-7

22. G.L. Holmes, Y. Ben-Ari. The neurobiology and consequences of epilepsy in the developing brain. *Pediatr Res* 2001;49:320-5
23. D.G. Fujikawa. Prolonged seizures and cellular injury: Understanding the connection. *Epilepsy & Behavior* 2005;7:3–11
24. L.J. Martin, N.A. Al-Abdulla, A.M. Brambrink, J.R. Kirsch, F.E. Sieber, C. Portera-Caillau. Neurodegeneration in excitotoxicity, global cerebral ischemia, and target deprivation: a perspective on the contributions of apoptosis and necrosis. *Brain Research Bulletin* 1998;46:281-309
25. F.J. Northington, D.M. Ferriero, E.M. Graham, R.J. Traystman, L.J. Martin. Early Neurodegeneration after Hypoxia-Ischemia in Neonatal Rat Is Necrosis while Delayed Neuronal Death Is Apoptosis. *Neurobiology of Disease* 2001;8:207-19
26. J.E. Natale, Y. Cheng, L.J. Martin. Thalamic neuronal apoptosis emerges rapidly after cortical damage in immature mice. *Neuroscience* 2002;112:665-76
27. F.J. Northington, E.M. Graham, L.J. Martin. Apoptosis in perinatal hypoxic-ischemic brain injury: how important is it and should it be inhibited? *Brain research Reviews* 2005;50:244-57









# Chapter 9

## DIFFUSION TENSOR IMAGING REVEALS ACUTE NETWORK INJURY IN NEONATAL ARTERIAL ISCHEMIC STROKE

---

J. Dudink  
S.J. Counsell  
M.H. Lequin  
A. Taselaar  
J.B. van Goudoever  
P.P. Govaert

*Submitted*

## **Abstract**

### ***Background and Purpose***

We used diffusion tensor imaging to study the effects of network injury in the ipsilateral thalamus after unilateral arterial ischemic stroke in the term newborn.

### ***Materials and Methods***

DTI images of 3 term infants with acute extensive unilateral cortical arterial ischemic stroke were analyzed. All infants were scanned on a 1,5 Tesla MRI scanner. We used probabilistic tractography postprocessing to define the regions of interest (ROI) in the thalamus. We evaluated the three eigenvalues and calculated the apparent diffusion coefficient (ADC).

### ***Results***

We found significantly lower ADC values in the voxels of the ROI's placed within the nuclei corresponding to ischemic cortex compared to the unaffected contralesional thalamic nuclei.

### ***Conclusion***

Our finding support the concept of acute network injury, showing how DTI enables to show how deep grey matter is directly affected after a primary hit to its connected cortex in neonatal stroke.

---

Neonatal arterial ischemic stroke (NAIS) is an important cause of long-term neurologic morbidity including cerebral palsy, epilepsy, and cognitive impairment.<sup>1-4</sup> The incidence of neonatally symptomatic NAIS is at least 1/4000 term liveborn infants.<sup>5</sup>

Magnetic resonance imaging is the investigation of choice in perinatal stroke. Diffusion-weighted imaging (DWI) can detect neonatal ischemic brain injury within 24 hours of its onset with the acute changes being seen for several days.

DWI also allows us to visualize acute secondary effects of neuronal injury on connected projection tracts. An example is the early stage of Wallerian degeneration seen on DWI, which is correlated with outcome in neonatal arterial ischemic stroke (NAIS).<sup>6-9</sup>

Recently Govaert et al. reviewed DWI scans of perinatal brain lesions looking for early secondary changes in distant nuclei and tracts associated with primary cortical or white matter injury.<sup>10</sup> We described for the first time a pattern of thalamocortical interaction where extensive cortical injury from neonatal stroke led to acute changes in pulvinar not explained by disturbances in vascular perfusion.

Diffusion Tensor Imaging (DTI) is an MRI sequence that offers to study effects of network injury on the thalamus, because it visualizes micro-architectural organization of tissue in life. It allows objective and reproducible assessment of tissue characteristics.<sup>11</sup> A relatively new DTI post-processing probabilistic tractography technique describes the cortical connectivity map of thalamus.<sup>12-13</sup>

Our aim is to use DTI and probabilistic tractography postprocessing for the study of the acute effects of NIAS on ipsilateral thalamus.

## Materials and Methods

### Subjects

We analyzed DTI images of 3 term infants with acute extensive unilateral cortical arterial ischemic stroke. Patient characteristics are shown in table 1. Longstanding antepartum injury was excluded by normal findings on routine first day ultrasound scanning in these infants. They were born in 2008 and 2009, scanned in the latter part of the first week and with artifact free DTI and T2 weighted scans.

**Table 1**  
Patient Characteristics.

	Patient 1	Patient 2	Patient 3
GA (weeks)	40 1/7	41	37 1/7
BW (grams)	3800	3750	3620
Pregnancy	Uncomplicated	Uncomplicated	Uncomplicated
Mode of delivery	Spontaneous vaginal	Cesarean section	Spontaneous vaginal
APGAR score (1 - 5 min)	9-9	3-6	7-9
Presenting signs	Focal (right sided) seizures	Apnea	Generalized seizures
Arterial territory	Left posterior truncal MCA stroke	Left PCA stroke	Left complete MCA stroke
Cortical area involved in stroke	Sensory-, Parietal- and Temporal cortex	Occipital cortex	Frontal-, Motor-, Sensory-, Parietal- and Temporal cortex

Table 1: showing patient characteristics: GA = gestational age, BW = birthweight, MCA = middle cerebral artery, PCA = posterior cerebral artery.

## MR imaging technique

### Image acquisition

All imaging was performed on a 1.5-T GE EchoSpeed scanner (GE Medical Systems, Milwaukee, Wis.). All studies were performed according to a protocol that included axial dual T2 spin echo, axial T1 spin echo or axial T13D SPGR, sagittal T1 spin echo, axial PD (proton density) and

---

coronal FLAIR. Diffusion tensor images (DTI) were acquired using multi repetition, single shot echo-planar sequence with a slice thickness of 3 mm with no gap. The images were gathered in 25 gradient directions with sensitivity of  $b = 1000 \text{ s/mm}^2$ , TR/TE = 8700–11725/83–98 ms, field of view 18–24 cm<sup>2</sup>, the scan matrix 128×128 and the reconstruction matrix 256×256.

DTI studies the motion of water along different non-collinear directions, from which a mathematical tensor can be calculated, which describes the motion of water in the studied tissue. This tensor can be conceptualised as an ellipsoid of which the long axis represents the direction with the highest diffusivity; the magnitude of its diffusivity is given by the major eigenvalue ( $\lambda_1$ ) and its direction is called the major eigenvector. Perpendiculars to the major eigenvector are the two short axes: the median and minimum eigenvectors, with their eigenvalues  $\lambda_2$  and  $\lambda_3$ .

With DTI, a mathematical tensor can be conceptualized as an ellipsoid of which the long axis represents the direction with the highest diffusivity; the magnitude of its diffusivity is given by the major eigenvalue ( $\lambda_1$ ) and its direction is called the major eigenvector. Perpendiculars to the major eigenvector are the two short axes: the median and minimum eigenvectors, with their eigenvalues  $\lambda_2$  and  $\lambda_3$ .

The patients were scanned using an MR-compatible incubator with a specialized high-sensitivity neonatal head coil (Lammers Medical Technology, Lubeck, Germany) that allowed DTI imaging at high spatial resolution and high signal-to-noise ratio (SNR). The incubator provided controlled temperature and humidity as well as MR-compatible pulse oximetry and ventilation. We used mouldable earplugs and neonatal earmuffs to reduce noise. No sedation was given. Pads around the infant's head kept movement to a minimum.

### ***Data analysis***

Data analysis was performed using FSL.<sup>14</sup> We minimized image artifacts due to eddy current distortions by registering the DT images to the b0 images. DTI data and T2 weighted imaging were skull stripped. Next au-

tomated image registration was used to co-register DTI data from each patient to a template image (ICBM-MNI 152) using 12-mode affine transformation.<sup>15</sup> The cortical seed masks were defined from the Harvard Oxford Cortical Structural Atlas. Results were visually inspected. Thalamic masks were generated on T2 weighted images and also co-registered onto the infant's native DTI data.

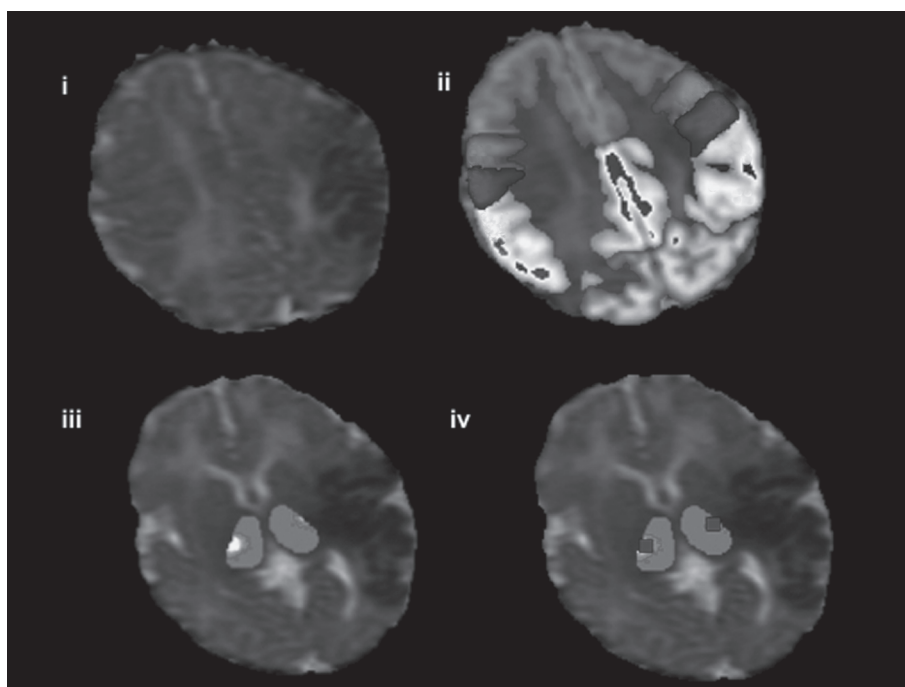


**Figure 1**

Images of a patient with a posterior truncal MCA stroke: (i) ADC map showing low SI in area of stroke (ii) same ADC-map after automated image registration software was used to co-register DTI data from the patient to standard cortical masks (Harvard Oxford Cortical Structural Atlas) (red-yellow = frontal cortex (minus the prim motor area), red = prim motor cortex, blue = sensory cortex, yellow = parietal cortex (minus the prim sens cortex) and light blue = occipital cortex) (iii) thalamo-cortical connections were assessed for every voxel in the thalamic masks (green) using connectivity-based seed classification with predefined thresholds; yellow-red area is the seed mask of the parietal cortex, there is a clear difference between right and left thalamus ( $R > L$ ) (iv) The thalamic connectivity seeds were used to place ROIs from which the DTI measurements were taken. (A full color version of this illustration can be found in the color section).



---

### ***Thalamo-cortical projections***

We manually delineated the thalamic masks on T2 weighted images and propagated them onto the infant's native DTI data. We used the third ventricle to form the medial border, the posterior limb of the internal capsules (PLIC) was used to delineate the lateral border and the subthalamic nuclei was used as the inferior border.<sup>13</sup> Posterior border was the posterior part of the pulvinar.

The cortex was divided into functional cortico-thalamic areas: the frontal cortex (with exclusion of the primary motor area), the primary motor cortex, primary sensory cortex, parietal cortex (primary sensory cortex excluded), temporal cortex and occipital cortex (Figure 1). Thalamo-cortical connections were assessed for every voxel in the thalamic masks using connectivity-based seed classification with predefined thresholds. The thalamic connectivity seeds were used to place regions of interest (ROIs) from which the DTI measurements were taken (Figure1).

### ***Statistical method***

The values of the voxels in the region of interests of the affected sides were compared with those of the healthy contralateral thalamus, using the paired T-test with two tails (Graphpad InStat for Macintosh).

## **Results**

### ***ADC values***

When comparing ADC values of the voxels of the ROI's between ipsi- and contralesional thalamus we found significantly lower ADC values in the ROI's placed within the nuclei corresponding to ischemic cortex (Table 2). Patient 1 suffered from a left posterior truncal MCA stroke with sensory, parietal and temporal cortex affected. In all connected ipsilateral thalamic nuclei we found significantly lower ADC values compared to corresponding nuclei of the contralesional thalamus ( $P < 0.05$ ). Patient 2 had left PCA stroke affecting occipital cortex on DWI and T2; a significantly lower mean ADC value was measured in ipsilateral compared to

contralateral pulvinar. Patient 3 had a (extensive) complete MCA stroke involving frontal, motor, sensory, parietal and temporal cortex; we found significantly lower ADC values in corresponding ipsilateral thalamic nuclei.

The ADC values found in the contralesional thalamus are of the order of magnitude of ADC values found in the thalami of healthy term infants reported by other authors.<sup>16-20</sup>

**Table 2**  
ADC values of thalamic nuclei.

		Frontal	Occipital	Parietal	Sensory	Motor	Temporal
Patient 1							
Ipsilateral	Mean	0.001132	0.001059	<b>0.000831*</b>	<b>0.000818*</b>	0.001048	<b>0.000897*</b>
	SD	0.000034	0.000145	0.000081	0.000075	0.000099	0.000099
Contralesional	Mean	0.001100	0.001055	0.000995	0.000983	0.001023	0.001018
	SD	0.000018	0.000105	0.000042	0.000044	0.000034	0.000072
Patient 2							
Ipsilateral	Mean	0.001850	<b>0.000425*</b>	0.0017303	0.001616	0.001633	0.001852
	SD	0.000119	0.000013	0.000194	0.000198	0.000179	0.000129
Contralesional	Mean	0.00185	0.00105	0.001743	0.001601	0.00167	0.001837
	SD	0.000092	0.000040	0.000224	0.000121	0.000160	0.000080
Patient 3							
Ipsilateral	Mean	<b>0.000634*</b>	0.00105	<b>0.000647*</b>	<b>0.000644*</b>	<b>0.000643*</b>	<b>0.000728*</b>
	SD	0.000019	0.0001	0.000036	0.000019	0.000020	0.000068
Contralesional	Mean	0.000909	0.001045	0.000936	0.000898	0.000903	0.001004
	SD	0.000018	0.000040	0.000038	0.000029	0.000036	0.000051

Table 2: showing mean and standard deviation (SD) ADC values (in mm<sup>2</sup>/s) measured in the regions of interests (ROIs) of different thalamic nuclei of the ipsilateral and contralesional thalamus.

\* Significant (p<0.05) lower ADC values compared to contralesional nuclei.

**L1, L2, L3 values**

All eigenvalues ( $\lambda_1$ ,  $\lambda_2$  and  $\lambda_3$ ) of the voxels in the ROI's of the affected ipsilateral thalamic nuclei were significantly lower compared to the corresponding contralesional nuclei. When comparing mean differences of  $\lambda_1$ ,  $\lambda_2$  and  $\lambda_3$  we found the 'absolute' mean difference  $\lambda_1 > \lambda_2 > \lambda_3$  in all affected thalamic nuclei. When comparing the relative mean difference

(which is the mean difference divided by the arithmetic mean) of the  $\lambda_1$ ,  $\lambda_2$  and  $\lambda_3$  we found the largest relative mean difference in the  $\lambda_1$  values (Table 3).

**Table 3**  
Mean differences between eigenvalues of affected thalamic nuclei.

		Frontal	Occipital	Parietal	Sensory	Motor	Temporal
Patient 1							
$\lambda_1$	MD			0.000265	0.000268		0.000276
	RMD			0.20	0.24		0.24
$\lambda_2$	MD			0.0001	0.00014		0.000126
	RMD			0.116	0.166		0.13
$\lambda_3$	MD			0.000129	0.000103		0.00004
	RMD			0.171	0.138		0.05
Patient 2							
$\lambda_1$	MD		0.000723				
	RMD		0.88				
$\lambda_2$	MD		0.000654				
	RMD		0.84				
$\lambda_3$	MD		0.000509				
	RMD		0.8				
Patient 3							
$\lambda_1$	MD	0.000376		0.000413	0.00039	0.000371	0.000364
	RMD	0.41		0.45	0.43	0.41	0.37
$\lambda_2$	MD	0.000248		0.000294	0.000223	0.000213	0.000281
	RMD	0.33		0.37	0.29	0.28	0.33
$\lambda_3$	MD	0.000201		0.000162	0.000147	0.000197	0.000183
	RMD	0.31		0.25	0.23	0.29*	0.24

Table 3: Shows the mean differences (MD) of L1, L2 and L3 between the ipsilateral and contral-  
esional thalamus of the significantly affected thalamic nulcei of Table 2. And the relative mean  
difference (RMD); which is the mean difference divided by the arithmetic mean of the L1, L2 and  
L3 between the ipsilateral and contralesional thalamus.

## Discussion

Our study shows significant changes in DTI values of voxels in the regions of the ipsilateral thalamus, which are connected to injured cortex, revealing acute secondary network injury. These results support the concept of acute network injury, showing how deep grey matter (specifically thalamic nuclei) is directly affected after a primary hit to its connected cortex.

For decades pathologists have reported the concept that primary cortical injury can lead to cell loss in thalamus. Global thalamic shrinkage has been associated with preterm white matter injury,<sup>21,22</sup> and long-term influence of perinatal venous white matter infarction on thalamus at 2 years of age has been shown with DTI probabilistic tractography.<sup>13</sup>

In 2005 Herve et al reported an early decrease in transient diffusion measured in the ipsilateral thalamus of adult patients with large infarctions involving the cortex and internal capsule.<sup>16</sup> It was noted their findings could not be attributed to direct ischaemic cytotoxic oedema because the location of the ischaemic lesions as detected on late T2-weighted scans only involved the MCA territory which does not include thalamus. In serial scans of the same patients they found a delay in diffusion decrease that was not observed in the primary areas of cytotoxic oedema.

Recently, Govaert et al. reported findings of acute secondary axonal effects of cell injury in nuclei connected to the primary lesion sites in NIAS.<sup>10</sup> The study evaluated term infants with cortical stroke, showing signal hyperintensities in the ipsilateral pulvinar on DWI and a decrease in ADC values during the acute phases on the injury. Because the pulvinar was outside of the primary territory of infarction and because these infants showed no evidence of hypoxia, the authors concluded that their findings suggested acute secondary injury to the pulvinar, i.e. following primary damage of their cortical targets and/or connecting axons.

In experimental animal models acute transient diffusion decrease in grey matter remote from the ischaemic area has also been reported.<sup>23</sup> This seemed to be temporally related to swelling of neurons and perivascular

---

astrocyte feet. Astrocytic and microglial activation may also account for the decrease mobility of water molecules in ipsilateral thalamus.

Several mechanisms have been suggested to explain secondary neuronal cell death in the ipsilateral thalamus.<sup>10,24</sup> First excitotoxic injury has been suggested to play a role: cortical neurons suffering from electrographic seizures transmit glutamatergic signals to connected thalamic nuclei.<sup>25,26</sup> This concept could explain the signal intensities on the diffusion weighted images. Following primary injury the connected thalamic nuclei may also undergo delayed neurodegeneration due to loss of trophic support from their cortical targets. This type of transsynaptic thalamic cell death is mainly apoptotic and develops over a period of a few days, peaking in intensity slightly later than necrosis in cortex or striatum.<sup>27-28</sup>

In the affected nuclei of the ipsilateral thalamus we found the primary eigenvalue to be the most reduced compared to the second and third eigenvalues. Our data are supported by Sorensen et al,<sup>29</sup> which showed that in abnormal grey matter regions of patients with acute ischemia the primary eigenvalue was reduced most. Combining histopathology with DTI will shed more light on the underlying mechanisms of these findings.

Our study has a few limitations. One is the absence of a large cohort of normal DTI data in different thalamic subnuclei. We used the contralateral thalamus as a reference. Although there are a number of studies reporting on normal DTI values in the thalamus which seem to be of the same order of magnitude as the values found in our study, to our knowledge none of these studies have used probabilistic methods to measure DTI values in different thalamic subnuclei.<sup>16-20</sup> Another limitation is the absence of histopathological studies of secondary thalamic lesions in term newborn. Also our patients only had a single scan and so our study did not allow to define optimal timing of DTI to pick up network injury. A low number of subjects is also a limitation of this study. Finally the absence of a quantitative estimate of the primary injury did not permit finding thresholds above which distant tracts and nuclei become affected.

## Summary

Our finding support the concept of acute network injury, showing how DTI enables to show how in NAIS deep grey matter is directly affected after a primary hit to its connected cortex. This intriguing concept may lead to better understanding of the variability in neurological outcomes in perinatal stroke.

Future research efforts should be directed at determining the relevance of delineating network injury, its influence on prognosis, and the impact of early treatment of a newborn with stroke.

## References

1. E. Mercuri, A. Barnett, M.A. Rutherford, et al. Neonatal cerebral infarction and neuromotor outcome at school age. *Pediatrics* 2004;113:95–100
2. A. Kirton, G. deVeber. Cerebral palsy secondary to perinatal ischemic stroke. *Clin Perinatol* 2006;33:367–86
3. B.B. Wulfeck, D.A. Trauner, P.A. Tallal. Neurologic, cognitive, and linguistic features of infants after early stroke. *Pediatr Neurol* 1991;7:266–9
4. D.A. Trauner, C. Chase, P. Walker, et al. Neurologic profiles of infants and children after perinatal stroke. *Pediatr Neurol* 1993;9:383–6
5. J.K. Lynch, K.B. Nelson. Epidemiology of perinatal stroke. *Curr Opin Pediatr* 2001;13:499–505
6. R.C. McKinstry, J.H. Miller, A.Z. Snyder, et al. A prospective, longitudinal diffusion tensor imaging study of brain injury in newborns. *Neurology* 2002;24: 824–33
7. L.S. De Vries, J. Van der Grond, I.C. Van Haastert, et al. Prediction of outcome in new-born infants with arterial ischaemic stroke using diffusion-weighted magnetic resonance imaging. *Neuropediatrics* 2005;36:12–20

8. F.M. Cowan, L.S. de Vries. The internal capsule in neonatal imaging. *Semin Fetal Neonat Med* 2005;10:461–74
9. F. Groenendaal, M.J. Benders, L.S. de Vries. Pre-wallerian degeneration in the neonatal brain following perinatal cerebral hypoxia–ischemia demonstrated with MRI. *Semin Perinatol* 2006;30:146–50
10. P.P. Govaert, A. Zingman, Y.H. Jung, et al. Network injury to pulvinar with neonatal arterial ischemic stroke. *NeuroImage* 2008;39:1850–7
11. C. Beaulieu. The basis of anisotropic water diffusion in the nervous system: a technical review. *NMR Biomed* 2002;15:435–55
12. T.E. Behrens, H. Johansen-Berg, M.W. Woolrich, et al. Noninvasive mapping of connections between human thalamus and cortex using diffusion imaging. *Nat Neurosci* 2003;6:750–7
13. S.J. Counsell, L.E. Dyet, D.J. Larkman, et al. Thalamo-cortical connectivity in children born preterm mapped using probabilistic magnetic resonance tractography. *NeuroImage* 2007; 34: 896–904
14. S.M. Smith, M. Jenkinson, M.W. Woolrich, et al. Advances in functional and structural MR image analysis and implementation as FSL. *Neuroimage* 2004;23:208-19
15. J.Zhang, A. Evans, L. Hermoye, et al. Evidence of slow maturation of the superior longitudinal fasciculus in early childhood by diffusion tensor imaging. *Neuroimage* 2007;38:239-47
16. D. Herve, N. Molko, S. Pappata, et al. Longitudinal thalamic diffusion changes after middle cerebral artery infarcts. *J Neurol Neurosurg* 2005;76:200-5
17. R.L. Wolf, R.A. Zimmerman, R. Clancy et al. Quantitative apparent diffusion coefficient measurements in term neonates for early detection of hypoxic-ischemic brain injury: Initial experience. *Radiology* 2001;218:825-33
18. P. Ward, S.J. Counsel, J. Allsop et al. Reduced fractional anisotropy on diffusion tensor magnetic resonance imaging after hypoxic-ischemic encephalopathy. *Pediatrics* 2006;117:619-30
19. A.I. Bartha, K.R. Yap, S.P. Miller et al. The normal neonatal brain: MR imaging, diffusion tensor imaging, and 3D MR spectroscopy in healthy term neonates. *AJNR Am J Neuroradiol* 2007;28:1015-21

20. M.A. Rutherford, S.J. Counsell, J. Allsop et al. Diffusion-Weighted Magnetic Resonance Imaging in Term Perinatal Brain Injury: A Comparison With Site of Lesion and Time From Birth. *Pediatrics* 2004;114:1004-14
21. Y. Lin, A. Okumura, F. Hayakawa et al. Quantitative evaluation of thalami and basal ganglia in infants with periventricular leukomalacia. *Dev Med Child Neurol* 2001;43:481-5
22. D. Ricci, S. Anker, F.M. Cowan et al. Thalamic atrophy in infants with PVL and cerebral visual impairment. *Early Hum Dev* 2006;82:591-5
23. M. Nakane, A. Tamura, Y. Sasaki et al. MRI of secondary changes in the thalamus following a cerebral infarct. *Neuroradiology* 2002;44:915-20
24. M. Dihné, C. Grommes, M. Lutzenburg et al. Different mechanisms of secondary neuronal damage in thalamic nuclei after focal cerebral ischemia in rats. *Stroke* 2002;33:3006-11
25. B.S. Meldrum, R.A. Vigouroux, J.B. Brierley. Systemic factors and epileptic brain damage: pro- longed seizures in paralyzed, artificially ventilated baboons. *Arch Neurol* 1973;29:82-7
26. G.L. Holmes, Y. Ben-Ari. The neurobiology and consequences of epilepsy in the developing brain. *Pediatr Res* 2001;49:320-5
27. L.J. Martin, N.A. Al-Abdulla, A.M. Brambrink et al. Neurodegeneration in excitotoxicity, global cerebral ischemia, and target deprivation: a perspective on the contributions of apoptosis and necrosis. *Brain Research Bulletin* 1998;46:281-309
28. F.J. Northington, D.M. Ferriero, E.M. Graham et al. Early Neurodegeneration after Hypoxia-Ischemia in Neonatal Rat Is Necrosis while Delayed Neuronal Death Is Apoptosis. *Neurobiology of Disease* 2001;8:207-19
29. A.G. Sorensen, O. Wu, W.A. Copen et al. Human acute cerebral ischemia: detection of changes in water diffusion anisotropy by using MR imaging. *Radiology* 1999;212:785-92









# Chapter 10

GENERAL DISCUSSION  
FUTURE DIRECTIONS  
SUMMARY  
SAMENVATTING  
DANKWOORD  
LIST OF PUBLICATIONS  
CURRICULUM VITAE  
PHD PORTFOLIO

---

## General discussion

Damage to the developing brain is associated with significant risk of life-long neurodevelopmental consequences<sup>1</sup>. Despite advances in neonatal intensive care in recent decades, dedicated brain-oriented care of the critically ill neonate has not yet been established<sup>2</sup>.

Although major successes have been achieved in experimental neuroscience, neuroprotective interventions for human newborns performed poorly in many clinical trials. This is partly explained by difficulties in diagnosis, timing, and determination of the severity of neonatal brain damage<sup>3</sup>.

Brain injury in infants is often unanticipated, and especially in premature infants, remains “silent,” until long after the threshold of irreversible injury has been crossed<sup>1</sup>. An important challenge is to define early proxy measurements of outcome. The gold standard end-point for neuroprotection strategies is functional neurodevelopmental outcome, defined for instance by the ‘Bayley-scores of neurodevelopment’<sup>4</sup>.

Advanced ‘cutting edge’ neuroimaging techniques have the potential to overcome many of these challenges<sup>5</sup>. Neuroimaging techniques are able to quantify various aspects of brain growth, connectivity, metabolism, perfusion, and function<sup>6</sup>. Diffusion weighted MR imaging has increased our ability to identify and quantify many aspects of brain injury. It has also proved useful to understand more about timing and evolution of structural injury to the immature brain. Ongoing developments of MRI post-processing software are providing researchers tools to design early proxy predictors of outcome.

DTI is a neuroimaging tool that has shown great advances in recent years with it’s application constantly expanding. The primary reason for success of DTI is because water diffusion in tissues is highly sensitive to differences in the microstructural architecture of cellular membranes. This sensitivity renders DTI a powerful method for detecting microscopic differences in tissue properties. In this thesis the application of DTI in neonatal neuroimaging was studied.

---

**Chapter 2** reviews the use of DTI to study white matter maturation and brain injury in the preterm brain. Research has shown how DTI allows to study brain connectivity and plasticity and how DTI has contributed to our understanding of preterm WM maturation, WM injury and plasticity. Methods for DTI acquisition and analysis are evolving rapidly. This has greatly improved the accuracy of DTI measurements in recent years. Both **chapter 2** and **chapter 3** illustrate the use of white matter tractography (fiber tracking). Despite promising results, there are several limitations of tractography. Estimates of the eigenvector directions, and hence the local tract directions, are sensitive to thermal noise, physiologic fluctuations and image artifacts. Algorithms based upon the major eigenvector are unable to resolve regions of crossing white matter pathways. New diffusion imaging methods, such as QBI (q Ball Imaging)<sup>7</sup>; HARDI (High Angular Diffusion Imaging)<sup>8</sup>; CHARMED (Combined Hindered and Restricted Diffusion)<sup>9</sup>; DSI (Diffusion Spectrum Imaging)<sup>10</sup>, may resolve intersecting crossing white matter regions more accurately. However, these methods require higher diffusion-weighting (typically 3,000–15,000 s/mm<sup>2</sup>) and take minutes more time to acquire.

**Chapter 3** describes the results of a retrospective study aimed at providing FA and ADC reference values for the clinical interpretation of DTI images in VLBW infants. However caution is warranted when interpreting changes in the measured diffusion tensor. Research is often focused on diffusion anisotropy (usually FA), which may not suffice to characterize tissue changes. Alternatively, recent studies started to measure either eigenvalues or the radial and axial diffusivities to provide more specific information about the diffusion tensor. Other pitfalls when interpreting DTI measurements is the sensitivity of the diffusion tensor, and the anisotropy in particular, to a broad spectrum of other factors: which include (1) image noise (both thermal and physiologic) (2) artifacts (i.e., misregistration of DW images from eddy currents or head motion), (3) partial volume averaging between tissues in large voxels (signal mixing of gray matter, white matter and cerebral spinal fluid), (4) and regions of crossing WM tracts. Many regions of the brain contain considerable areas of fiber crossing, which have corresponding low FA. Thus crossing WM fiber groups within a voxel can result in significant anisotropy changes without any white matter abnormalities. Within healthy WM, FA

can range between values and crossing WM fibers causes much of this variation. The variability in FA can be reduced considerably by focusing on white matter tracts in specific anatomic regions.

**Chapter 4** reports FA and ADC values of subplate and cortical plate in VLBW infants with normal developmental outcome, to be used as reference values. Because the subplate is a site of early neural activity and considered selectively vulnerable to hypoxic/ischemic injury, it is of great interest in the study of preterm brain injury. The study uses manually placed ROI measurements, a commonly used technique enabling easy clinical use. However manual ROI placement is observer dependent and so easy automatic segmentation of the subplate would be preferred. Our research group is currently looking into this option.

**Chapter 5** shows the results of a study in which DTI scans of the neonatal brain obtained at high b values are evaluated. It was found that the increase in diffusion image contrast observed at high b values could be useful in identifying lesions in the neonatal brain. However one of the disadvantages of high b values DTI are reduced signal to noise ratios (SNR). Multiple signal averages were required to achieve adequate SNR, which increases image acquisition time and hence susceptibility to image degradation due to patient motion, which is of particular importance when imaging neonates. The dependence of FA and ADC values on the preset b values should always be taken into account when comparing data<sup>11</sup>.

**Chapter 6** summarizes the current literature on neuroimaging of neonatal stroke. Showing the important role of DWI in the acute stages of the infarction. DWI (including DTI) seems to be inadequate to predict future neurodevelopment. The way forward has to be to combine cutting-edge neuroimaging techniques to quantify various aspects of brain injury, including: connectivity, metabolism, perfusion, and function in a complementary manner.

**Chapter 7** describes the evolution of unilateral perinatal arterial ischemic stroke (PAIS) on serial conventional and DW MR scans from symptomatic term infants. In this study the “healthy” hemisphere was used

---

as an internal control. As described in **chapter 6 and 8** trans-synaptic degeneration causes network injury, which might even affect the healthy contralesional hemisphere. This makes a case for using healthy term controls in future studies.

**Chapter 8** and **Chapter 9** show how primary cortical damage leads to secondary network injury in thalamus. There is still a lack of objective reproducible quantitative estimates of primary stroke injury. This estimates the need to find the thresholds (size and location) above which distant tracts and nuclei become affected. The relevance of delineating network injury, its influence on prognosis, and the impact of early treatment of a newborn with stroke are still largely unknown and needs further investigation.

## Future directions

Vast improvements have been made in DTI in the past years and it is expected that the next decade will lead to even more important new developments in cerebral diffusion measurements with MRI. Incorporating these advanced DTI techniques into daily clinical neonatal intensive care is one of the challenges we face in the near future. Only by combining knowledge of specialized MR physicists, pediatric radiologists and neonatologists these new DTI techniques will become new clinical tools: automated, and user friendly.

Different neuroimaging and monitoring techniques have shown great improvements in the last decade. Near infrared spectroscopy (NIRS), continuous (a)EEG, cerebral ultrasound (3D, new Doppler techniques, raw preprocessed signals) have all booked vast improvements in technique and postprocessing. Selecting and combining specific measurements into a 'multimodel neuromonitoring' will be needed to evaluate those aspects of brain metabolism, perfusion, and microstructure involved in acute injury and to assess anticipated effects of neuroprotection trials.

In vivo analysis of inflammation patterns is of great interest for neonatal neuroscientists. Because of unique cerebrovascular anatomy and physiology, the white matter of the preterm infant is very sensitive to the abnormal milieu present in extrauterine life, in particular ischaemia and inflammation<sup>12</sup>. Inflammation imaging could be the next MRI technique, which could (combined with existing MRI tools) help us answer the remaining questions concerning preterm brain damage. Iron oxide particles such as superparamagnetic iron oxide (SPIO) and ultrasmall SPIO (USPIO) are phagocytosed by hematogenous macrophages upon systemic application into the circulation and allow in-vivo tracking of infiltration to the CNS due to their paramagnetic effect by MRI<sup>13</sup>.

Another possible new direction in which DTI might be heading is functional DTI (fDTI). The concept is, that a pathway whose axons are actively conveying action potentials at high frequency (in communication with another area), as compared to a "silent" or low activity one, should display modifications in the FA or other diffusion measures. This would



---

be caused by a higher flow of water molecules associated with ion currents -close to Ranvier nodes-, such as Na<sup>+</sup> and K<sup>+</sup>. In 2008 Mandl et al looked at the change in FA along white matter tract during motor and visual task and found a significant change in the white matter. If proven correct, this new concept has great potential<sup>14</sup>.

Finally on a short term, clinical studies could use DTI measurements to pick up changes in tissue micro-architecture. For instance after a nutritional intervention study, anisotropy indices of white matter tracts can be evaluated to compare study patients to controls. These surrogate markers of brain growth or damage should be validated with long-term outcome. At present we have to wait at least two years to evaluate the effects of our interventions. Providing reliable biomarkers in neuroimaging will mean a great step towards interpreting interventions in a short time.

## References

1. J.J. Volpe. Brain injury in premature infants: a complex amalgam of destructive and developmental disturbances. *Lancet Neurol* 2009;8:110-24
2. C. Limperopoulos. Advanced neuroimaging techniques: their role in the development of future fetal and neonatal neuroprotection. *Semin Perinatol* 2010;34:93-101
3. P.D. Barnes. Neuroimaging and the timing of fetal and neonatal brain injury. *J Perinatol* 2001;21:44–60
4. N. Bayley (1993) Bayley scales of infant development, 2nd edn. Psychological Corporation, San Antonio, TX
5. P.S. Huppi, T.E. Inder. Magnetic resonance techniques in the evaluation of the perinatal brain: recent advances and future directions. *Semin Neonatol* 2001;6:195–210
6. S.J. Counsell, S.L. Tranter, M.A. Rutherford. Magnetic resonance imaging of brain injury in the high-risk term infant. *Semin Perinatol* 2010;34:67-78
7. D.S. Tuch, T.G. Reese, M.R. Wiegell, V.J. Wedeen. Diffusion MRI of complex neural architecture. *Neuron* 2003;40:885–95

8. L.R. Frank. Characterization of anisotropy in high angular resolution diffusion-weighted MRI. *Magn Reson Med* 2002;47:1083–99
9. Y. Assaf, P.J. Basser. Composite hindered and restricted model of diffusion (CHARMED) MR imaging of the human brain. *Neuroimage* 2005;1:48–58
10. V.J. Wedeen, P. Hagmann, W.Y. Tseng WY et al. Mapping complex tissue architecture with diffusion spectrum magnetic resonance imaging. *Magn Reson Med* 2005;54:1377–86
11. D.K. Jones, M.A. Horsfield, A. Simmons. Optimal strategies for measuring diffusion in anisotropic systems by magnetic resonance imaging. *Magn Reson Med* 1999;42:117–21
12. O. Khwaja, J.J. Volpe. Pathogenesis of cerebral white matter injury of prematurity. *Arch Dis Child Fetal Neonatal Ed.* 2008;93:153-61
13. G. Stoll, M. Bendszus. New approaches to neuroimaging of central nervous system inflammation. *Curr Opin Neurol* 2010;23:282-6
14. R.C. Mandl, H.G. Schnack, M.P. Zwiers, A. van der Schaaf, R.S. Kahn, H.E. Hulshoff Pol. Functional diffusion tensor imaging: measuring task-related fractional anisotropy changes in the human brain along white matter tracts. *PLoS One.* 2008;3:3631



## Summary

In this thesis use of diffusion weighted imaging (DWI) - including diffusion tensor imaging (DTI) - in neonatal neuroimaging was explored. The thesis was based on clinical and research questions likely to be encountered by neonatologists and paediatric radiologists, and focused on the use of DTI in describing 'normal' white matter development and subplate evolution of the very-low-birth-weight (VLBW) infant and perinatal stroke.

**Chapter 1** describes the background and aims of the studies presented in this thesis. In this chapter the physical basis of diffusion in tissue is explained and how this can be used to visualize biological structures using DTI.

**Chapter 2** presents an overview of the literature on applications of DTI in neonatal brain research. DTI has been shown to provide non-invasive and quantitative means for evaluating neonatal brain maturation and injury in vivo. DTI allows to study brain connectivity and plasticity and has contributed to our understanding of preterm white matter (WM) maturation, WM injury and plasticity. DTI research offers great potential to gain new insights and bring us a step further in reducing WM damage of the preterm infant. DTI reference values however are often still lacking.

**Chapter 3** demonstrates the results of a study, which was set up to provide DTI reference values for white matter tracts of VLBW infants for clinical use. Advances in neonatal intensive care have not yet reduced the high incidence of neurodevelopmental disability among very low birth weight (VLBW) infants. As neurological deficits are related to white matter injury, early detection is important and DTI is a tool for assessment of white matter injury. DTI images of 28 VLBW infants (26-32 weeks gestational age) without evidence of white matter abnormalities on conventional MRI sequences, and normal developmental outcome (assessed at age 1-3 years), were retrospectively analyzed. Fractional anisotropy (FA) and apparent diffusion coefficient (ADC) of different white matter tracts were measured. Quantitative investigation characterized age related trends in FA in pyramidal tracts. In conclusion norma-

---

tive data are provided for white matter tracts in preterm infants scanned within the first week of life.

Many intervention studies in preterms aim to improve neurodevelopmental outcome, but short-term proxy outcome measurements are lacking. Cortical plate and subplate development could be such a marker. **Chapter 4** reports the results of a study aimed at providing 'normal' DTI reference values for the cortical plate and subplate of preterm infants. DTI images of 19 preterm infants without evidence of injury on conventional MRI, with normal outcome, and scanned in the first four days of life were analyzed. FA and ADC values in frontal and temporal subplate and cortical plate were measured in single and multiple voxel regions-of-interest (ROIs) placed on predefined regions. A significant inverse correlation was found between gestational age and FA of the frontal and temporal cortical plate. ADC values had a significant positive correlation with gestational age in the frontal and temporal subplate. These results show how DTI allows in vivo exploration of the evolving cortical plate and subplate.

In **Chapter 5** a study is presented that explored the use of DTI with high b-values when studying the neonatal brain. The aims were to assess isotropic diffusion weighted image contrast and lesion conspicuity at b values between 350 and 3000s/mm<sup>2</sup> and to assess whether ADC or FA in the neonatal brain change with increasing b value. This study considered whether DTI obtained at high b values would be useful in evaluating pathology in the neonatal brain. DTI scans of 17 neonates were analyzed. DTI was performed with b values of 350, 700, 1500 and 3000 s/mm<sup>2</sup>. ROIs were positioned in the central white matter at the level of the centrum semiovale, frontal and occipital white matter, splenium of the corpus callosum, posterior limb of the internal capsule and the thalamus. Isotropic diffusion image contrast and lesion to normal tissue contrast increased with increasing b value. ADC values decreased with increasing b value in all regions studied. However, there was no change in FA with increasing b value. It was concluded that an increase in diffusion image contrast observed at high b values can be useful in identifying lesions in the neonatal brain.

The second part of the thesis focuses on the use of DTI in neonatal stroke. First of all an introduction is given in **Chapter 6**. This chapter reviews the MR neuroimaging modalities that assist the clinician in the detection of neonatal stroke in which DWI and DTI play an important current and future role.

**Chapter 7** presents a study in which serial changes are documented on T1 and T2-weighted and DW images over 3 post-natal months after symptomatic unilateral perinatal arterial ischemic stroke (PAIS) in term infants. Knowledge of the sequence of signal intensity (SI) change on conventional and DW imaging following PAIS is limited, adding to the difficulty in timing the onset of PAIS. A visual SI scoring system was used compared to the contralesional hemisphere. In this study 43 scans from 21 term infants were analyzed. Changes in SI on conventional T1 and T2 images were remarkably consistent between infants. The cortex was of low SI on T1 and high SI on T2 until day 6 when SIs reversed and cortical highlighting was seen for 1-2 months. The white matter showed high SI on T1 in the first 8-9 days and on T2 for >2 weeks before becoming low SI. Secondary SI changes remote from the infarction were seen in thalamus and brainstem in the first week and atrophy was seen from 4 weeks. All DW images showed high SI of the affected region until at least day 4, which fell to  $\approx$ /below that of the contralesional hemisphere by day 12. This study conclude that the pattern of SI change on conventional and DW images following PAIS was remarkably consistent between patients, suggesting that PAIS in symptomatic term-born infants occurs within a very limited time frame around birth.

For years now, DWI plays an important role in diagnosing neonatal stroke. However DWI after neonatal stroke only allows to partly predict future neurodevelopmental outcome. There is a large variability in outcome seen after perinatal stroke. New DTI postprocessing techniques permit to visualize and quantify secondary network injury and may lead to better understanding of the variability seen in neurodevelopmental outcome. In **Chapter 8** a study is described which was aimed at establishing that newborn stroke involving extensive parts of cerebral cortex immediately leads to secondary network injury in pulvinar. Seven term infants with acute cortical stroke are presented with hypersignal

---

in pulvinar on DWI. ADC values in secondarily injured pulvinar were significantly higher than in the area with primary (sub)cortical injury. It was concluded that in the absence of asphyxia and because pulvinar is outside of the primary area of infarction, there are suggestions from imaging for acute secondary injury to pulvinar following primary damage of their cortical targets and/or connecting axons. In **Chapter 9** DTI images of 3 term infants with acute extensive unilateral cortical arterial ischemic stroke were analyzed and state-of-the-art probabilistic tractography postprocessing was used to define the regions of interest (ROI) in the thalamus. The three eigenvalues were evaluated and from them the ADC was calculated. Significantly lower ADC values were found in the voxels of the ROI's placed within the nuclei corresponding to ischemic cortex compared to the unaffected contralesional thalamic nuclei. These findings support the concept of acute network injury, showing how DTI enables to show how deep grey matter is directly affected after a primary hit to its connected cortex in neonatal stroke.

In **Chapter 10** the findings of this thesis are discussed. Furthermore recommendations are made for future studies.

The main conclusions obtained from the studies described in this thesis are:

- DTI allows us to study the evolution of the white matter, subplate and cortical plate in VLBW infants in vivo.
- There is a statistically significant correlation between gestational age and FA of the PLIC in VLBW infants scanned within the first week of life.
- There is a statistically significant inverse correlation between gestational age and FA of the frontal and temporal cortical plate in VLBW infants. ADC values have a significant positive correlation with gestational age in the frontal and temporal subplate.
- Isotropic diffusion image contrast and lesion to normal tissue contrast increases with increasing b value in the neonatal brain and may be useful in identifying lesions.
- ADC values decreased with increasing b value in different regions in the neonatal brain. No change in FA values was found.

- The pattern of SI change on conventional and DW images following PAIS was remarkably consistent between patients suggesting that PAIS in symptomatic term-born infants occurs closely around the time of birth.
- Within days DWI SI changes in pulvinar follow focal infarction involving cortex and white matter, suggesting secondary network injury.
- In neonatal stroke patients significantly lower ADC values are found in ROIs placed within the nuclei corresponding to ischemic cortex compared to the unaffected contralesional thalamic nuclei, supporting the concept of secondary network injury.



---

## Samenvatting

De incidentie van te vroeg geboren kinderen (prematuren) in Nederland, volgens de klassieke definitie (i.e. < 37 weken), is ongeveer 14.000 levendgeborenen per jaar. Hiervan zijn rond de 2300 zeer vroeg levendgeborenen (i.e. <32 weken). Er lijkt volgens de gegevens van het RIVM / Nationaal Kompas Volksgezondheid een trend van toename van vroeggeboorten in Nederland en in andere westerse landen.

Deze trend heeft deels te maken met de stijging in de aangifte van extreem vroeg geboren kinderen en deels met de toename in risicofactoren zoals meerlingzwangerschappen, hogere leeftijd van de moeder en de toename van vruchtbaarheid bevorderende behandelingen.

Door de vooruitgang in de prenatale en neonatale (intensieve) zorg in de afgelopen decennia is er een duidelijke verbetering gekomen in de overlevingskansen van de premature pasgeborenen. Echter ondanks een vermindering van de morbiditeit van de overlevenden, is er voor deze kinderen echter nog steeds een grote kans op hersenschade met (cognitieve en motorische) ontwikkelingsproblemen.

Gewoonlijk wordt schade aan de witte stof verantwoordelijk geacht voor de meeste ontwikkelingsachterstanden die gezien worden bij zeer prematuur geboren. Meer recent wordt de aandacht ook gericht op abnormale ontwikkeling (schade) ter hoogte van de corticale grijze stof (hersenschors) en diepere grijze stof (hersenkernen en cerebellum).

Vroege objectieve detectie van hersenschade is belangrijk voor het opzetten van interventiestudies en het beoordelen van de effecten daarvan. Er is tot nu toe een tekort aan referentiewaarden van de normale maturatie van verschillende hersenstructuren voor het premature brein.

Bij de voldragen pasgeborenen zijn asfyxie en infarcten vaak voorkomende vormen van hersenschade. Asfyxie wil zeggen dat er bij de foetus een situatie van (tijdelijk) gebrekkige zuurstofoverdracht van de moeder is geweest, met mogelijk ernstige gevolgen voor de neurologi-

sche ontwikkeling van het kind. Door vooruitgang in de perinatale zorg lijkt de incidentie van perinatale asfyxie gelukkig te dalen.

Een herseninfarct (beroerte) is de beschadiging van hersenweefsel door een al dan niet tijdelijke afsluiting van een bloedvat in de hersenen. Ook infarcten kunnen zorgen voor ernstige neurologische gevolgen van variabele aard. Herseninfarcten bij pasgeborenen worden, in tegenstelling tot asfyxie, echter steeds vaker gerapporteerd. Incidenties van 1:2300 worden nu beschreven. We vinden dit ook terug in het aantal infarcten gezien op de NICU in het Sophia Kinderziekenhuis van de afgelopen jaren.

Beeldvorming van de hersenen is van groot belang voor de diagnose en (voorzichtige) voorspelling van de neurologische prognose. Voor patiënten met een herseninfarct is een precieze voorspelling van de neurologische effecten moeilijk. Verbeterde kennis zou veel kunnen betekenen voor de informatie verstrekking aan ouders en artsen en zou kunnen dienen als basis voor interventiestudies.

De twee technieken die gebruikt worden voor de beeldvorming van de hersenen in de neonatale periode zijn schedelechografie en 'magnetic resonance imaging' (MRI).

Met MRI kan men zeer gedetailleerde opnames maken van het hele neonatale brein. MRI sequenties (scan instellingen) geven verschillende soorten informatie over het bestudeerde weefsel. De 'diffusie sequenties', de zogenaamde 'diffusion weighted imaging' (DWI), zijn scansequenties die de diffusie van atomen in materie kunnen meten. Er wordt bij DWI niet naar de anatomische structuur wordt gekeken maar naar de thermodynamische beweging van watermoleculen. De willekeurige bewegingen van atomen zijn o.a. verstoord in de acute fase van celsterfte (door zwelling van de hersencellen). Met DWI zijn we in staat dit te visualiseren.

DTI staat voor 'diffusion tensor imaging' en is een vrij recent ontwikkelde MRI techniek dat door middel van het meten van de diffusie parameters van watermoleculen (in verschillende richtingen) objectieve en

---

kwantificeerbare meetwaarden kan geven van weefselkarakteristieken in vivo.

Het belangrijkste doel van dit proefschrift is het bestuderen van de mogelijkheden van het gebruik van DTI bij de beeldvorming van de hersenen van pasgeborenen. Meer specifiek: het gebruik van DTI voor het bestuderen van 'normale' witte- en grijze stof ontwikkeling (maturatie) bij prematuur geboren en onderzoek naar herseninfarcten bij voldragen pasgeborenen.

In **Hoofdstuk 2** wordt een overzicht gegeven van de literatuur over de toepassingen van DTI bij neonataal hersenonderzoek. Omdat DTI een non-invasieve objectieve, kwantificeerbare methode is om neonatale hersenontwikkeling en schade te evalueren, heeft DTI de potentie om nieuwe inzichten te verwerven.

**Hoofdstuk 3** beschrijft een studie met als doel DTI referentiewaarden te geven van witte stof banen bij prematuren. Deze prematuren waren gescand in de eerste week na de geboorte, hadden geen afwijkingen op de conventionele (anatomische) MRI scansequenties en hadden een normale ontwikkeling op 1-3 jarige leeftijd. Als maat voor gemiddelde diffusie werden de 'apparent diffusion coefficient' (ADC) waarden bekeken. Tevens werd er gekeken naar de fractionele anisotropie (FA). Een FA van 0, betekent vrije diffusie van de watermoleculen (isotrope diffusie), als de FA waarde maximaal 1 is, dan is de diffusie ideaal lineair. Het meten van referentiewaarden in prematuren laat een leeftijdsgerelateerde trend zien van FA waarden gemeten in de pyramidebanen (motorische witte stof banen).

**Hoofdstuk 4** beschrijft de resultaten van een studie bij dezelfde patiëntengroep waarin werd gekeken naar DTI (ADC en FA) normaalwaarden gemeten in de 'subplate' en de 'cortical plate'. De subplate is een tijdelijke laminaire structuur, die tijdens de foetale hersenontwikkeling een rol speelt in het maken van de verbindingen van de cortex (oa met de thalamus) en zorgt voor de functionele maturatie van de cortex. De subplate neuronen zijn selectief gevoelig voor hypoxische schade, die geassocieerd is met cognitieve en motorische problemen. Deze studie

laat zien hoe de ADC waarden van de temporale en frontale subplate positief gecorreleerd zijn met toename van de zwangerschapsduur en hoe de FA waarden van deze structuren negatief gecorreleerd zijn met de zwangerschapsduur.

**Hoofdstuk 5** beschrijft een studie waarin gekeken wordt naar de invloed van de hoogte van de 'b' waarde van diffusie gewogen MRI scans. Deze 'b' waarde is normaal rond de 700-750 voor prematuren. Er is onderzocht of hersenschade beter zichtbaar wordt door een toename van contrast van de scans. Ook werden FA en ADC waarden van verschillende hersenstructuren gemeten bij verschillende 'b' waarden. Er zijn aanwijzingen dat een hogere 'b' waarde neonatale hersenschade duidelijker kan laten zien. De ADC waarden gemeten in verschillende hersenstructuren zijn lager met hogere 'b' waarden, de FA waarden blijven gelijk.

In **Hoofdstuk 6** wordt een overzicht gegeven van de verschillende soorten MRI technieken die gebruikt kunnen worden voor het bestuderen van neonatale herseninfarcten: bijvoorbeeld DTI.

Het aspect van een neonataal herseninfarct op een MRI scan verandert met de tijd. Er is weinig literatuur over de evolutie van neonatale herseninfarcten op MRI. Een beschrijving van het patroon van veranderingen van signaal intensiteit op MRI kan gebruikt worden voor de diagnostiek. In **Hoofdstuk 7** wordt hierover een studie beschreven. Zowel op conventionele MRI opnamen (T1- en T2-gewogen) als op de DWI scans werd gekeken naar de evolutie van het aspect van de neonatale infarcten. Het patroon van veranderingen is bij een geselecteerde groep (voldragen, symptomatische pasgeborenen met unilaterale arteriële infarcten) opvallend consistent.

**Hoofdstuk 8 en 9** richten zich op het onderzoek naar secundaire effecten van neonatale corticale infarcten op de thalamus. De thalamus kan gezien worden als een verbindingstation in de hersenen. Informatiestromen tussen het perifere zenuwstelsel en de hogere lagen van de hersenen worden hier aangepast. Met behulp van DTI werd gezien dat er sprake is van 'netwerk' schade in de gebieden van de thalamus, die overeenkomen met de aangedane cortex: een effect op afstand. Verdere

---

kennis over dit fenomeen zou de variabiliteit van kunnen verklaren die gezien wordt in de neurologische gevolgen van de neonatale patiënten die een herseninfarct hebben doorgemaakt.

In **Hoofdstuk 10** wordt een algemene discussie gevoerd over de beschreven hoofdstukken. Bovendien worden voorstellen voor toekomstig onderzoek besproken.

## Dankwoord

*"If I have seen a little further it is by standing on the shoulders of Giants";  
Sir Isaac Newton.*

Graag bedank ik allen die het mogelijk hebben gemaakt om dit proefschrift tot stand te laten komen. Een paar mensen wil ik hier speciaal noemen.

Ten eerste alle kinderen en ouders die belangeloos hebben meegewerkt aan de verschillende onderzoeken.

Mijn promotor Prof. dr. J.B. van Goudoever. Beste Hans, sla een willekeurig boek over motiverende leiders open en jij voldoet aan alle kenmerken die beschreven worden. Door je 'pep-talks' en je optimisme heb ik veel uit mezelf kunnen halen. Mijn dank is groot!

Mijn co-promotor dr. P.P. Govaert. Beste Paul, het was een enorme eer om onder jouw begeleiding een thesis te mogen maken. Je bent voor mij zeker een van de 'giants' en ik hoop nog lang van je te mogen leren. Naast je enorme kennis van de neonatale neurologie en hersenbeeldvorming, was je voor mij ook een leermeester in de dagelijkse kliniek. Jou motto 'de patiëntenzorg en de directe verbetering daarvan gaat altijd voor' zal ik proberen hoog in het vaandel te houden. Ik kijk uit naar onze koffiemeetings in de toekomst.

Mijn co-promotor dr. M.H. Lequin. Beste Maarten, bedankt voor je bereidheid om mij altijd te woord te staan. Ook ben ik zeer dankbaar voor de vrolijke noot die je bracht in onze research meetings. Ik heb veel van je kunnen leren. Ik wens je een hele mooie toekomst waarin we hopelijk veel gaan samenwerken.

De leden van de kleine commissie: Prof. dr. W.F.M. Arts, Prof. dr. G.P. Krestin, Prof dr. D. Tibboel dank ik hartelijk voor het beoordelen van het manuscript. Prof. dr. P.J. vd Spek, dr. F. Groenendaal en dr. F.M. Cowan wil ik bedanken voor het zitting nemen in de grote commissie.

---

Prof. dr. M.A. Rutherford and Prof. dr. A.D. Edwards. Thank you very much for the opportunity to spend a year working in the Robert Steiner MR Unit and the NICU of the Hammersmith Hospital in London. It has been a great year. I felt very honored working in one of the leading neonatal neuroimaging research centers of the world. I have met many researchers and clinicians dedicated at exploring all aspects of the newborn brain. I hope one day I will be back.....

Dr. F. M. Cowan. Dear Frances, I would like to thank you for all your help during my stay in London. You made me feel very welcome. You have taught me so much.

Dr. S.J. Counsell. Dear Serena, I owe you so many "thank you's". Thank you, thank you, thank you... times a million. Thank you for all your optimism, for all your help, for your motivational speeches and for being so nice all the time. You have become my role model as a future researcher.

The Robert Steiner MR Unit: J.M. Allsop, Dear Joanna, thanks for helping me out with so many things and thank you for being the sunshine on foggy days in London. Thanks to all the radiographers and researchers, who are all lovely. Tayyib and Andrew, we had so much fun. I would like to thank you for a wonderful time together. I miss our discussions at moments we were all in the Robert Steiner Unit. And like promised, if I find a cure for a regressing hairline you will be the first I share it with.

De paranymfen dr. J.T. van Asseldonk en dr. J.E. Bunt. Thies als grote vriend en inspiratiebron ben ik je eeuwig dankbaar. Onder het genot van een Jupiler hebben we (vanaf dat we elkaar hebben ontmoet in Leuven) zo ongeveer alles besproken. Ik kijk nu alweer uit naar ons volgende gesprek. *"I choose to live, not just to exist"; James Hetfield*. Beste Jan Erik, op onze kamer sk-3202 hebben we veel gelachen zodat de zware diensten op de NICU dragelijk werden. Ik kijk uit naar ons volgende congres of café ('de club' of 'de Twister') bezoek.

De afdeling neonatologie van het Sophia Kinderziekenhuis. Grote dank aan alle neonatologen die het voor mij mogelijk hebben gemaakt om deze thesis te maken en mij de kans hebben gegeven om een jaar naar

Londen te gaan. Dank ook voor de ondersteuning van de arts-assistenten, NP-ers en verpleegkundigen.

Mentoren drs. J. Bosman en dr. N. vd Lely. Beste Judith, je bent voor mij een van de grote 'gaints'. Als mentor hebt je mij beschermd, opgeleid, sterk gemaakt, een introductie gegeven in de wetenschap en mij geleerd wat een IC dokter is. Ik ben je daarvoor nog elke dag dankbaar en vandaar dat ik deze thesis aan je heb opgedragen. Beste Nico, je hebt me (samen met de andere kinderartsen uit het Reinier de Graaf) geleerd om een kinderarts te worden. Bedankt voor je blijvende mentorschap. Lang leve de 'Heeren van Delft'.

M. v Roon. Beste Monique, we boffen met jou als NP-er met speciale interesse in de neonatale neurologie. Heel veel dank voor je inzet voor de neuro-database, het "Dr. D lijstje".

BRAINS (Brain Research And Imaging Neonatology Sophia). Onder de leiding van dr. P.P. Govaert en Prof. dr. J.B. van Goudoever heb ik de grote eer gehad de neurogroep te mogen helpen uitbereiden. Dank aan iedereen van de BRAINS groep. Ik heb veel zin in de toekomst.

De afdeling radiologie van het Sophia Kinderziekenhuis. Bedankt alle radiologen en laboranten die mij hebben geholpen ten tijde van het maken van dit proefschrift en die mij ook nu blijven ondersteunen. Mijn dank is groot!

Dr. E. Vansteenkiste. Beste Ewout, bedankt voor de hulp bij het nakijken van de introductie van deze thesis. Mede dank aan Jan Aelterman hiervoor. Ik kijk uit naar de gezamenlijke onderzoeksprojecten.

A.W. Everaers. Beste Ton, bedankt voor de opmaak van dit proefschrift. Heel veel plezier in Australië.

D.M.T. vd Laar. Beste Daan, bedankt voor alle ondersteuning voor dit proefschrift en tijdens mijn opleiding tot neonatoloog.



---

De Leuven boys. *“Country road, take me home to the place were I belong... Leuven” (de Wink)*. Geweldig hoe de ‘mannen van Leuven’ nu nog steeds bij elkaar komen. Dank aan de ‘chairmen of the board’: Sander, Thies, Ton, Martijn, Jippe, Bram, Jur, Arthur en Ralf. Tot de volgende ‘board-meeting’.

Mijn ouders wil ik bedanken voor de kansen die ze me hebben gegeven en voor hun onvoorwaardelijke steun. Jullie staan altijd voor ons klaar. Mam, bedankt voor alles wat je continu voor ons doet. Pap, bedankt voor je motivatie. Ook dank voor mijn zussen (Suus en Tess) waarop ik erg trots ben.

Mijn dochters, Mara, Linde en Iris. Jullie maken mijn leven compleet. Ik heb altijd een glimlach op mijn gezicht als ik aan jullie denk. Ik hou heel veel van jullie.

Lidia, mijn liefste: *“How wonderful life is, now you are in my world”*. Niemand is voor mij zo belangrijk geweest tijdens het maken van deze thesis als jij. Jij geeft mij rust en je geeft me energie. Ik kijk uit naar onze grote reis door Australië en naar onze toekomst daarna. Ik hou zielsveel van je!

## List of publications

### *Manuscripts based on this thesis*

**Dudink J**, Counsell SJ, Lequin M, Taselaar A, van Goudoever JB, Govaert PP. Diffusion tensor imaging reveals acute network injury in neonatal arterial ischemic stroke. Submitted.

**Dudink J**, Buijs J, Govaert P, van Zwol AL, Conneman N, van Goudoever JB, Lequin M. Diffusion tensor imaging of the cortical plate and subplate in very-low-birth-weight infants. *Pediatr Radiol*. 2010 Mar 27 [Epub ahead of print]

Lequin MH, **Dudink J**, Tong KA, Obenaus A. Magnetic resonance imaging in neonatal stroke. *Semin Fetal Neonatal Med*. 2009 Oct;14(5):299-310

**Dudink J**, Mercuri E, Al-Nakib L, Govaert P, Counsell SJ, Rutherford MA, Cowan FM. Evolution of unilateral perinatal arterial ischemic stroke on conventional and diffusion-weighted MR imaging. *AJNR Am J Neuroradiol*. 2009 May;30(5):998-1004

**Dudink J**, Kerr JL, Paterson K, Counsell SJ. Connecting the developing preterm brain. *Early Hum Dev*. 2008 Dec;84(12):777-82

**Dudink J**, Larkman DJ, Kapellou O, Boardman JP, Allsop JM, Cowan FM, Hajnal JV, Edwards AD, Rutherford MA, Counsell SJ. High b-value diffusion tensor imaging of the neonatal brain at 3T. *AJNR Am J Neuroradiol*. 2008 Nov;29(10):1966-72

Govaert P, Zingman A, Jung YH, **Dudink J**, Swarte R, Zecic A, Meersschaut V, van Engelen S, Lequin M. Network injury to pulvinar with neonatal arterial ischemic stroke. *Neuroimage*. 2008 Feb 15;39(4):1850-7

**Dudink J**, Lequin M, van Pul C, Buijs J, Conneman N, van Goudoever J, Govaert P. Fractional anisotropy in white matter tracts of very-low-birth-weight infants. *Pediatr Radiol*. 2007 Dec;37(12):1216-23

---

## ***Other publications***

Ecurey-Goossen GM, **Dudink J**, Lequin M, Feijen-Roon M, Horsch S, Govaert P. The clinical presentation of preterm cerebellar haemorrhage. *Eur J Pediatr*. 2010 May 18 [Epub ahead of print]

Govaert P, Smith L, **Dudink J**. Diagnostic management of neonatal stroke. *Semin Fetal Neonatal Med*. 2009 Oct;14(5):323-8

Govaert P, Ramenghi L, Taal R, **Dudink J**, Lequin M. Diagnosis of perinatal stroke II: mechanisms and clinical phenotypes. *Acta Paediatr*. 2009 Nov;98(11):1720-6

Verkerk AJ, Schot R, Dumee B, Schellekens K, Swagemakers S, Bertoli-Avella AM, Lequin MH, **Dudink J**, Govaert P, van Zwol AL, Hirst J, Wessels MW, Catsman Berrevoets C, Verheijen FW, de Graaff E, de Coo IF, Kros JM, Willemsen R, Willems PJ, van der Spek PJ, Mancini GM. Mutation in the AP4M1 gene provides a model for neuroaxonal injury in cerebral palsy. *Am J Hum Genet*. 2009 Jul;85(1):40-52

Govaert P, **Dudink J**, Visser G, Breukhoven P, Vanhatalo S, Lequin M. Top of the basilar artery embolic stroke and neonatal myoclonus. *Dev Med Child Neurol*. 2009 Apr;51(4):324-7

**Dudink J**, Lequin M, Weisglas-Kuperus N, Conneman N, van Goudoever JB, Govaert P. Venous subtypes of preterm periventricular haemorrhagic infarction. *Arch Dis Child Fetal Neonatal Ed*. 2008 May;93(3):F201-6

**Dudink J**, Roeten BM, van der Meer-Kappelle LH, Walther FJ. [A painful skin disorder in two newborn babies: neonatal subcutaneous fat necrosis]. *Ned Tijdschr Geneesk*. 2003 Nov 22;147(47):2337-40

**Dudink J**, Walther FJ, Beekman RP. Subcutaneous fat necrosis of the newborn: hypercalcaemia with hepatic and atrial myocardial calcification. *Arch Dis Child Fetal Neonatal Ed*. 2003 Jul;88(4):F343-5

**Dudink J**, Mearin LM, Sukhai RN. [Ileus after the use of loperamide in a child with acute diarrhea]. *Ned Tijdschr Geneeskd*. 2003 Apr 5;147(14):670-2

---

## Curriculum Vitae

Jeroen Dudink was born in Amsterdam on June 19th, 1973. He passed his secondary school exam at the “Montesori Lyceum Amsterdam” in 1991. He started his medical training at the Medical Faculty of the Catholic University of Leuven (Belgium) in 1992, and received his medical degree cum laude in 1999. He became a resident Paediatrics at the “Leiden University Medical Center” (Prof. dr. J.M. Wit), and the “Reinier de Graaf Hospital” (dr. N. vd Lely). In 2004, he started his fellowship neonatology in the “Sophia Children’s Hospital” of the “Erasmus University Medical Center” in Rotterdam (Prof. dr. J.B van Goudoever and dr. B.J. Smit). He became a neonatologist in 2007. October 2006 he started working on his thesis. In October 2007 he went to London to spend a year as a research fellow at the “MR Robert Steiner Unit, Hammersmith Hospital” of the “Imperial College London” (Prof. dr. M.A. Rutherford and Prof. dr. A.D. Edwards). He is one of the founding members of the neonatal neuroimaging group “BRAINS” (Brain Research and Imaging Neonatology Sophia). Next to clinical work and research he is also involved in advanced life support training. He became an instructor for the “Paediatric and Neonatal Save Transport and Retrieval (PaNSTaR)” course and is a ‘Course Director’ of the “Neonatal Life Support (NLS)” course.

The author lives happily together with his wife, Lidia and their three daughters: Mara, Linde and Iris in ‘the Bilt’, the Netherlands.

## PhD Portfolio

Name PhD student: Jeroen Dudink  
 ErasmusMC Department: Neonatology  
 PhD period: Oct 2006 – Mar 2010  
 Promotor: Prof. dr. J.B. van Goudoever  
 Supervisors: dr. P.P. Govaert  
 dr. M.H. Lequin

	year	Workload (hours)
<b>Courses</b>		
Da Vinci European Neonatology training course	2006	25
ESPR Fellowship course	2006-2008	50
Hands on fMRI-DTI course, Leuven	2007	25
Neonatal Cranial Ultrasound, London	2008	25
Neonatal Brain MRI, London	2008	25
Good Clinical Practice course, London	2010	10
<b>Seminars and Workshops</b>		
Research meetings 'Moeder en Kind' Center	2006-2010	25
"Schedelechografie-cursus": I and II, Rotterdam	2007-2008	50
Research meetings Hammersmith Hospital, London	2007-2008	25
<b>Presentations</b>		
Presentation "Vlaams-Nederlandse Neonatologiedag", Leuven	2006	25
Presentation "Nederlandse Vereniging Neuro-neonatologie"	2007	25
Presentation "ESMRN", Tübingen	2007	40
Presentation "ESPR", Nice	2008	60
Posterwalk "ESPR", Nice	2008	25
Presentation "Nederlandse Vereniging Neonatale Follow Up"	2008	25
Posterwalk "ESMRN", Zurich	2009	25
<b>Teaching</b>		
Introduction training Internship pediatrics	2006-2010	100
NLS-training (ALSG), Riel and London	2006-2010	100
PaNSTaR-course training, Manchester	2008-2010	50
NICU nurses education, Rotterdam and London	2006-2010	25
Medical training Pediatric residents, Rotterdam and London	2006-2010	50









# Chapter 10

## COLOR SECTION

---

Chapter 1

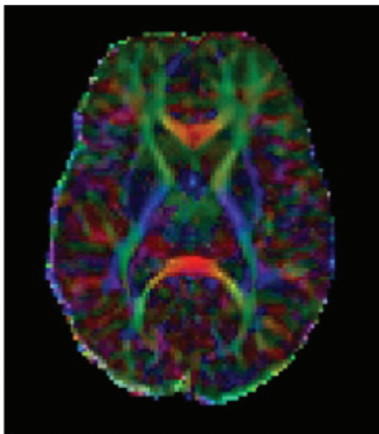


Figure showing a typical DTI color map: the major eigenvector direction indicated by color (red = R/L, green = A/P, blue = S/I) weighted by the FA (note that specific tract groups can be identified).

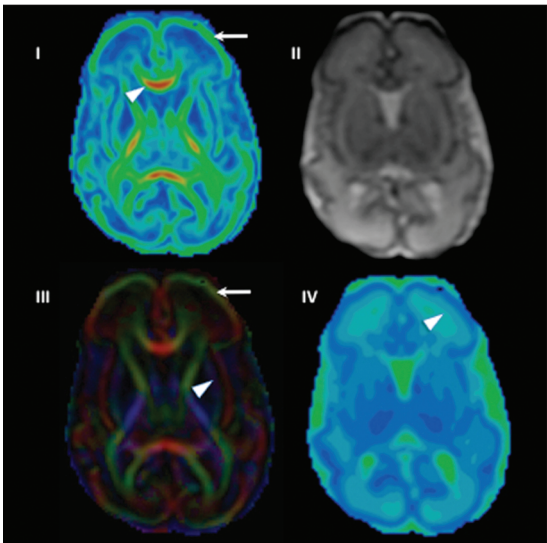
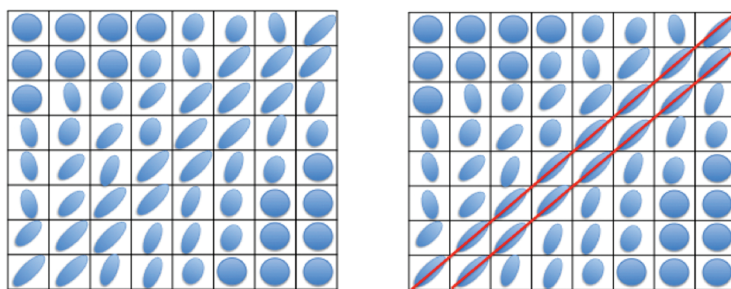
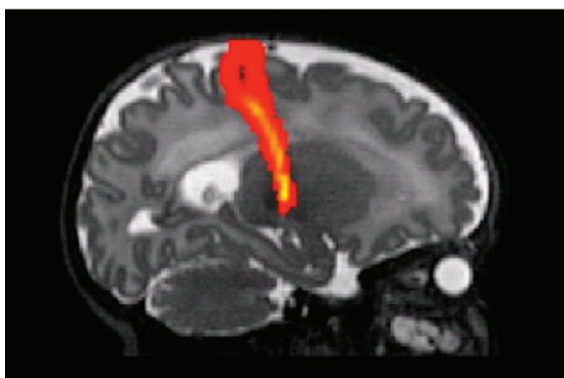


Figure showing different representations of a DTI scan of a patient of 30 weeks gestation. (I) FA-map showing a relatively high FA values (green) of the cortex (arrow) and the highest FA values (red) of the genu of the corpus callosum (arrowhead). (II) Showing a B0 map. (III) Color map in which the major eigenvector direction is indicated by color (red = R/L, green = A/P, blue = S/I) signal intensity weighted by FA values. Different white matter tracts can be delineated such as the external capsule (arrowhead). Note the radial organization of the cortex (arrow). (IV) ADC map showing a clear radial organization of the cortex (cortical plate and subplate).



Figures showing an abstract representation of an 8 x 8 grid (left and right). Within the voxels the averaged ellipsoids are shown. Streamline tractography (right) propagates a fiber tract (red lines) in the direction of principal eigenvector, preserving voxel-to-voxel directional information.



Sagittal image of connectivity distributions in the corticospinal tracts in a preterm infant imaged at 42 weeks gestational age obtained using probabilistic tractography.

## Chapter 2

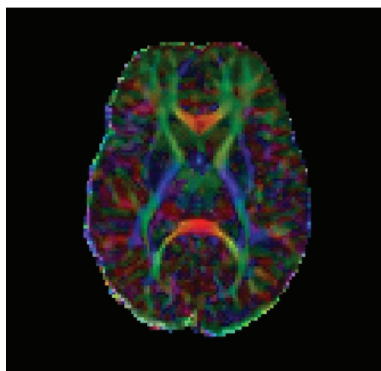


**Figure 1.**

Red-green-blue FA color map. Red represents fibres in the left-right direction, blue represents fibres in the superior-inferior direction and green represents fibres in the anterior-posterior direction.

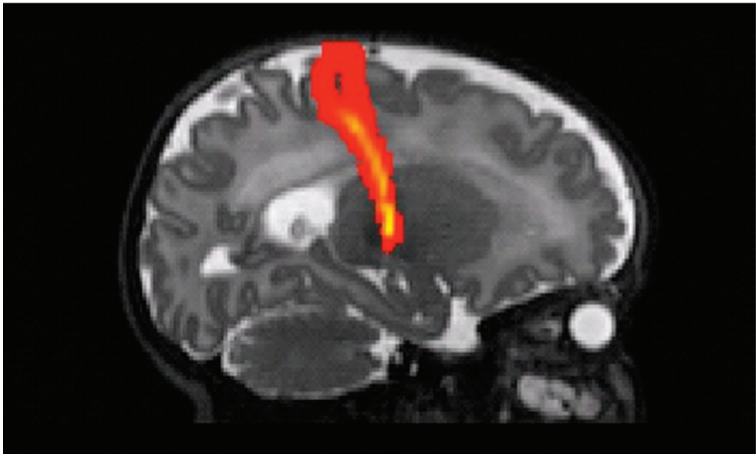


**Figure 2.**  
Sagittal image of connectivity distributions in the corticospinal tracts in a pre-term infant imaged at 42 weeks gestational age obtained using probabilistic tractography.

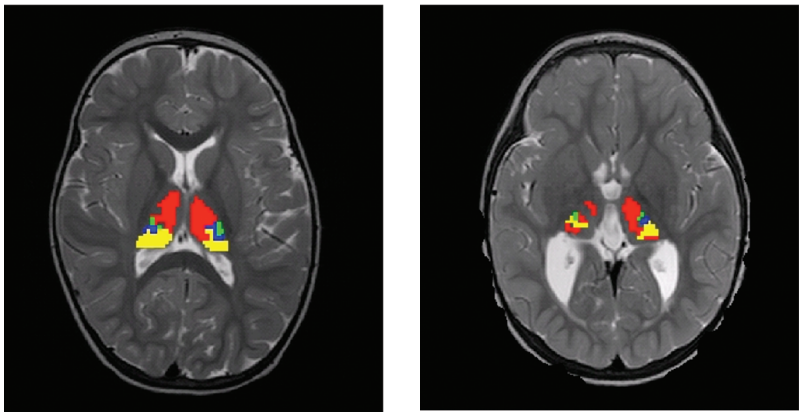


**Figure 3.**  
Thalamo-cortical projections displayed on the infants native T2 weighted image in (a) infant with normal imaging and (b) infant with porencephalic cyst (key: red = connections from frontal/temporal cortex, y = connections from parietal/occipital cortex, green = connections from motor cortex and blue = connections from somato-sensory cortex). Reprinted from SJ Counsell, LE Dyet, DJ Larkman, RG Nunes, JP Boardman, JM Allsop, JA Fitzpatrick, L Srinivasan, FM Cowan, JV Hajnal, MA Rutherford, AD Edwards. Thalamo-cortical connectivity in children born preterm mapped using probabilistic magnetic resonance tractography. *NeuroImage* 2007; 34: 896-904 with permission from Elsevier.

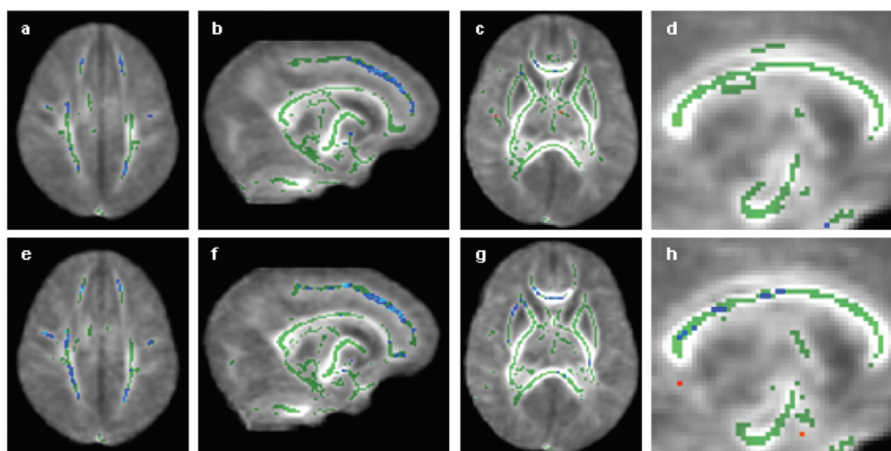


**Figure 4.**

The effect of preterm birth on FA at term equivalent age. Mean FA skeleton overlaid on the mean FA map. Regions of the mean FA skeleton in green represent areas where there were no significant differences in FA values in the preterm infants imaged at term compared to the term-born controls. Areas in blue are regions where the FA was significantly lower in the preterm group (a–d), and can be observed in the centrum semiovale (a), frontal white matter (b) and genu of the corpus callosum (c). Those infants born  $\leq 28$  weeks gestational age (e–h) had greater regions of reduced anisotropy within the centrum semiovale (e), frontal white matter (f) and genu of the corpus callosum (g), and displayed additional reductions in FA in the posterior aspect of the posterior limb of the internal capsule (g) and the external capsule (g). Reprinted from: M Anjari, L Srinivasan, JM Allsop, JV Hajnal, MA Rutherford, AD Edwards, SJ Counsell. Diffusion tensor imaging with tract-based spatial statistics reveals local white matter abnormalities in preterm infants. *NeuroImage* 2007;35: 1021-7 with permission from Elsevier.

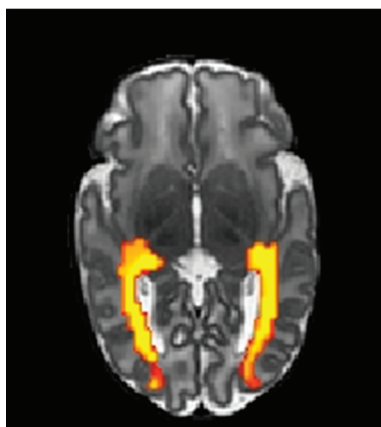


**Figure 5.**

Probabilistic tractography of the optic radiations in an infant who was born at 26 weeks gestational age and imaged at 40 weeks post-menstrual age shown on the infant's native T2 weighted image. Reprinted from: L Bassi, D Ricci, A Volzone, JM Allsop, L Srinivasan, A Pai, C Ribes, LA Ramenghi, E Mercuri, F Mosca, AD Edwards, FM Cowan, MA Rutherford, SJ Counsell. Probabilistic Diffusion Tractography of the Optic Radiations and Visual Function in Preterm Infants at Term Equivalent Age. *Brain* 2008; 131: 573-582. by permission of Oxford University Press.

### Chapter 3

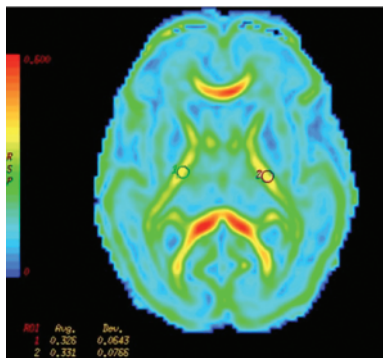


**Figure 1**  
Example of a fractional anisotropy map (gestational age 30 weeks) on which the ROIs were placed.

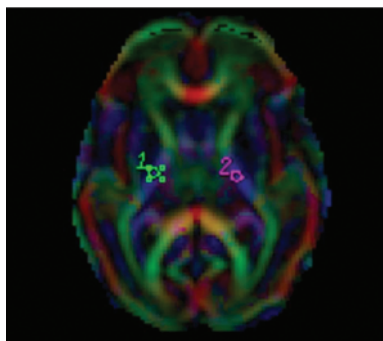


**Figure 2**  
We performed fiber tracking in each of the ROIs to confirm the right location (example showing the corticospinal tracts (gestational age 28 weeks)).

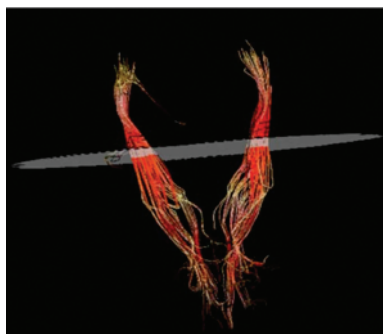


**Figure 3**  
We confirmed ROI placement on the colormaps (example showing the colormaps of a patient with gestational age of 30 weeks).

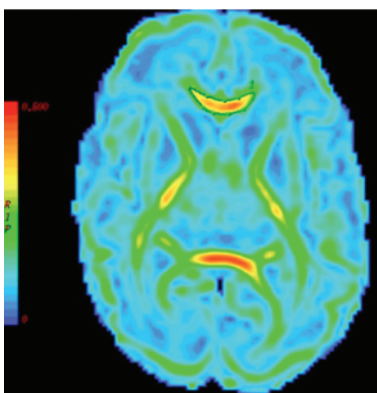


**Figure 4**

Delineating the Corpus Callosum with a free hand ROI placement on a FA map. .

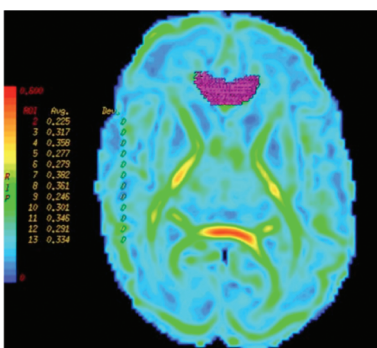


**Figure 5**

Automating calculation of the maximum FA pixel value within the ROI on a FA map.



Chapter 4

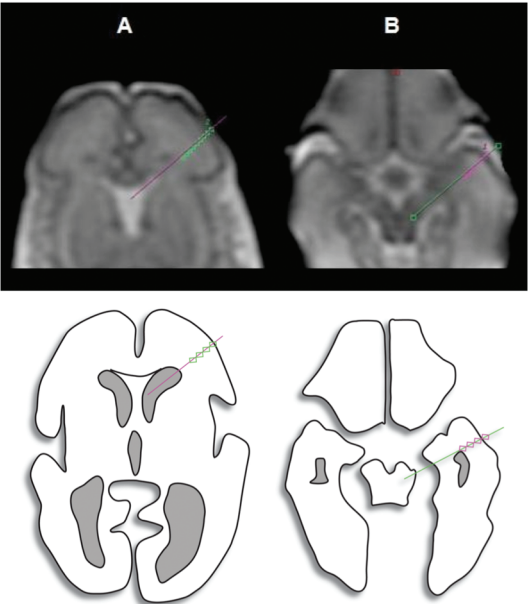


**Figure 1.** Top image shows ROI placement (row of single voxels) both frontal (A) and temporal (B) regions. The image below shows the same ROI placement on a cartoon.

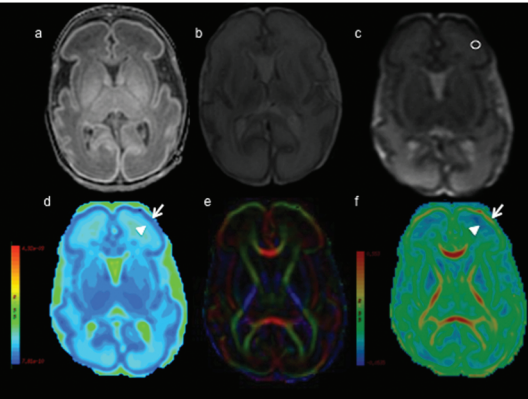


**Figure 2.** Showing different scan sequences of the same patient (GA 30w). (a) T1-weighted image, (b) T2-weighted image, (c) B0-image showing low signal intensity (SI) of CP and a ROI placed in area of the subplate, (d) ADC map showing low (dark blue) ADC value of the cortex (arrow) and intermediate ADC values of the subplate (arrowhead), (e) colour map (red representing right-left, green representing antero-posterior, and blue representing supero-inferior anatomical directions), (f) FA map, showing high FA values of the cortex (arrow) and low FA values (blue) of the subplate zone (arrowhead).



## Chapter 6

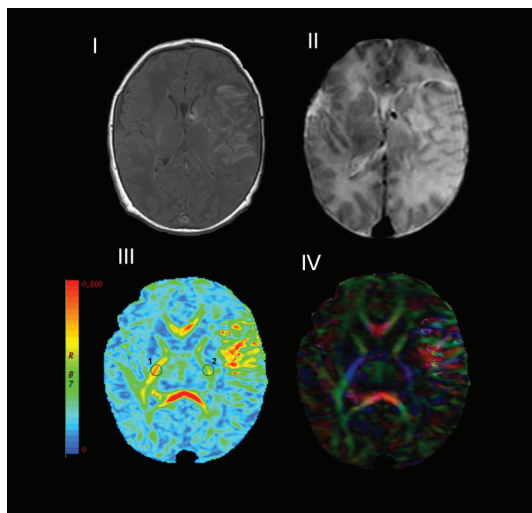


**Figure 2**

Diffusion tensor imaging. A magnetic resonance image of a term infant with left complete middle cerebral artery infarction: (I) T1-weighted image, (II) T2-weighted image, (III) fractional anisotropy (FA) map showing distorted FA values in the region of the infarction and (IV) RGB (red–green–blue) directionality color map. Two regions of interest (ROIs) are placed on the FA map (III) on the posterior limbs of the internal capsules showing clear differences in FA values between the contralesional (1 = 0.447) and the ipsilateral (2 = 0.295) sides.

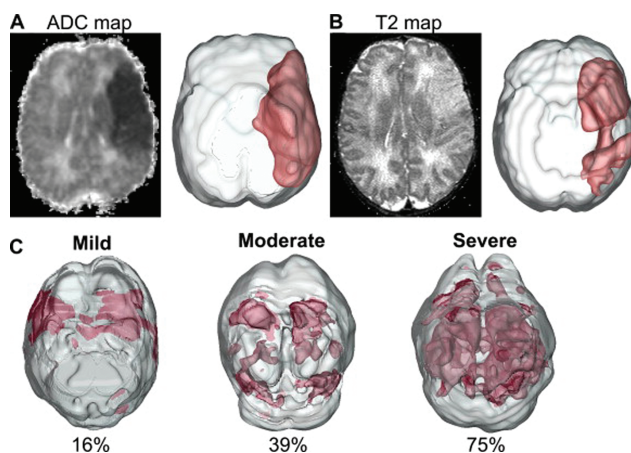


**Figure 6**

Volumetric reconstructions assist in localizing neonatal hypoxic ischemic injury. Volumetric reconstructions of magnetic resonance datasets can assist in localizing regions of injury in the arterial ischemic stroke and hypoxic ischemic injury neonate. (A) Using apparent diffusion coefficient (ADC) maps we can threshold for all ADC values below a value ( $<50 \times 10^{-6} \text{ mm}^2/\text{s}$ ), allowing rapid 3D localization of the lesion

(patient was scanned at 4 days after birth). (B) In the same patient the T2 maps can also be used to localize the lesion. Note that the injury location and volume are different within this patient between the two imaging modalities and these differences may represent salvageable tissues. The 12-month outcome of this left middle cerebral artery occlusion patient was right hemiplegic cerebral palsy. (C) 3D volumetric hypoxic ischemic injury volumes from axial MRI scans of three newborns. The severity scaling (mild, moderate, severe) was determined from 12-month outcomes using their neurological outcome score. Individuals with poorer outcomes had higher percentage of injury (Courtesy of S. Ashwal).

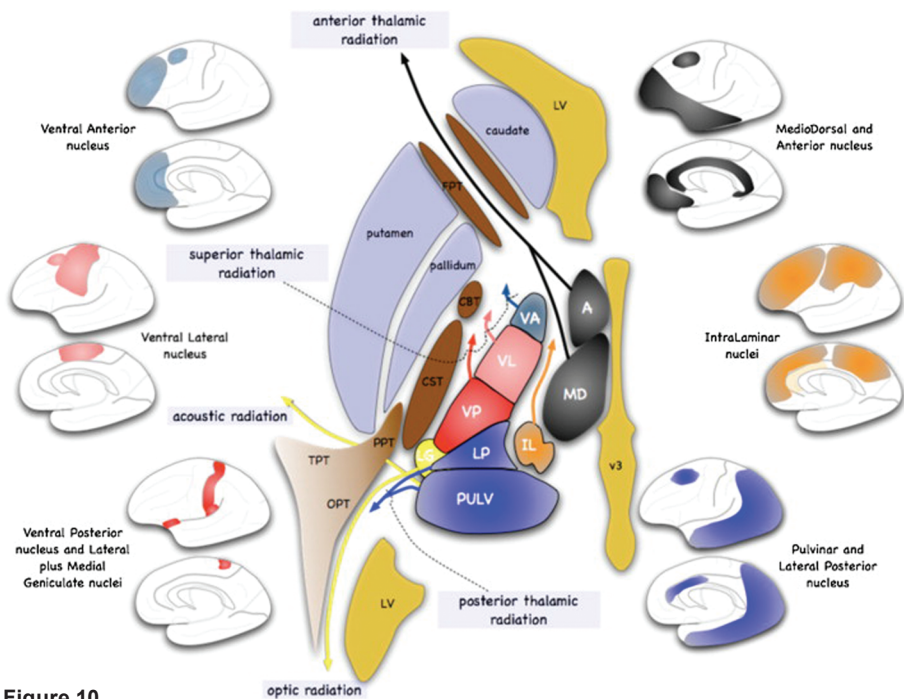


**Figure 10**  
Corticothalamic network injury. Examples of possible network injuries from primary injury to various cortical areas resulting in secondary injury to different nuclei (in matching colors).

## Chapter 8

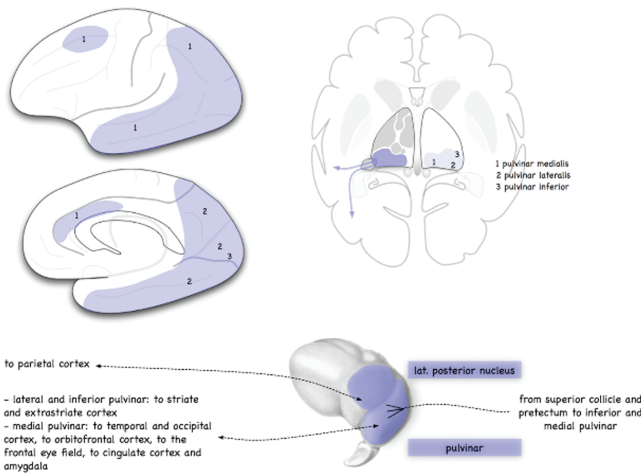


**Figure 1**  
Afferents and efferents of pulvinar and lateral posterior nucleus (adapted from Nieuwenhuys et al. 1988). Cortical connections are mainly with parietal, occipital and temporal lobes.

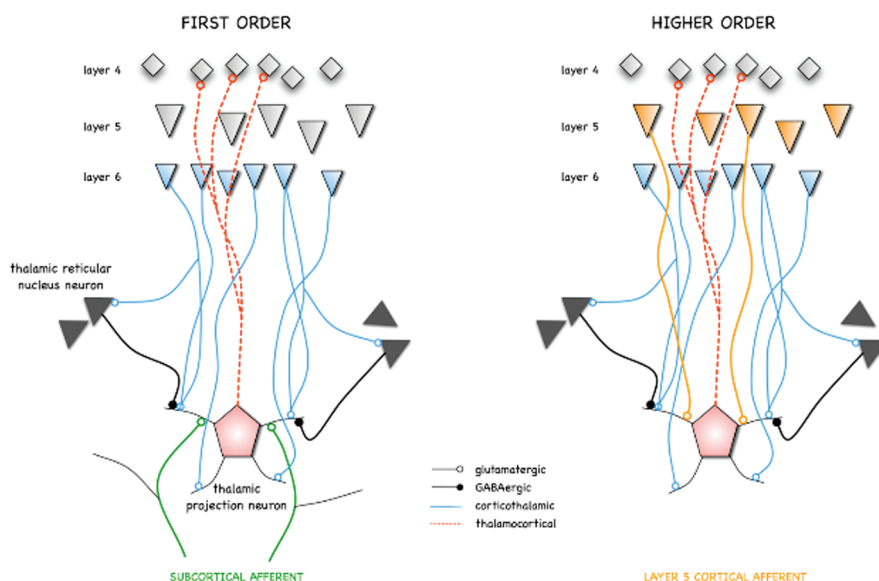


**Figure 6**

FIRST ORDER driving thalamic afferents transfer peripheral (subcortical) information to cortex for further processing. Specific first order afferents (mainly to layer 4, also to 3 and 6) come from thalamic relay nuclei in one of the sensory brain modes: VPL for somatosensory perception, lateral geniculate for visual and medial geniculate for auditory perception. The columnar cortical module is largely built on thalamocortical input. Reciprocal projections from these cortical areas to their thalamic nuclei and corresponding parts of the thalamic reticular nucleus come from layer 6. One thalamic cell forms synapses with many cells within a cortical column. The reciprocal corticothalamic axon number is an order of magnitude (at least 10 x) greater than the number of thalamocortical axons. Each cortical axon (most coming from layer 6) innervates many thalamic neurons, therefore there is considerable convergence and divergence in specific first order corticothalamic pathways. Non-specific first order afferents come from association thalamic nuclei that function in different systems: e.g. VL between cerebellum/pallidum and (pre)motor cortex in the motor system. There is more overlap in cortical areas innervated from these non-specific thalamic nuclei. Driving projections of HIGHER ORDER type come from neocortex onto nuclei like mediodorsal nucleus, pulvinar and intralaminar nuclei. Reciprocal connections emanate not only from layer 6 but also from layer 5 pyramidal cells to these thalamic nuclei, which depend heavily on the intact function of these neocortical areas because subcortical input to them is limited. Corticothalamic connections are glutamatergic. MODULATORS to thalamus come from thalamic reticular nucleus (inhibitory), hypothalamus, raphe nuclei, reticular formation, locus coeruleus. They filter information by switching the transmission mode of thalamic cells between tonic firing, rhythmic (quiet sleep or non-REM sleep) or arrhythmic bursting. When awake the burst mode acts like a "wake-up" system whereas the tonic mode works on a linear relay basis and permits faithful, detailed signal analysis. Thalamus as a whole filters and transforms information to the cortex and thereby becomes a tool for attention to events (adapted from Sherman and Koch 1998).

Chapter 9

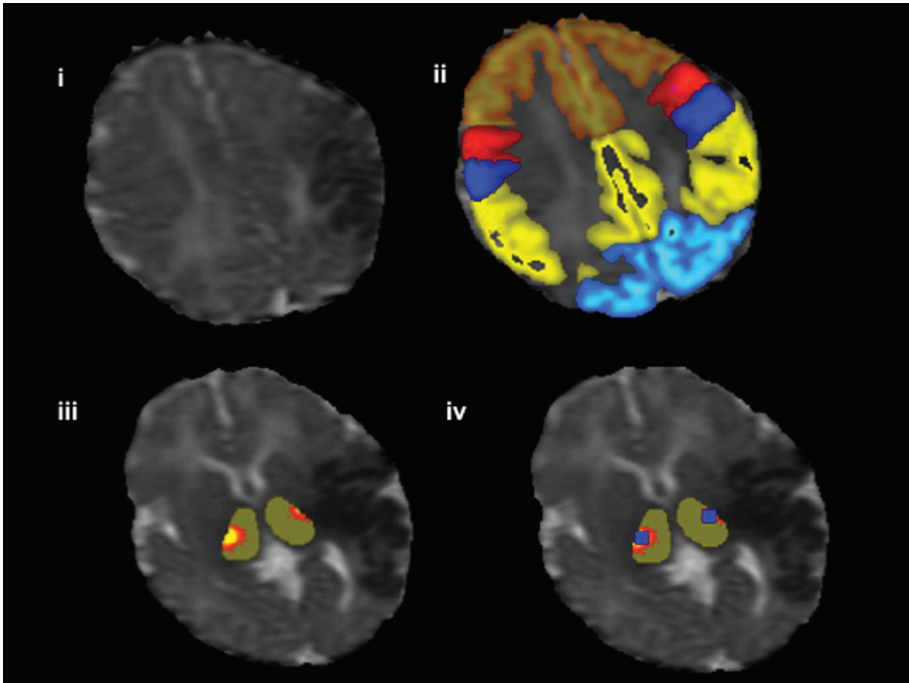


**Figure 1**  
Images of a patient with a posterior truncal MCA stroke: (i) ADC map showing low SI in area of stroke (ii) same ADC-map after automated image registration software was used to co-register DTI data from the patient to standard cortical masks (Harvard Oxford Cortical Structural Atlas) (red-yellow = frontal cortex (minus the prim motor area), red = prim motor cortex, blue = sensory cortex, yellow = parietal cortex (minus the prim sens cortex) and light blue = occipital cortex) (iii) thalamo-cortical connections were assessed for every voxel in the thalamic masks (green) using connectivity-based seed classification with predefined thresholds; yellow-red area is the seed mask of the parietal cortex, there is a clear difference between right and left thalamus (R>L) (iv) The thalamic connectivity seeds were used to place ROIs from which the DTI measurements were taken.